Effects of coastal structures on the shoreline change in Phan Thiet bay, Vietnam

Miss Hoai Thi Phuoc Pham

A Thesis Submitted in Partial Fulfillment of the Requirements
for the Degree of Master of Engineering in Water Resources Engineering
Department of Water Resources Engineering
Faculty Of Engineering
Chulalongkorn University
Academic Year 2023

ผลกระทบของโครงสร้างชายฝั่งทะเลต่อการเปลี่ยนแปลงชายฝั่งที่อ่าวฟานเถียต ประเทศเวียดนาม

น.ส.ฮอย ที พอค ฟาม

วิทยานิพนธ์นี้เป็นส่วนหนึ่งของการศึกษาตามหลักสูตรปริญญาวิศวกรรมศาสตรมหาบัณฑิต
สาขาวิชาวิศวกรรมแหล่งน้ำ ภาควิชาวิศวกรรมแหล่งน้ำ
คณะวิศวกรรมศาสตร์ จุฬาลงกรณ์มหาวิทยาลัย
ปีการศึกษา 2566

Thesis Title	Effects of coastal structures on the shoreline change in Phan Thiet bay, Vietnam
By	Miss Hoai Thi Phuoc Pham
Field of Study	Water Resources Engineering
Thesis Advisor	Assistant Professor Anurak Sriariyawat, Ph.D.

Accepted by the FACULTY OF ENGINEERING, Chulalongkorn University in Partial Fulfillment of the Requirement for the Master of Engineering

.... Dean of the FACULTY OF ENGINEERING
(Professor SUPOT TEACHAVORASINSKUN, Ph.D.)

THESIS COMMITTEE

.... Chairman
(Assistant Professor BUTSAWAN BIDORN, Ph.D.)

.... Thesis Advisor
(Assistant Professor Anurak Sriariyawat, Ph.D.)

.... Examiner
(TANAWAT TANGJARUSRITARATORN, Ph.D.)

.... External Examiner
(Assistant Professor Thamnoon Rasmeemasmuang, Ph.D.)

ฮอย ที พอค ฟาม : ผลกระทบของโครงสร้างชายฝั่งทะเลต่อการเปลี่ยนแปลงชายฝั่งที่อ่าวฟานเถียต ประเทศเวียดนาม. (Effects of coastal structures on the shoreline change in Phan Thiet bay, Vietnam) อ.ที่ปรึกษาหลัก : ผศ. ดร.อนุรักษ์ ศรีอริยวัฒน์

วิทยานิพนธ์นี้เป็นศึกษาผลกระทบของโครงสร้างชายฝั่งต่อการเปลี่ยนแปลงชายฝั่งในอ่าว Phan Thiet จังหวัด Binh Thuan ประเทศเวียดนาม ตั้งแต่ปี ค.ศ.1988 - 2021 โดยมีวัตถุประสงค์หลักสองประการ คือ การตรวจสอบการเปลี่ยนแปลงของชายฝั่งในอดีต และผลกระทบของโครงสร้างชายฝั่งต่อการเปลี่ยนแปลงชายฝั่งโดยการเปรียบเทียบแนวชายฝั่งในกรณีที่มีและไม่มีโครงสร้างชายฝั่งด้วยแบบจำลอง GENESIS อีกทั้งยังได้การประยุกต์ใช้แบบจำลอง SWAN เพื่อจำลองคลื่นซึ่งเป็นข้อมูลนำเข้าที่สำคัญสำหรับแบบจำลอง GENESIS

จากผลการศึกษาการเปลี่ยนแปลงชายฝั่ง พบว่ามีอัตราการสูญเสียพื้นที่ดินชายฝั่งตั้งแต่ 0.9 – 8.7 เฮกแตร์ต่อปี ระหว่างปี 1988 – 2016 ขณะที่อัตราการสูญเสียนี้เพิ่มขึ้นถึง 11.2 เฮกแตร์ต่อปี หรือคิดเป็นร้อยละ 83 ของพื้นที่ชายฝั่งที่ถูกกัดเซาะระหว่างปี 2016 - 2021 นอกจากนี้ผลลัพธ์การศึกษายังพบว่าอัตราการเปลี่ยนแปลงชายฝั่งมีความสัมพันธ์กับการมีอยู่ของโครงสร้างชายฝั่งและความถี่ของพายุไต้ฝุ่น

แบบจำลอง GENESIS สามารถจำลองแนวชายฝั่งในพื้นที่ด้านตะวันตกและด้านตะวันออกของอ่าว Phan Thiet ได้อย่างมีประสิทธิภาพ โดยมีค่าเฉลี่ยความคลาดเคลื่อนสัมบูรณ์ (MAE) ของอัตราการเปลี่ยนแปลงชายฝั่งที่ 2.34 ม./ปี และ 5.32 ม./ปี ตามลำดับ ผลจากแบบจำลอง GENESIS ยืนยันทิศทางหลักของการเคลื่อนตัวของตะกอนตามแนวชายฝั่งในพื้นที่ศึกษาจากทิศตะวันออกไปทิศตะวันตก สำหรับผลกระทบของโครงสร้างต่อการเปลี่ยนแปลงชายฝั่ง พบว่าโครงการถมดินบนชายหาดส่งผลกระทบต่อพื้นที่กัดเซาะห่างออกไป 1,600 เมตรจากที่ตั้งโครงการ ขณะที่คันดักทรายและกำแพงกันคลื่นมีอิทธิพลต่อแนวชายฝั่งที่อยู่ติดกันเป็นระยะทาง 2,500 เมตร และ 1,700 เมตร ตามลำดับ โดยสรุปแล้วการศึกษานี้ได้นำเสนอผลของการเปลี่ยนแปลงชายฝั่งในอดีตและผลกระทบของโครงสร้างชายฝั่งบางชนิดต่อการเปลี่ยนแปลงชายฝั่งในอ่าว Phan Thiet ซึ่งเป็นข้อมูลพื้นฐานสำหรับการประยุกต์ใช้โครงสร้างป้องกันชายฝั่งเพื่อโครงการบรรเทาผลกระทบการกัดเซาะชายฝั่งในพื้นที่นี้ในอนาคต

สาขาวิชา	วิศวกรรมแหล่งน้ำ	ลายมือชื่อนิสิต ....
ปีการศึกษา	2566	ลายมือชื่อ อ.ที่ปรึกษาหลัก ....

6170419621 : MAJOR WATER RESOURCES ENGINEERING
KEYWORD: Shoreline change coastal structures ArcMap SWAN GENESIS

Hoai Thi Phuoc Pham : Effects of coastal structures on the shoreline change in Phan Thiet bay, Vietnam . Advisor: Asst. Prof. Anurak Sriariyawat, Ph.D.

This thesis examined the effects of coastal structures on shoreline change in Phan Thiet Bay, Vietnam from 1988 to 2021. This thesis explored two key objectives; that were the investigation of historical shoreline changes and the effects of structures on shoreline based on the comparison of simulated shorelines with and without structures by using GENESIS model. Moreover, the SWAN model was used for simulating wave data which is an important input for the GENESIS model.

From the shoreline evolution results, it was found that the land loss rate ranged from 0.9 to 8.7 ha/year in 1988 to 2016, while this loss rate increased up to 11.2 ha/year or 83% of the eroded coastline in 2016 to 2021. Moreover, the results found that the shoreline change rate was strongly correlated with the presence of structures and the frequency of typhoons.

The GENESIS model effectively simulated the shoreline in the Western area and the Eastern area in Phan Thiet Bay, with an average Mean Absolute Error (MAE) of shoreline change rate as 2.34 m/year and 5.32 m/year, respectively. The results from GENESIS model reaffirmed the predominant longshore sediment transport direction in this study area was East to West. For the effects of structures to the shoreline change, it found that the beach reclamation project affected the erosion areas up to 1600 m away from its location, while groins and seawalls influenced adjacent shorelines up to 2500 m and 1700 m, respectively. In conclusion, this study contributed results on the historical shoreline change and effects of some specific structures on shoreline change in Phan Thiet Bay, providing fundamental data for applying the coastal structures in future coastal erosion resilience project in this area.

Field of Study:	Water Resources Engineering	Student's Signature ....
Academic Year:	2023	Advisor's Signature ....

ACKNOWLEDGEMENTS

I am grateful for the support I have received from various individuals and organizations during the completion of this thesis on the effects of coastal structures on shoreline change in Phan Thiet Bay.

I would like to express my sincere thanks to Asst. Prof. Dr. Anurak Sriariyawat for his patient supervision throughout this study and his efforts training me on working skills such as rational thinking, making decision, clear communication, and many other precious skills. In addition, I really appreciate his financial and emotional support which has given me more courage to keep going until now.

I would like to thank the examination committee including Asst. Prof. Dr. Butsawan Bidorn, Dr. Tanawat Tangjarusritaratorn, Asst. Prof. Dr. Thamnoon Rasmeemasmuang, for their time and valuable feedback on this thesis.

Besides, I am extremely grateful for being a part of Water Resource Engineering department, Chulalongkorn University. I would like to thank all professors, seniors, and juniors in our department for going through this thesis with me. Their generous sharing of knowledge, encouragement, and insights into this beautiful country, Thailand, have enriched my experience here.

I would like to acknowledge the ASEAN University Network/ Southeast Asia Engineering Education Development network (AUN/Seed-net) for granting me the scholarship that made this opportunity possible.

Special thanks to the Port and Coast Engineering Department of Ho Chi Minh University of Technology for being the foundation for me to know about this field. Thanks to all the lecturers from there, especially Assoc. Prof. Dr. Nguyen Danh Thao for introducing me to AUN/Seed-net and Chulalongkorn University, and their advises on this thesis.

I would like to thank Binh Thuan Provincial Hydrometeorological Center, Department of Agriculture and Rural Development of Binh Thuan province, and Institute of Meteorology Hydrology and Climate Change Vietnam for providing wind data, and wave data for this thesis.

I would like to thank Super Wind Energy company for the opportunity to work while doing this study. Their valuable support and the lessons in working skills are greatly appreciated. It is an honor to have had the chance to work with such a reputable organization.

Finally, I would like to acknowledge the numerous contributors of related studies whose valuable references have significantly enriched my research. I hope that this thesis will also serve as a contribution to the field of coastal engineering.

I sincerely appreciate the support of everyone who has been the special and necessary part of this journey.

Hoai Thi Phuoc Pham

TABLE OF CONTENTS

Page

LIST OF TABLES

Page

LIST OF FIGURES

Page

CHAPTER 1
INTRODUCTION

1.1 Background

The coastal shoreline serves as the dynamic interface between water, land, and air, constantly undergoing changes in its position. Global studies spanning from 1984 to 2015 have revealed that the extent of coastal erosion, covering an area of 28,000 km^2, was twice as large as the accretion area of 14,000 km^2 (Mentaschi et al., 2018).

These changes can be influenced by a combination of natural factors, such as wind, waves, currents, river flow, tides, storms, and rising sea levels, as well as human activities, including water resource projects, mineral mining, construction of structures along the coast, land use practices, and deforestation of coastal mangroves.

Whether driven by natural processes alone or exacerbated by human activities, shoreline change can have significant consequences for coastal areas (Horikawa, 1988). Erosion results in the loss of land and related things such as communities, beaches, water resources systems, and ecosystems (Phillips & Jones, 2006). On the other hand, coastal accretion in navigation channels, river mouths, and lagoon inlets obstructs water flow and hampers navigation, posing challenges to coastal transportation systems (Swift et al., 1976).

As other areas in the world, Vietnam has experienced the shoreline change. Vietnam coastline is divided into 3 parts which are the Northern part, Central part, and Southern part in Figure 1-1 (Thao et al., 2014). Vietnam features an expansive coastline stretching 3,260 km, with 28 provinces and municipalities out of the total 63 situated in the coastal zone. The coastline is important for Vietnam with the most world's charming and peaceful destinations. Further, Vietnam's coastline plays a vital role as a strategic international trade hub as key connections in the Southeast Asian region . However, Vietnam's coastal areas face persistent risks and hazards, including shoreline changes, saltwater intrusion, and flooding, with erosion emerging as a particularly severe challenge along the central coastline (Thao et al., 2014). Managing coastal erosion and accretion poses a significant challenge for the Vietnamese, particularly with the escalating severity of erosion (Tien et al., 2003).

The study area of this study is Phan Thiet, the capital city of Binh Thuan province which is located in the south of the middle part of Vietnam as shown in Figure 1-1. The study was done from Ke Ga to Mui Ne, including 3 segments separated by Ca Ty river and Phu Hai river. The coastal region plays a crucial role in the socio-economic development of Phan Thiet, primarily driven by the tourism industry and fisheries. Phan Thiet is well-known as one of the most productive fishing sectors in Vietnam (Takagi et al., 2014).

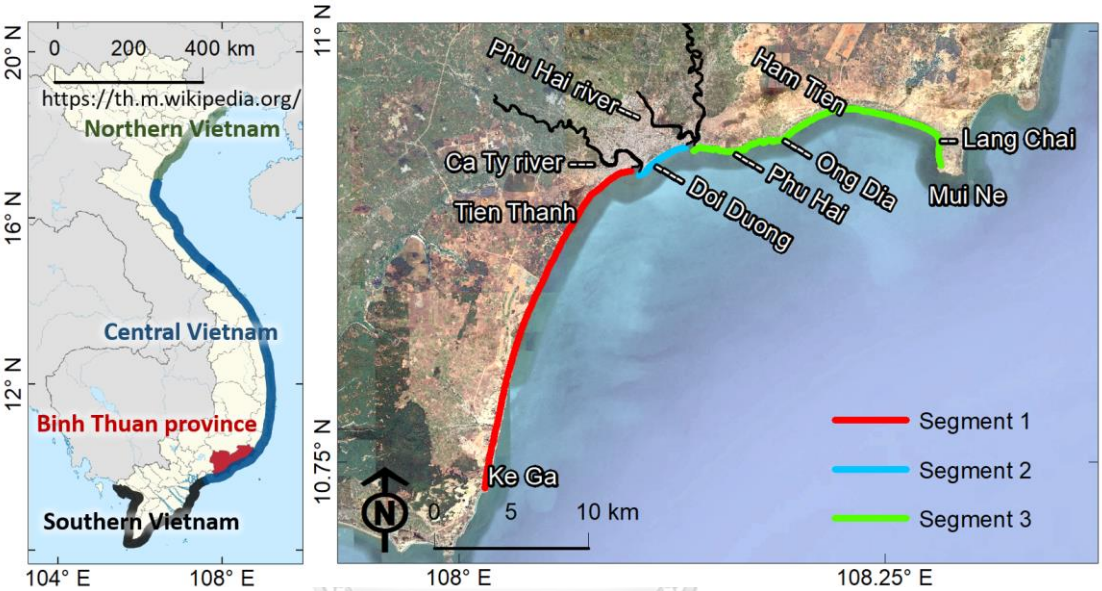

Figure 1-1 Study area: Phan Thiet bay, Binh Thuan province, Vietnam

Unfortunately, Binh Thuan province has witnessed changes in shoreline positions, with erosion being a prevailing issue (Duc & Luan, 2014). Binh Thuan province is one of the most eroded areas in the south of the central part of Vietnam (Hue & Thanh, 2019). To mitigate these challenges, various coastal structures have been constructed in Binh Thuan province to control shorelines and maintain estuary navigation in Ca Ty river mouth and Phu Hai river mouth, accidentally leading to shoreline changes in the area (Van To, 2006). Beginning in 2004, land reclamation efforts have been undertaken in Tien Thanh for commercial purposes. However, after that, significant erosion occured near the mouth of the Ca Ty River, leading to the formation of steep coastal cliffs housing vulnerable structures. A field survey conducted in January 2012 by Takagi et al. (2014) revealed that, as a consequence of coastal erosion, six households were forced to elevate their houses, and four had to relocate entirely. Trung and Mau (2011) showed that the shoreline from Phu Hai to Mui Ne was eroded from 3 m/year to 5 m/year. Tien Thanh experienced erosion during the NE monsoon season. In particular, in 2007 and 2008, erosion resulted in the destruction of 3 to 4 rows of houses. The situation worsened in 2008 and 2009 when a staggering 104 houses collapsed. Furthermore, during the survey, the houses destroyed with steep slope in Tien Thanh were observed as shown in Figure 1-2.

Figure 1-2 Coastal community in Tien Thanh

Moreover, some other areas have also experienced severe erosion, adversely impacting tourist beaches, causing them to narrow down and even disappear altogether (Trung & Mau, 2011). Consequently, the tourism industry has been negatively affected as well. Despite an increase in service establishments and tourist numbers, the degradation of beach views due to the use of various groins, sandbags, geotubes, and the loss of sandy beach areas has been evident (Vo et al., 2018).

Despite the implementation of various shoreline protection structures, shoreline change, particularly erosion, continued to occur in Phan Thiet bay. While studies have examined shoreline in specific areas within the bay, it also necessary to do research on the long-term effects of coastal structures on the entire bay to effectively manage and protect the coastal area of Phan Thiet bay.

This study aims to investigate the effects of coastal structures in whole Phan Thiet bay. To achieve that, the historical shoreline change should be understood by investigating the behaviors of shoreline changes which possibly affected by the presence of structures and typhoon. Selected tools were ArcMap, Digital Shoreline

Analysis System (DSAS), numerical wave model Simulating Waves Nearshore (SWAN), and GENEralized model for SImulating Shoreline change (GENESIS). The effects of structures on shoreline were analyzed through the comparison of shoreline simulation results with and without structures. Those results of historical shoreline change and structural effects are the contribution as the basic data providing additional fundamental understanding for future coastal resilience in Phan Thiet bay.

1.2 Objective of study

From the reasons mentioned above, the objectives of this study are:

1) To investigate the behaviors of shoreline changes in Phan Thiet bay, Vietnam

2) To investigate the effects of coastal structures to the shoreline in Phan Thiet bay, Vietnam

1.3 Scope of research study

1) The study focuses on about 50 km of Phan Thiet bay, located in Binh Thuan province, Vietnam, from Ke Ga to Mui Ne as shown in Figure 1-1. The bay consists of three distinct segments, namely segment 1, segment 2, and segment 3, which are separated by the Ca Ty River and Phu Hai River.
2) Landsat satellite images were obtained from United States Geological Survey (USGS) from 1988 to 2021.
3) Google Earth images in 2011 and 2021 were obtained from Maxar Technologies Inc.
4) Wave data at 1 offshore station were obtained from Institute of Meteorology Hydrology and Climate Change Vietnam.
5) Wave data at 2 nearshore stations and bathymetry survey data in 2012 were obtained from the survey of Vuong (2012).
6) Wave data at 2 nearshore stations and bathymetry survey data in 2014 were obtained from the survey of Vuong (2014).
7) Bathymetry data is the gridded bathymetry data of the General Bathymetric Chart of the Oceans (GEBCO).
8) Observed wind data was from Binh Thuan provincial Hydrometeorological center.

9) Global wind data was from the fifth generation ERA5 of ECMWF.
10) Global wave data was from Wavewatch from the National Centers for Environment Prediction (NOAA/NCEP).
11) Data of structures were obtained from Google Earth images, Landsat images, and Department of Agriculture and Rural Development of Binh Thuan province.
12) DSAS tool in ArcGIS was used to determine the shoreline change rate.
13) SWAN model was used to simulate wave nearshore from 1988 to 2021.
14) GENESIS model was used to simulate shoreline change with and without structures from 1988 to 2021.

1.4 Expected outcomes

The expected outcomes of this study are as follows.

1) Understanding the situation of coastal erosion and accretion of in Phan Thiet bay, Binh Thuan province.
2) Understanding the effect on shoreline of structures in Phan Thiet bay, Binh Thuan province.

1.5 Research procedures

The procedures of this study include literature reviews, compiling data, extracting shoreline, wave simulation, shoreline change simulations, and writing thesis as shown in Figure 1-3. Firstly, literature reviews were conducted to gain insights into the study area, related research, and theories. During this phase, surveys were also conducted to establish contact with the Binh Thuan Provincial Hydrometeorological Center and the Department of Agriculture and Rural Development of Binh Thuan province. Additionally, sediment samples were collected in Binh Thuan province for sieve analysis, providing a better understanding of coastal erosion consequences.

Subsequently, all the necessary data, such as Landsat satellite images, wind data, wave data, bathymetry, and structural information, were downloaded and prepared. This preparation was essential for digitizing shorelines and inputting them into shoreline simulation models. As shoreline change models require more wave data than the available global and observational data, a wave simulation model was employed to generate the required wave data for shoreline change models. The simulated shorelines, along with the necessary input data, were then used to determine the shoreline positions in scenarios with and without structures. Finally, the thesis was written, marking the completion of this study.

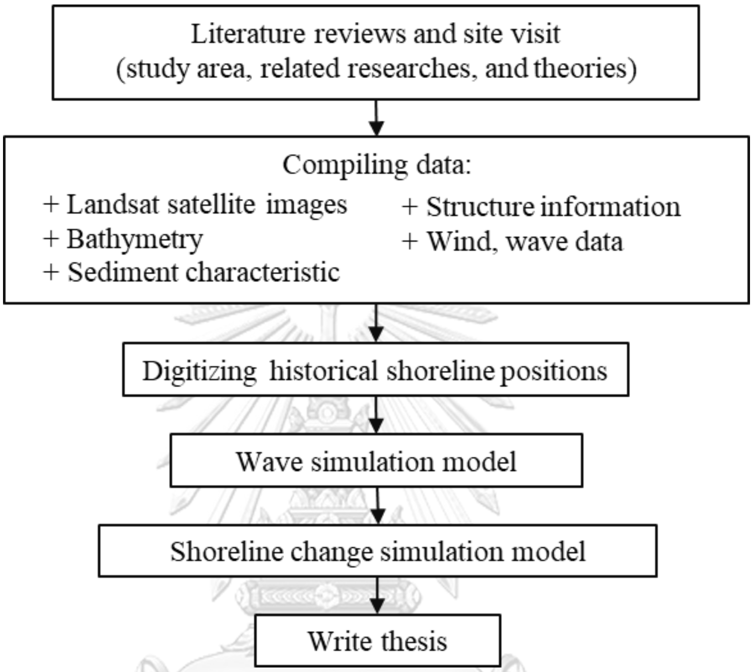

Figure 1-3 Research procedure of this study

CHAPTER 2
THEORIES AND LITERATURE REVIEWS

This chapter provides an overview of theories and literature related to the study area. It covered essential theories about coastal processes, shoreline change investigation, shoreline simulation models, and related researches to study area. The related researches to study area, Binh Thuan province in Vietnam, explored relevant research conducted in the region, offering insights into the existing knowledge and gaps within the context of Binh Thuan province. By reviewing these theories and relevant literature, this chapter established a solid foundation for investigating the behavior of historical shoreline change, and investigating the effects of coastal structures on the shorelines.

2.1 Coastal processes

This section presents theories related to shoreline change, encompassing the causes of shoreline change, mechanisms of coastal sediment transport, and theories regarding the two primary factors considered in this study: waves and engineering solutions.

2.1.1 Shoreline change

Shoreline is the interaction of land, sea, and water changes continuously. Depending on the objective of the research, the considered period could be some seconds or some years. The shoreline is determined at a certain time is the instantaneous shoreline. The average shoreline is better for being used if that is possible to obtain. The shoreline positions could move some centimeters to tens of meters (or more) respectively to the different tidal levels. Therefore, the shoreline should be collected at the same tidal level as much as possible (Boak & Turner, 2005)

There are some indicators following which the shoreline position is determined, such as the discernible coastal feature, tidal level, and the index of the remote sensing technique. That discernible coastal feature can be the vegetation boundary or the wet/dry boundary, which can be physically recognized. The tidal level can be the mean high water or mean sea level (Boak & Turner, 2005). The index of the remote sensing technique could be the Normalized Difference Water Index (NDWI) or Normalized Difference Vegetation Index (NDVI) (Pham & Prakash, 2018).

Consider in a certain period, the shoreline may be eroding, accreting, or in the equilibrium stage. When shoreline change happens, it could be coastal erosion or coastal accretion. Coastal erosion is the process when the shoreline retreats landward; and the width of the beach is narrowed down. Coastal accretion is the process when the shoreline moves seaward and extends the width of the beach (Pilkey, 1991). The equilibrium stage means that the average shoreline positions in months or years are relatively stable, even though the shoreline position keeps moving back and forth (Sorensen, 2006). Natural beaches are generally stable and in dynamic equilibrium (Horikawa, 1988).

Even when the shoreline is eroded, accreted, or in the equilibrium stage, it is continuously responding to variable wind, waves, currents, beach fills, sediment from the river, dredging, and other factors (Sorensen, 2006). All those factors could be classified into 3 main reasons that are sediment movements, sediment supply or removal by humans, and relative differences in elevation between land and sea surface.

When a certain coastal area is considered in a certain period, if the sediment amount from the inflow is less than the sediment amount taken out by the outflow, erosion happens. On the other way around, if the sediment amount that the inflow supplies to that area is more than the sediment moves out with the outflow, that area is accreted. Those movements of the sediments are called littoral drift. The littoral drift could be created by waves and other related factors. Meanwhile, the sediment transport rate and direction could be affected by the structures or other coastal projects along the shore (Horikawa, 1988).

Not only built many structures, but humans also had other activities affecting shoreline such as mining natural resources which are titanium and sand in coastal areas (Chisholm & Dumsday, 1987), dredging sediment in accretion areas, changing land use and releasing water from water drainage systems (Tien et al., 2003).

The shoreline is possibly changed without the effect of sediment transport because of the change in water surface elevation and sea bed elevation which are sea level rise and land subsidence. When the sea level rises, the shoreline moves landward. The movement of the shoreline depends on the beach slope. If the beach slope is high, the shoreline change is small, and vice versa (Narayana, 2016).

2.1.2 Coastal sediment transport mechanisms

Based on the direction of the littoral drift, 2 types of processes are longshore sediment transport and cross-shore sediment transport. Longshore sediment transport referring to the movement of sediment along the shoreline is the significant factor controlling shoreline change in long-term and large-scale. On the other hand, cross-shore sediment transport refers to the movement perpendicular to the shoreline; and significantly controls shore-term variations in beach profile (Horikawa, 1988).

Longshore sediment transport is mainly driven by the effect of longshore wave-induced current, and the longshore wave on the bedload sediments and suspended sediment induced by wave breaking. The process of wave inducing the current is shown in Figure 2-1. When the oblique incident wave comes to the shore from offshore, after passing the wave breaking line and reaching the surf zone, the wave breaks and keeps moving shoreward. Thereby the water level and pressure near the breaking waves are high, while the ones further away from the breaking waves are low. Additionally, the breaker line is not parallel to the shoreline. That means there are pressure differences along the shoreline. Since the water flows from the higher-pressure area to the lower pressure area, the longshore current that flows parallel to the shoreline is generated. This current can move the sediment with it (Sorensen, 2006).

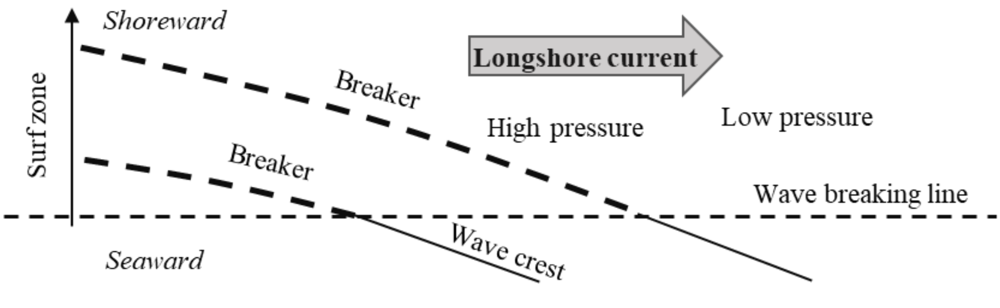

Figure 2-1 Wave-induced current (Sorensen, 2006)

The main factor creating cross-shore sediment transport is the wave orbital motion in the swash zone (Horikawa, 1988). After the wave breaks is the swash meaning the wave continues moving up seaward, and the backwash that is the water flow is pulled down seaward by gravity. In those swash and backwash processes, the sediments are transported by the wave orbital motion. If the swash is stronger than the backwash, the sediment is moved to the onshore direction, and vice versa (Sorensen, 2006). The swash not only causes cross-shore sediment transport but also distributes to the longshore sediment transport when the wave direction is not perpendicular to the shoreline (Horikawa, 1988). The fluctuation of sea level which is tidal can also transport sediment. However, tidal currents have a small effect on the sediment, especially in the straight coastline area (Narayana, 2016).

2.1.3 Wave dynamic

Waves continuously arrive at the coast and are followed by several coastal processes such as wave breaking, wave inducing the longshore current, wave moving longshore, wave causing swash, and gravity pulling down the backwash. The nearshore sediments are correspondingly responding to those processes (Sorensen, 2006).

According to Sorensen (2006) and Horikawa (1988), the wave can be generated by wind, storms, earthquakes called tsunamis, the moon and the sun called tides. The wind-generated wave is the most common in terms of coastal sediment processes. The wind generates the wave as the capillary waves first. The wave propagates, and travels outward from the wind source with steep, random irregular waves. Within the wind fetch, the wave is called sea wave or wind wave. The sea wave can be developed until those waves reach a maximum state respective to the given wind source. In that fully developed sea, theoretically, the wave characteristics are relatively more uniform, with waves of similar height, period, and direction. Practically, the term fully developed wind with uniform characteristics rarely happens due to the continuous change of the wind.

In case the wind fetch is close to and over the coast, the developed sea interacts with the sea floor, the waves become irregular and complex. In case the wind fetch is distant from the coast. Beyond the wind fetch, depending on many factors such as wind characteristics, the swell waves possibly form after the wind-generated waves. For example, if the wind duration is not long, or the wind speed is not stable, the wind waves do not change to the swell waves.

When waves come to the shallow water and the surf zone, several processes might happen, leading to changes in wave characteristics. These processes include wave shoaling, wave refraction, wave diffraction, wave breaking, and wave reflection. Waves characteristics include their wavelength (L), period (T), height (H), and speed (c). The wavelength is the distance between two consecutive wave crests or troughs. The period is the time it takes for one full wavelength to pass a fixed point. The height of a wave is the vertical distance between the crest and trough of wave, while the wave magnitude is the vertical distance from the still water level to the crest or trough. Wave celerity is the speed at which a wave crest moves across the ocean. Wave steepness is the ratio of wave height (H) to wavelength (L).

The wave can be classified into sea waves (wind waves) and swell waves based on their origin and characteristics. Wind waves are generated by the transfer of energy from the local wind of the considered area to the water surface, resulting in steep, random, and irregular wave patterns. Swell waves, on the other hand, are created by distant storms or weather systems out of the considered area; or swell waves can form after the wind-generated wave moves out of the wind fetch as show in Figure 2-2. The condition for the storm or wind to generate the swell are that the wind must move faster than the wave crests for energy transfer to continue; the wind duration must be long enough; and the fetch should be far enough. That wave can travel across the long distance of hundreds or even thousands of kilometers and come to the considered area as the swell with the longer wavelengths, lower wave height, longer wave crest-line, and nearly uniform periods compared to the wind wave by local wind (Sorensen, 2006).

In terms of coastal sediment processes, wind waves are more important than other types of waves due to their occurring frequency. The wind is always blowing and creating wind waves. Wind waves create the largest energy from the sea to the shore (Sorensen, 2006).

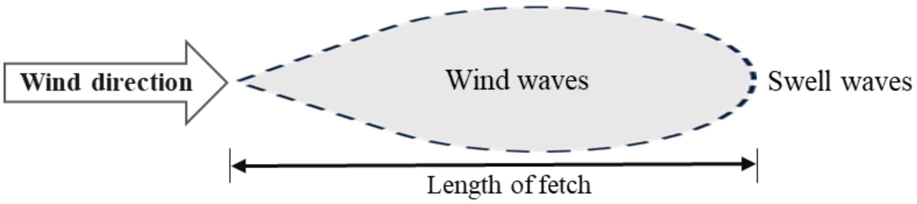

Figure 2-2 Wind waves to swell waves (Brooks & Cole, 2002)

2.1.4 Engineering solution of shoreline change problem

When erosion or accretion occurs, humans have the option to respond with engineering solutions, or do nothing and allow the shoreline to naturally reach an equilibrium state. In cases of coastal erosion, various interventions were employed by humans to protect and develop coastal land. For example, beach reclamation, breakwaters, seawalls, groins, and jetties, which help absorb wave energy and regulate sediment distribution. On the other hand, in areas of coastal accretion, where sediment accumulation disrupts navigation, dredging was often performed to remove the obstructing sediment (Sorensen, 2006).

Beach reclamation is a method helping to solve the main reason for erosion, which is the lack of sand. Detached breakwaters are structures built parallel to the shore to obstruct the incident wave energy, in turn, reduce the sediment transport induced by those waves (Sorensen, 2006). Seawalls could protect the upland behind the wall, however when the waves hit the seawall, it creates the downward forces of water removing the sand in front of the wall and scouring the wall. Groins are structures built perpendicular to the shoreline and interrupting the longshore sediment transport. For the protected beach, that could either accumulate sand on the shore or retard sand losses. For the downdrift shore, that could cause the lack of sand supply from the updrift (Horikawa, 1988). Jetties are structures to support the navigation of vessels. The jetty could prevent the buildup of sediment inside that navigation channel. In most cases, in order to achieve these purposes, two jetties should be built on both sides of the river mouth; and dredging activity by humans is necessary to support the jetty. Although the main purposes of the jetty and groin are different, they give a similar effect to sediment transport since their shape and material can be the same (Sorensen, 2006).

These above coastal structures could affect the coastal processes by changing the energy of incident waves approaching the shore, which indirectly affected the sediment transport induced by those waves, and by directly disturbing the existing sediment transport (Sorensen, 2006). That resulted in the change of shoreline as well. By the time, more and more structures were built, and can affect not only the protected shoreline, but also seriously to the adjacent coastal zone. The partial or inadequate solutions of structures in one area may even accelerate the shoreline change problem in other areas. The careful consideration of the structures in the whole regional shore is important for creating an effective and economical plan to manage the coastal zone (US Army Corps of Engineers, 1984).

2.2 Shoreline change investigation

Shoreline change analysis is crucial because coastlines constantly shift due to factors like waves, tides, and sea-level changes. It's essential for dealing with scientific, engineering, and management challenges, especially in areas with long histories of coastal human settlement. The origins of shoreline change analysis date back to the 19th century when early researchers described shoreline movements based on hydrographic charts and topographic maps. However, it gained significant development in the 1970s due to better technology like aerial photos and computers. As coastal populations grew, so did the need to understand shoreline changes. This led to the development of methods for measuring and analyzing shorelines, which continue to improve, now using various data types and techniques (Burningham & Fernandez-Nunez, 2020).

Multiple data sources and analytical methods can be utilized to assess shoreline positions. These sources for shoreline determination may include satellite imagery, aerial photography, beach surveys, and GPS-based measurements, among others. (Boak & Turner, 2005). Zuzek et al. (2003) analyzed shoreline change rates and identify areas of erosion and accretion along the coast of Lake Michigan in Ottawa and Allegan Counties, Michigan, USA. In this study, the aerial photographs were used due to their availability with high resolution of 0.65 m to 1.33 m.

In many coastal areas, historical data was often scarce or entirely absent. Consequently, the selection of data sources for a particular site is typically guided by data availability (Boak & Turner, 2005). Do et al. (2019) explored the potential of Landsat satellite images with resolution of 28 m in monitoring shoreline-change rates and changes in volumes of coastal sediments that can be applied to beach locations where data are lacking or scarce. The study evaluated the accuracy of the developed method by comparing the extracted shorelines from Landsat images with in situ observations from the JAaRlijkse KUStmeting (JARKUS) database, yearly survey program for the Dutch coastal area, between 1985 and 2010. The main result of this study was that Landsat satellite images could be used as a reliable and cost-effective method for monitoring shoreline-change rates and changes in volumes of coastal sediments over decadal periods.

Landsat satellite images were also used for extracting shorelines in other research for different objectives. Dewidar and Bayoumi (2021) forecasted the future coastal location of Egyptian Nile Delta coast for the year 2041 based on the observed shoreline changes and trends. Vallarino Castillo et al. (2022) examined the historical progression of shoreline changes of the Pacific Coast of Panama, and discerned the influential factors behind these alterations. Ozturk and Sesli (2015) investigated and quantified the temporal changes that occurred in the shorelines of the Kizilirmak Lagoon Series before and after the construction of Altinkaya and Derbent Dams.

In Vietnam, the observational source of data for shoreline extraction was limited. Satellite images became a useful source. For doing the study of shoreline change in Da Nang, Vietnam from 2009 to 2015, Google Earth satellite images were used (Hoang et al., 2015). For the case of long-term shoreline change from 1973 to 2015 in Mekong Delta river, in order to analyze how the shoreline has continuously changed in response to shifts in relative sea levels, transformations in land use, and variations in sediment supply, Liu et al. (2017) utilized Landsat satellite images due to its availability over other sources of data. Landsat satellite images were also used in other research in other area of Vietnam for monitoring the shoreline such as Thinh and Hens (2017) in the north of Vietnam, and Quang Tuan et al. (2017) in the central of Vietnam.

2.3 Shoreline simulation models

This section provides literature reviews of the methodology for determining shoreline change, the SWAN model used to simulate waves as input in the shoreline change model, and the GENESIS one-line shoreline model.

Empirical methods, physical models, and numerical models could be used to predict beach evolution. The empirical method was based on observation of beach evolution in the past and comparison of the study area and other beaches which have similar conditions. The physical model was the scale model with corresponding conditions of real conditions of the study area (Horikawa, 1988). Although measurement and analysis of historical shoreline position was the most accurate method to analyze shoreline evolution, this method did not consider the effects of specific coastal structures or climate change (Thomas & Frey, 2013).

According to Horikawa (1988), as the computer has come into wide use, numerical models along with empirical methods and physical models had been gradually become an useful tool for predicting beach evolution. The development of numerical models had been accelerated by the requirement for faster and more cost-efficient method in the prediction of beach evolution. However, empirical methods were more practical to be applied in cases where computational resources were limited. While the physical models could represent the physical process better. Each method had its strengths and limitations. Combining numerical models, empirical methods, and physical models could provide a more comprehensive understanding of shoreline evolution, mitigating the individual limitations of each approach. This study utilized the numerical model due to the objectives of investigating the effects of coastal structures on shoreline change, and the large scale of a study area compared to the size of sediment and structures.

Cross-shore movement and longshore movement are two main types of sediment movement caused by waves. The cross-shore transport effects are the erosion by storm, and the cyclical movement of shoreline position by season. Whereas the longshore sediment transport affects the evolution of shoreline in long term. The cross-shore sediment transport contribution to shoreline change can usually be neglected, if long periods more than 1 year are being treated.

One-line model: In this model, shoreline change is caused by longshore sediment transport. The model was most suitable for simulating shoreline long-term change with effects of structures such as the groin, jetty, and breakwater (Hanson, 1989). One-line model was well-developed and became the most typical line model (Horikawa, 1988). The one-line model, based on longshore sediment transport and conservation of sand volume, had been preferred for simulating shoreline change with effect of nature and human factors (Thomas & Frey, 2013). One-line represents shoreline, while shapes of all contour lines are similar. One-line models could be used to simulate shoreline change in long time scale from 1 year to many years (Horikawa, 1988).

N-line model, which is the improvement of one-line model, is based on longshore and cross-shore sediment transport, and the continuity of sediment transportation (Uda, 2018); However, N-line model had not been popularly applied. Obtaining consistent results of N-line model was the challenge when the beach is complicated and not straight (Reeve & Valsamidis, 2014).

Three-dimensional bottom topography change model is predicted from wave and current data which was used to determine the spatial distribution of the sediment transport rates. Although the three-dimensional model uses less assumptions and idealization, it is more complicated to use and takes a longer time of computation than the line model. Three-dimensional models can be used for spatial scale from hundred meters to less than 10 km and used for time scale in one storm or some months (Horikawa, 1988).

In this study, the shoreline of the study area is longer than 10 km and time scale in many years, so the three-dimensional model is not appropriate to use. One-line model is applied. The one-line model, which came closest to satisfying these requirements generally includes a considerable level of empiricism and may be termed top-down or data-drive models (Prasad & Kumar, 2014). Beside the one-line model, wave simulation model also was used in order to provide the input data for one-line model.

2.3.1 SWAN Wave simulation model

One of the main factors affecting shoreline change is waves which cause both cross-shore and alongshore sediment transport. Waves are generated by many sources such as wind, earthquakes, the effects of Moon and Sun, movement of the Earth and surface tension (Sorensen, 2005). Those factors control the wave characteristics. Wind predominate in generating wave almost all the time (WMO, 1998).

Ocean wave characteristics are mainly determined through field measurement, numerical simulation, physical models and analytical solutions. Each method has its advantages and disadvantages. Numerical models emerged as one of the most powerful tools for the study of surface water waves (Janssen, 2008). Due to lack of observed wave data which was most reliable data in the study area, the wave data can be hindcasted by computer model which had been developed with acceptable reliable result (Thomas & Dwarakish, 2015).

SWAN is the third-generation numerical wave model which is used to compute random, short-crested wave in the coastal region with shallow water and inland water. SWAN can be applied in the area whose width is less than 20-30 km and water depth less than 20-30 m. The model is based on an Eulerian formulation of the discrete spectral balance of action density that accounts for refractive propagation over arbitrary bathymetry and current fields (Booij et al., 1999). SWAN can consider shallow water physics and provide large scale of time simulation. More theories of SWAN were mentioned in APPENDIX A.

There were many researchers used the SWAN model in their work. Polsomboon and Sriariyawat (2019) used the SWAN model to determine significant wave height with the study area in the Gulf of Thailand. The results from SWAN were well verified with observed data from GISTDA's buoys. Akpınar et al. (2012) assess the SWAN model in the Black Sea. The results which were wind-wave climate and wave energy was well verified with the measured data of the buoy.

Ris et al. (1999) verified the third-generation wave model SWAN in stationary mode with 29 observations from 17 buoys and 1 wave gauge in five cases in the Southern North Sea coast. The wavefields were highly variable. The result showed that the triad wave-wave interactions almost do not have an effect on the significant wave height and have a slight effect on the mean wave period (8%). The result of significant wave height and mean wave period was well verified. The difference between model and reality could be came from the physical processes, the bathymetry, the driving wind field, the wind-induced setup, the wave-induced setup, and the current field.

2.3.2 GENESIS One-line shoreline change model

Coastal managers, scientists and engineers have long sought a practical methodology for the prediction of shoreline change along sandy coastlines, over time-scales spanning several years to decades. Probably the best known and most widely used example was the GENESIS model (Hanson, 1989) which is applicable to predict generalized platform shoreline evolution for the special case where alongshore gradients in longshore sediment transport dominate (Davidson et al., 2013). Coastal Engineering Design and Analysis System (CEDAS) is the design and analysis system for coastal engineering. A Generalized Shoreline Change Numerical Model (GENESIS) is one of the programs in the system of CEDAS for simulating shoreline response. More details of theories of GENESIS was shown in APPENDIX B.

Hung and Larson (2014) used GENESIS to simulate coastline of Hai Hau province in Red River delta, Vietnam. In their study, the wave climate was assumed to remain unchanged during the simulation period from 1912 up to 1965 to find the best fit calibration coefficient K1, K2 which were used to simulate shoreline evolution from 2001 to 2005. The result showed that the computed results can reproduce well the real situation of shoreline retreat along the Hai Hau coastline. Finally, the cause of the erosion at Hai Hau beach was confirmed. That was because of NE monsoon with effect of 2 estuaries.

Sutikno et al. (2015) used satellite image data to extract coastline which was analyzed by using the digital Shoreline Analysis System (DSAS) in Tanjung Motong beach in Indonesia. Then authors used those data to calibrate K1 and K2 coefficients in the GENESIS model. The result showed the good correlation between simulated shoreline and historical shoreline. Therefore, satellite data is reasonable way to calibrate the GENESIS model.

Kakisina et al. (2016) used GENESIS to model the erosion mitigation at the Northern Coast of Ambon Bay in Indonesia with 3 scenarios, i.e., without protection, with groin series and with groin and seawall combination.

2.4 Researches related to study area

Shoreline change is a global issue that has attracted significant research attention worldwide. Numerous studies have been conducted in various regions to understand the dynamics of coastal areas. Binh Thuan, in Vietnam, with many locations as shown in Figure 2-3, has also seen several research projects dedicated to understanding and addressing coastal issues in the area such as beach erosion, sediment transport, and the impact of coastal structures. These studies had contributed to our understanding of the bay's unique characteristics and provided ideas for this study.

Van To (2006, 2008) conducted research utilizing the parabolic model based on the Hsu and Evan model (1989). The focus of these studies was to investigate the causes of beach erosion in Doi Duong and propose effective measures to combat the erosion. Additionally, Van To (2006, 2008) estimated the equilibrium stage of the bay-shape shoreline in Phan Thiet bay, both with and without the presence of an imaginary structure. The shoreline in Phan Thiet bay, Ham Tien and fishing port breakwater were dynamical equilibrium. The parabolic model and spectral numerical model were used to discuss the causes of beach erosion in terms of crossshore and longshore direction. In terms of crossshore direction, the beach was eroded by high waves and water level rises. In terms of longshore, the shoreline was simulated with coastal works and without coastal works. The shoreline in Binh Thuan province was not equilibrium and continued retreat landward. If there had been structures with the location tip recommended in Mui Ne, the beach from Mui Ne to Mui Ong Dia would have been stable.

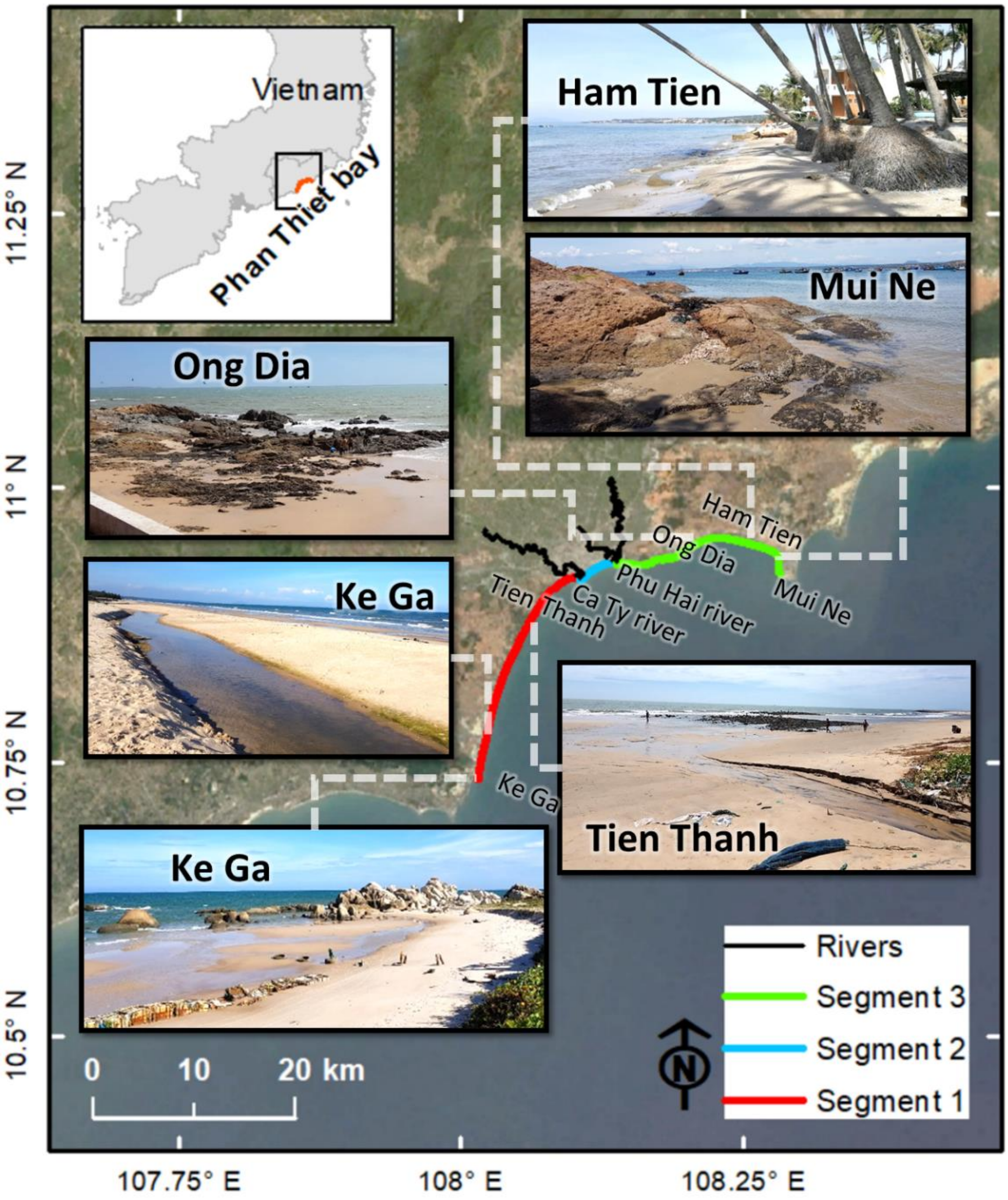

Figure 2-3 Morphology at some locations along study area

Trung and Mau (2011) assessed the status of erosion – deposition processes along the coast of Binh Thuan province. In this study, they used satellite images to determine shoreline in 2004 and December 2008. The result of this study showed that in Binh Thuan province, erosion occurred in the NE monsoon period, while accretion occurred in the SW monsoon period. The erosion rate is higher than the accretion rate. There were many hard structures protecting seriously eroded areas and caused erosion – deposition process in other areas.

Duc and Luan (2014) and Vuong et al. (2015) used Mike 21/3 coupled model to assess impacts of the nearshore hydrodynamic regime to accretion and erosion process of Phan Thiet coastline, analysis and research on sediment and erosion development at the La Gi - Dinh estuary, Binh Thuan province, and determined accretion and erosion causes which were waves in NE monsoon combined with the typhoon, sediment characteristics, and structures. Duc and Luan (2014) calibrate simulated data with measured data in 3 stations (S1 measures velocity and water level at the river mouth, S2 measures nearshore velocity, S3 measures wave nearshore from). The vigorous influence of wave height directly act on the coastline and nearshore current results in lack of sedimentation, causes erosion at Doi Duong beach (Duc & Luan, 2014). Vuong and Dat (2015) used the Wavewatch III model and wind data from NOAA with MIKE 21 coupled FM to simulate coastal erosion and accretion in Ca Ty river mouth which is near the study area of this study.

Linh (2018) assessed coastal vulnerability in Binh Thuan province and Vung Tau province after determining shoreline location in 10 years in the past (1990, 1995, 1998, 2001, 2003, 2005, 2009, 2011, 2015, 2017) by using Landsat satellite image and DSAS of GIS. The erosion and accretion rate that are NSM, EPR, and LRR were determined. The coastal vulnerability depends on coastline change rate, coastal elevation, coastal slope, geomorphology, mean sea level rise, mean significant wave height and mean tidal range.

There were research that proposed the effects of structures on shoreline. Trung and Mau (2011) mentioned that the erosion and deposition has happened because of ineffective coastal protect structures that were built in most of the eroded shoreline areas and cause erosion – deposition in other areas. According to Vuong and Dat (2015), the adjacent shoreline has been changed due to change of wave, current and sediment distribution after jetties in Ca Ty river mouth were built.

In conclusion, previous research on the shoreline in Phan Thiet bay has primarily focused on specific areas, mentioning the presence of structures to control shoreline dynamics. However, a comprehensive understanding of the shoreline across the entire bay has not been explored. Therefore, this study aims to investigate the shoreline dynamics throughout Phan Thiet bay and examine the effects of existing structures on shoreline change. By filling this research gap, the study will provide a more comprehensive analysis of the shoreline in the whole bay and contribute to a better understanding of the role and impact of coastal structures in shaping the shoreline in Phan Thiet bay.

CHAPTER 3

STUDY AREA AND METHODOLOGY

Firstly, this chapter provides an overview of the study area. Secondly, this chapter provides the framework dividing the study into three parts including (1) shoreline change investigation, (2) wave simulation, and (3) simulating shoreline change and investigating effects of coastal structures on shoreline change. These 3 parts were designed to achieve 2 objectives of this study. Thirdly, the chapter presents the methodologies guiding each part of this study.

3.1 Study area

This section aims to provide an understanding of key characteristics of the study area relevant to the shoreline change process, including meteorological and hydrological conditions, morphology, and existing structures..

3.1.1 Meteorology and hydrology

Wind is one of the main factors causing waves which affect the shoreline. The observed wind data was available only in Phan Thiet station from 2000 to 2019 as shown in Figure 3-1. The observed wind data showed that there were 2 main wind directions that are from the East (E) and from the West (W) as shown in Figure 3-2. According to Van To (2006), there were two monsoon seasons which are dominated by Northeast (NE) and Southwest (SW) monsoon seasons. The mild windspeeds from West Southwest (WSW) were predominant from May to October. The gusty wind speeds from East Northeast (ENE) were mainly from November to April.

The wave characteristics in Phan Thiet bay were primarily influenced by wind patterns. Waves originating from the East direction were dominant in this area. During the SW monsoon season, the waves were generally not strong, except during the occurrence of typhoons. The maximum nearshore wave height in Phan Thiet reached 0.47 m in June and 1.45 m in November (Vuong, 2009). At the Bach Ho station located 60 km from the shoreline as shown in Figure 3-2 from 1987 to 2008, the highest monthly average wave height was recorded as 3 m in December, while the lowest monthly average wave height was 0.9 m in May as shown in Figure 3-3.

Additionally, the highest monthly average wave period was 6.5 seconds, whereas the lowest monthly average period was 4.8 seconds. The parameter Htb is the average monthly wave height. Ttb is average monthly wave period. Hmax is highest wave height. Tmax is highest wave period.

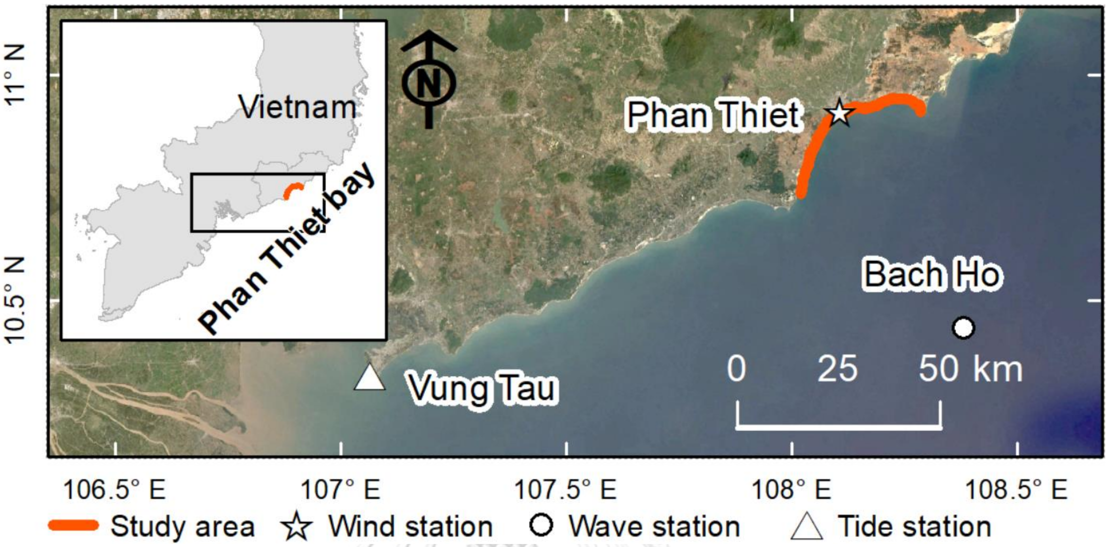

Figure 3-1 Locations of observed wind data (Phan Thiet station), observed wave data (Bach Ho station), observed sea level (Vung Tau gauge)

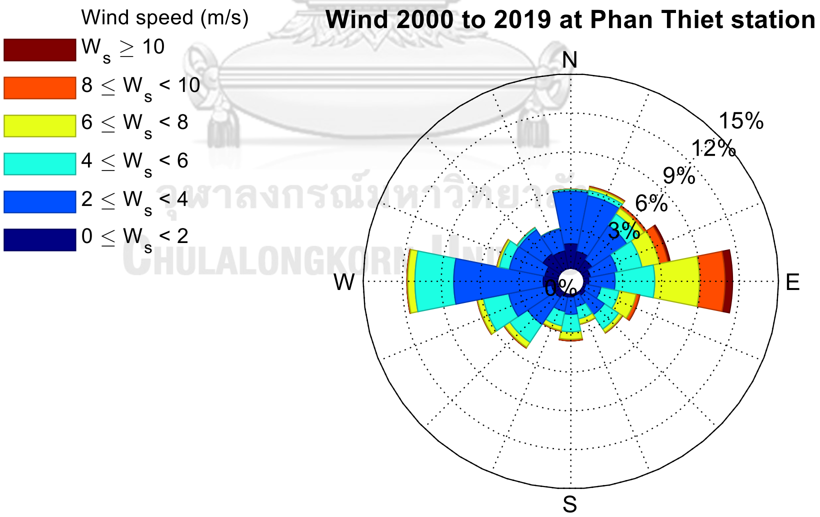

Figure 3-2 Windrose from 2000 to 2019 in Phan Thiet station

Climate change phenomena such as sea level rise may affect shoreline position. The average global sea level rise rate was 3.2 mm/year in the period 1993 to 2010 (Church et al., 2013). In Vietnam, the average sea level rise was 2.7 mm/year in 57 years between 1961 and 2018 based on 15 gauges along the coast. The gauge near

Binh Thuan province was Vung Tau gauge level, as shown in Figure 3-1, measuring the height of the sea. The sea level rise was estimated about 2.9 mm/year from 1978 to 2018 (MONRE, 2020). This indicates that the sea level rise in the Vung Tau area exceeded the national average in Vietnam, yet remained below the global average.

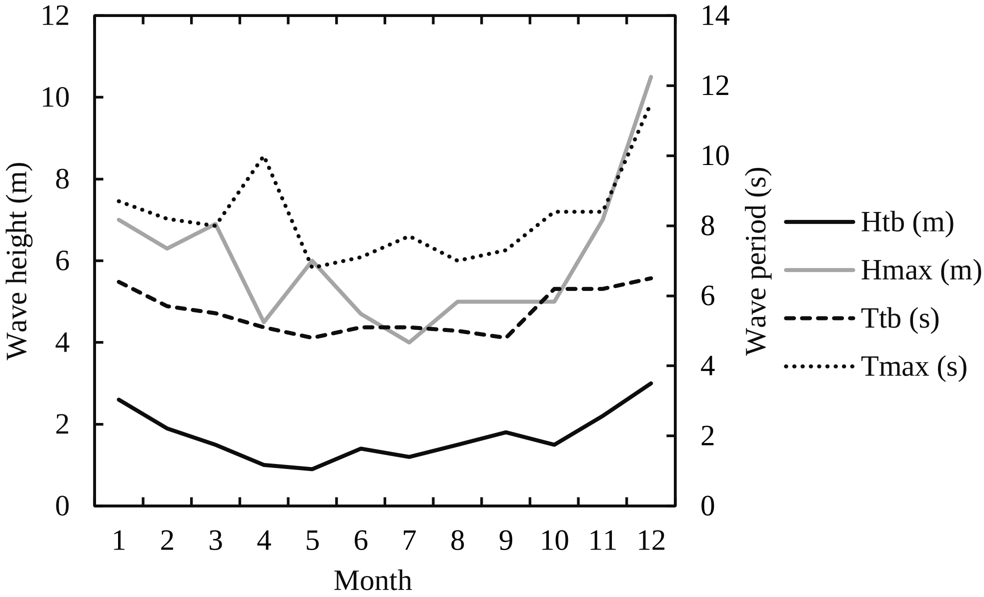

Figure 3-3 Wave data in Bach Ho station (Vuong, 2009)

From the data of Center of Meteology and hydrography Vietnam (2021), it showed that there were 8 typhoons that hit Phan Thiet from 1988 to 2020 as shown detail in Table 3-1 with the tracking route in Figure 3-4. From 24th to 26th November 2018, typhoon Usagi (typhoon number 9 in Vietnam) caused strong wind, high waves, and sea level increase which attacked the shoreline and caused 2000 m beach erosion in Ham Tien (Center of Meteology and hydrography Vietnam, 2021).

Table 3-1 List of typhoons (T), storms (S), and depression (D) in Binh Thuan Vietnam (Center of Meteology and hydrography Vietnam, 2021)

No.	**Name**	**Time**	**No.**	**Name**	**Time**
1	Manny (S)	Dec 1993	**5**	Pakhar (S)	Mar 2012
2	Teresa (S)	Oct 1994	**6**	Kirogi (D)	Nov 2017
3	Chip (T)	Nov 1998	**7**	Tembin (T)	Dec 2017
4	Durian (T)	Nov 2006	**8**	Usagi (S)	Nov 2018

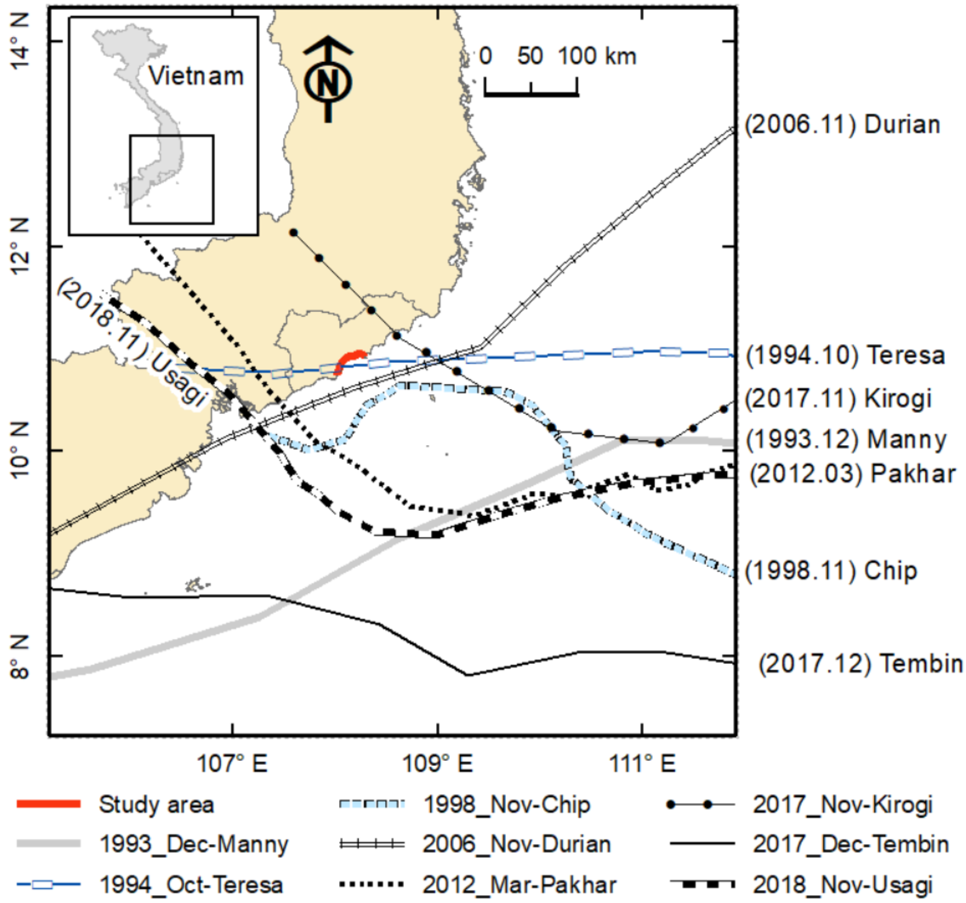

Figure 3-4 Tracking routes of typhoon come to 100 km near the study area (adapted from Center of Meteology and hydrography Vietnam)

3.1.2 Morphology and Structures in the study area

As mentioned, the shoreline of Phan Thiet bay is from Ke Ga to Mui Ne, separated into 3 segments by 2 river mouths as shown in Figure 2-3. Through satellite image analysis and field surveys, it was identified that Phan Thiet bay includes several key structures as shown in Figure 3-5. There was 1 beach reclamation project, 4 jetties situated at 2 river mouths, 8 seawalls, and 28 groins. Those structures were built from 1996 to 2021.

Binh Thuan province is characterized by steep and relatively short rivers. These rivers played a crucial role in transporting sediment, which was subsequently deposited at their respective river mouths. However, excessive sand pumping and filtration activities for construction purposes within these rivers were observed. This overexploitation had resulted in several consequences, including an imbalance in the coastal sediment budget (Van To, 2006).

The shoreline length of Segment 1, extending from Ke Ga to Ca Ty River, spans approximately 23 km in a NE-SW direction. Notably, Ke Ga headland was characterized by rocky terrain as shown in Figure 2-3. Furthermore, the survey of segment 1 recorded several small rivers and sand dunes along the beach which might affect the shoreline digitization process. Moreover, they also have the potential to influence shoreline change as they can disrupt the natural longshore transport of sediment and the supply of sediment to the beach. The interaction between these rivers and the coastal processes may result in alterations to the shoreline dynamics in the area.

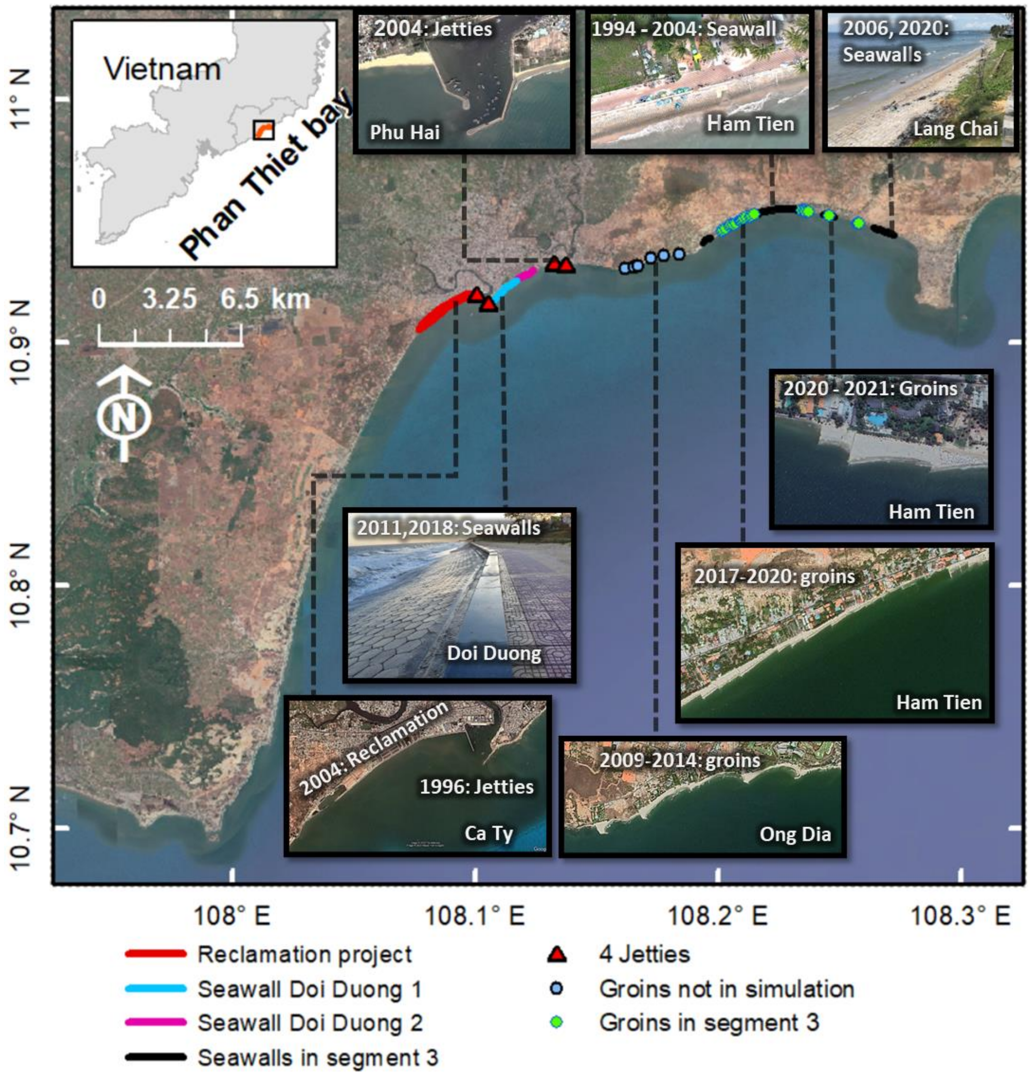

Figure 3-5 Structures and their years of construction

In order to understand the real situation of the study area, the survey was conducted in 2019 and 2020. One notable project observed during the survey was a beach reclamation project named Hamubay in segment 1 as shown in Figure 3-5. It was the structures with seawall along the edge composed by tetrapods, and the landfills inside as shown in Figure 3-6 (a and b). Right next to beach reclamation project Hamubay was Jetty Ca Ty 1, which was well constructed as shown in Figure 3-6 (c and d). Jetty Ca Ty 1 was one of 4 jetties at Ca Ty river mouth, and Phu Hai river mouth.

Figure 3-6 Beach Reclamation Project Hamubay
(a) Landfill of beach reclamation project, (b) Seawall of beach reclamation project
Jetties at c) Ca Ty river mouth, and d) Phu Hai river mouth

Segment 2 spans approximately 3.5 km of shoreline, extending from the mouth of Ca Ty River to the mouth of Phu Hai River. Within this segment, the most severely eroded area was the 1.5 km shoreline of Doi Duong, located to the west of Ca Ty River mouth. In 2007, a geotube structure was constructed in Doi Duong to combat erosion, but it eventually collapsed due to a combination of human and natural factors (Trung & Mau, 2011). As a subsequent measure, a concrete seawall was constructed in Doi Duong in 2011, and it has been effectively protecting the shoreline (Quoc, 2019) as shown Figure 3-7. Seawall Doi Duong 1 and Seawall Doi Duong 2 stand side by side, even though they were constructed in different years.

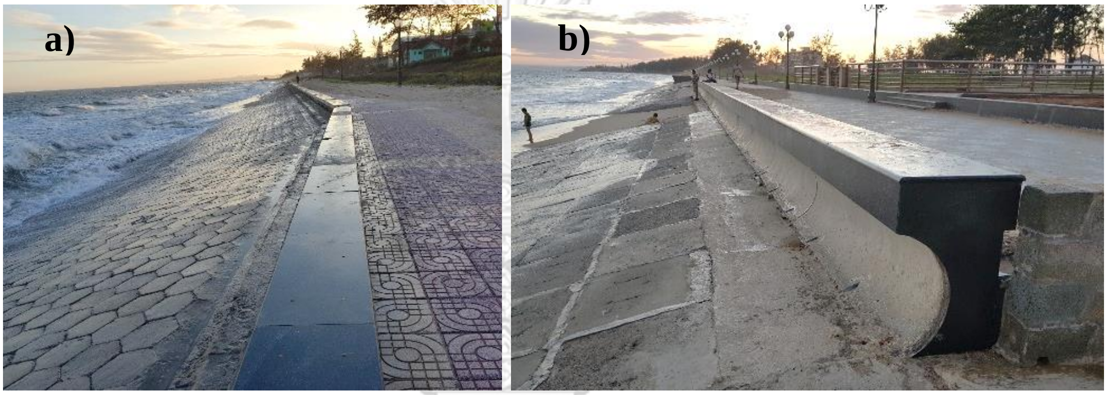

Figure 3-7 Seawalls at Doi Duong
a) Seawall Doi Duong 1, and b) Seawall Doi Duong 2

Segment 3 covers a shoreline length of 20 km, running from the mouth of Phu Hai River to Mui Ne in an E-W direction. This stretch of coastline was home to various seaside resorts, restaurants, and service establishments. However, the area experienced erosion at an average rate of 3 to 5 m per year. To protect the shoreline on the western side, several groin structures had been built (Trung & Mau, 2011). Most of them were the structures of huge sandbag as shown in Figure 3-8. Along with those sandbags were several seawalls and the buildings along the coast with the exhibition as similar to the seawall. Additionally, during the survey conducted in 2019 and 2020, evidence of erosion was observed in other areas of segment 3. Moreover, field observations revealed that at Ong Dia and Mui Ne in segment 3, the shoreline predominantly consisted of rocky beaches as shown in Figure 2-3.

Figure 3-8 structures in segment 3
a) groins, and b) seawalls and buildings along the coast

3.2 Framework of this study

The framework of methodology to achieve 2 objectives of this study was shown in Figure 3-9. To initiate the process, data was gathered from multiple sources, including field surveys, local authorities, and global data sources. Subsequently, the study was divided into three parts, each serving a distinct purpose.

The first part of this study investigated the shoreline change by calculating the shoreline change rate, and erosion and accretion area from 1988 to 2021. The Landsat satellite images were utilized to be the input in ArcMap, a component of Esri's ArcGIS, for digitizing the historical shorelines. In ArcMap, the Normalized Difference Water Index (NDWI) of each cell was calculated based on the color bands of Landsat images for defining land and sea. The shorelines were digitized as the contour line between them. The shoreline positions from Landsat images were used for determining EPR which is the net cross-shore movements divided by the interval time in Digital Shoreline Analysis System (DSAS), an ArcGIS extension for calculating shoreline change developed by the USGS (Thieler et al., 2009). Beside calculating the shoreline change rate, the areas of land loss and land gain were calculated in ArcMap. The better understanding of how shoreline changed correspondingly to the presence of structures in Phan Thiet bay as the first objective of this study was gained after these steps in part 1.

In the second part, SWAN version 41.31 was used for simulating waves which is one of the main inputs of GENESIS shoreline change model in this study. This wave simulation model was necessary due to the spatial and temporal limitations of both observed wave data and global wave data. The first step was setting up the SWAN model by specifying the model simulating grid, inputting bathymetry and wind, and the boundary condition of wave. In SWAN, whitecapping, bottom fiction, wave breaking were the processes counted through the parameters WCAP, FRIC, and BREAK correspondingly. The following steps were sensitivity analysis, calibration, and validation of the model to get an appropriate set of those parameters. The output was wave characteristics including depth representing water level, wave height, wave period, and wave direction by location from 1988 to 2021, as same as the time of shoreline change simulation.

The third part used GENESIS model of Coastal Engineering Design and Analysis System (CEDAS) which is the design and analysis system for coastal engineering. A Generalized Shoreline Change Numerical Model (GENESIS) is one of the programs in the system of CEDAS for simulating shoreline response. In GENESIS model, the shorelines were simulated from the initial shoreline and other input such as wave data, bathymetry data, sediment size, and structures. The initial shoreline is from part 1 shoreline change assessment of this study. While wave data is from part 2 wave simulation of this study. In GENESIS, after setting up the model is the sensitivity analysis, calibration, and validation for determining the parameters including K1, D_c, D_{50}, D_b, K2. The outputs of this process are the positions of shorelines with the difference between initial shoreline and final shoreline, and longshore sediment transport rate. Through a comparison of shoreline change in simulation results with and without these structures, insights were gained into the effects of such structures on shoreline dynamics as the second objective of this study.

The result of part 1 (Shoreline change investigation) to achieve objective 1 of this study (to investigate the behaviors of shoreline changes) is shown in CHAPTER 4. The result of part 2 (Wave simulation) and part 3 (Simulating shoreline change and investigating effects of coastal structures on shoreline change) to achieve objective 2 of this study (To investigate the effects of coastal structures to the shoreline) is shown in CHAPTER 5.

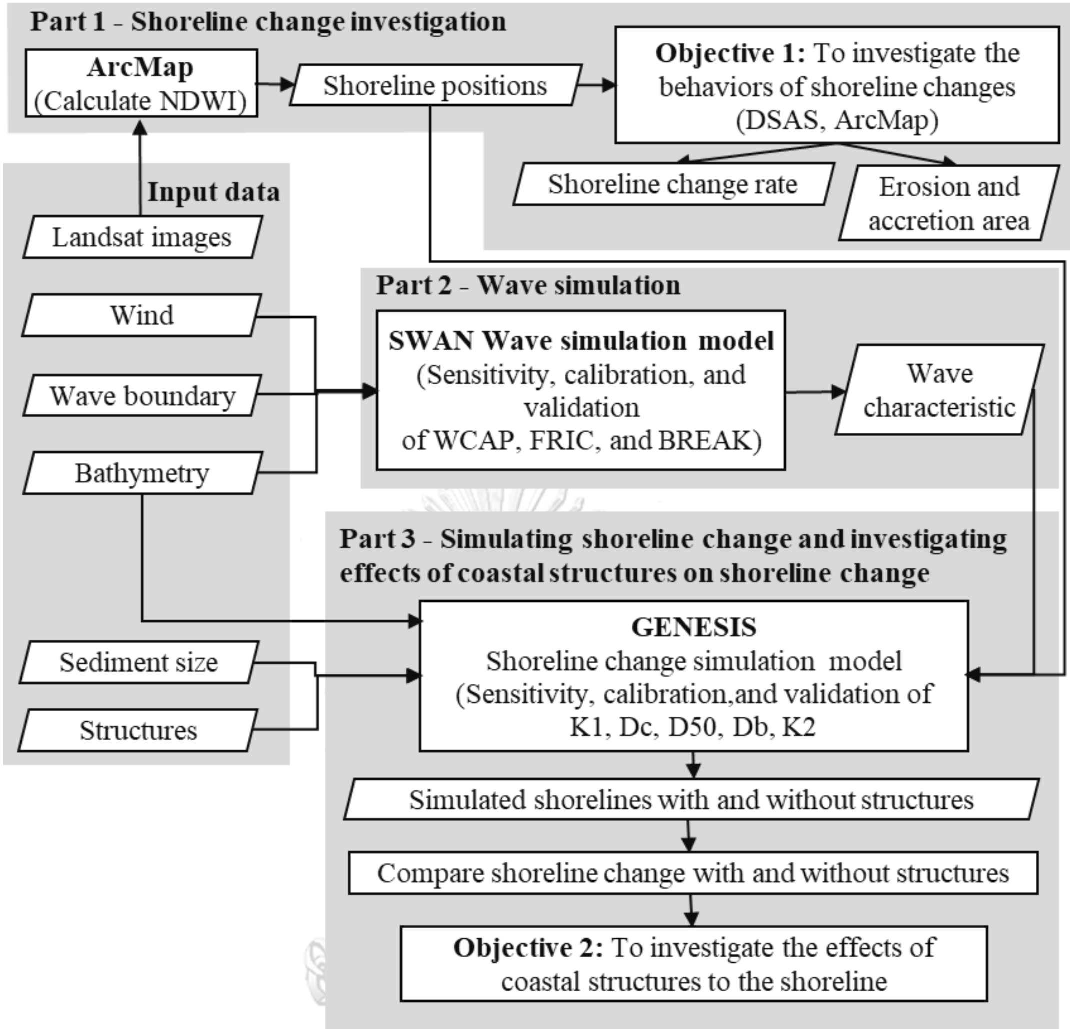

Figure 3-9 Framework of this study

3.3 Methodology of Shoreline change investigation

This section explained the methodology of shoreline change investigation, which is part 1 of this study. This part was to achieve the first objective of investigating the behaviors of shoreline changes in Phan Thiet bay, Vietnam.

3.3.1 Landsat image collection

Assessing the shoreline positions is the fundamental job of coastal scientists, coastal engineers, and coastal managers (Boak & Turner, 2005). In this study of Phan Thiet bay, the available sources were Landsat satellite image, Sentinel-2 satellite images, and Google Earth satellite images. The Landsat satellite image is remote sensing images which is free, available in many areas, and possibly used for investigating the long term shoreline change (Mullick et al., 2019).

The shoreline positions are determined in ArcMap from the color of the satellite images. Landsat satellite images have a drawback of low resolution of 30 m, but they were available over a long period of time, especially before the construction of structures around 1994 in Phan Thiet bay. This makes them useful for understanding the shoreline change before and after the presence of structures.

Although higher-resolution imagery like Google Earth Images (5-meter resolution) and Sentinel-2 satellite images (10-meter resolution) would improve accuracy, they were not available before the construction of coastal structures in Phan Thiet bay (Maxar, 2023; The European Space Agency, 2015). Therefore, for investigating the relationship between shoreline change and structures in Phan Thiet bay, Landsat satellite images are the most suitable option. Despite the lower resolution, their long-term coverage helps analyze the historical shoreline dynamics in relation to the structures.

Landsat satellite images, distributed from United States Geological Survey (USGS), are available from 1972 to the present with the images from 7 Landsat satellites. In this study, the shorelines are assessed from 1988, the first year Landsat image of Phan Thiet bay was recorded, to 2021. This time was divided into four periods of time that are 1988 to 1995, 1995 to 2004, 2004 to 2016, and 2016 to 2021 corresponding to the time of coastal structures construction as shown in Table 3-2 and Table 3-3.

Table 3-2 Four periods in this study and the related structures

Years	Details
1988 - 1995	1988 was the first year of available Landsat images in this area.
1995 - 2004	Around 1996, jetty Ca Ty 1 and jetty Ca Ty 2 were built. The Landsat images in 1996 is not qualified in whole study area.
2004 - 2016	Before 2004, jetty Phu Hai 1 and jetty Phu Hai 2 were built. From 2004 to 2016, the beach reclamation 1, 1 seawall in segment 2, and 4 seawalls in segment 3 were built.
2016 to 2021	There were 31 coastal structures built. Most of them were the groins in segment 3, except the 1 seawall in segment 2 and 1 seawall in segment 3.

The shoreline along the coast changes naturally by the season with different wind, wave and current characteristics. In long-term shoreline change assessment, the season change of shoreline was ignored by digitizing the shoreline in the same season of the year, and the map after the storm was not recommended in order to maximize the accuracy of the result (Crowell et al., 1991).

Depending on the year, the Landsat images could be from Landsat 5 or Landsat 8. In both of them, the Green band and Near-Infrared band have the 30 m resolution (United States Geological Survey, 2023a, 2023b). The details of the Landsat images used for assessing the shoreline change was shown in Table 3-3. Beside choosing the time based on the structures, these Landsat images were chosen because the shorelines of whole study area were able to be digitized. In some other Landsat images at other times, the quality might be degraded by the cloud. Beside these above reasons, the Landsat images of 1990 and 2017 were used for the comparison to another research, which will be discussed in CHAPTER 4.

Table 3-3 Landsat images to do shoreline digitization for historical shoreline change assessment

Date (dd/mm/yyyy)	Time (UTC+7:00)	Type of Landsat
07/01/1988	09:36	Landsat 5
17/03/1990	09:28	Landsat 5
10/01/1995	09:20	Landsat 5
03/01/2004	09:46	Landsat 5
08/03/2016	10:07	Landsat 8
06/01/2017	10:07	Landsat 8
06/03/2021	10:07	Landsat 8

3.3.2 Shoreline digitization

The shoreline could be manually or automatically extracted. Tracing the shoreline manually is feasible in area that shoreline does not stretch complicatedly. Tracing the shoreline automatically is based on the density slice to analyze multiple bands corresponding multi-spectral images (Bagli et al., 2004). Therefore, automatic method is more consistent across entire bay over times, reducing human error, which is suitable for tracking changes of shoreline by time. That multi-band method also could decrease the error of shadow noise of the images due to the reflective differences of each involved bands (Xu, 2006). In this study, the shorelines were automatically extracted by using ArcMap, the analyzing geospatial processing program from ESRI’s ArcGIS. However, it's important to note that while automated methods offer consistency and objectivity, they may not capture all nuances or subtleties in shoreline changes, especially in areas with complex features or where the shoreline dynamics are influenced by a combination of natural and anthropogenic factors. The shoreline that automatically digitized on Landsat image was then compared to the shoreline manually digitized on Google Earth image as discussed in CHAPTER 4.

Pham and Prakash (2018) compared Normalized Difference Vegetation Index (NDVI) and Normalized Difference Water Index (NDWI) which are spectral band ratios used for automatic shoreline extracting using the multi-band method. NDWI band ratio was more effective in determining water bodies and extracting shoreline. The NDWI was the popular index of remotely sensed imagery (Li et al., 2013). In Phan Thiet bay, the beach is not covered by vegetation. Therefore, NDWI is more suitable for defining the shoreline.

In NDWI map, the water features are enhanced and have positive values, while the other features have value of equal or less than 0. The NDWI maximizes reflectance of water in Green band, and minimizes the low reflectance of near-infrared lights (Xu, 2006). NDWI value is determined by the equation (2-1) (McFeeters, 1996). Where the *Green* is the reflectance of green spectral band. *NIR* is the reflectance of near-infrared (NIR) spectral band of the Landsat images. Resolution of Green band and NIR band maps are 30 m. The shoreline digitized from the Landsat image was then compared to the shoreline manually digitized on Google Earth image as shown in CHAPTER 4.

$$NDWI = \frac{Green - NIR}{Green + NIR} \tag{2-1}$$

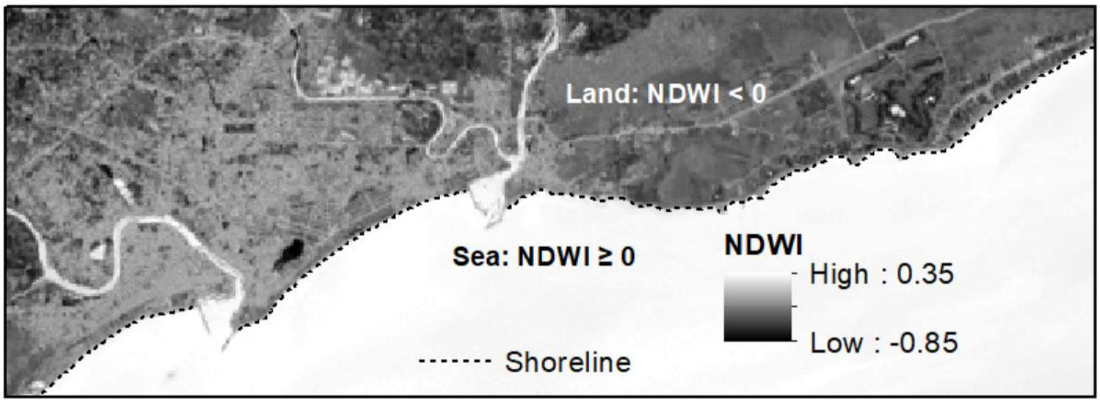

Figure 3-10 NDWI value to classify land and sea

3.3.1 Determining shoreline change rate, and erosion and accretion area

As the shoreline was digitized in the coordinate UTM zone 49N with the unit of meter, the shoreline change rate could be subsequently calculated in the Digital Shoreline Analysis System (DSAS) version 5.0, which is the software extension for ArcGIS and developed by USGS DSAS development team. To begin the analysis of shoreline changes over a specific period, the DSAS required the initial shoreline and final shoreline data to be imported into the program. After that, the baseline which should be parallel to both the initial and final shoreline was generated. Based on that baseline, DSAS can create a set of transects that are perpendicular to the baseline and cross the shorelines as shown Figure 3-11. Therefore, the baseline should be smooth as much as possible to keep the constant distance between transects. In this study, the distance between 2 transect lines was about 50 m. The shoreline change rate was calculated by the distances of initial shoreline and final shoreline (Crowell et al., 1991). Subsequently, End Point Rate (EPR) (m/year) was calculated as the movement of shoreline by time in 4 time periods as shown in Table 3-2.

The area of erosion and accretion were the area of the polygon bound by the initial shoreline and final shoreline as shown in Figure 3-11. Arcmap was used to generate those polygons whose area were calculated subsequently. In this study, the annual average erosion and accretion areas of every period were determined in the whole Phan Thiet bay and each segment. This annual rate was used for comparing how much the coastal areas change in different periods from 1988 to 2021. The amounts of erosion accretion areas were used for analyzing the balance of land loss and land gain in each area by time.

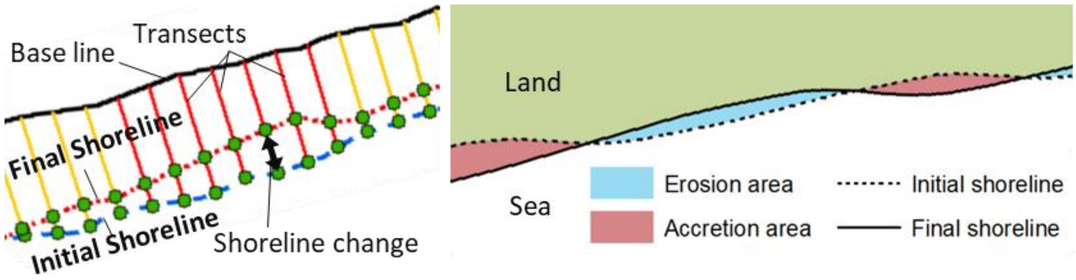

Figure 3-11. a) Determining shoreline change rate
b) Determining erosion and accretion area

The first part provided a better understanding of shoreline change rates, erosion, and accretion areas from 1988 to 2021 in correlation with the presence of structures in Phan Thiet Bay, addressing the first objective of this study.

3.4 Wave simulation methodology

This section explains the methodology of wave simulation, which is part 2 of this study. The objective of this part is to generate wave data with higher spatial and temporal resolution due to the limitation of observational wave data and global wave data. There was only one offshore station providing data for specific days in 2017. Additionally, three nearer stations had data for only three days each in 2012 and 2014. The resolution of global wave data is 0.5 degree. Subsequently, simulated wave results from part 2 were utilized in part 3 of the study to simulate shoreline changes.

There were several numerical models for simulating wave data such as WAM (Wave model), WAVEWATCH model, or PHIDIAS (Program for Hindcasting of Waves in Deep, Intermediate and shallow water). In those models, the deep ocean waves can be well simulated. However, in shallow water, those models could not practically simulate the waves due to lack of the simulation of depth-induced wave breaking. However, Simulating Waves Nearshore (SWAN) model contained some additional formulations for shallow water with the result that SWAN is able to simulate the nearshore wave by integrating of (1) a reformation of the whitecapping in term of wave number rather than frequency; (2) adding bottom dissipation; and (3) depth-induced wave breaking (Delft University of Technology, 2007).

Bathymetry data was the gridded bathymetry data of the General Bathymetric Chart of the Oceans (GEBCO), whose website for downloading data was https://download.gebco.net/ (GEBCO Compilation Group, 2020). The grid resolution is 15 arc-second which is about 0.004167 arc-degree or 0.4624 km. The elevation value represented the elevation at the center of each grid cell.

For using wave simulation model, observational wind data is important and preferable compared to other sources of wind data. In Phan Thiet bay, observational wind data was collected at the Phan Thiet meteorological station, as shown in Figure 3-12, from 2015 to 2018 only. Although this data should be the most accurate data for SWAN model, it has limitations in terms of spatial coverage, as it does not encompass the entire computational grid. Nevertheless, it serves as a representative sample for the area. However, there is an additional challenge regarding the limited duration of the observational data which could not cover from 1988 to 2021. To overcome these space and time limitations, alternative sources of data were employed, specifically global wind data, to supplement the analysis and provide a broader perspective.

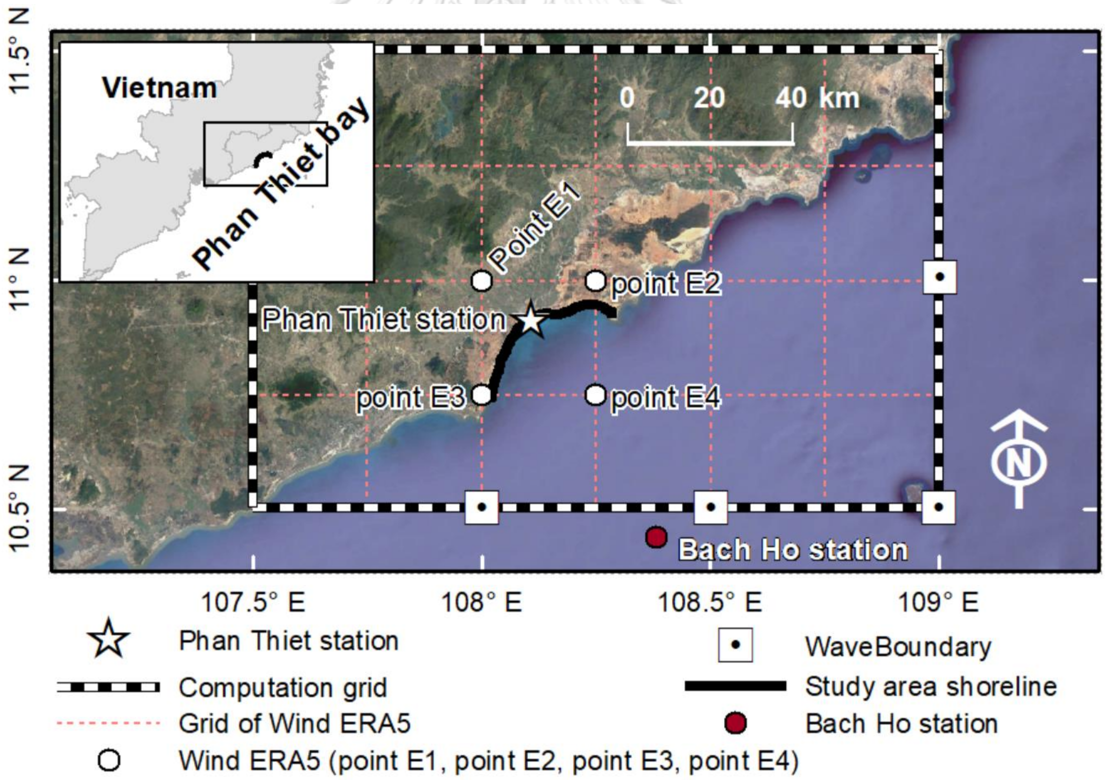

Figure 3-12 The boundary of computation grid, Wind data grid, Phan Thiet station of observed wind data, and locations of Wave boundary

The global wind data fifth generation ERA5 from European Centre for Medium-Range Weather Forecasts (ECMWF) is adequate for use in SWAN since wave data is available from 1940 onward with an interval time is 1 hour and a resolution is 0.25 arc-degree (approximately 27.75 km) (ECMWF, 2020). Compared to other sources of wind data, for example, Climate Forecast System Reanalysis (CFSR) is available only to 2017 (NCAR, 2023); or National Centers for Environmental Information (NCEI) of National Oceanic and Atmospheric Administration (NOAA) has only 1 location of wind data in Phan Thiet bay (NOAA, 2023a). The fifth generation ERA5 of ECMWF provides hourly wind data at the standard elevation of 10 m above the mean sea surface (ECMWF, 2020), which is the data that SWAN wave simulation model requires. ERA5 wind data from 1988 to 2021 with an interval time of every hour was used for simulating the wave in this study. The analyze of ERA5 wind input data and observed wind data at Phan Thiet station was shown in APPENDIX C.

Wavewatch III from the National Centers for Environment Prediction (NOAA/NCEP) is considered to meet the requirements in quality and quantity as the wave boundary. The resolution is 0.5 arc-degree and the interval time is 3 hours, available more than from 1988 to 2021 (NOAA, 2023b) which is the simulation time that SWAN does. Meanwhile, although ERA-20C Ocean Wave has better resolution of 0.25 arc-degree, it is available until only 2010 (ECMWF, 2021). In the case of DHI MetOcean Data Portal, the data is not available in the study area (DHI, 2023). Moreover, Wavewatch III data were compared to the observed wave data at Bach Ho station as location shown in Figure 3-12. The comparison showed that Wavewatch III was compatible to the observed wave data as discussed in APPENDIX D. Wave Therefore, Wavewatch III data were used for simulating waves in this study.

Once the model setup was completed as shown in APPENDIX E, comprehensive processes of sensitivity analysis, calibration, and validation were undertaken. These processes focused on three key parameters: whitecapping parameter (WCAP), bottom friction parameter (FRIC), and depth-induced wave breaking parameter (BREAK). Calibration and validation involved a comparison between the simulated significant wave height (Hs) and wave direction to the observational Hs and wave direction data collected by Vuong (2012) and Vuong (2014) from Agriculture and Rural Development of Binh Thuan province. The details and locations of the observational wave data were presented in Table 3-4 and Figure 3-13.

Table 3-4 Observational wave data for calibration and validation of SWAN

Points	Year	Starting time	Ending time	Time step
PH01	2012	26/11/2012	29/11/2012	30 mins
PH02	2012	26/11/2012	29/11/2012	30 mins
PH02TN	2014	22/08/2014	25/08/2014	
PH01TN	2014	22/08/2014	25/08/2014	30 mins

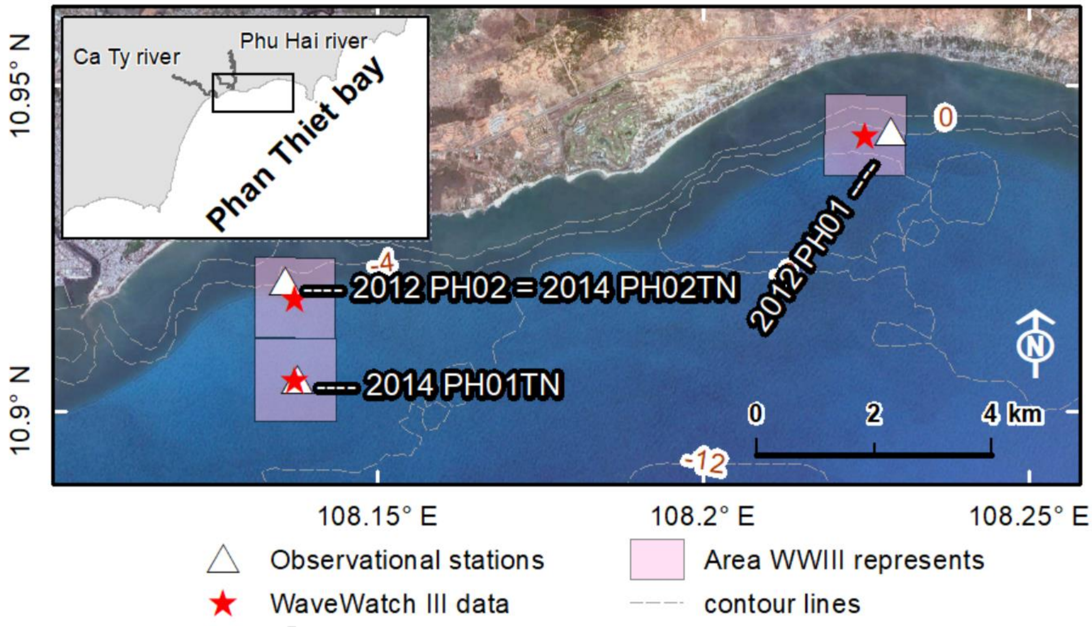

Figure 3-13 Observational wave data for calibration and validation of SWAN

Following a thorough evaluation of the SWAN model's accuracy and reliability in hindcasting wave conditions, the simulation of wave patterns in Phan Thiet bay from 1988 to 2021 was initiated. This extensive simulation aimed to capture the wave characteristics for being the input of GENESIS shoreline change model following.

The data used in this study, including bathymetry from GEBCO, wind data from ERA5, and wave data from Wavewatch III, were chosen for their suitability; however, they introduced potential sources of uncertainty in the SWAN model's results. This uncertainty arose because these global datasets lack validation against local observational data in certain locations. Additionally, SWAN, as a modeling tool, had inherent limitations. Notably, it did not account for tidal effects, which can generate waves. Moreover, SWAN did not incorporate swell waves into its simulations. To ensure the reliability of SWAN's results for subsequent use in the GENESIS shoreline simulation model, it became necessary to assess how well the results obtained from the GENESIS model, which used SWAN-generated wave data, aligned with the results obtained directly from observational wave data.

3.5 Methodology of simulating shoreline change and investigating effects of coastal structures

In this part 3, the shoreline of segment 1, segment 2, and segment 3 were simulated to get the result the shoreline change in these areas from 1988 to 2021, 34 years. The locations were shown in Figure 3-14. The shoreline change results simulated with and without structures were subsequently compared in order to investigate the effects of those structures on shoreline.

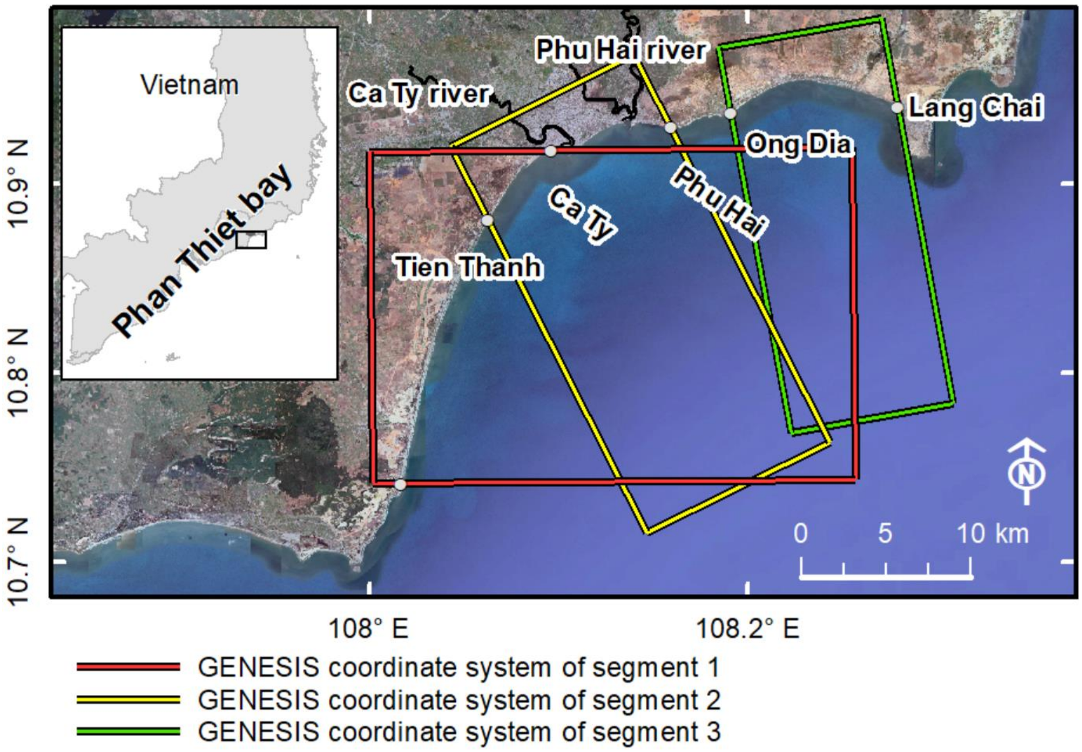

Figure 3-14 Locations of segment 1, segment 2, and segment 3 in GENESIS model

Segment 1 was from Ke Ga to Ca Ty, about 23 km. Segment 2 was from Tien Thanh to Phu Hai, about 12 km. Segment 3 was from Ong Dia to Lang Chai, about 10 km. GENESIS model was used in this study due to its applicability to the long-term shoreline change in the long-stretch shoreline of more than 10 km as mentioned in 2.3.

Bathymetry data was the GEBCO data as same as the data downloaded for SWAN model. The grid resolution was still 15 arc-second. The shoreline was extracted with the same method as in part 1 of this study. In segment 1 and segment 2, the wave data of point 1 was used, while in segment 3, the wave data of point 1, additionally point 2, and point 3 was used for simulation. Because there was a considerable headland in the East of segment 3. More details of those 3 points of wave data were discussed in section 5.1.

Another main input in GENESIS was the structure information, which was obtained by observing Landsat satellite images, Google Earth images, during the site visit, and contacting Department of Agriculture and Rural Development of Binh Thuan province. In this study, there was 1 beach reclamation project, 4 jetties at 2 river mouths, 8 seawall, and 22 groins. Table 3-5 gave the information of the structures such as No. for identifying the structure, the year of construction, the type, the name of the structure, and the segment that structure belong to. The location maps of structures were shown in APPENDIX F. Those structures started being constructed from 1996 until now. The numbering system to define the No. of structures is for easily recording all structures. The No. increases with time and by location from the West to the East.

In segment 1, there was only structure number (3) the beach reclamation project named Hamubay, built from 2004 until later than 2021. Hamubay was the extended coastal land for commercial shopshouse, hill villas, and other services. In segment 2, 7 structures were assigned in the model. While there were particularly various structures in segment 3, in total 28 structures.

Table 3-5 List of all structures that were assigned in GENESIS

No.	Year of construction	Structure type	Name	Segment	Dimension (m)
1	before 1996.07.07	Jetty	Ca Ty 2	2	380
2	after 1996.07.07	Jetty	Ca Ty 1	2	500
3	after 2004.01.03 until now	Reclamation	Hamubay	1 and 2	1250
4	before 2004	Jetty	Phu Hai 1	2	440
5	before 2004	Jetty	Phu Hai 2	2	403
6	1994 to 2004	Seawall	Mot Nang	3	2951
7	2006	Seawall	Anam	3	406
8	2006	Seawall	Aloha	3	85
9	2006	Seawall	Centara	3	1007
10	2011	Seawall	Doi Duong 1	2	1630
11	August 2017	Seawall	Sunrise	3	359
12	Jan 2018	Groin	Sunrise 2	3	44
13	2018	Seawall	Doi Duong 2	2	870
14	Sep 2018	Groin	Tien Dat 1	3	54
15	Sep 2018	Groin	Tien Dat 2	3	48
16	Nov 2018	Groin	Blue Ocean 1	3	51
17	Nov 2018	Groin	Lam Vien	3	64
18	Nov 2018	Groin	Aria 1	3	53
19	Nov 2018	Groin	Hong Di	3	41
20	Nov 2018	Groin	Sunrise 1	3	37
21	Jan 2019	Groin	Novela 1	3	65
22	Jan 2019	Groin	Novela 3	3	41
23	Apr 2019	Groin	Sunsea	3	44
24	Apr 2019	Groin	Lang Nghi Mat	3	34
25	Apr 2019	Groin	Sunny	3	37
26	Apr 2019	Groin	Sunshine 1	3	27
27	Apr 2020	Groin	Joe's	3	28
28	Apr 2020	Groin	Blue Ocean 3	3	43
29	Apr 2020	Groin	Hoang Ngoc 1	3	96
30	Apr 2020	Groin	Hoang Ngoc 2	3	86
31	Apr 2020	Groin	Thai Hoa	3	39
32	Apr 2020	Groin	Canary	3	31
33	Apr 2020	Seawall	Glamour	3	499
34	Apr 2020	Groin	Ravenala	3	31
35	Apr 2020	Groin	Meraki	3	58

Another input in GENESIS was the sediment size D_{50}. The sediment size was determined based on the beach profile, and the sediment collected at the study area. In order to determine the value of sediment size from the beach profile, that beach profile needed to be compared to the graph between distance offshore and elevation by the equations (*3-1*) of Bruun (1954) and Dean (1977). The beach profiles were from beach profile survey conducted by Vuong (2012) and Vuong (2014), and GEBCO bathymetry data.

$$D = Ay^{2/3} \qquad (3\text{-}1)$$

Where

A is the empirical scale parameter whose value depends on the median sediment size (D_{50}) as shown below.

$$\begin{aligned}
A &= 0.41(D_{50})^{0.94} && , D_{50} < 0.4 \\
A &= 0.23(D_{50})^{0.32} && , 0.4 \leq D_{50} < 10.0 \\
A &= 0.23(D_{50})^{0.28} && , 10.0 \leq D_{50} < 40.0 \\
A &= 0.46(D_{50})^{0.11} && , 40.0 \leq D_{50}
\end{aligned} \qquad (3\text{-}2)$$

Another way of estimating the sediment size in this study was done by the laboratory work for the sediment samples collected from study area. Since the sediment size was estimated to be about 0.15 mm to 0.45 mm based on the beach profile; and US Army Corps of Engineers (1995) recommended to use sieve analysis for the sediment between 0.0625 mm to 32 mm. Therefore, sieve analysis should be the suitable method to determine the size of sediment samples in this study. More details are in APPENDIX G.

Once the model setup was completed, the calibration and verification processes were conducted on several key parameters of the GENESIS model, including the azimuth angle, K1, depth of closure (D_c), sediment size (D_{50}), berm height (D_b), and K2, based on the insights gained from a sensitivity analysis as shown in APPENDIX H. Calibration and validation were carried out by comparing the model's simulated outcomes to observed data on shoreline position and shoreline change End Point Rate (EPR). The observed data were sourced from Landsat satellite images, as discussed in section 3.3.

The methodology employed in this study carried uncertainties arising primarily from limitations within the GENESIS model and the available data. The first assumption of the GENESIS model was that the shape of the beach profile was constant over time and locations. The second limitation of the Genesis model was that it assumed constant shoreward and seaward limits of sediment transport. The third limitation was that the predictions of the total longshore sand transport rate were assumed to be influenced by the height and direction of breaking waves along the shore, without considering the details and effects of the nearshore current pattern. The fourth limitation was that the shoreline changes following the long-term trend, which was controlled by the waves inducing longshore sediment transport, and by the boundary conditions of structures or other barriers (Hanson, 1989).

The limitations associated with our dataset encompass various sources of uncertainty and missing information. These limitations included the uncertainty of shoreline and wave data collected in both part 1 and part 2 of this study. Additionally, a constraint arose from the absence of structure-related information, which could not be documented by local authorities due to the presence of illegally constructed structures. Moreover, the absence of sediment transport data presented a challenge, particularly in the context of the calibration process.

Following an evaluation of the accuracy and reliability of the GENESIS model in simulating shorelines, simulations were conducted to compare the resulting shoreline positions and End Point Rate (EPR) between scenarios with and without various coastal structures. Several types of structures, including beach reclamation projects, jetties, groins, and seawalls, were investigated in this study to assess their impact on coastal dynamics as the second objective of this study.

CHAPTER 4

SHORELINE CHANGE INVESTIGATION

The shorelines were extracted by using NDWI in Landsat images from 1988 to 2021. This chapter shows the results of shoreline investigation in segment 1, segment 2, and segment 3 as objective 1 of this study. In this part, the 3 main results and discussion were about shorelines digitization, shoreline change rate, and area of land loss and land gain. These findings revealed dynamic changes in different segments in the whole Phan Thiet bay during different periods from 1988 to 2021.

4.1 Shoreline digitization and method verification

The shoreline digitization was done to obtain 5 shorelines, as shown in Figure 4-1, corresponding to the beginning time and ending of 4 periods spanning from 1988 to 2021. Due to the extensive length of the shorelines, zoomed-in figures of shorelines at Ong Dia were utilized as illustrative examples to highlight the varying positions of the shoreline across different years.

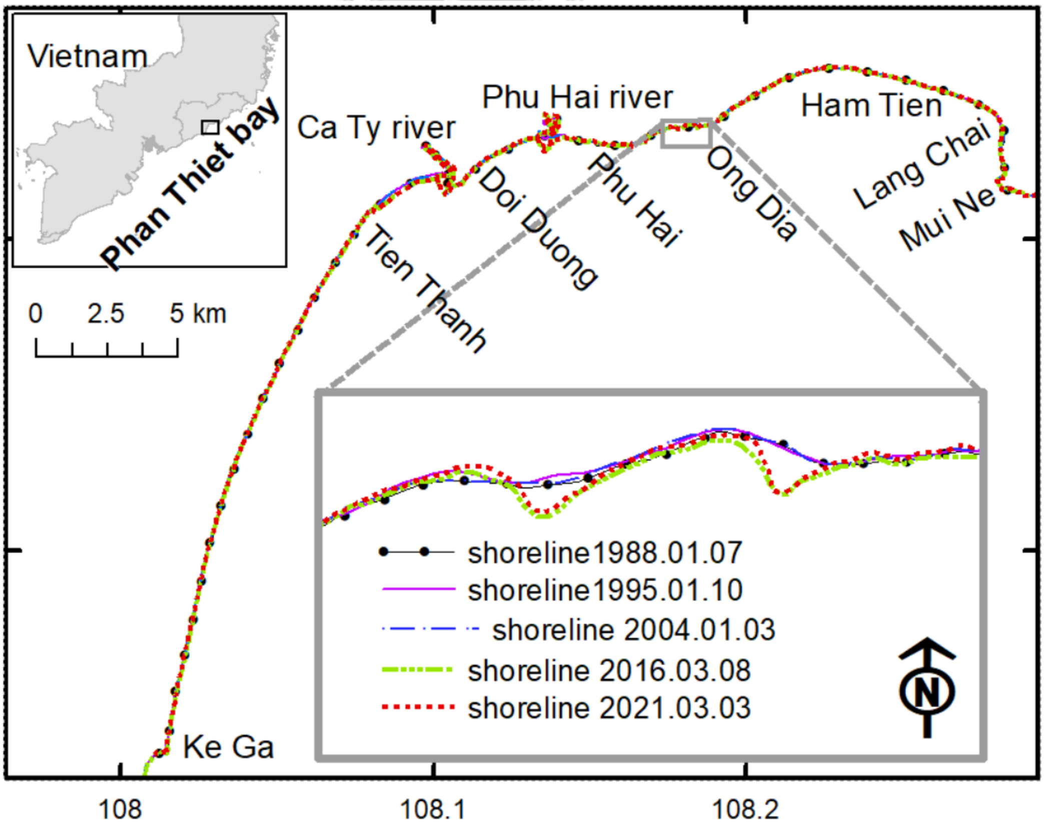

Figure 4-1 Shorelines 1988, 1995, 2004, 2016, and 2021

To validate the accuracy of the NDWI-based shoreline digitization method using Landsat image, a comparison was made between the automatically digitized shoreline with NDWI as shown in Figure 4-2 and a manually digitized shoreline derived from Google Earth image in March 2021. The difference, which is the distance between 2 shorelines at every 50 m, was shown in Figure 4-3. The mean absolute difference was found to be 9.36 m, with a median absolute difference of 8.72 m. The high differences were mostly at the beach cusps and the rocky area where the shoreline was complex rather than smooth stable shoreline. The shoreline digitization on Landsat images has limitations on the complex shoreline shape.

The difference less than 5 m accounts for 30.08% of the total 964 locations along the shoreline. That number is 24.59% and 44.40% for the difference ranging from 5 m to 10 m, and from 10 m to 30 m, respectively. Only 0.93% of positions along the shoreline exhibited variations exceeding 30 m. Considering the 30 m resolution of Landsat image, these differences suggest the reliability of the NDWI method. Nonetheless, the application of higher resolution images would further enhance the accuracy of the digitized shorelines.

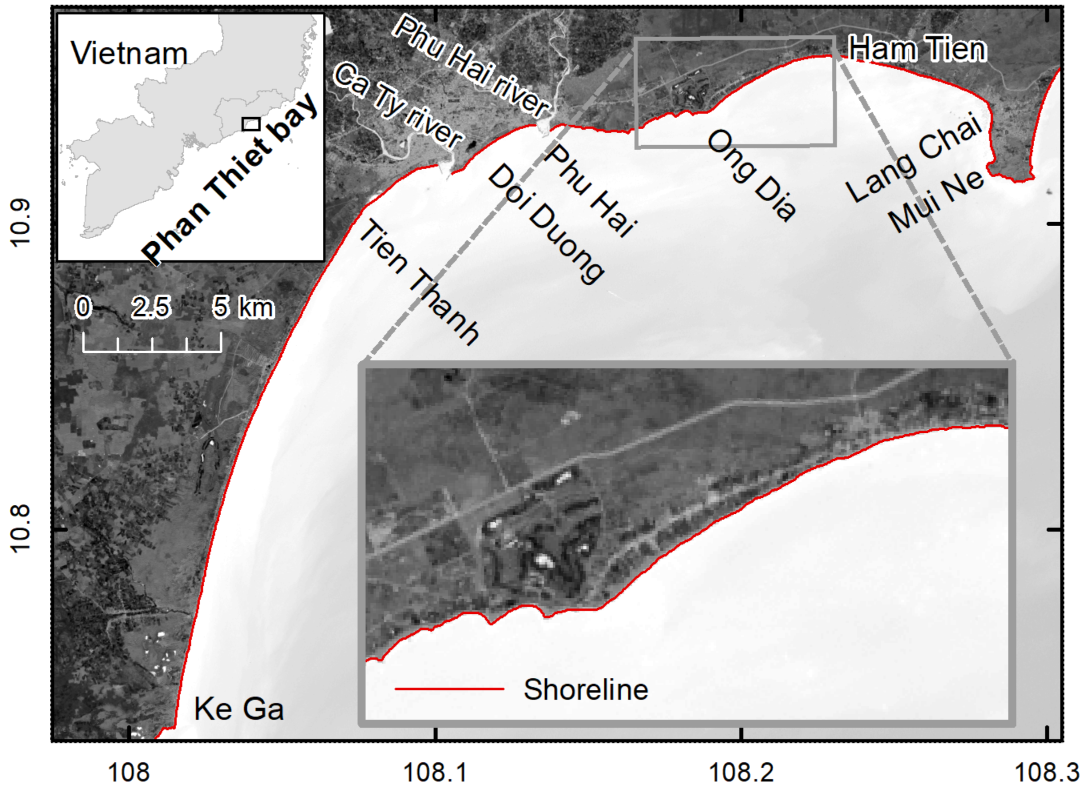

Figure 4-2 Shoreline digitized based on NDWI on Landsate image

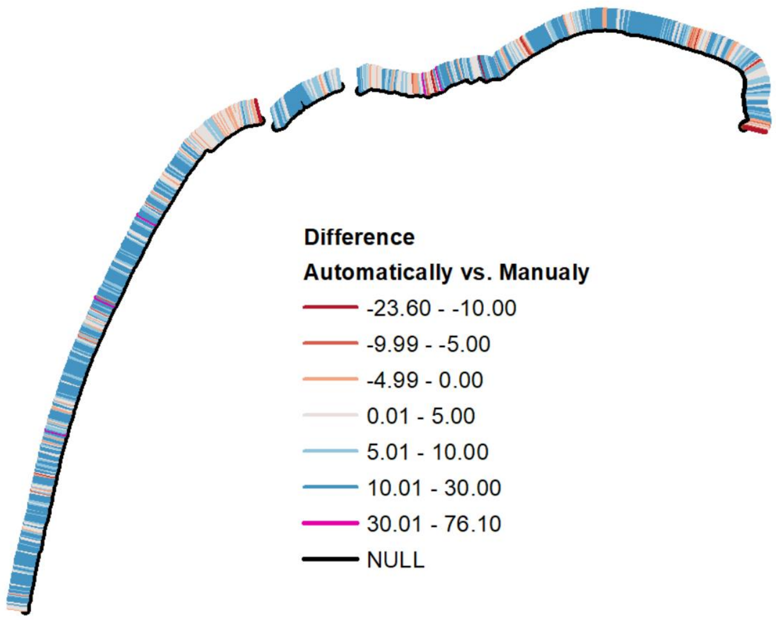

Figure 4-3 The differences between shoreline digitized on Landsat image and Google Earth image in March 2021

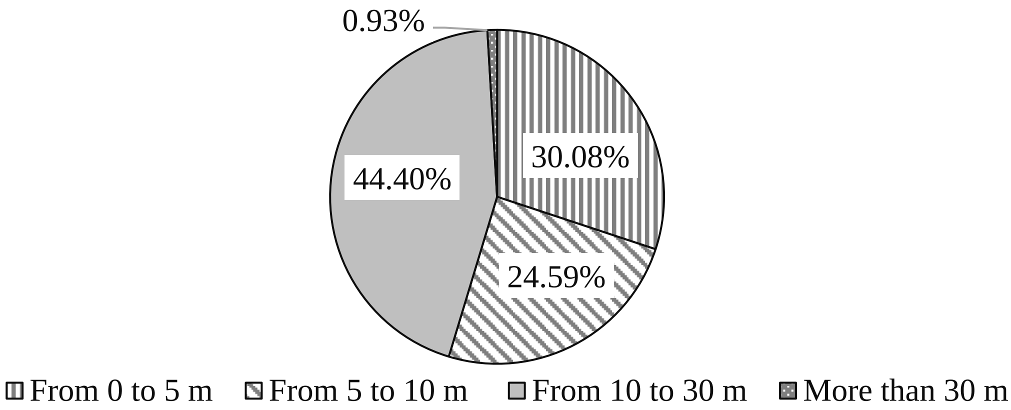

Figure 4-4 Statistical results for 964 locations to calculate the differences between two shorelines.

In order to validate the shoreline change rate calculation, the result of this study should be compared to the observed data of shoreline positions. However, due to the shortage of observed data in Phan Thiet bay in this study, the comparison of this study was compared to Linh (2018) instead. The comparison of the shoreline change rate in 3 segments (from Ke Ga to Mui Ne) from 17 Mar 1990 to 06 Jan 2017 gave the same pattern as shown in Figure 4-5. The average values of the shoreline change rate were compared in Tien Thanh and Ham Tien. The percent difference in shoreline change rate in Tien Thanh was 5.30%. In Ham Tien, the percent difference was -6.84% for EPR, as shown in Table 4-1. Since the percentage differences between two study results were small, this can be implied that this study's method can be used for further discussion.

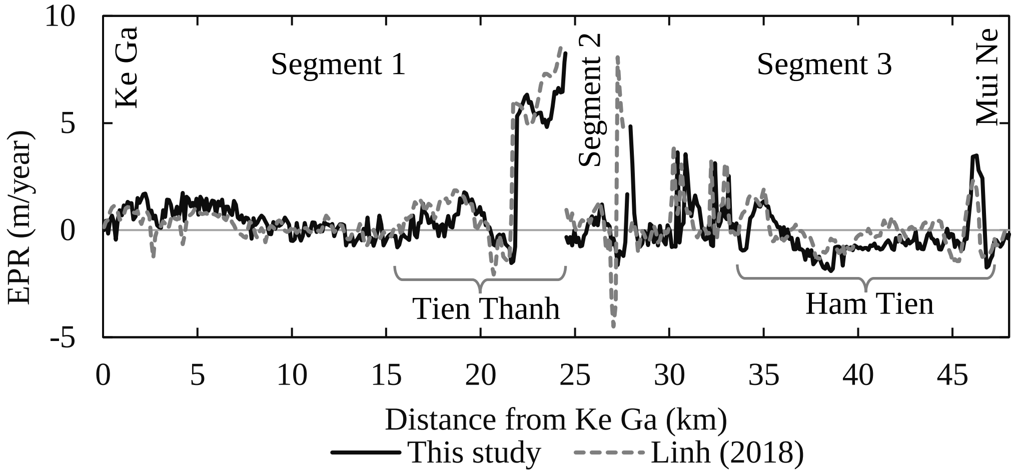

Figure 4-5. End Point Rate result (m/year) from 1990 to 2017 of (Linh, 2018) and this study

Table 4-1. Comparing the result of this study and the result of Linh (2018)

	Result	Tien Thanh	Ham Tien
Mean NSM	Linh's (m)	-16.55	-13.60
	This study (m)	-17.24	-13.75
	diff	0.69	0.15
	% diff	**-4.19**	**-1.12**
Mean EPR	Linh's (m/year)	-0.61	-0.48
	This study (m/year)	-0.64	-0.51
	diff	0.03	0.03
	% diff	**-5.30**	**-6.84**

4.2 Shoreline change rate and land balance over time

The shorelines of 3 segments were assessed in 4 periods based on the presence of structures. After applying ArcMap to extracting the shoreline, the details of the shoreline change rates along the coast from Ke Ga to Mui Ne were shown in Figure 4-6. Land balance in the whole Phan Thiet bay and each segment in each time period were shown Figure 4-7. Land balance was calculated as the difference between the accretion area and the erosion area. The summary of shoreline change rate and land balance was shown in Table 4-2. A positive value represents the seaward accretion, while the negative value means landward erosion. According to Cat et al. (2006), the shoreline change rate could be classified into 4 levels as shown in Table 4-3.

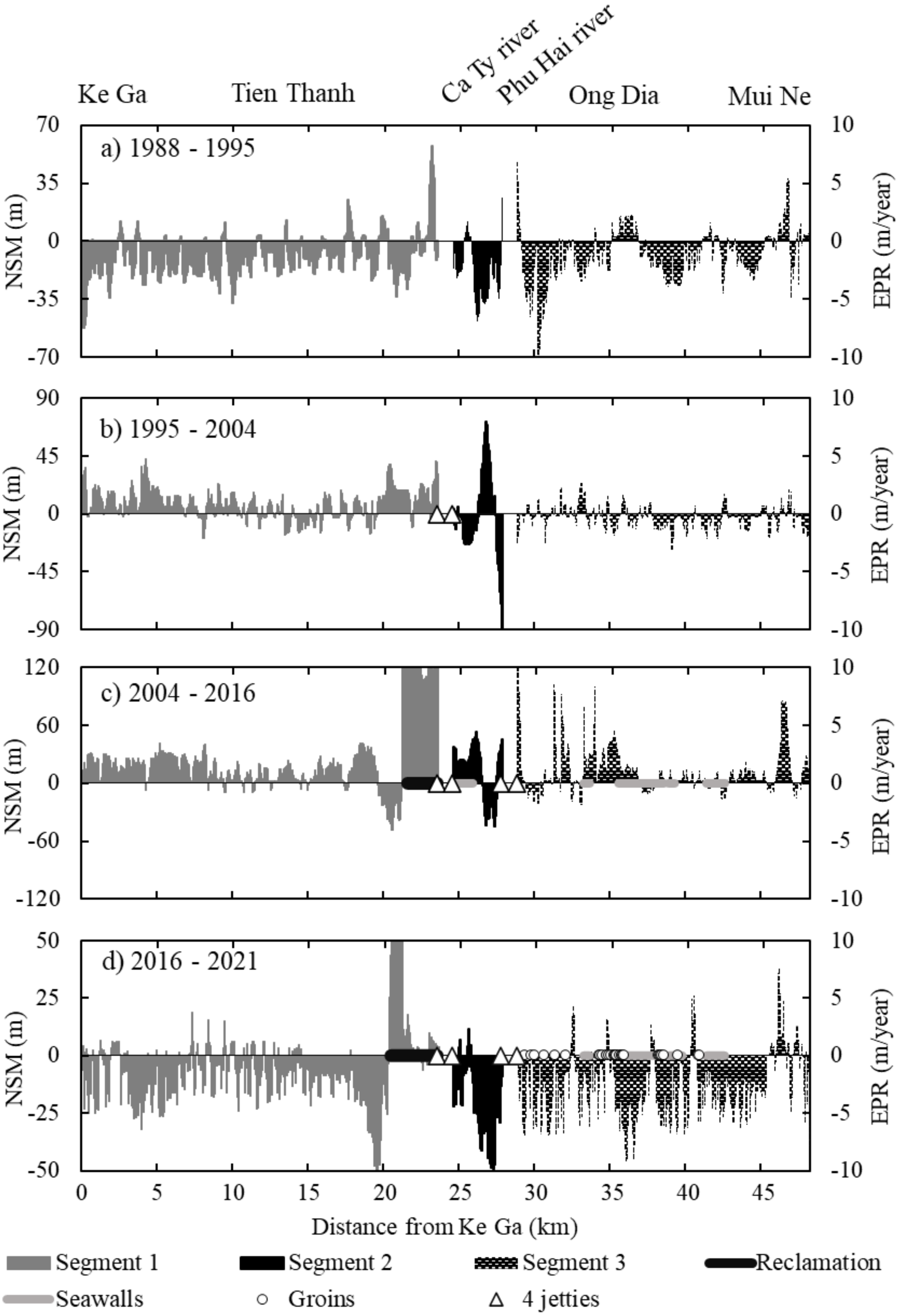

Figure 4-6. EPR result in Segment 1, segment 2, and segment 3 a) 1988-1995 b) 1995-2004 c) 2004-2016 and d) 2016-2021

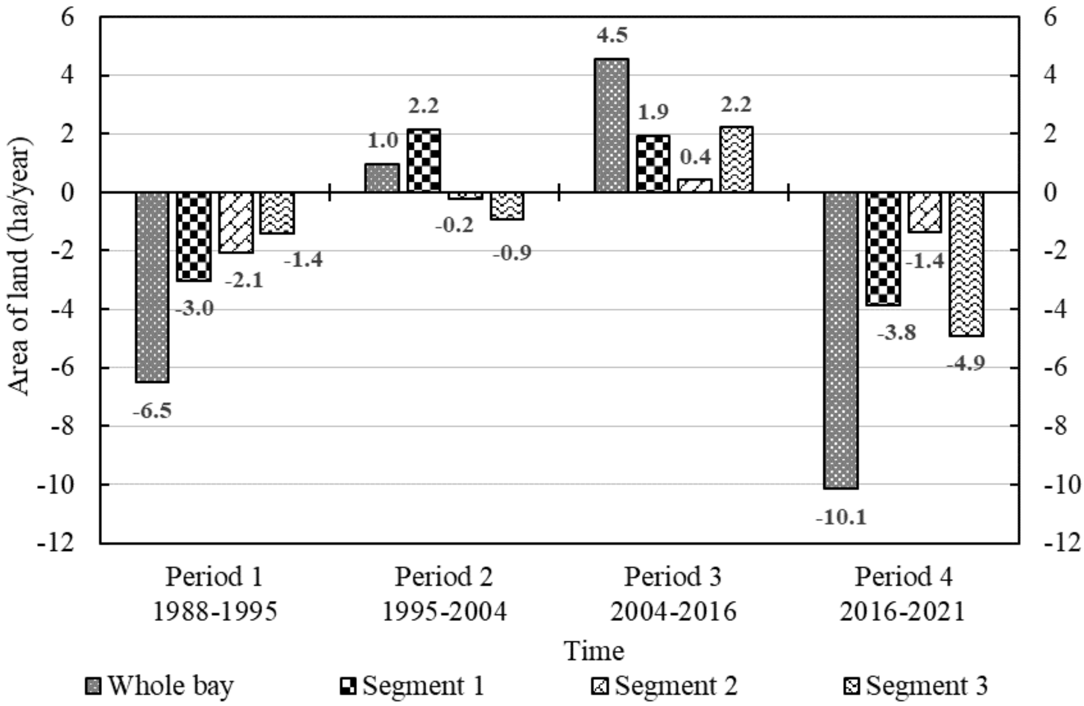

Figure 4-7. Land balance (Accretion area – Erosion area) in the whole bay and each segment during 4 periods from 1988 to 2021

Table 4-2 Result of shoreline change rate (EPR), and land balance (erosion and accretion area) in 4 periods

Parameter	**1988 - 1995**	**1995 - 2004**	**2004 - 2016**	**2016 - 2021**
Erosion (percentage of transect)	76%	50%	19%	83%
Erosion area (ha)	61.0	23.8	10.5	55.9
Erosion area (ha/year)	8.7	2.6	0.9	11.2
Mean erosion EPR (m/year)	-2.17	-0.87	-1.21	-3.22
Maximum erosion EPR (m/year)	-9.91	-10.01	-4.06	-11.77
Erosion rate (m/year)				
Low (< 5)	95%	99%	100%	80%
Moderate (5 – 15)	5%	1%	0%	20%
High (15 – 30)	0%	0%	0%	0%
Accretion (percentage of transect)	24%	50%	81%	17%
Accretion area (ha)	15.4	32.6	65.9	5.2
Accretion area (ha/year)	2.2	3.6	5.5	1.0
Mean accretion EPR (m/year)	1.19	1.40	1.49	1.41
Maximum accretion EPR (m/year)	8.22	7.97	10.81	8.70
Accretion rate (m/year)				
Low (< 5)	95%	98%	97%	96%
Moderate (5 – 15)	5%	2%	3%	4%
High (15 – 30)	0%	0%	0%	0%
Land balance (Accretion area - Erosion area) (ha)	-45.6	8.8	55.4	-50.7

Table 4-3 Classification of shoreline change rate (Cat et al., 2006)

Type	Rate (m/year)
Low rate	< 5
Moderate rate	5 – 15
High rate	15 – 30
Very high	> 30

Shoreline Change before the presence of structures (1988 - 1995)

During the first period (1988 - 1995), the shoreline exhibited a substantial erosion rate, with erosion accounting for 76% of the transect. This resulted in a significant erosion area of 61.0 ha (8.7 ha/year), primarily attributed to erosion processes. The accretion rate was comparatively lower at 24%, accompanied by an accretion area of 15.4 ha (2.2 ha/year). Consequently, there was a notable negative land balance of -45.6 ha. The mean erosion End Point Rate (EPR) was calculated at -2.17 m/year, while the maximum erosion EPR reached -9.91 m/year. The majority of the erosion events fell into the "Low" category (< 5 m/year), accounting for 95%. However, near Ca Ty river, the accretion was up to 57.54 m (8.22 m/year), which was classified as moderate shoreline change.

Shoreline Change after the construction of 2 Jetties at Ca Ty river mouth

In the second period (1995 - 2004), the shoreline experienced a reduced erosion rate, amounting to 50% of the transect. Land loss decreased to 23.8 ha (2.6 ha/year), while accretion increased significantly, amounting to 50% of the transect. The accretion area expanded to 32.6 ha (3.6 ha/year), resulting in a positive land balance of 8.8 ha. The mean erosion EPR reduced to -0.87 m/year, with the maximum erosion EPR at -10.01 m/year. Both erosion and accretion primarily fell into the "Low" category, correspondingly covering 99% and 98% of the observed events. After the construction of jetties near Ca Ty river mouth, the accretion rate was 40.68 m (4.52 m/year), which was lower compared to previous period.

Shoreline Change during the implementation of reclamation project

During the third period (2004 – 2016), since 2006, the beach reclamation project has been implemented in Tien Thanh of segment. The shoreline underwent a transformation, with erosion accounting for only 19% of the transect. The mean erosion EPR was recorded at -1.21 m/year, with the maximum erosion EPR reaching

-4.06 m/year. Remarkably, 100% of erosion events were categorized as "Low”. Erosion area continued to decrease, totaling 10.5 ha (0.9 ha/year), while accretion increased, encompassing 81% of the transect. The accretion area expanded significantly to 65.9 ha (5.5 ha/year), yielding a substantial land balance of 55.4 ha. Mean accretion EPR and maximum accretion EPR were higher than other periods, at 1.49 m/year and 10.81 m/year respectively.

Shoreline Change during recent year with 25 coastal structures built

In the most recent period (2016 - 2021), the shoreline faced heightened erosion, accounting to 83% of the transect. Erosion area amounted to 55.9 ha (11.2 ha/year), significantly higher the accretion area of 5.2 ha (1.0 ha/year). This resulted in a notable negative land balance of -50.7 ha. The mean erosion EPR during this phase was recorded at -3.22 m/year, with the maximum erosion EPR peaking at -11.77 m/year. Highest erosion EPR occurred next to the reclamation project in segment 1 and between 2 rivers in segment 2. Erosion events in this period were characterized by 80% falling within the “Low” category and 20% categorized as “Moderate”.

4.3 Discussion and conclusion of shoreline change investigation

In this part of shoreline change investigation, three main processes were digitizing shoreline, analyzing shoreline change rate, and determining the areas of land loss and land gain. The following contents are about limitation of shoreline digitization methodology, limitation of shoreline change rate and land area calculation, and mechanism of shoreline change in Phan Thiet bay.

4.3.1 Limitation of shoreline digitization methodology

The digitization of the shoreline was performed using Landsat satellite images. To validate the accuracy of the digitized shorelines, a manual extraction of the shoreline was conducted on Google Earth images for comparison. The results of the comparison revealed differences ranging from -23.6 m to 35.62 m. These disparities can be attributed to the limitations of the resolution of Landsat images, and the shoreline complexity.

Landsat images had a resolution of 30 m, which was generally adequate for some applications, they struggled to identify shoreline changes less than 30 m, especially in the range of 15 to 30 m. In coastal studies in Vietnam, changes within this range can be significant and could be classified as high-rate erosion or accretion as shown in Table 4-3. Therefore, using Landsat images may not be a good idea for identifying shorelines. However, due to limitations of other available sources for detecting shoreline changes, using Landsat images was a reasonable attempt.

The Landsat images were collected during the same season of the year, from January to March, as recommended by Crowell et al. (1991). Duc and Luan (2014) conducted a study that recognized the seasonal changes in the shoreline in Phan Thiet bay. Collecting images in the same season helped eliminate the influence of seasonal factors on the shoreline. Moreover, during January to March, Landsat images were clearer with fewer effects from clouds.

Employing higher-resolution images would enhance the accuracy of digitized shorelines. Unfortunately, in the specific case of Phan Thiet bay, options for higher-resolution images like Google Earth Images starting in 2006 (resolution of 5 m) and Sentinel-2 satellite images starting in 2016 (resolution of 10 m) were not accessible prior to the construction of coastal structures in 1996 (Maxar, 2023; The European Space Agency, 2015). Therefore, in this case of Phan Thiet bay, Landsat satellite images are the most suitable for digitizing the shoreline in order to investigate the relation of shoreline change to the structures.

Therefore, in future investigations or other timeframes where higher-resolution images were available, it was strongly recommended to utilize these images for achieving more precise shoreline positions and improved results. Moreover, it was recommended to gather observed shoreline positions to correct and validate the shorelines extracted from satellite images for long-term shoreline change investigations.

The digitization process did not incorporate tide and beach slope. Unfortunately, observed tide data specific to Phan Thiet bay was unavailable. As an alternative, tide data from Vung Tau was utilized for reference. Notably, the patterns of tides by years demonstrated considerable consistency. Moreover, from January to March which is the time of collected Landsat images, the pattern of tide level were quite similar. Therefore, the tidal effects on shoreline position can be supposed to be similar. Noteworthy, the period spanning from day 1 to day 4 experienced the highest tidal magnitude as shown in Figure 4-8.

Landsat images were taken in January and March between 9:20 am and 10:07 am UTC+7. During this time, maximum fluctuation of water level was from day 1 to day 4 at 0.5 m as shown in Figure 4-9. While the average beach slope within -2.5 m water depth from the survey conducted by Vuong (2012) and Vuong (2014) was 1/40. This could approximate that the tide could potentially induce shoreline movement of 20 m, which was smaller than the 30 m grid size of the Landsat images. Therefore, the error resulting from the absence of tide level and beach slope correction was smaller than the inherent uncertainty associated with the Landsat images themselves. To achieve more precise shoreline positioning, it was recommended to employ higher resolution images and incorporate corrections based on tide level and beach slope. Consequently, it was recommended to carry out measurements of beach slope and tide level to enhance the accuracy of the results.

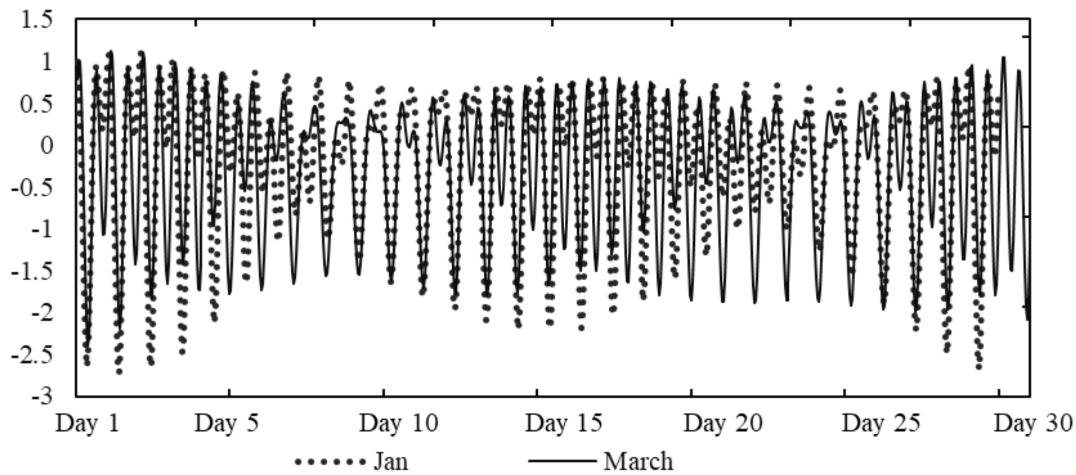

Figure 4-8 Tide level at Vung Tau gauge in January and March 2010

The above limitations possibly gave impact on the accuracy of shoreline results. For instance, the utilization of Landsat images with a resolution of 30 meters gave constraints in accurately capturing complex shorelines characterized by changes occurring within distances less than the 30-meter resolution. Consequently, this limitation contributes to the generation of less precise shoreline digitization, particularly evident in rocky areas and beach cusps where the changes happen within less than 30 m shoreline length.

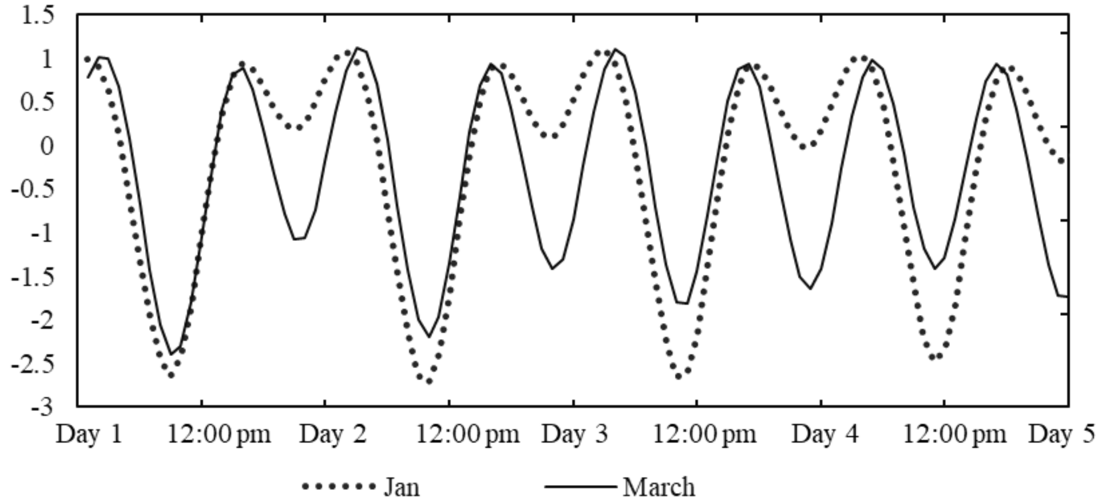

Figure 4-9 Tide level at Vung Tau gauge from day 1 to day 4 in January and March 2010

4.3.2 Limitation of shoreline change rate, and land area calculation

In this study, the results of shoreline positions with above limitations were used for calculating the shoreline change rate, and the amount of land loss and land gain in Phan Thiet bay in long term from 1988 to 2021 according to the presence of structures in this area. That helps to obtain more understanding on the mechanism of shoreline change behaviors. Considering the long-term duration of this study, even though it would be better with the more precise shoreline, some details in the shoreline change could be neglected.

The Digital Shoreline Analysis System (DSAS) was utilized to analyze the EPR of shoreline change in four time periods in Phan Thiet bay. The result of EPR should be compared to the observed data, but it was compared to Linh (2018) due to the shortage of observed data. The graphs of EPR from 1990 to 2017 in this study and Linh (2018) exhibited a similar pattern. The difference of mean NSM and mean EPR between the 2 results were from 1.12% to 6.84%. This difference could be attributed to the difference in the transect distances employed in 2 studies. Nevertheless, overall, this method proved to be acceptable in investigating shoreline dynamics.

To further improve the analysis, it is strongly recommended to collect additional observed data on the shoreline position and shoreline change rate, as well as images with higher resolution. The inclusion of better data will enhance the accuracy and reliability of shoreline digitization results. Furthermore, to achieve more accurate results in the calculation of shoreline change rate, it is important to improve the accuracy of the input data that were the shoreline positions themselves. When utilizing the DSAS, it is essential to carefully consider the selection of baselines and transects. It is better to maintain uniform spacing between the transects while ensuring their perpendicular alignment with the shoreline. In order to do that, the baseline is better to be smooth and parallel to the initial and final shorelines as much as possible.

4.3.3 Mechanism of shoreline change in Phan Thiet bay

The correlations between shoreline change and the presence of structures and typhoons were evaluated as demonstrated in Table 4-4. In the first period of 7 years, the shoreline eroded in many locations without any structures yet, however with 2 typhoons. The second period of 9 years and third period of 12 years showed similar patterns of EPR, and land loss and land gain. However, the third period appeared more severe, with 4 jetties, 1 beach reclamation project, 5 seawalls, and 2 typhoons compared to the second period with only 2 jetties and 1 typhoon. In the fourth period of only 5 years, which had 41 structures in total and 3 storms which were more than the previous periods, shoreline change became more complex with a higher erosion rate and land loss. These findings indicate that typhoons and structures play a major role in shoreline change.

Table 4-4 Correlation between shoreline change and the presence of typhoons and structures

Parameter	1988 - 1995	1995 - 2004	2004 - 2016	2016 - 2021
Number of years	7	9	12	5
Number of typhoons	2	1	2	3
Number of structures	0	2	10	41
Erosion (percentage of transect)	76%	50%	19%	83%
Mean erosion EPR (m/year)	-2.17	-0.87	-1.21	-3.22
Accretion (percentage of transect)	24%	50%	81%	17%
Mean accretion EPR (m/year)	1.19	1.40	1.49	1.41

The results also indicate that typhoons possibly caused more serious erosion, leading to severe land loss along the shoreline. Moreover, the process of cross-shore reclamation to restore the eroded land after typhoons may extend beyond the one-year timeframe, which is different from what mentioned in existing literature. This difference suggested the importance of considering the specific characteristics and dynamics of the study area, as local factors can influence the duration and effectiveness of post-typhoon land restoration efforts.

The relationship between typhoons and shoreline behavior could be further investigated through the analysis of wave data. However, the present study was constrained by the lack of long-term observed wave data. To facilitate more comprehensive investigations into the interaction between typhoons and the shoreline in Phan Thiet bay, it is recommended to conduct long-term wave measurements and field observation on shoreline erosion after typhoon. These extended observations would provide valuable insights and enhance our understanding of the dynamics between typhoons and the shoreline.

Structures are the solution made by humans. They should be carefully considered before building. As the number of structures increases, shoreline change becomes more complex with higher rate of both erosion and accretion, and higher amount of land loss. The land spit was observed at several locations of groins of segment 3 as shown in Figure 4-10, which showed the evidence of the impact of coastal groins on longshore sediment transport. Moreover, during the third period and fourth period, when the beach reclamation project existed, the shoreline downdrift of it eroded with higher rate compare to other locations, which also the evidence the interaction between the coastal structures and longshore sediment transport.

The oblique incident waves as mentioned in section 3.1 could cause longshore sediment transport in Phan Thiet bay. The direction of these waves dominated by East direction, in conjunction with the orientation of the shoreline, suggests that the primary direction of alongshore sediment transport is likely from the East to the West. The above discussion leads to the necessity of understanding the effects of these structures on the alongshore sediment transport as well as the shoreline change of entirety Phan Thiet bay. This understanding is vital for formulating effective coastal management plans. To gain insights into these effects of structures on shoreline, the study utilized the GENESIS model to simulate long-term shoreline change through longshore sediment transport. Those effects investigated were the change in EPR, the change in erosion and accretion area, and the length of shoreline that got affected by the presence of structures.

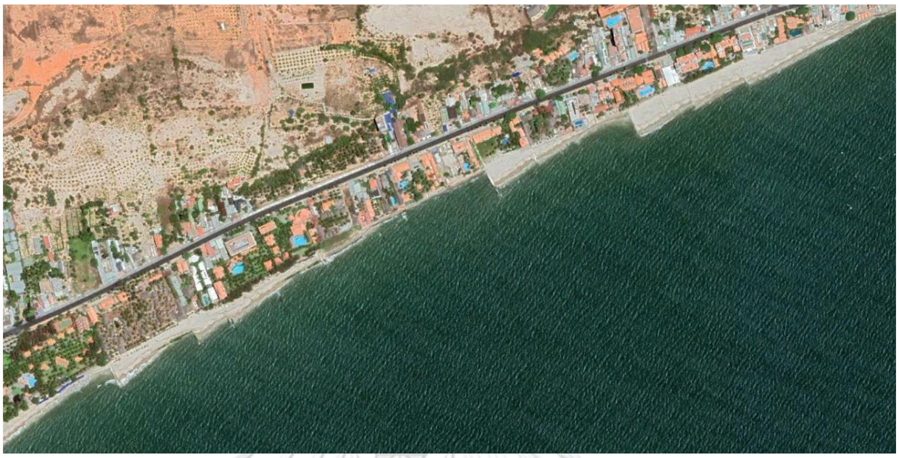

Figure 4-10 groins in segment 3 with land spit

Apart from structures and typhoons, there were other factors that were not considered in this study due to data limitations which could possibly impact the shoreline. Shoreline changes can occur when there are alterations in sediment storage, which could be influenced by the sediment from Ca Ty river and Phu Hai river. During the initial period, prior to the construction of jetties near the Ca Ty River, an erosion trend of shoreline erosion was observed. However, in the second period, a shift occurred, with shoreline dynamics indicating accretion. Particularly, in the adjacent shoreline of the Ca Ty River, the accretion rate during the second period was nearly twice that of the initial period. This observation implied that these jetties may have contributed to a reduction in accretion rates in the vicinity of the Ca Ty River. Consequently, it becomes evident that sediment originating from the Ca Ty River holds relevance for the adjacent shoreline. Near Phu Hai river, from 1988 to 1995, an unusual accretion was observed, possibly due to sediment deposits from the river. However, from 1995 to 2004, there was high erosion, which might be linked to sand dredging.

Human activities like dredging sediment from river navigation channels and relocating it along the coast, as well as sand mining and exploitation of other natural resources, can also contribute to shoreline changes. Trung (2019) mentioned dredging activities at the mouth of Ca Ty River to facilitate ship access to the port, providing evidence of sediment movement from the river to the coast. The above results of this study also showed the abnormal erosion near Phu Hai river from 1995 to 2004, which could be the evident of sand dredging. Additionally, Vietnamnet (2017) reported on the issue of sand overexploitation in Phan Thiet city for local use and illegal exportation abroad.

The shoreline also changes when the relative differences in elevation between land and sea surface changes according to the sea level rise, land subsidence, or tidal. Vung Tau gauge, the nearest nearshore tidal gauge to Phan Thiet bay, showed the sea level rise of 2.9 mm/year (from 1978 to 2018), which is higher than the average of Vietnam sea level rise of 2.7 mm/year (from 1961 to 2018) (MONRE, 2010), and which is lower than the average of global sea level rise of 3.2 mm/year (from 1993 to 2010) (Church et al., 2013). The difference in elevation should be considered with the beach slope in order to determine the impacts of them on shoreline positions.

It is recommended to collect more observed data of sediment from rivers, sand dredging and exploitation, tide, and sea level rise for incorporating those factors into the analysis of shoreline change rate.

In conclusion, in Phan Thiet bay from 1988 to 2021, correlations were observed between shoreline change rate and the presence of structures, as well as the frequency of typhoons during that period. The rates of shoreline change, including erosion, accretion, and land loss, increased with the construction of more structures. These findings emphasize the need to raise awareness regarding the unintended consequences of coastal structures on the coastal zone in Phan Thiet bay, Vietnam. The results can contribute to the development of coastal management plans, including risk assessments that consider shoreline change in relation to typhoons and structures. However, further research is necessary to investigate additional factors such as sediment from rivers, sand dredging or exploitation, sea-level rise, and tidal influences, in order to develop a more comprehensive understanding of the mechanisms driving shoreline change in Phan Thiet bay. In the subsequent part of this study, the application of the GENESIS model facilitated a deeper understanding of the effects of different structures on shoreline change, which can further inform mitigation strategies within the coastal management plan.

CHAPTER 5
EFFECTS OF COASTAL STRUCTURES ON SHORELINE CHANGE

The effects of coastal structures on shoreline change in Phan Thiet Bay were analyzed based on shoreline simulation in the GENESIS model as objective 2 of this study. The SWAN wave simulation model was used to generate wave data as input for the GENESIS model. Therefore, this chapter begins by describing the results and discussion of wave simulation in SWAN. Secondly, it details the setup of the GENESIS shoreline simulation model. Thirdly, the effects of each structure on shoreline change were described based on a comparison of shoreline simulation results with and without each structure. The structures considered include beach reclamation projects, jetties, groins, and seawalls. The final section is a discussion on shoreline simulation.

5.1 Wave simulation

This section provides (1) the result of wave simulation including the results of calibration and validation, wave characteristics; and (2) the discussion and conclusion of those results. The results of wave characteristics from this section are one of the main inputs for shoreline simulation model in the next part.

5.1.1 Calibration and validation of wave simulation

The calibration and validation process of the SWAN model involved comparing the simulated wave heights and wave directions generated by SWAN with observational wave data. The objective was to identify the optimal combination of whitecapping (WCAP), bottom friction (FRIC), depth-induced wave breaking (BREAK) parameters that would yield the closest match between the model's predictions and the observed wave heights. For the calibration phase, the wave data collected at PH01 and PH02 in 2012, were utilized as the observational dataset. The validation was done at PH01TN and PH02TN observed in 2014 as shown in Figure 5-1. The variation of WCAP, FRIC, and BREAK in the process of calibration varied between 1.3×10^{-5} to $1,7\times10^{-5}$, 0.02 to 0.05, and 0.5 to 0.9. As a result, the values of

WCAP, FRIC, and BREAK were adjusted to achieve the closest match between the simulated wave heights and the observational wave heights, as well as simulated wave direction and the observational wave direction. The optimized parameter values resulting in the best agreement with the observational data are as follows: WCAP = 1.4×10^{-5}, FRIC = 0.037, and BREAK = 0.7.

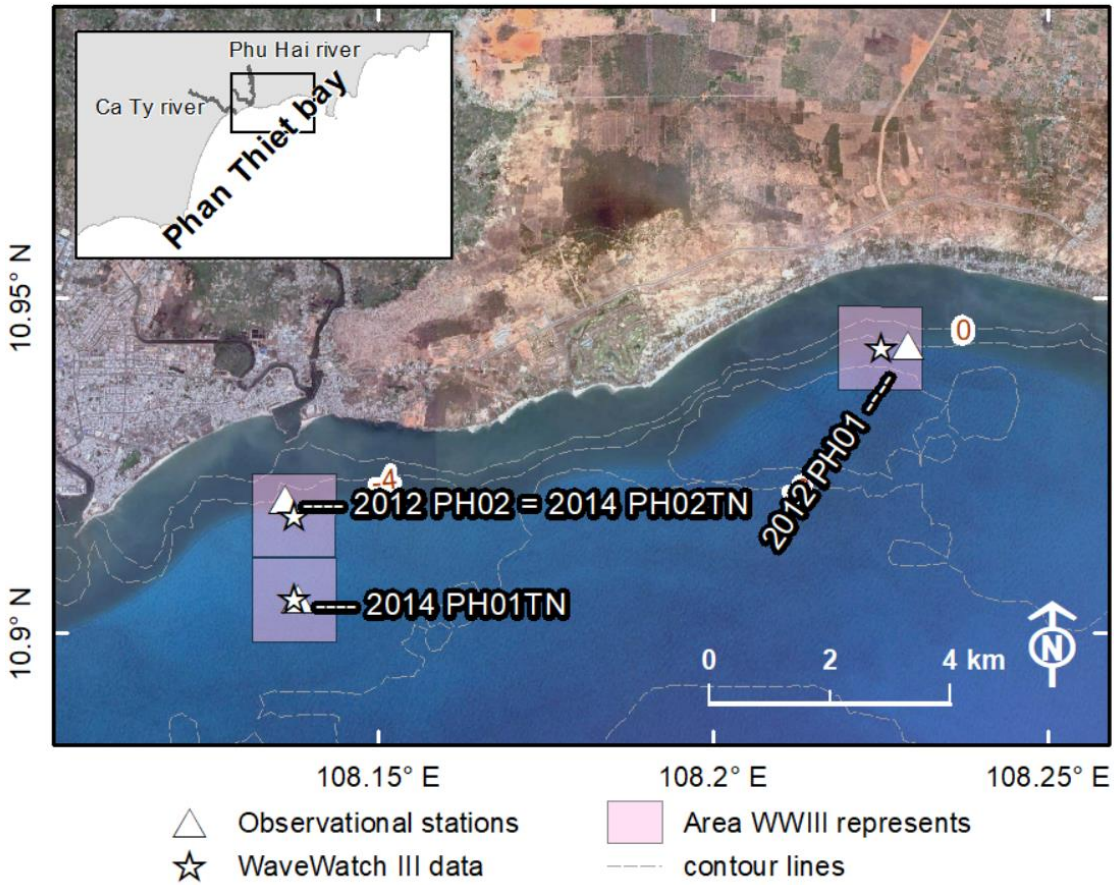

Figure 5-1 Locations of observational wave data

The simulated wave heights generated by the SWAN model exhibited overall good agreement with the observational wave data at station PH01 and station PH02 in the calibration phase, as depicted in Figure 5-2 and Figure 5-3. The patterns of peak and trough values were largely consistent between the simulated and observed wave heights. Notably, on 28th November 2012, the simulated wave height closely resembled the actual wave height. However, at other times, some minor differences were observed. For instance, the calibrated wave heights exhibited a slightly narrower range compared to the observed wave heights. In the station PH01, the range of simulated wave height was from 0.37 m to 0.60 m, while the actual range was from 0.14 m to 0.81 m.

a) *Calibration result of station PH01*

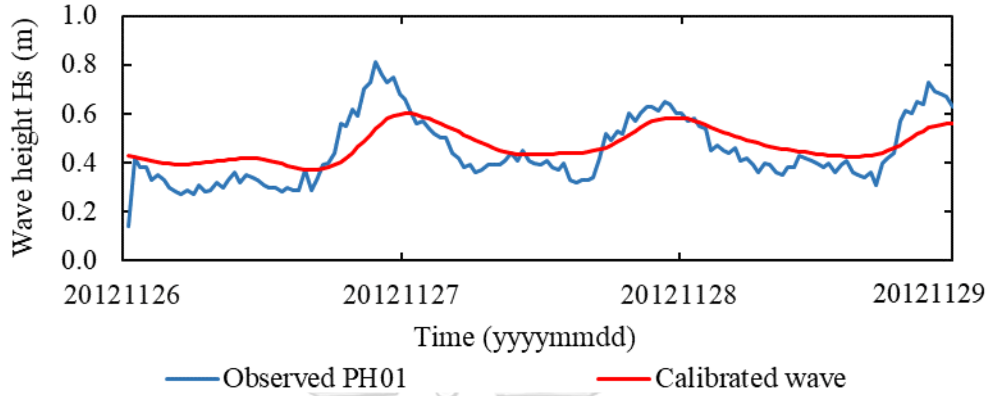

b) *Calibration result of station PH02*

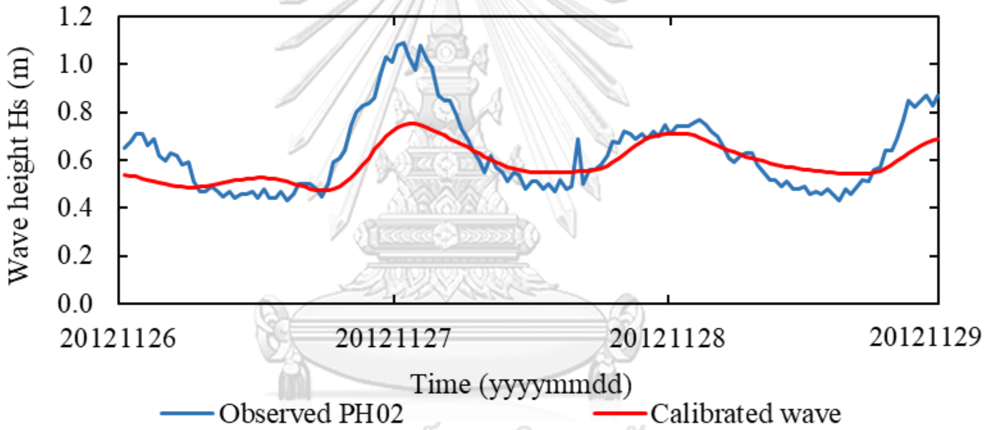

Figure 5-2 Calibration result of SWAN (wave height)

The comparison between the wave directions obtained from the SWAN model and the observed wave data, as shown in Figure 5-3, revealed the agreement. Specifically, the model captured the dominant wave directions. Nevertheless, it is important to note that the wave directions simulated by the model exhibited a higher level of stability, primarily aligning with a limited range of angles. In contrast, the observed wave directions displayed a wider range of angles.

In addition to the visual agreement displayed in the graph, the agreement between the simulated and actual wave heights can be further evaluated using quantitative metrics such as Mean Absolute Error (MAE), and relative bias as presented in the Table 5-1.

The MAE values indicate that, on average, the simulated wave heights deviate from the actual wave heights by approximately 0.08 to 0.9 meters. Considering the range of the wave heights being analyzed, this MAE value can be considered relatively small, indicating a reasonably good agreement between the simulated and actual wave heights.

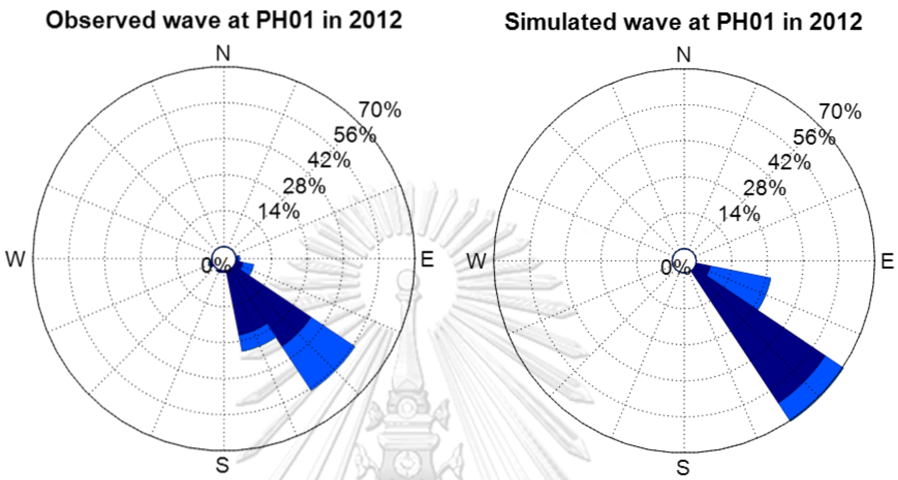

a) Calibration result of station PH01

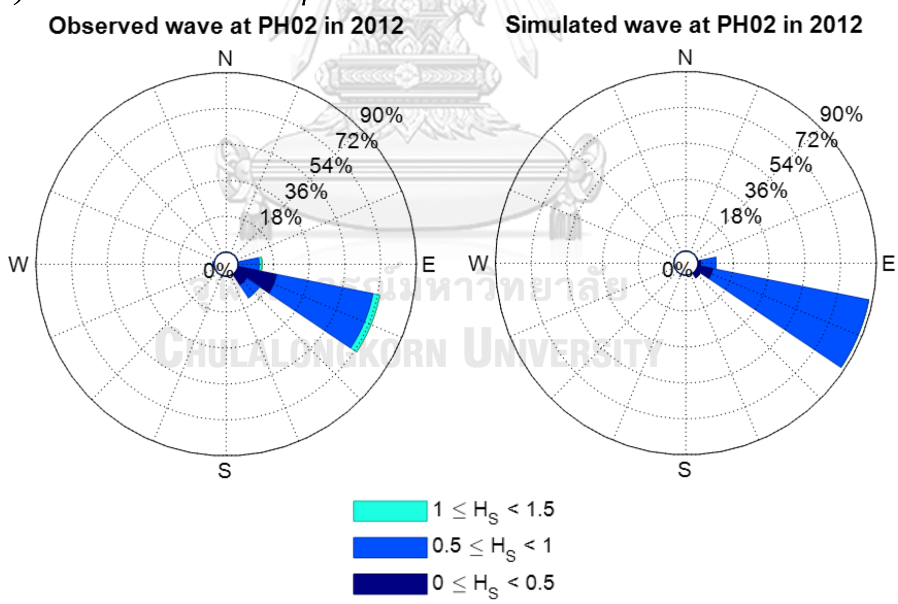

b) Calibration result of station PH01

Figure 5-3 Calibration result of SWAN (wave direction)

The relative bias values ranging from -0.04 to 0.11 indicate that, on average, the simulated wave heights tend to be overestimated by approximately 11% for station PH01 and underestimated by approximately 4% for station PH02 of the observed wave heights.

Despite these slight discrepancies, the model's performance in replicating the general wave characteristics was satisfactory, demonstrating its capability to capture the main features of the wave field of Phan Thiet bay in 2012.

Table 5-1 Calibration result of SWAN

	PH01	**PH02**
MAE (m)	0.08	0.09
Relative bias	0.11	-0.04

After completing the calibration phase, the next step is model validation, which aims to assess the performance of the calibrated model. Specifically, we evaluate how well the chosen set of parameters (WCAP, FRIC, and BREAK) can be utilized to hindcast the wave characteristics at station PH01TN and PH02TN in 2014. Their locations and details of those stations were mentioned in Figure 5-1. Through validation, the degree of agreement between the simulated wave heights and the corresponding observed wave heights at these stations were examined.

The validation results, depicted in the Figure 5-4 and Figure 5-5, highlighted several key observations. Firstly, the simulated wave heights exhibited greater stability compared to the actual wave heights. However, it is important to note that the simulated wave heights closely followed the general pattern of the observed wave heights.

Similarly as the calibration results, the model simulated dominant wave directions that aligned well with the observed data in the validation phase. However, the simulated wave directions were not as broad as those in the observed data. This difference can be attributed to variations in the wind input data, as the directions of the global wind data that were used in SWAN model were also not as broad as those in the observed wind data.

In addition to the graphical representation, various statistical metrics were calculated to assess the agreement between the simulated and observed wave heights at two stations in 2014. These metrics included Mean Absolute Error (MAE), and relative bias, as summarized in the Table 5-2.

Considering the average wave heights in the validation phase, the simulation showed good agreement with the observations, which was consistent with the findings from the calibration phase. This suggested that while the model may not capture the exact wave heights at specific instances, it provided an accurate representation of the average wave behavior.

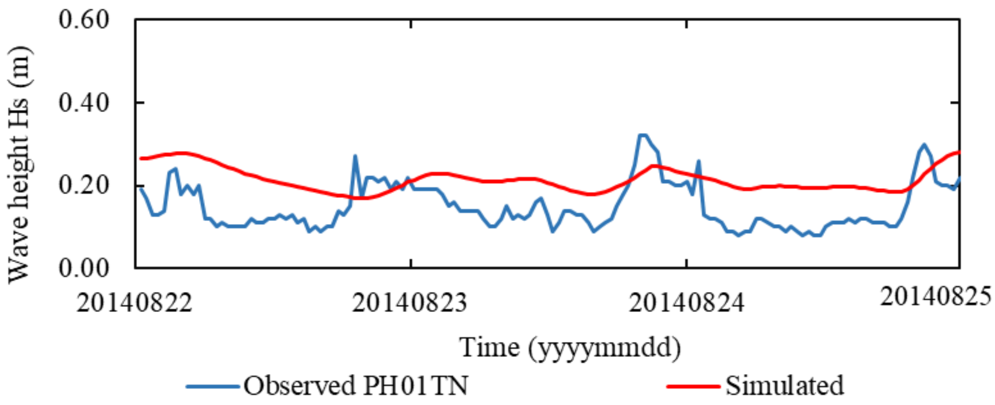

a) *Validation result of station PH01TN*

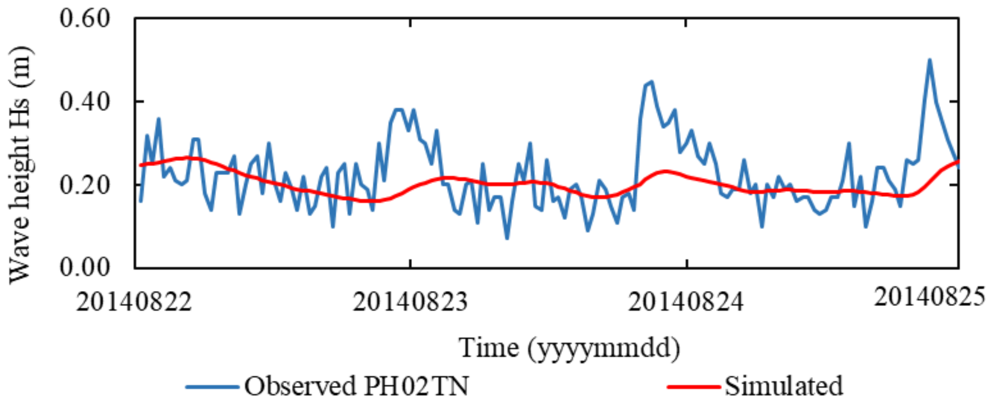

b)Validation result of station PH02TN

Figure 5-4 Validation result of SWAN model

In conclusion, while the model's performance in matching individual data points was not as precise, it demonstrated good agreement with observed average wave heights. The validation phase confirmed that the SWAN model can effectively simulate wave heights, making it a suitable tool for generating wave inputs for shoreline change models. Future enhancements could focus on improving the model's ability to capture extreme wave events.

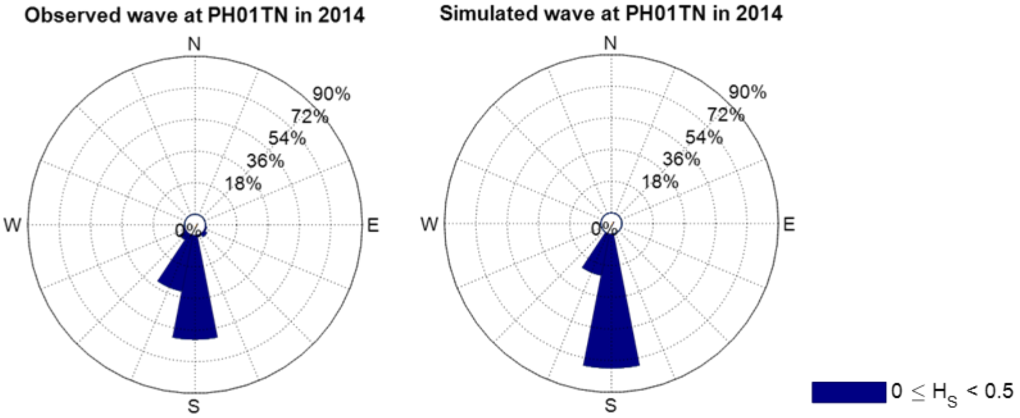

a) Validation result of station PH01TN

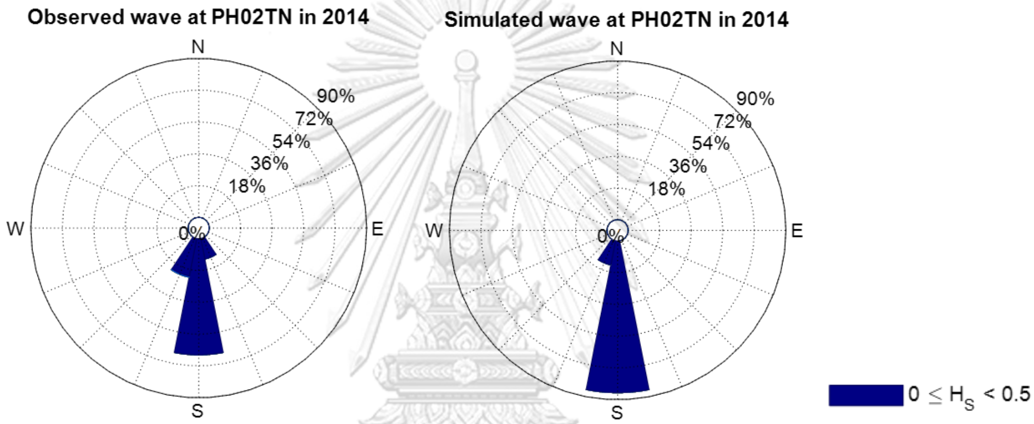

a) Validation result of station PH02TN

Figure 5-5 Validation result of SWAN (wave direction)

Table 5-2 Validation result of SWAN

	PH01TN	PH02TN
MAE (m)	0.08	0.06
Relative bias	0.58	0.01

5.1.2 Wave characteristic results

The waves of every hour from 1988 to 2021 at various locations of the resolution of 0.0125 were simulated. The result were collected and presented in this part. To investigate the behavior of wave simulation result from 1988 to 1993, 3 sample points, both offshore and nearshore were chosen as point 1, point 2, and point 3 as shown the location in Figure 5-6.

At all 3 points, the wave pattern showed the stable wave height by years. However, they exhibited the seasoning changing as shown in Figure 5-7. At point 1 and point 2, the wave heights closely followed the wind data pattern. When the wind speeds were higher, the wave heights also increased, and vice versa. That includes the abnormal event of high wind speed and wave height in the end of 1988. As shown in Figure 5-6, during the NE monsoon season, spanning the end of the year until the beginning of the following year, wind speeds were generally higher compared to the SW monsoon season in the middle of the year.

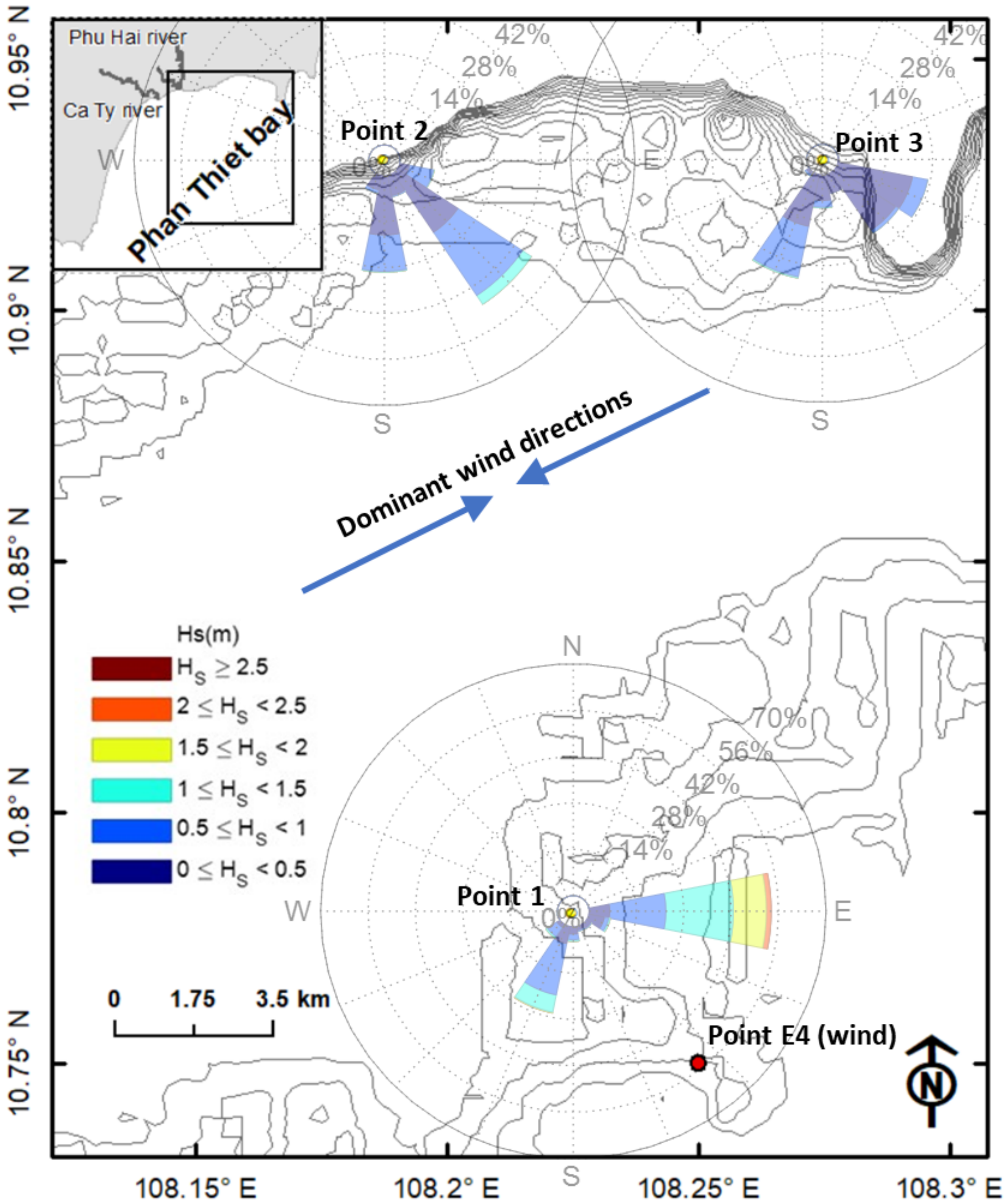

Figure 5-6 Wave at point 1, point 2, point 3 from 1988 to 2021

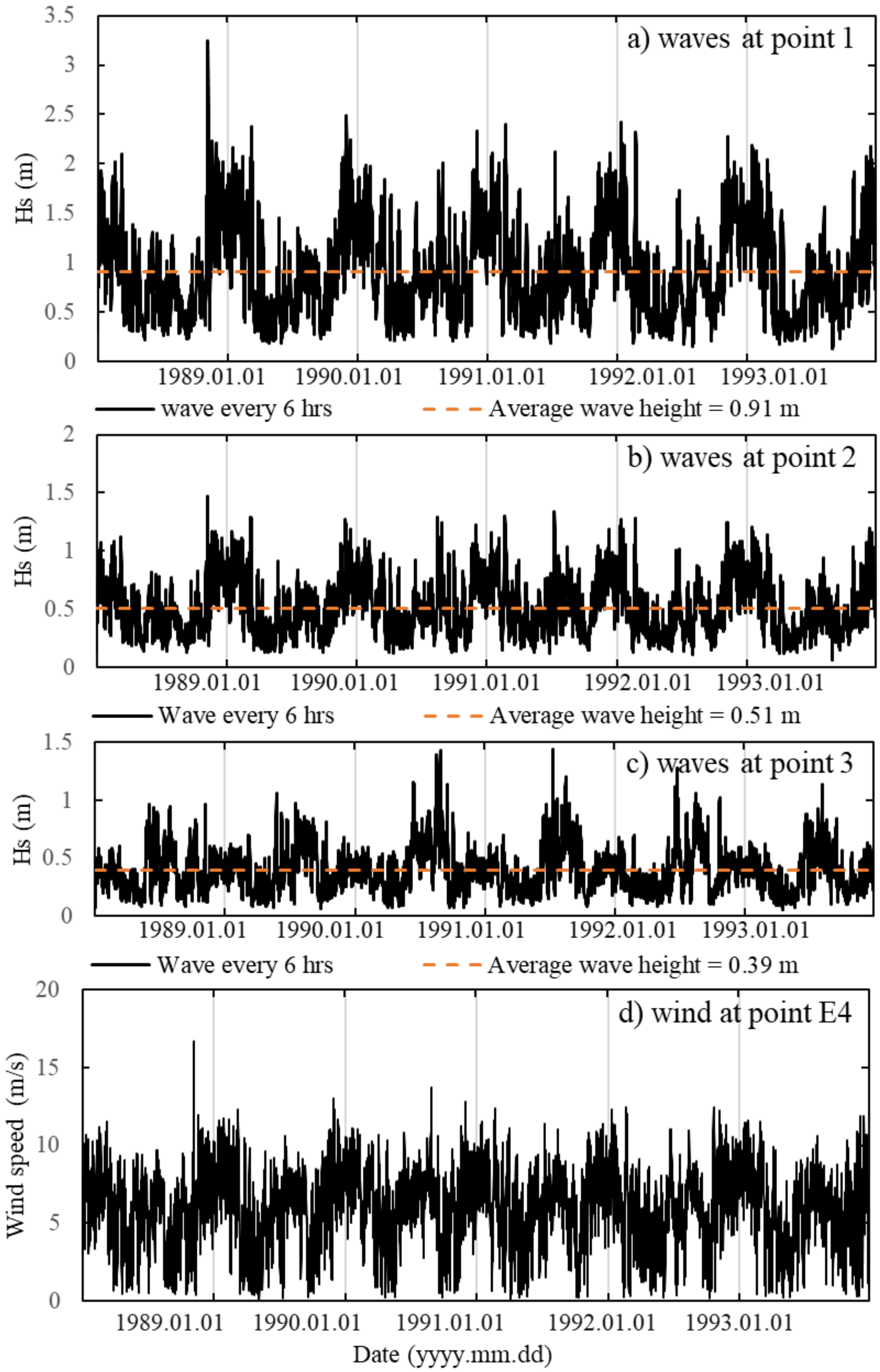

Figure 5-7 Wave pattern from 1988 to 1993 of
a) point 1, b) point 2, and c) point 3,
d) Wind pattern from 1988 to 1993 at point E4

However, at point 3, the wave height pattern was different. It was lower during the NE season when the wind speeds were higher. This disparity can be attributed to the presence of the Mui Ne headland on the east side of the bay, which acts as a barrier, preventing the waves generated by the NE wind from reaching point 3.

Comparing wave characteristics at different locations, point 1, point 2, and point 3 revealed variations influenced by factors such as water depth, wind characteristics, and bathymetry as shown in Figure 5-6 and Table 5-3.

The significant wave height (Hs) tended to be higher at point 1, where the water depth was also greater. This relationship can be attributed to factors such as bottom friction, wave shoaling, and breaking, which result in decreased wave energy.

Table 5-3 Details of waves, winds, and bathymetry at point 1, point 2, and point 3

	Point 1	**Point 2**	**Point 3**
Depth (m)	20	4.4	4.4
Median Hs (m)	0.84	0.48	0.36
Average Hs (m)	0.91	0.51	0.39
Dominant wave direction	From E And from SSW	From SE And from S	From ESE And from SSW
Wind direction		From ENE And from WSW	
Contour line direction in the East	N-S	NE - SW	NW - SE and Mui Ne headland
Contour line direction in the West	NNW - SSE	E - W	NW - SE

Wave directions were closely related to both wind direction, bathymetry, and shoreline orientation. At offshore point 1, the wave direction tended to align with the wind direction, even though with slight differences. However, the wave directions also showed sensitivity to the bathymetry, adjusting to become more perpendicular to the contour lines. At points 2 and 3, wave directions appeared to be influenced more significantly by the bathymetry rather than the wind direction. Point 2 exhibited wave directions perpendicular to both the contour lines as well as the shoreline. Point 3, which was impacted by the presence of a headland, showed a deviation from being perpendicular to the contour line close to the wave point, but remained perpendicular to the shoreline, reflecting the influence of the headland.

5.1.3 Discussion and conclusion of wave simulation

The calibration and validation processes have shown that the SWAN model was effective in simulating wave characteristics in Phan Thiet bay. The model well reproduced the average wave height, but it could not capture the full magnitude of the waves, resulting in an underestimation compared to the observed data. This limitation may be due to not simulating swell waves from storms, or not accounting for tidal effects. It is recommended that the swell and the tidal effects should be added into some numerical model to gain better results.

The SWAN model simulated the dominant wave directions, aligning closely with the observed wave data. However, the model exhibited a narrower range of wave directions compared to the observed data. This discrepancy can be attributed to the limited range of the wind input from ERA5 data, which had a narrower range compared to the observed wind data. It is recommended to collect more observed data of wind and wave for better input data and better calibration and validation processes.

The analysis of wave data revealed consistent patterns in wave heights over the years, exhibiting seasonal variations. At a distant point (point 1) and along the open coast (point 2), the wave patterns closely aligned with the corresponding wind patterns. However, in proximity to the headland (point 3), the presence of the headland significantly influenced the wave heights by obstructing incident waves.

In general, wave heights tended to be higher at the distant point compared to the waves near the coast. This difference can be attributed to wave dissipation during propagation and transformation processes along the coastal region.

Wave directions were influenced by multiple factors, including wind direction, bathymetry, and shoreline orientation. In the absence of shoreline orientation, the wave direction at the distant point was primarily shaped by the wind direction and the seabed characteristics. As waves approached the coast, all three factors, wind direction, bathymetry, and shoreline orientation, played a significant role in determining wave directions, with the shoreline orientation at the headland causing a notable influence.

The SWAN model was employed to provide data for the GENESIS shoreline simulation model due to the limited availability of observed wave data in Phan Thiet bay, although observed wave data was considered the most accurate input. The comparison between the GENESIS results obtained using observed wave data and simulated wave data from SWAN, as shown in Figure 5-8, revealed minimal differences. This was further supported by the Mean Absolute Error Difference of EPR, indicating a reasonably close match between the two. Hence, the simulated wave data from SWAN could serve as an alternative choice for input in the GENESIS model. However, to attain a more accurate outcome, it is recommended to conduct measurements of observed wave data.

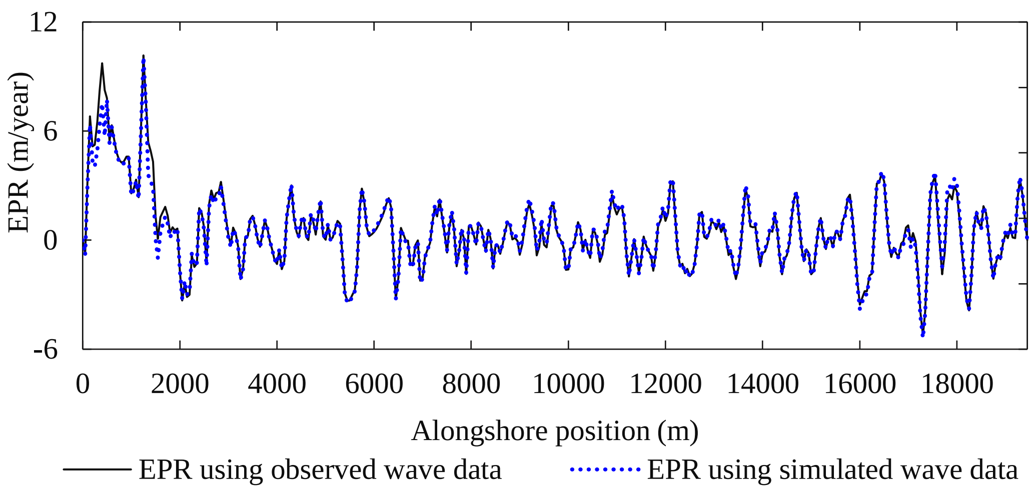

Figure 5-8 The comparison of GENESIS result by using observed wave data and simulated wave data

5.2 Shoreline simulation setup

This section provides the results of GENESIS shoreline simulation model including (1) results of calibration and validation of shoreline simulation in 3 segments of study area, and (2) sediment transport result corresponding to the calibration result.

In all 3 segments, X axis and Y axis originated from the starting point of each segment as shown in Figure 5-9, Figure 5-10, and Figure 5-11. The value of Y was used to determine the location of the shoreline at every 50 m interval of X (m). In segment 1, at the left boundary of the GENESIS simulation, Ca Ty, X was set to 0 m, while at the right boundary, Ke Ga, X was set to 19450 m as shown in Figure 5-9. In segment 2, at the left boundary of the GENESIS simulation, Phu Hai, X was set to 0 m, while at the right boundary, Tien Thanh, X was set to 11850 m as shown in Figure 5-10. In this segment, there were 2 rivers which are Phu Hai river and Ca Ty river. The simulation of shoreline change was assessed in 3 parts separated by Phu Hai river and Ca Ty river. In segment 3, at the left boundary of the GENESIS simulation, Lang Chai, X was set to 0m, while at the right boundary, Ong Dia, X was set to 9550 m as shown in Figure 5-11.

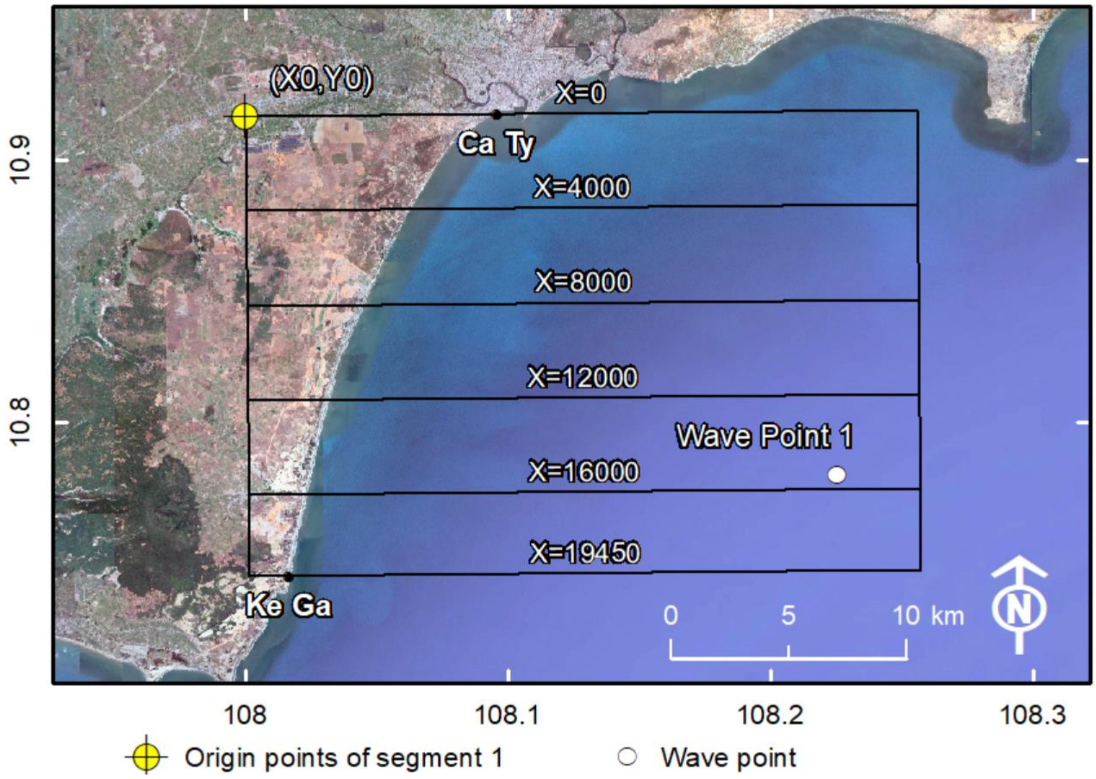

Figure 5-9 Calculation system of segment 1

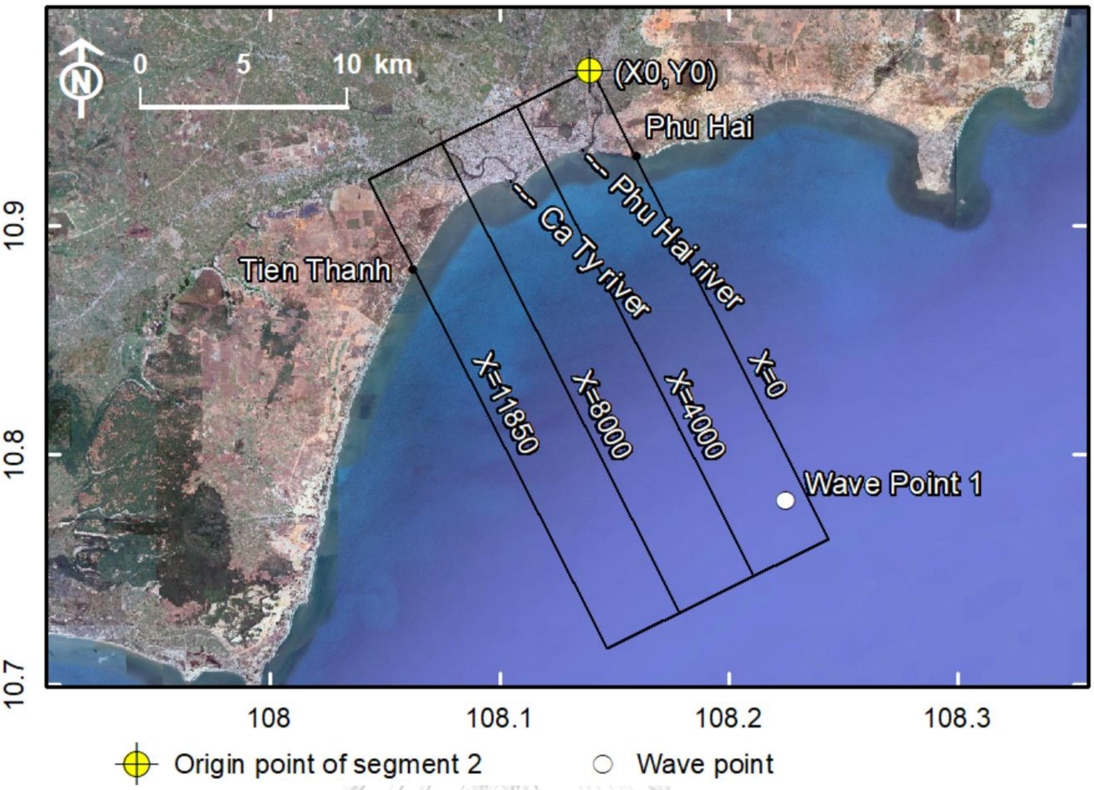

Figure 5-10 Calculation system of segment 2

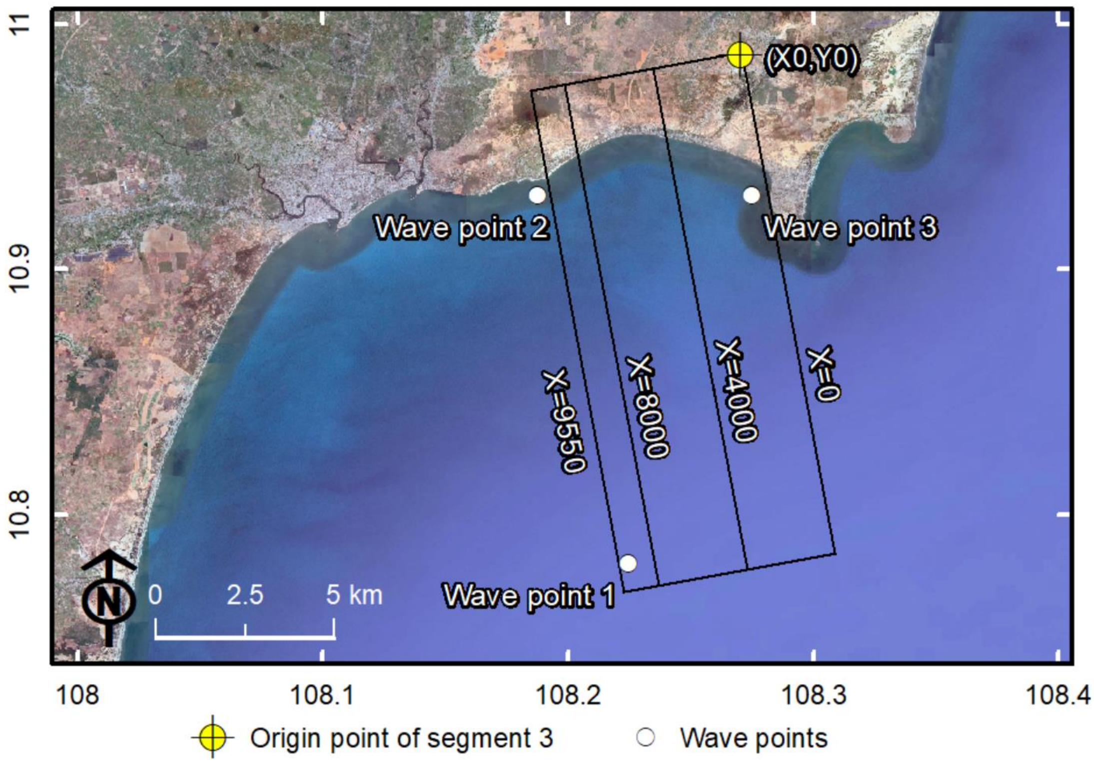

Figure 5-11 Calculation system of segment 3

5.2.1 Calibration and validation of shoreline simulation

In this study, the calibration process was conducted to optimize several key parameters of the GENESIS model, including the azimuth angle, K1, depth of closure (D_c), sediment size (D_{50}), berm height (D_b), and K2 as shown in Table 5-4 with more details of calibration process in APPENDIX I. The calibration involved the comparison between the simulated shoreline change and the actual shoreline change, as measured by the shoreline position (Y) in meters, Net Shoreline Movement (NSM) in meters, and EPR in meters per year. Following the calibration, a validation process was carried out to verify the model's capability in simulating shoreline changes in Phan Thiet bay. Mean Absolute Error (MAE) was used for evaluating how well the model predictions match the observed data, including MAE of shoreline position (Y) and MAE of EPR.

Table 5-4 Set of parameters of 3 segments (calibration result)

Segment	Azimuth angle	K1	D_c (m)	D_{50} (mm)	Berm height D_b (m)	K2
1	0	0.1	9	0.25	0.6	0.2
2	334	0.1	9	0.2	0.2	0.2
3	350	0.1	9	0.25	0.2	0.2

Not only the shorelines were used for the comparison, NSM and EPR also were used due to the big scale of the whole shoreline segment compared to the net shoreline movement, and it was difficult to visualize and discuss with only shoreline position. Net shoreline movement was the cross-shore movement of the shoreline from initial year to final year, while EPR was NSM divided the number of the years during that time. Therefore, NSM and EPR had the same pattern. EPR which showed the rate of shoreline change per year, was used as the determination parameter for comparing the shoreline change rate among different periods of time.

Calibration and validation of segment 1

The calibration of the model in segment 1 was performed by simulating from 07 Jan 1988 to 09 Mar 1993 (about 5 years). In segment 1, the comparison of the actual EPR and the simulated EPR in Figure 5-12 showed that the simulated EPR closely followed the pattern of the actual EPR, with only minor deviations that the magnitudes of EPR were slightly different at some locations. However, it can be observed that the shoreline evolution of erosion and accretion is correctly simulated in most of the positions. The MAE of shoreline position was found to be 13.27 m. The MAE of EPR was 2.57 m/year. Overall, the calibration results showed that GENESIS could simulate the shoreline evolution in the study area.

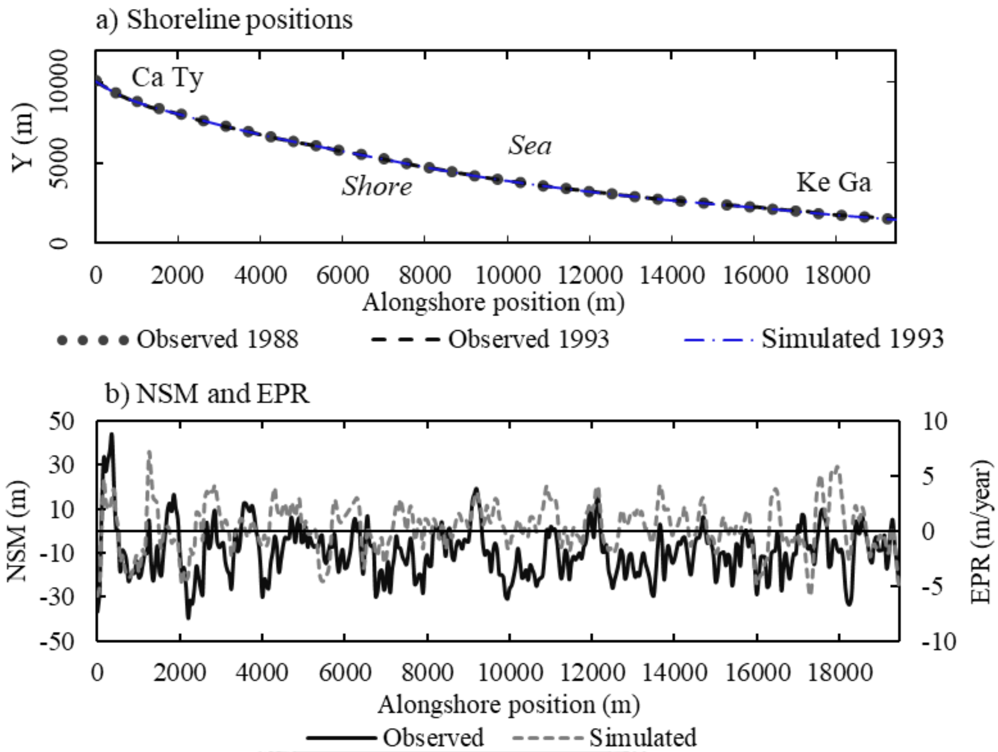

Figure 5-12 Calibration result of segment 1 (07 Jan 1988 to 09 Mar 1993)

The results of the validation, shown in Figure 5-13, provided strong evidence that the simulated EPR was in good agreement with the actual EPR for most shoreline positions. Although some minor differences exist in the magnitudes of EPR at certain locations, the model correctly captured the shoreline erosion and accretion evolution. Although there was a slight shift in the estimated location of accretion, the model still produced satisfactory results. Near Ca Ty boundary, in this validation phase, the model could not simulate the erosion, which was different from calibration phase. The MAE was only 6.82 m for shoreline position (which was lower than in the calibration phase), and 3.71 m/year for EPR (which was more or less the same as in the calibration phase).

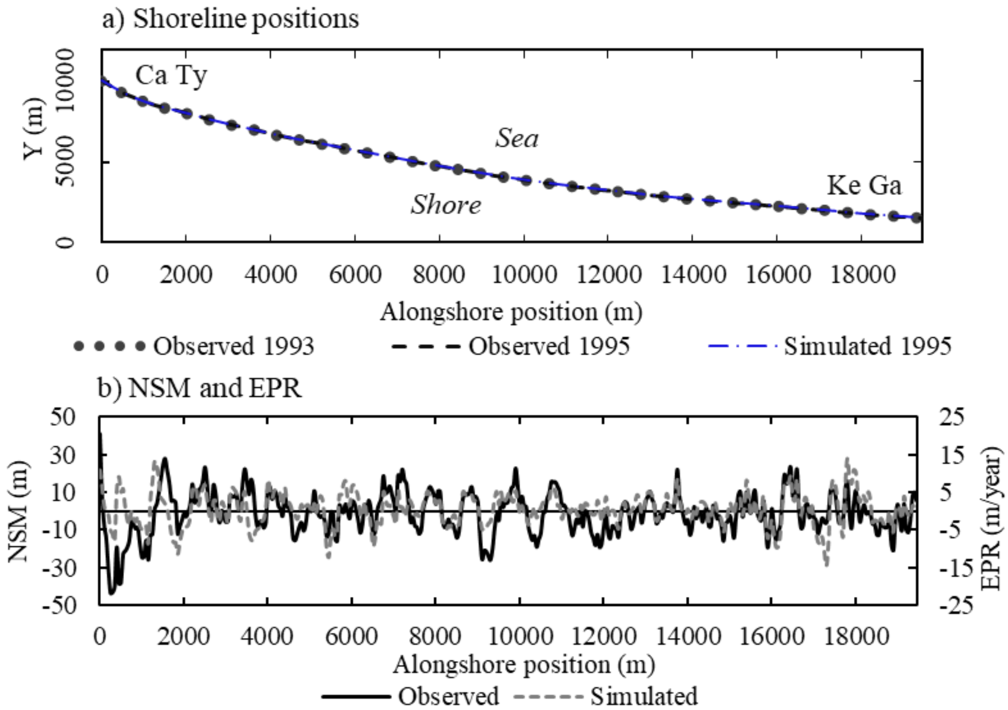

Figure 5-13 Validation result of segment 1 from 09 Mar 1993 to 10 Jan 1995

Calibration and validation of segment 2

The model calibration in segment 2 involved simulating from 03 Jan 2004 to 15 Feb 2008 in 3 parts as shown in Figure 5-14. Part 1 of segment 2, located near Jetty Ca Ty 1, included beach reclamation project Hamby that was simulated in segment 1 as well. The calibration generally gave a good result in this part with MAE of 14.12 m for the shoreline, and 9.08 m/year for EPR. Notably, the simulation could capture the erosion occurring downdrift of Hamubay, aligning closely with the actual shoreline changes.

In part 2 of segment 2 which located between two rivers, despite extensive efforts in calibration process to achieve the highest level of accuracy, the model failed to capture the shoreline evolution in this specific area with MAE 37.40 m of the shoreline and 10.47 m/year of EPR. The actual shoreline exhibited a relatively stable pattern with a low EPR. However, the GENESIS model produced a result indicating significant erosion downstream of Jetty Phu Hai 1.

The calibration results for part 3, characterized by a complex shoreline shape compounded by the presence of nearby structures, demonstrated a generally good alignment between the calibrated EPR values and the actual EPR, effectively capturing the shoreline's erosion and accretion patterns at most shoreline positions with MAE 29.65 m for the shoreline, and 11.21 m/year for the EPR. However, some deviations existed where the EPR magnitudes differed at some locations.

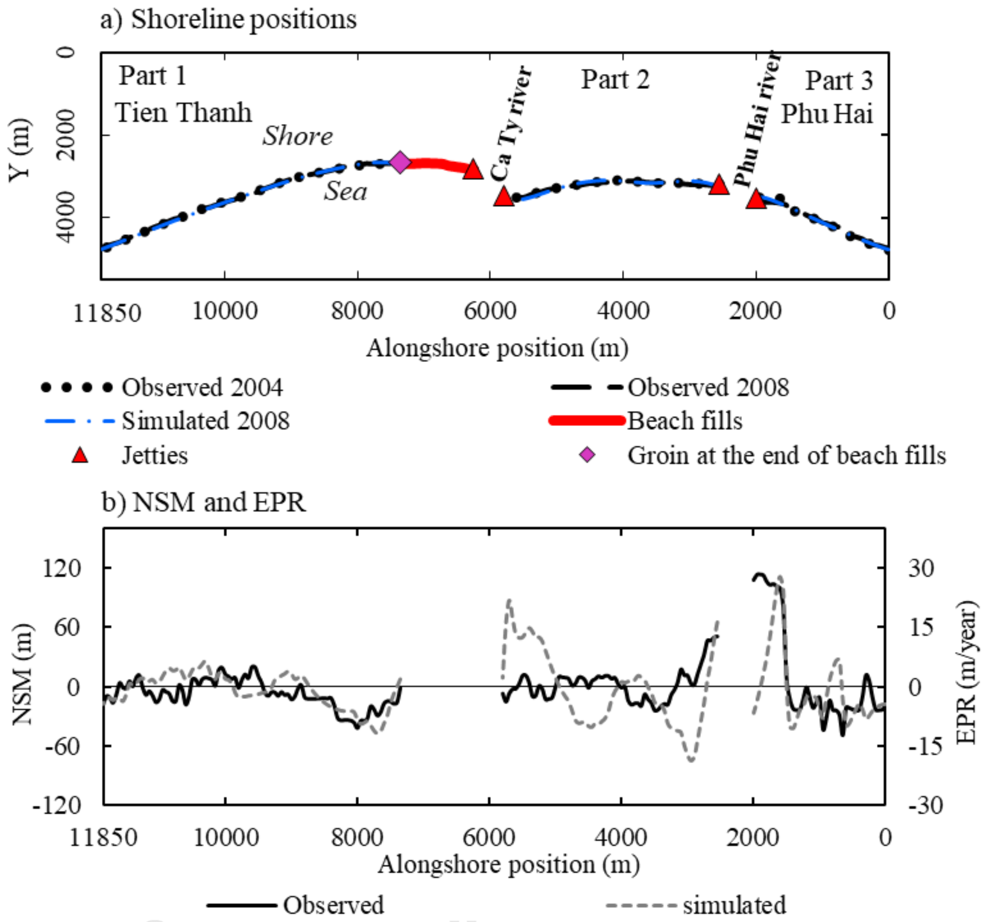

Figure 5-14 Calibration result of segment 2 (03 Jan 2004 to 15 Feb 2008)

The validation results of segment 2, shown in Figure 5-15, exhibited similarities to the calibration outcomes with slightly diminished performance. Despite the disparities in the magnitudes of the EPR between the simulated and actual shoreline changes in part 1, their patterns aligned closely, exhibiting comparable locations of peaks and troughs. In part 2 and part 3, the model struggles to capture the shoreline change pattern. The MAE of this period according to each part is shown in Table 5-5. Generally, GENESIS ineffectively simulated the shoreline change in segment 2.

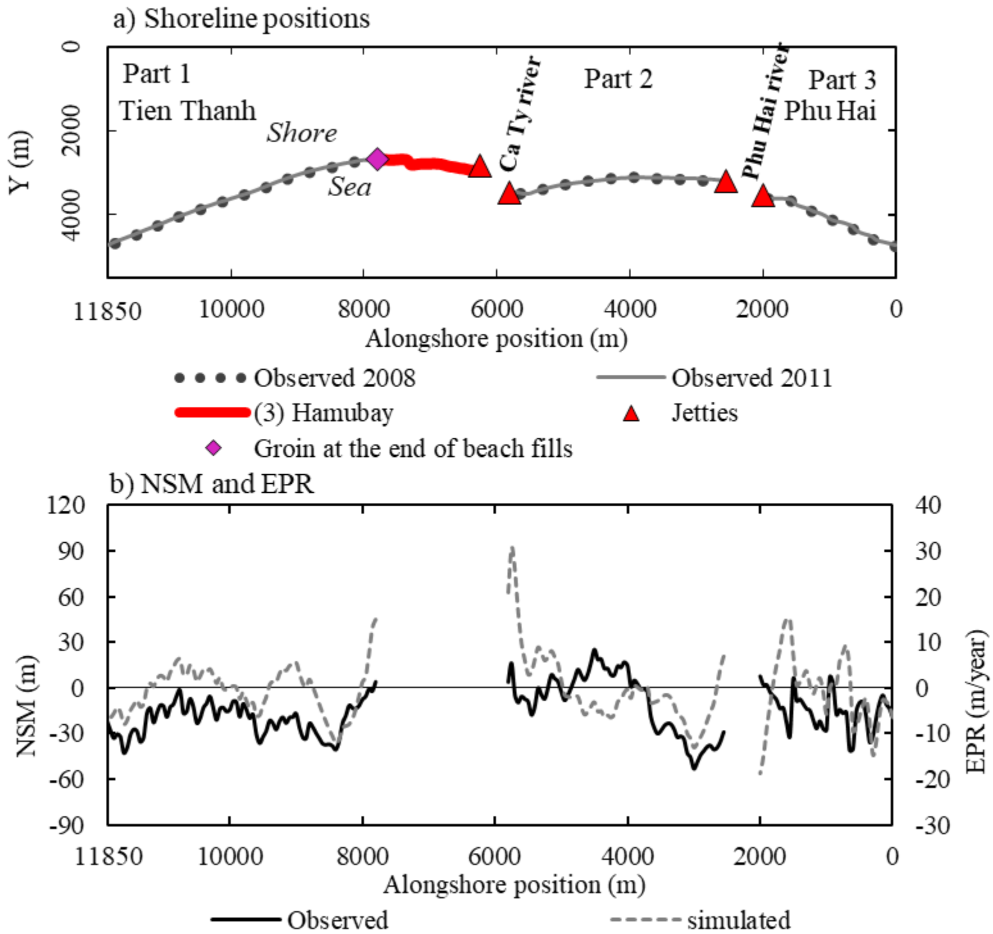

Figure 5-15 Validation result of segment 2 (15 Feb 2008 to 15 Mar 2011)

Table 5-5 The MAE of GENESIS from 2008 to 2011 in segment 2

Simulation	MAE of Y (m)	MAE of EPR (m/year)
Part 1	27.78	6.30
Part 2	25.37	11.58
Part 3	20.99	10.60

Calibration and validation of segment 3

The calibration of the model in segment 3 was performed by running the simulation from 07 Jan 1988 to 09 Mar 1993 (about 5 years) as the result shown in Figure 5-16. The calibration results for segment 3, revealed a general agreement between the calibrated EPR values and the actual EPR, effectively capturing the erosion and accretion patterns along the shoreline, with consistent peak and trough locations. The calibration process yielded a MAE of 8.31 m for the shoreline and 4.24 m/year for the EPR. However, some discrepancies were observed, particularly in the magnitudes of the EPR at some locations, where the actual shoreline change exhibited erosion, whereas the simulation showed a combination of erosion and accretion with a relatively small magnitude.

The set of parameters in segment 3 was validated by running simulations from 1993 to 1996. The validation results, presented in Figure 5-17, strongly support the agreement between the simulated EPR and the actual EPR for most shoreline positions. However, minor differences in EPR magnitudes were evident at certain locations, where the actual shoreline experienced erosion while the simulation showed greater stability. The MAE was found to be only 6.71 m for shoreline position (which is lower than in the calibration phase) and 4.59 m/year for EPR (which is more or less the same as in the calibration phase). Despite the slight deviations in magnitude, the calibrated GENESIS model successfully captured the general behavior and trends of shoreline dynamics in segment 3.

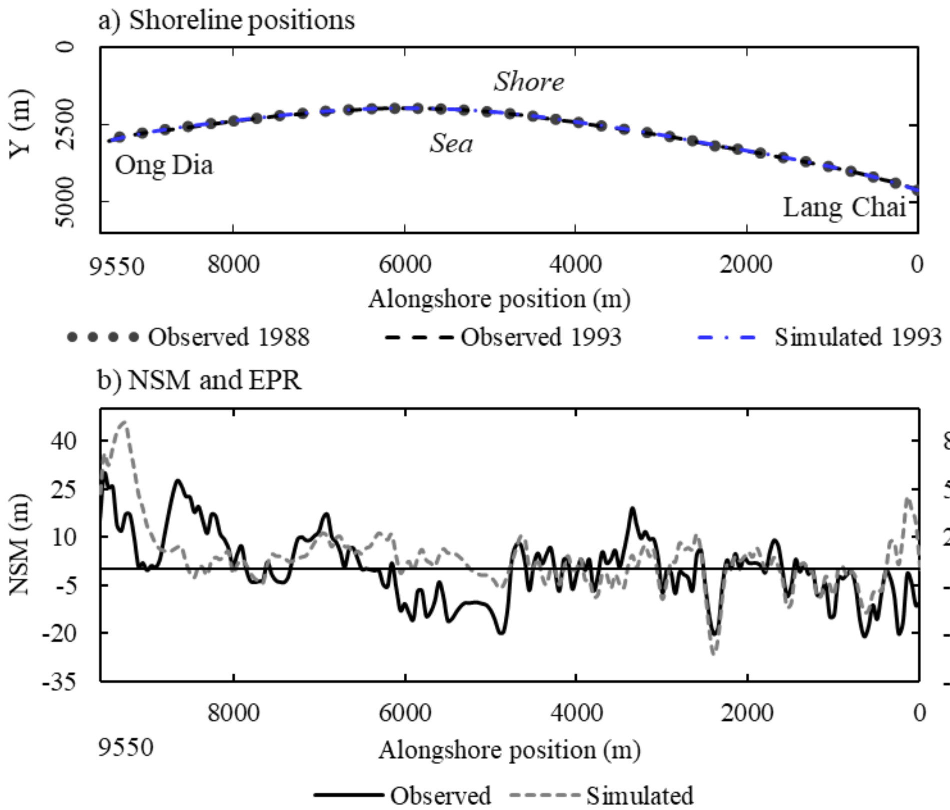

Figure 5-16 Calibration result of segment 3 (07 Jan 1988 to 09 Mar 1993)

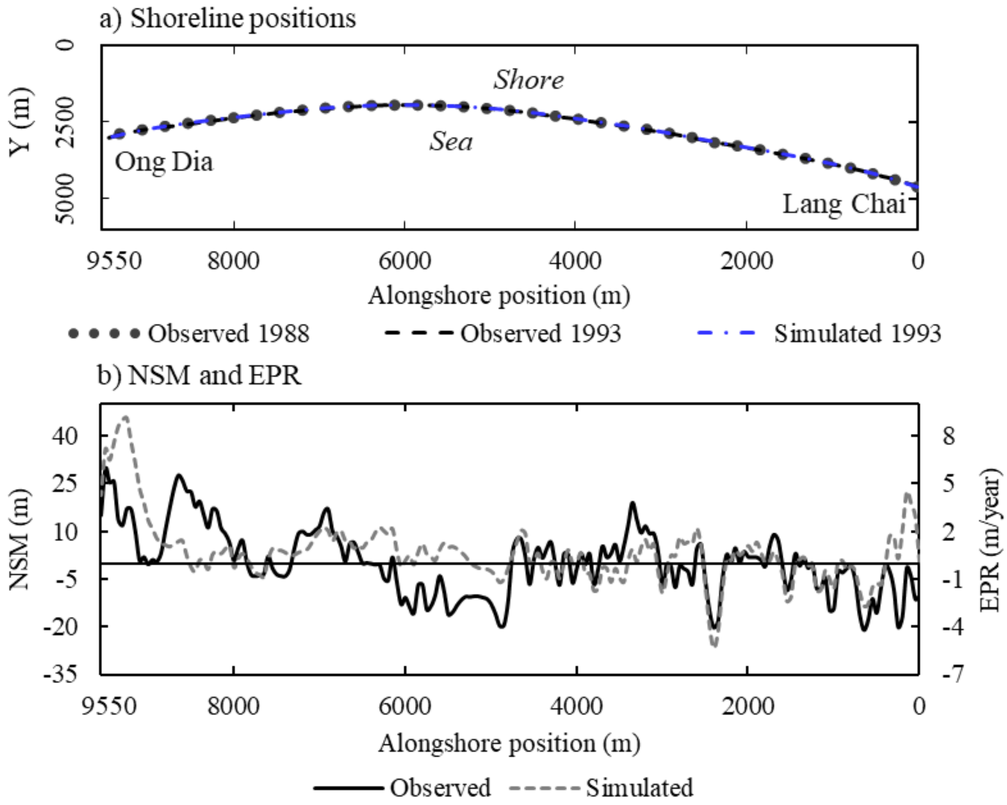

Figure 5-17 Validation result of segment 3 from 09 Mar 1993 to 04 May 1996

GENESIS effectively captured the shoreline positions with the EPR pattern aligning well with the actual EPR in order to provide valuable insights into the shoreline change evolution in segment 1 and segment 3, but not in segment 2. The current results demonstrated the model's reliability and highlight its potential as a useful tool for further part of this study.

5.2.2 Sediment transport results

The net longshore transport rate is the balance between the longshore sediment transport toward 2 directions. In all 3 segments, the net longshore transport rate was positive as shown in Figure 5-18, Figure 5-19, and Figure 5-20, indicating a same dominant sediment transport direction from Ca Ty to Ke Ga in segment 1, Phu Hai to Tien Thanh in segment 2, and Lang Chai to Ong Dia in segment 3. This sediment transport direction aligned with the expected sediment transport patterns in the study area, which was supposed to be influenced by the main wave direction from East and from SE, while the shoreline orientation from North-Northeast (NNE) to South-Southwest (SSW) as shown in Figure 5-21.

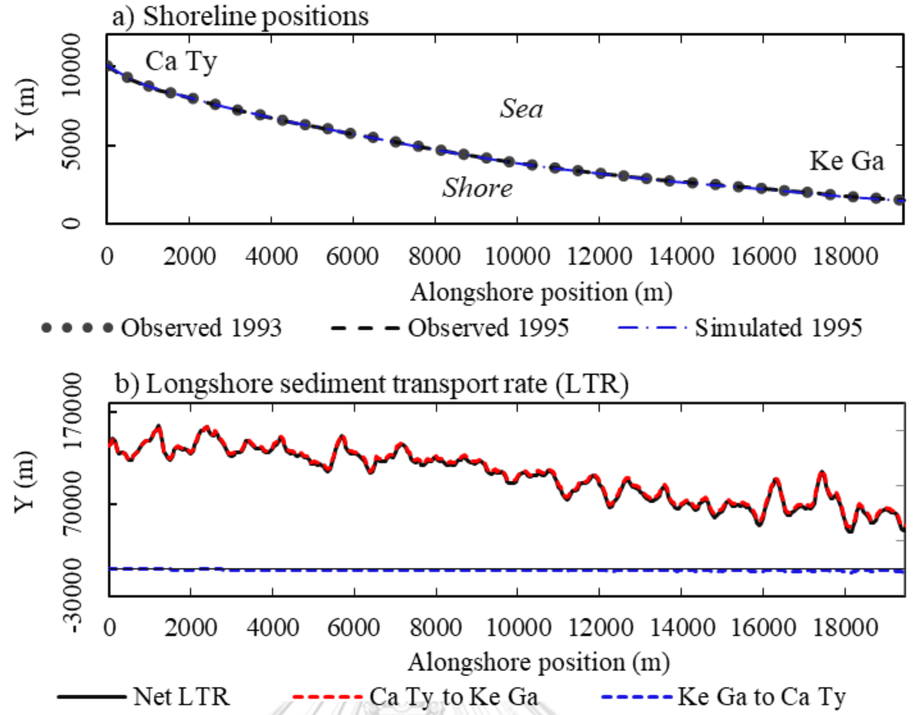

Figure 5-18 Longshore sediment transport rate of segment 1 from 1988 to 1993

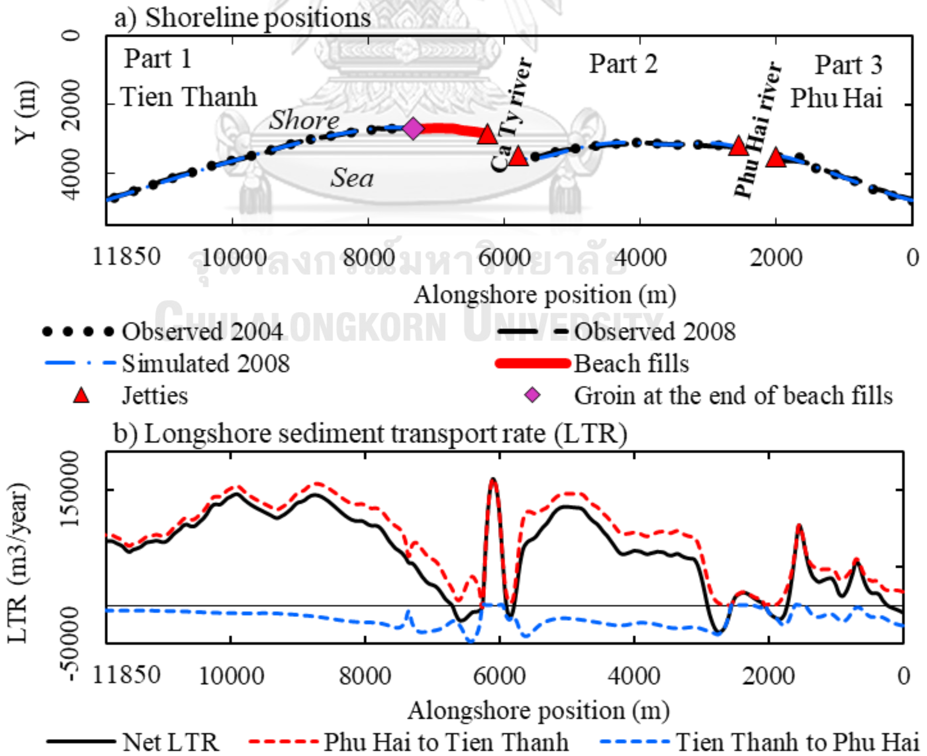

Figure 5-19 Longshore sediment transport rate of segment 2 from 2004 to 2008

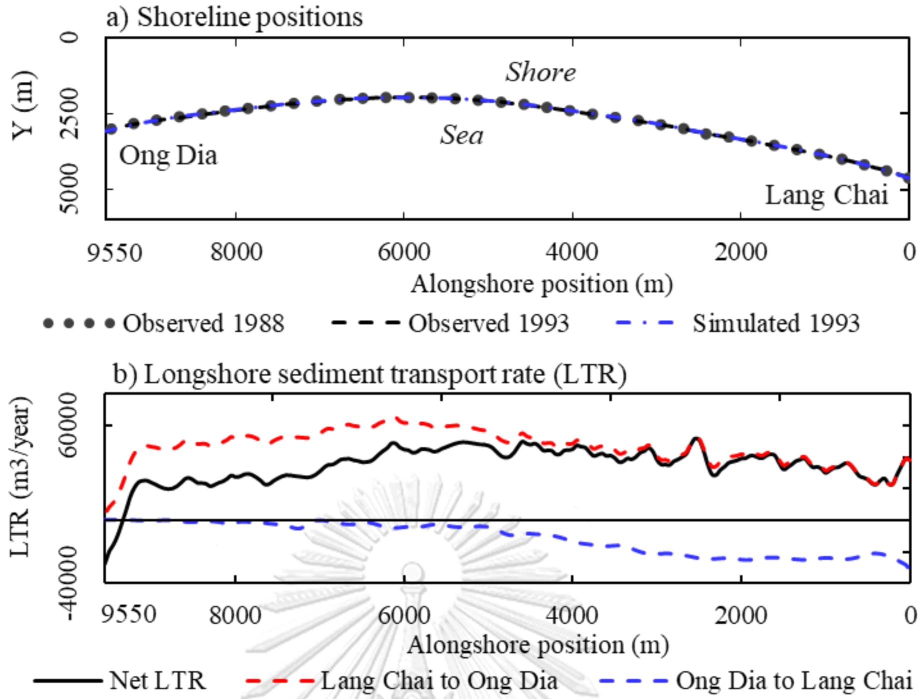

Figure 5-20 Longshore sediment transport rate of segment 3 from 1988 to 1993

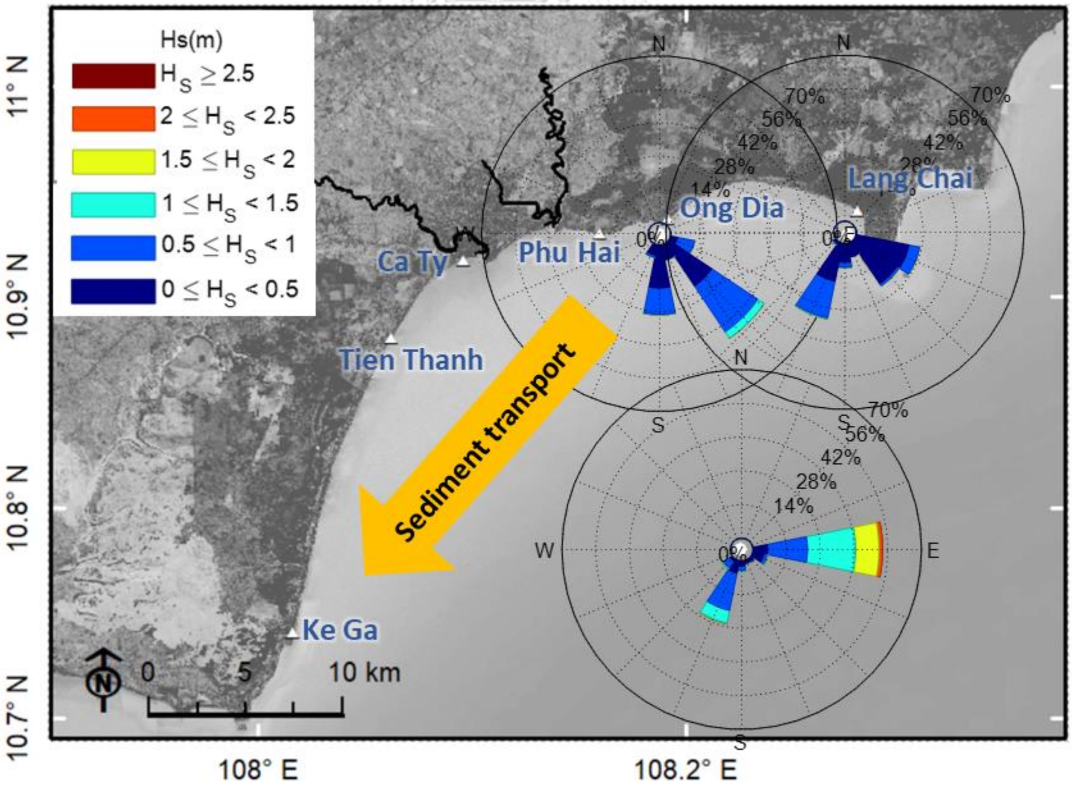

Figure 5-21 Sediment transport direction, shoreline orientation, and wave characteristics from 1988 to 1993

5.3 Simulations for structure effects on shoreline

In all three segments of Phan Thiet bay from 1988 to 2021, various structures were built along the coast including beach reclamation project, jetties, groins, and seawalls. The previous part of this study showed that those structures likely gave the impacts to the shoreline. It is necessary to investigate those effects, which was done by comparing the shoreline change in the case of with and without structures.

The impact of the Hamubay reclamation project on shoreline change was done in segment 1 from 2004 to 2021. The effects of four jetties near two river mouths was examined from 2011 to 2018 in segment 2. The effects groins in segment 3 was done from 2017 to 2021. The effects of 4 seawalls in segment 3 were done from 2006 to 2017. The following showed the performance of GENSIS on simulating the shoreline change, and the result of shoreline change with and without structures including beach reclamation project, jetties, groins, and seawalls.

5.3.1 Beach reclamation project

The Hamubay beach reclamation project was located in segment 1 near Ca Ty river as shown in Figure 3-5. It was extended from 2004 to 2021 as in Figure 5-22. To capture the variability of the project's progress, the simulation period would be divided into 5 periods starting in 2004 and ending in 2008, 2011, 2014, 2018, and 2021. This approach allowed for the observation of the effect of the beach reclamation project on the shoreline after each period, taking into account the starting year of the project and the length of extension during the considering time.

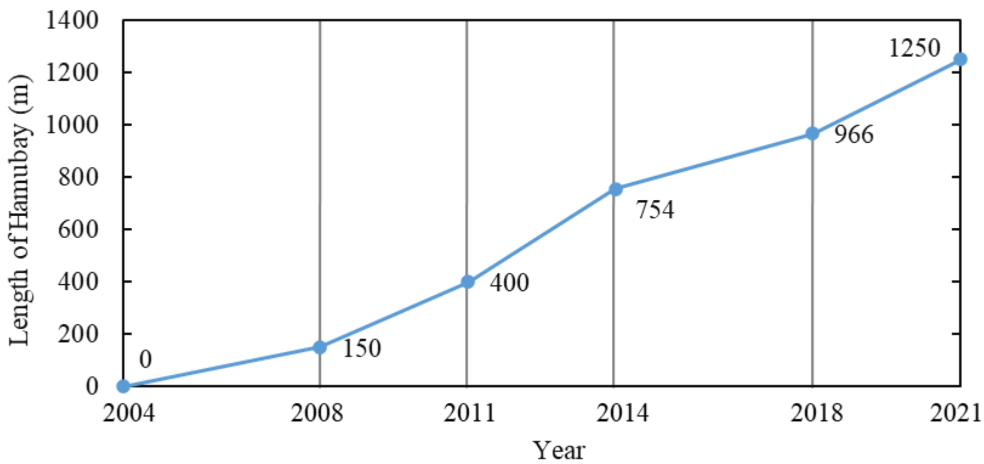

Figure 5-22 Accumulative length of beach reclamation project Hamubay by time

In Genesis, there was no available option to assign the beach reclamation project into the model. The beach reclamation project involves the process of filling an area of the sea to create new land, and in this case, it was protected by a seawall along the edge of the beach fills as shown in Figure 5-23. Based on the test of multiple simulations as more details in APPENDIX F, the beach reclamation project Hamubay was assigned to the GENESIS model as beach fills with a groin at the end for the period between 2004 to 2018. However, for the simulation with the final year of 2021, where the end of the beach reclamation project was more aligned with the shoreline, it is suggested to adjust the initial shoreline to match the final edge of Hamubay and add a seawall along that edge.

Figure 5-23 Beach reclamation project Hamubay

From 2004 to 2021, the simulated EPR values tracked closely the actual EPR, showcasing a strong agreement between the model's predictions and the actual shoreline changes as shown in Figure 5-24. The MAE for the shoreline position was calculated to be 10.70 m, while the EPR's MAE stood at 0.62 m/year, affirming the accuracy of the model. GENESIS captured the erosion downdrift of Hamubay reclamation project well. The model captured the general pattern of shoreline change, with areas near the beach reclamation project experiencing more significant changes compared to distant areas. Besides the overall agreement between the simulated and actual EPR values, minor deviations are present. For example, between X=9000 m and X=11000 m, the actual shoreline exhibited minimal change. However, the model predicts shoreline accretion, which aligned with the calibration phase. This indicated the effectiveness of the GENESIS model in simulating the shoreline with the beach reclamation project Hamubay from the start year 2004 to 2021.

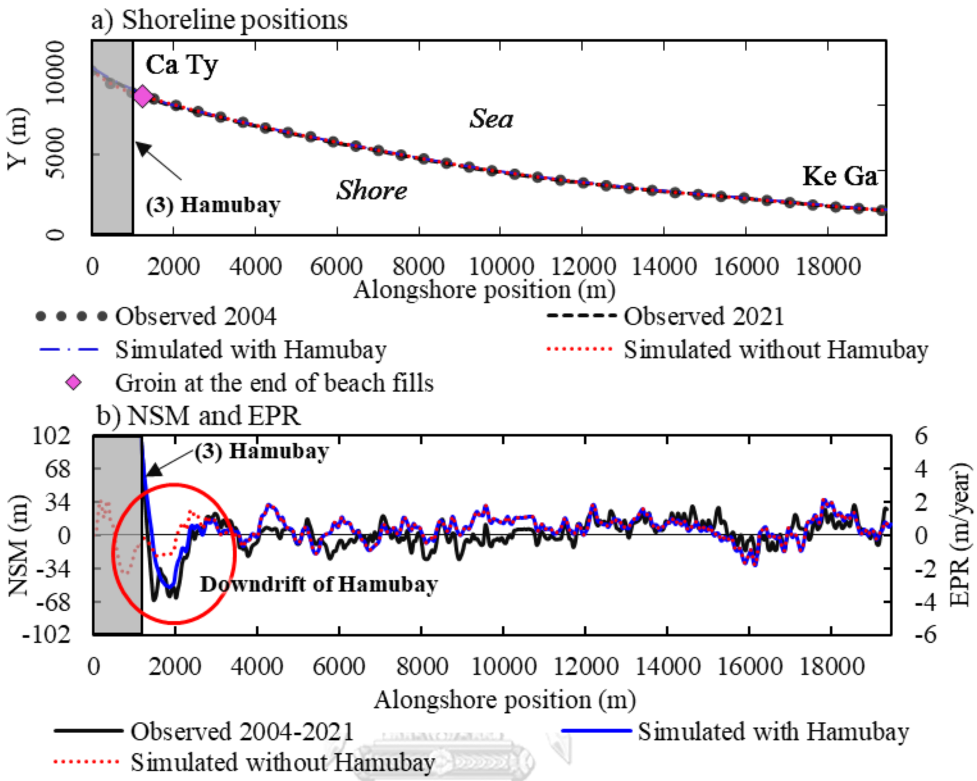

Figure 5-24 Simulation results with and without Hamubay project from 2004 to 2021 in segment 1

The simulation results, with and without the presence of the Hamubay beach reclamation project from 2004 to 2021, were shown in Figure 5-24 and zoomed in as presented in Figure 5-25. In the down-drift area, the simulation with Hamubay showed a higher erosion rate (-3.11 m/year) compared to without it (-1.23 m/year) as shown in Table 5-6. The erosion area with Hamubay was 5.0 ha (2.1 ha more than without it), and the accretion area with Hamubay (29.1 ha) was higher than without it (2.4 ha), a difference of 26.7 ha due to external land fill.

However, beyond 1600 m from Hamubay, no significant difference was observed. This observation indicated that the influence of Hamubay was localized, primarily affecting areas in close proximity to the project.

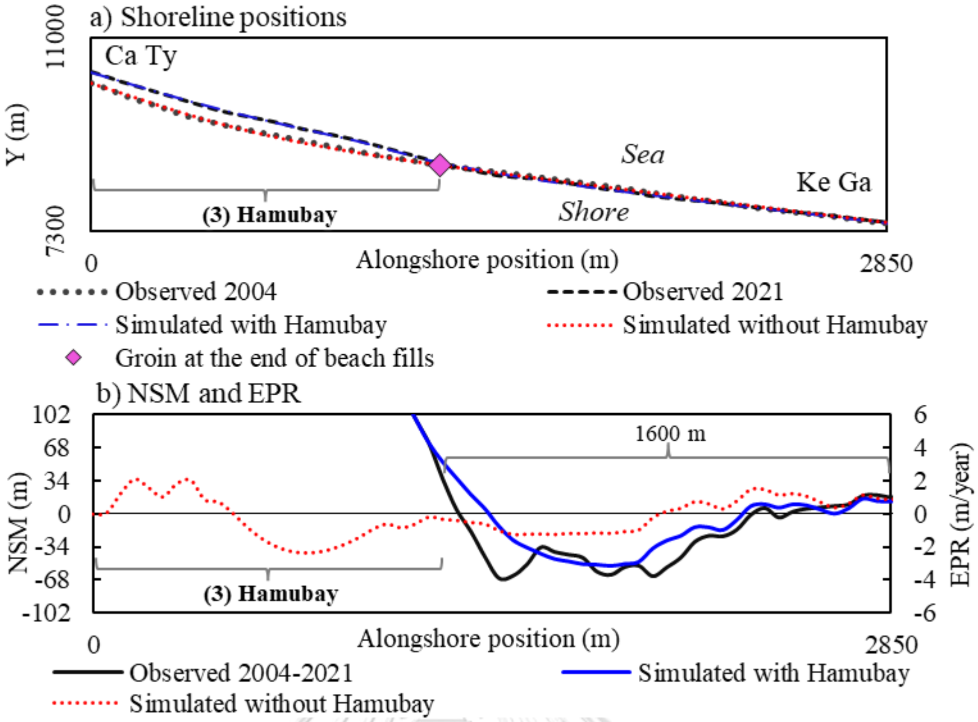

Figure 5-25 Simulation results with and without Hamubay project from 2004 to 2021 at affected area of Hamubay project

Table 5-6 Comparison of simulated shoreline changes of with and without the Hamubay beach reclamation project

	Without beach reclamation project	**With beach reclamation project**	**Diff**
Maximum erosion rate (m/year)	-1.23	-3.11	-1.88
Erosion area (ha)	-2.9	-5.0	-2.1
Accretion area (ha)	2.4	29.1	26.7
Balance (ha)	-0.5	24.1	24.6

GENESIS could simulate the shoreline change from 2004 to 2021 with the presence of the Hamubay beach reclamation project. To capture how the shoreline responded to the step-by-step expansion of the that structure over time, four additional simulations were conducted.

Shoreline evolution during the construction of beach reclamation projects

The results of periods from 2004 to each year of 2008, 2011, 2014, 2018 with and without Hamubay reclamation project were shown in Figure 5-26 to Figure 5-29, respectively. Overall, the simulated shoreline changes incorporating the Hamubay beach reclamation project (beach fills and the groin) exhibited a satisfactory agreement with the observed shoreline changes in most locations, as seen in previous periods of segment 1. The Mean Absolute Error (MAE) values for shoreline position and (EPR) for each period were provided in the Table 5-7. There were differences in the down-drift areas of the beach reclamation project for each period, where the simulated erosion rates were higher than the actual rates. Particularly from 2004 to 2011, the model predicts more severe erosion compared to what actually occurred.

The simulation results with and without the presence of the Hamubay beach reclamation project was shown from Figure 5-24 to Figure 5-29. All simulations provided similar results where the simulation with the beach reclamation project gave the higher rate of erosion compared to the simulation without the beach reclamation project. That meaned while reclamation project was constructed step by step, it possibly gave the higher erosion rate on shoreline downdrift.

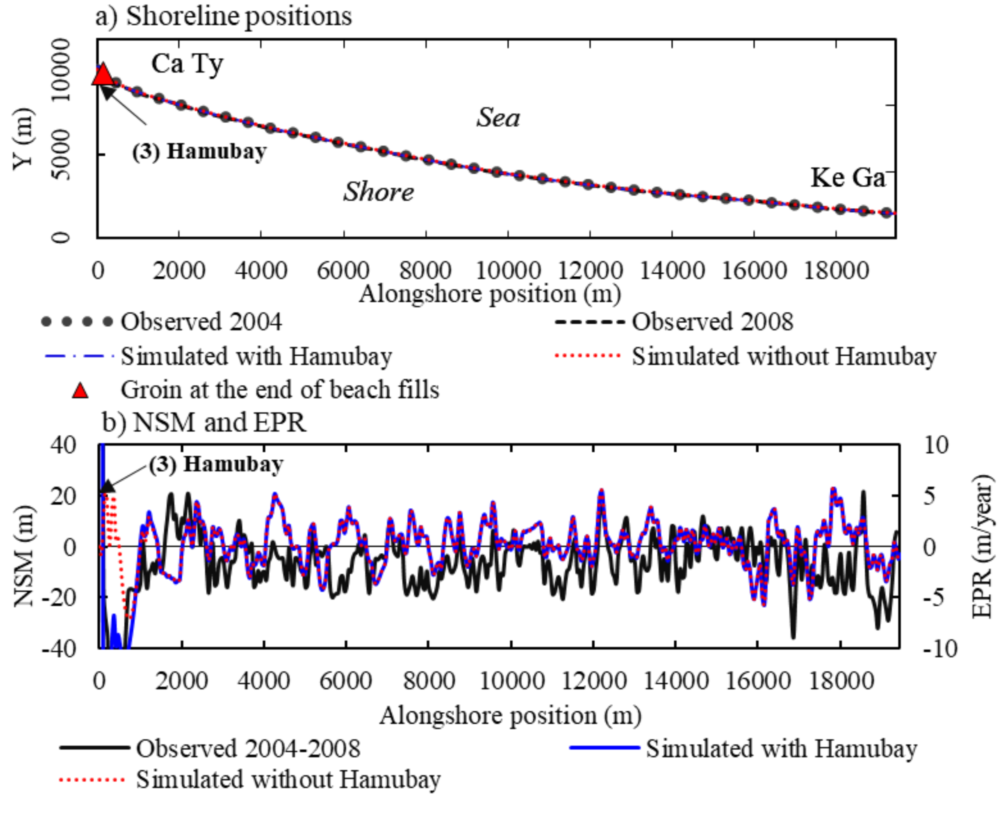

Figure 5-26 Simulation results with and without Hamubay project from 2004 to 2008 in segment 1

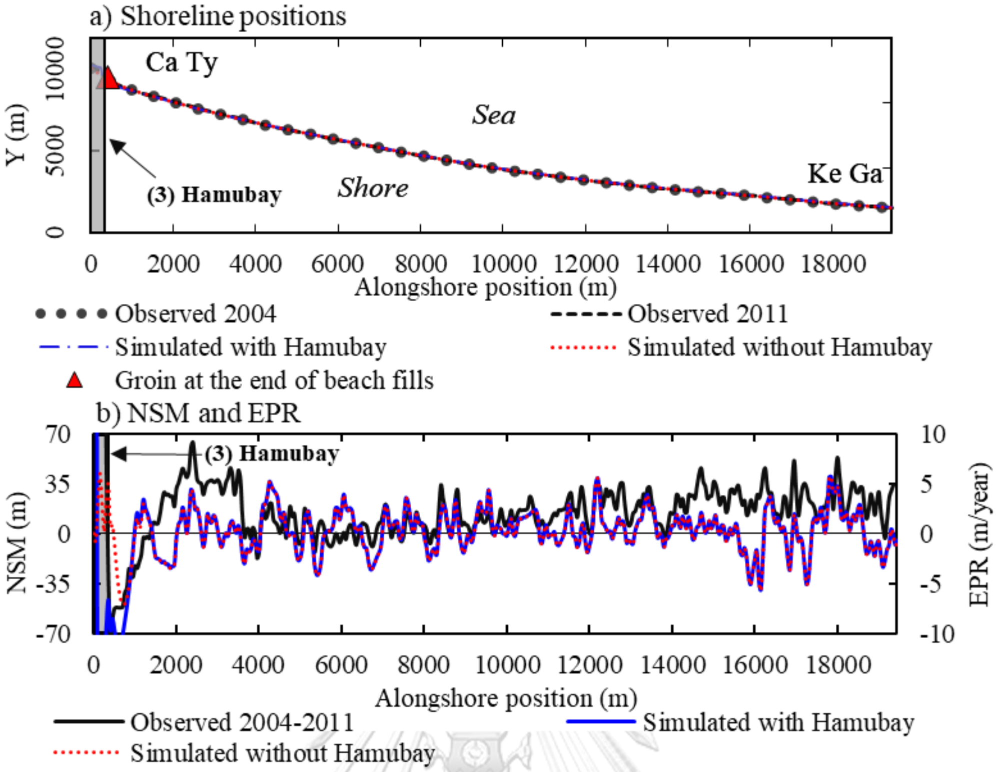

Figure 5-27 Simulation results with and without Hamubay project from 2004 to 2011 in segment 1

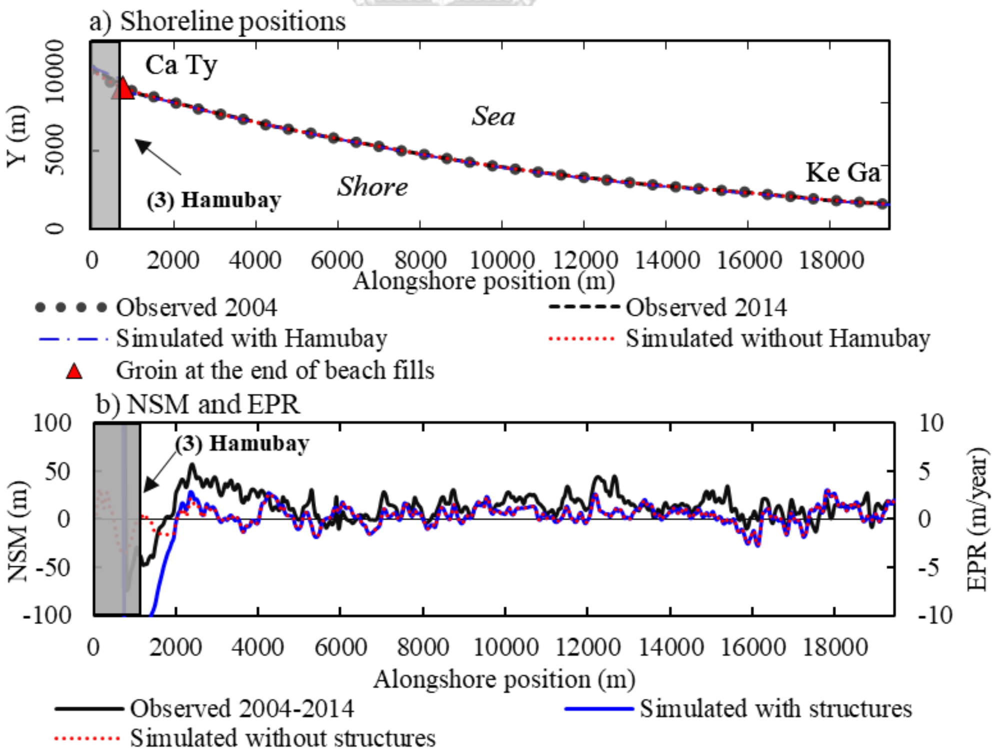

Figure 5-28 Simulation results with and without Hamubay project from 2004 to 2014 in segment 1

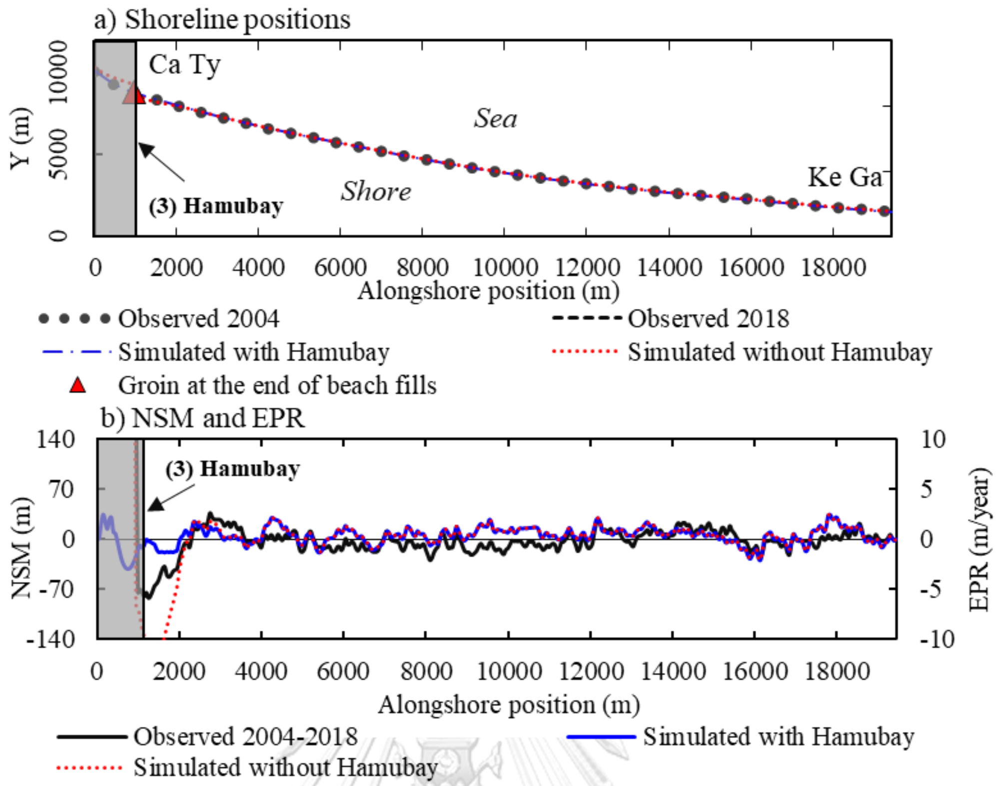

Figure 5-29 Simulation results with and without Hamubay project from 2004 to 2018 in segment 1

Table 5-7 The MAE of GENESIS from 2004 to 2021 in segment 1

Simulation	**MAE of Y (m)**	**MAE of EPR (m/year)**
From 2004 to 2021	10.70	0.62
1/ From 2004 to 2008	11.00	2.73
2/ From 2004 to 2011	19.93	3.94
3/ From 2004 to 2014	22.57	2.22
4/ From 2004 to 2018	21.50	1.52

5.3.2 Jetties

In segment 2, from 2011 to 2018, there were 4 jetties located at Ca Ty river mouth and Phu Hai river mouth as shown in Figure 3-5. The performance of the GENESIS during that time in 3 parts of segment 2, as shown in Figure 5-30, was consistent with the calibration and validation phases. In part 1 of segment 2, corresponding to the down-drift of the Hamubay beach reclamation project, the simulated magnitude was not precise; however, the locations of erosion and accretion were accurately captured. In part 2, the magnitude of the simulated EPR was much higher than the actual EPR. GENESIS captured shoreline changes in certain positions within part 3. The MAE values of shoreline (m) and EPR (m/year) for all three parts were provided in Table 5-8. Generally, GENESIS ineffectively simulated the shoreline change in segment 2.

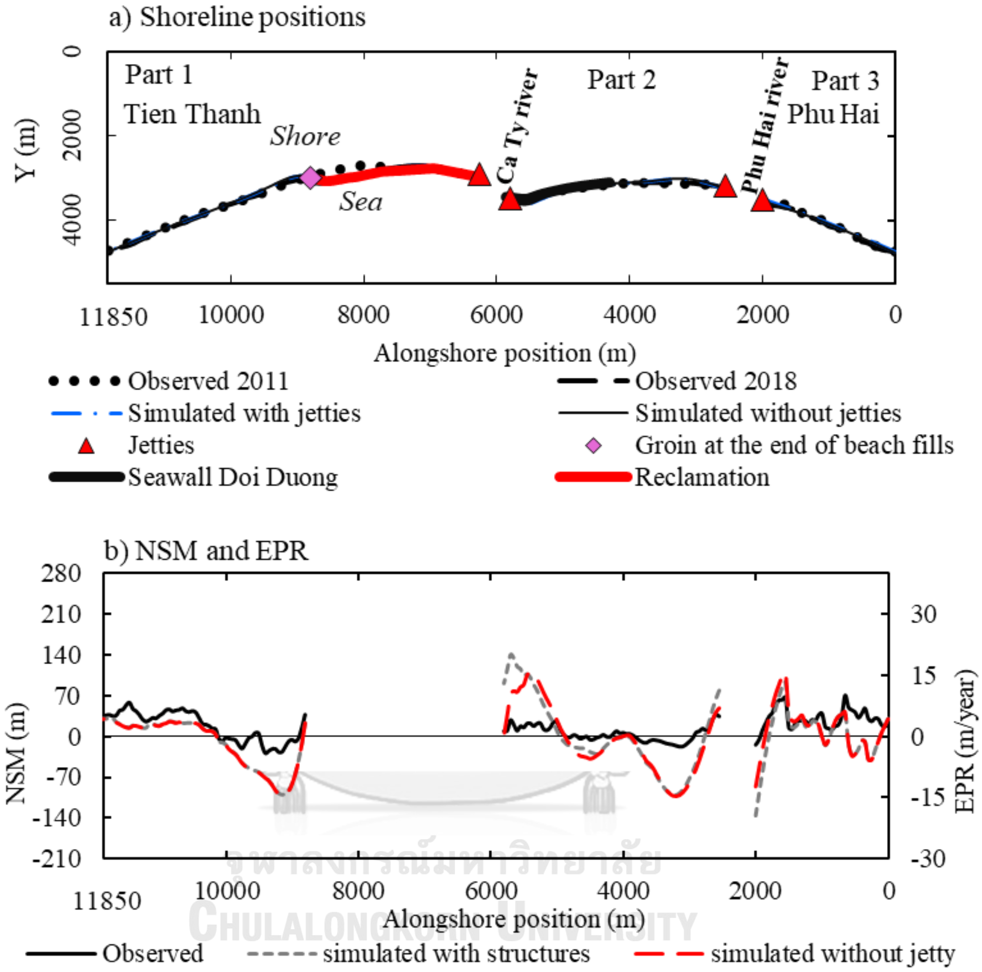

Figure 5-30 Simulation results with and without jetty from 2011 to 2018 in segment 2

Table 5-8 The MAE of GENESIS from 2011 to 2018 in segment 2

Simulation	MAE of Y (m)	MAE of EPR (m/year)
Part 1	34.04	4.96
Part 2	45.66	11.33
Part 3	17.37	15.67

From 2011 to 2018 in segment 2, the simulation results with and without four jetties showed minimal differences in shoreline change, were shown in Figure 5-30 and zoomed in as shown in Figure 5-32. Differences were observed at the shoreline of within 700 m to within 1500 m from the jetties. The simulation with jetties showed a higher maximum erosion rate (-19.5 m/year) and accretion rate (19.91 m/year) compared to without it (-12.3 m/year and 14.98 m/year, respectively) as shown in Table 5-9. The erosion area with jetties was 10.1 ha (1.6 ha less than without jetties), and the accretion area with jetties (10.4 ha) was 0.4 ha lower than without jetties (10.8 ha).

Although the shoreline change investigation gave the evidence of the increasing of shoreline change rate near the 4 jetties at Ca Ty river mouth and Phu Hai river mouth as presented in CHAPTER 4, GENESIS gave the result of minimal impact of 4 jetties on the shoreline nearby. This discrepancy could be attributed to the low performance of GENESIS in segment 2 due to the sediment supply from those rivers that was not obtained for this study.

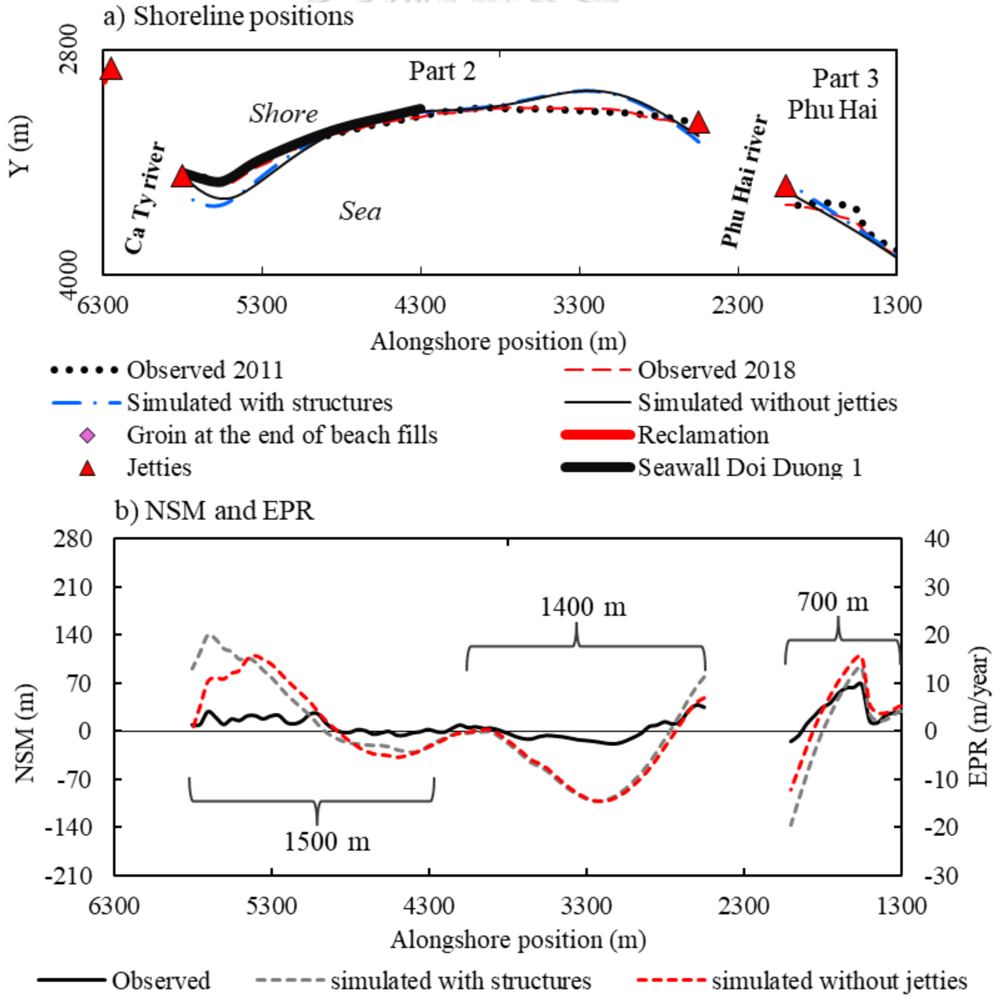

Figure 5-31 Simulation results with and without jetties from 2011 to 2018 at affected area of those jetties

Table 5-9 Comparison of simulated shoreline changes of with and without jetties

	Without jetties	With jetties	Diff
Maximum erosion rate (m/year)	-12.31	-19.53	-7.22
Maximum accretion rate (m/year)	14.98	19.91	4.93
Erosion area (ha)	-11.7	-10.1	1.6
Accretion area (ha)	10.8	10.4	-0.4
Balance (ha)	-0.9	0.3	1.3

5.3.3 Groins

In segment 3, from 15 Jun 2017 to 06 Mar 2021, there were 6 seawalls and 22 groins in total as shown in Figure 5-32. Due to the large number of the groins, the numbering system was designed to keep track on their construction year as shown the details in Table 3-5, while the smallest number represented the oldest structure.

The performance of the GENESIS model in simulating shoreline changes in segment 3 from 2017 to 2021 was shown in Figure 5-33. In this period, GENESIS exhibited shoreline changes in most of the shoreline well. However, there are some small differences of EPR magnitude at up-drift the groin, and near Ong Dia boundary, while their patterns remained consistent. The MAE values of shoreline (m), and MAE of EPR (m/year) were 9.82 m and 10.13 (m/year) respectively. Generally, GENESIS can give the shoreline change result of this segment 3 for the consideration of further purposes.

The simulation results, with and without the presence of the groins from 2017 to 2021, are shown in Figure 5-33. As expected, groins generally led to shoreline accretion updrift of them and erosion down-drift of them. In adjacent areas of those groins with the length of 300 m to 2250 m, the simulation with groins showed a higher erosion rate (-5.61 m/year) compared to without it (-4.84 m/year) as shown in Table 5-10. The maximum accretion rate with groins (10.62 m/year) was also higher than without groins (7.38 m/year). The erosion area with groins was 1.1 ha (0.8 ha more than without it), and the accretion area with groins (2.2 ha) was higher than without it (1.5 ha), exhibiting 0.7 ha difference.

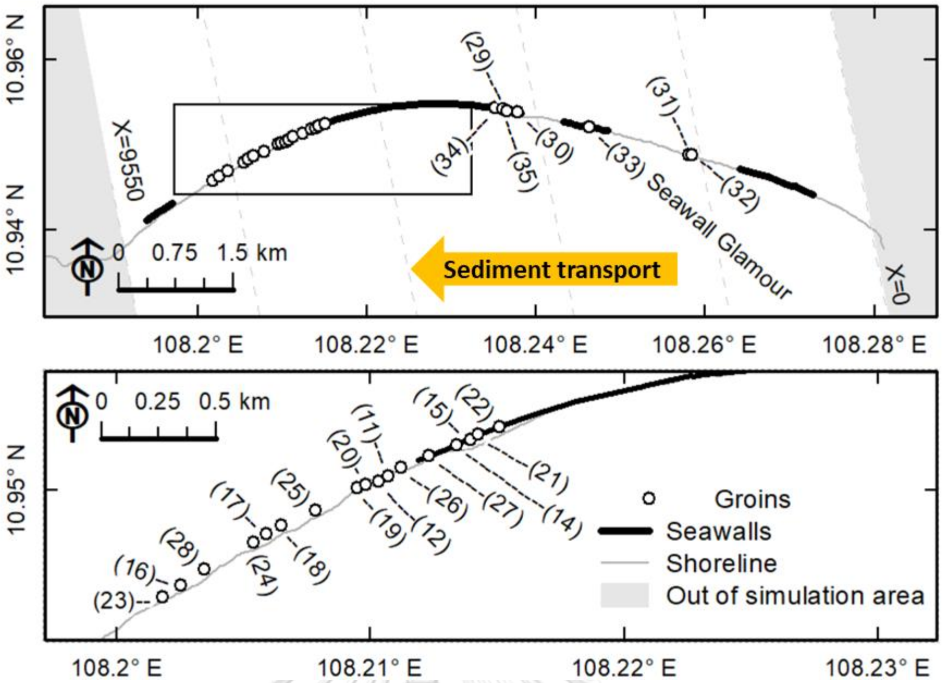

Figure 5-32 Groins in segment 3 from 2017 to 2021

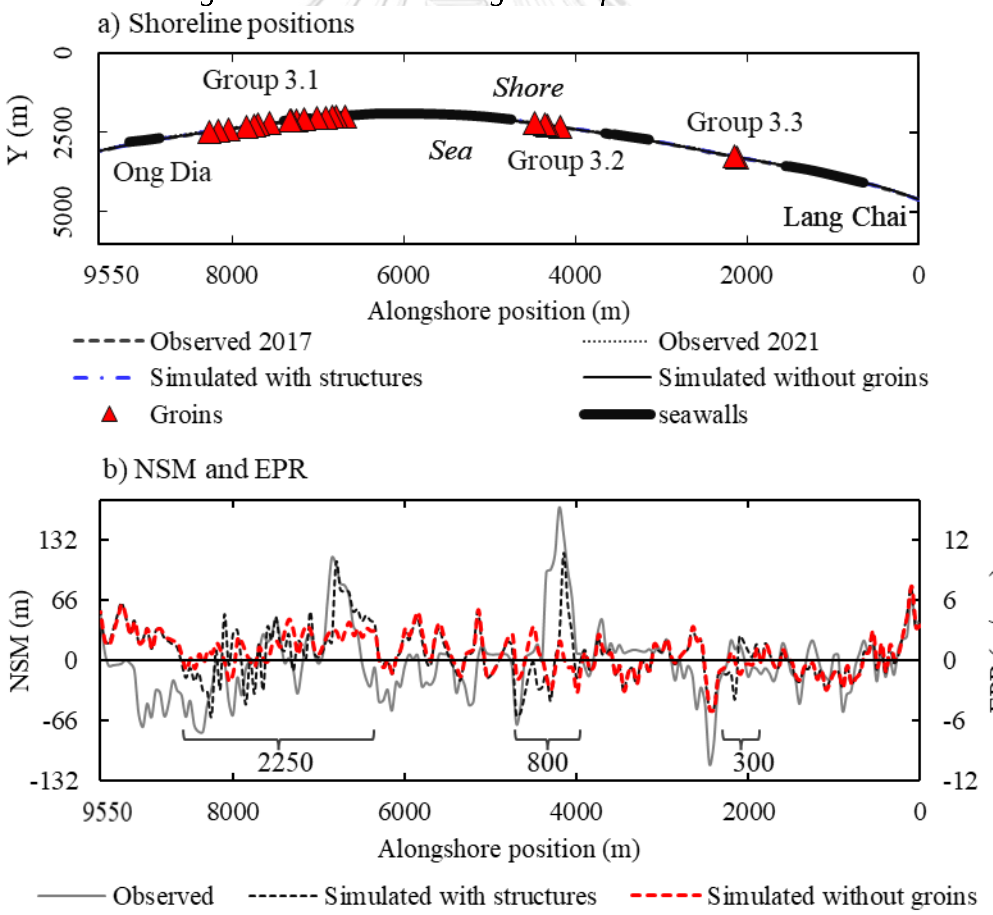

Figure 5-33 Simulation results with and without groins from 2017 to 2021 in segment 3

Table 5-10 Comparison of simulated shoreline changes of with and without the groins

	Without groins	With groins	Diff
Maximum erosion rate (m/year)	-4.84	-5.61	-0.77
Maximum accretion rate (m/year)	7.38	10.62	3.24
Erosion area (ha)	-0.4	-1.1	-0.8
Accretion area (ha)	1.5	2.2	0.7
Balance (ha)	1.1	1.0	-0.1

5.3.4 Seawalls

In segment 3, from 2006 to 2017, there were 4 seawalls (namely Anam, Mot Nang, Aloha, and Centara) existing as shown in Figure 5-34. The simulated EPR values tracked closely the actual EPR in most of the locations, showcasing an agreement between the model's predictions and the actual shoreline changes as shown in Figure 5-35. The MAE of shoreline position and MAE of EPR were 13.55 m and 2.32 m/year respectively, which reconfirmed the effectiveness of GENESIS model. However, some differences of EPR magnitude were observed. For example, from X=6000 m to X=8200 m, the simulated EPR deviated from the actual EPR, although their patterns remained consistent. This location corresponded with the area that exhibited limited model efficiency during the calibration and validation phases. Consequently, it can be inferred that this specific area may be a challenge to the effectiveness of the GENESIS model in segment 3.

Simulation results of shoreline changes with and without the presence of 4 seawalls from 2006 to 2017 in segment 3 showed minimal differences at seawalls Aloha, Mot Nang, and Anam as shown in Figure 5-35. However, for seawall Centara, some differences in EPR were noted. The erosion area with seawall Centara was 2.2 ha (0.2 ha lower than without it), and the accretion area with seawall Centara (6.4 ha) was lower than without it (6.5 ha). The seawall Centara kept shoreline more stable with the lower of both erosion and accretion rate updrift and downdrift of its location.

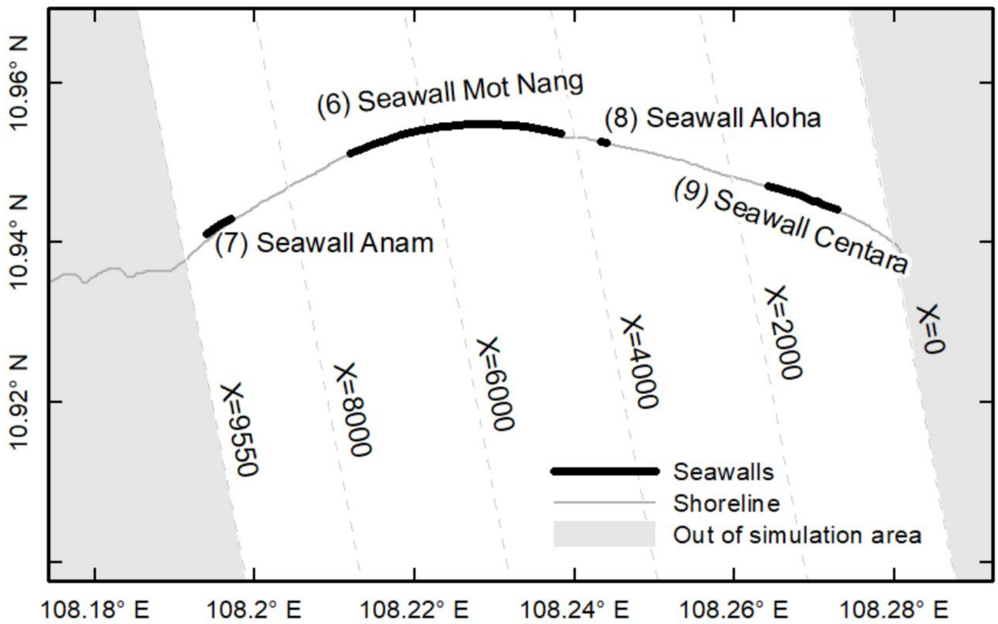

Figure 5-34 Seawalls in segment 3 from 2006 to 2017

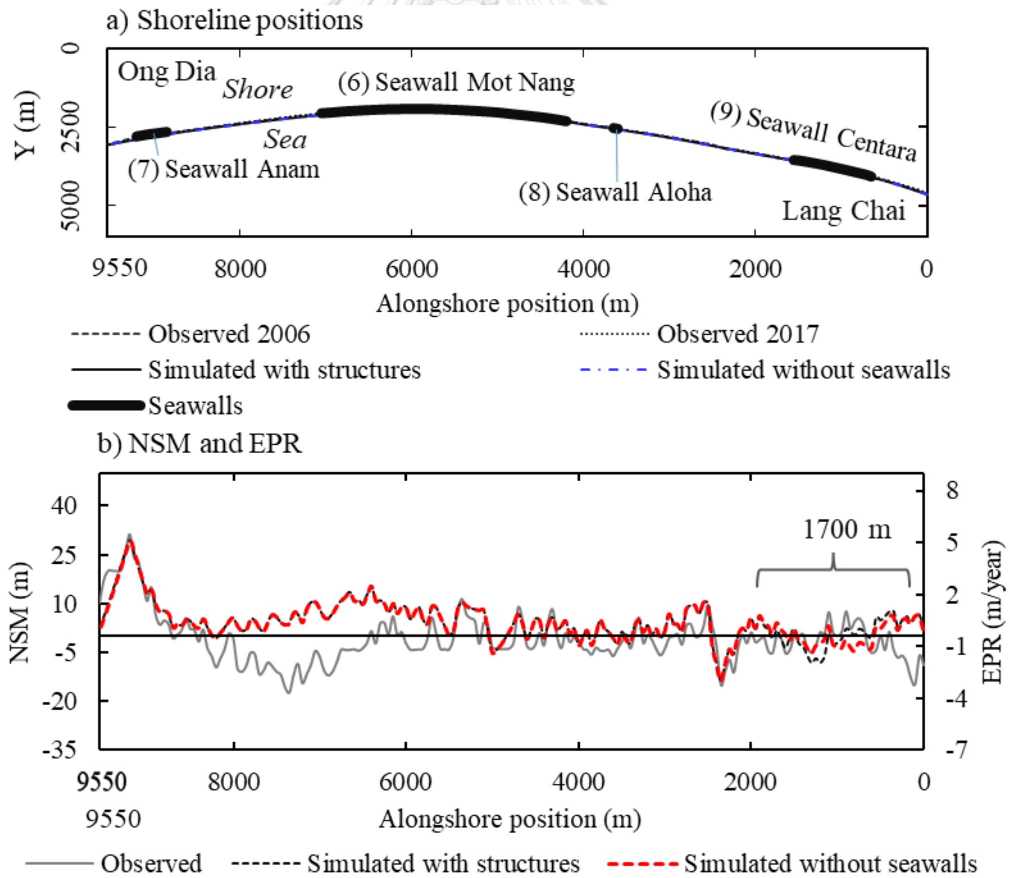

Figure 5-35 Simulation results with and without 4 seawalls from 2006 to 2017 in segment 3

Table 5-11 Comparison of simulated shoreline changes of with and without seawall Centara

	Without seawalls	With seawalls	Diff
Erosion area (ha)	-2.40	-2.20	-0.2
Accretion area (ha)	6.4	6.5	0.1
Balance (ha)	4.0	4.3	-0.1

The different impacts observed among the various seawalls on the shoreline possibly were attributed to their orientation in relation to the direction of incident waves. In segment 3, Seawall Centara gave the effects to the longest shoreline of 1700 m around its location. This seawall least perpendicular to the direction of incoming wave gave more effect on the adjacent shoreline. This implied that the relative angle between shoreline orientation where seawall built and wave direction should be considered carefully in order to enhance its function of protecting the land, and to reduce the unintended erosion in adjacent area.

5.3.5 Conclusion of structure effects

In conclusion, the findings demonstrate that the GENESIS model was able to simulate shoreline change, and sediment transport patterns in segment 1 and segment 3 for investigating the effects of beach reclamation project, jetties, groins, and seawalls on shoreline specifically in Phan Thiet bay. The effects of structures on shoreline change in Phan Thiet bay from 1988 to 2021 was assessed by comparing shoreline changes with and without the presence of structures, using the GENESIS model.

The Hamubay beach reclamation project was found to be a possible cause of increased erosion up to 1600 m downdrift, leading to a rise of 2.1 ha in erosion area and 26.7 ha in accretion area within segment 1.

The effects of 4 jetties at the river’s mouth in segment 2 were attempted to be investigated. However, despite efforts to calibrate the GENESIS model, there were noticeable discrepancies between the simulated and actual shorelines, possibly due to the sediments amount from rivers in segment 2, which there was no observed or study information.

In segment 3, groins demonstrated the expected effect of causing higher accretion updrift and increased erosion downdrift, impacting up to 2250 m around their location. Groins contributed to a rise of 0.8 ha in erosion area and 0.7 ha in accretion area.

Seawall Centara was found to give effects on the longest shoreline stretch, covering 1700 m around its location, compared to the minimal impacts of three other seawalls in segment 3. Seawall Centara led to an increase of 0.2 ha in erosion and 0.1 ha in accretion.

5.4 Discussion on shoreline simulation

This section aimed to describe the discussion on GENESIS model calibration and validation, focusing on the limitations of using GENESIS model in this study. Moreover, the result of sediment transport direction was also discussed in this section.

5.4.1 GENESIS model calibration and validation

The performance of the GENESIS model exhibited variations across different segments of Phan Thiet bay and throughout different study periods. Comparing the average MAE of EPR among the three segments, segment 1 exhibited the best agreement with an MAE of 2.34 m/year, followed by segment 3 with 5.32 m/year, and segment 2 with 8.98 m/year. The minimum MAE for shoreline position was 6.71 m, reflecting the model's best performance in predicting shoreline position in Phan Thiet bay with an accuracy of approximately 6.71 meters. Similarly, the minimum MAE for EPR was 0.62 (m/year) in segment 1, indicating the model's best performance in predicting the shoreline change rate with an accuracy of approximately 0.62 m/year. Overall, the model's simulations which accounted for the alongshore sediment transport and structures, demonstrated reasonable agreement with the actual shoreline change, capturing the general erosion or accretion trends observed at various shoreline positions in segment 1 and segment 3. However, GENESIS model in this study did not capture the shoreline change in segment 2 well. Therefore, the interpretation was based on GENESIS simulation results in segment 1 and segment 3, excluding segment 2.

In this study, the model performed well the shoreline change in long term in areas where the shoreline was smooth and featured beach reclamation projects, seawalls, and groins in segment 1 and segment 3. GENESSIS well determined erosion and accretion locations in these areas. This result could be contributed to the coastal management plan in Phan Thiet bay. Furthermore, the effects of those structures could be investigated by assessing the length of adjacent shoreline that got the impacts from their presence.

In certain areas, there were discrepancies in the shoreline change rate observed between the simulated shoreline change and the actual shoreline change, which can be attributed to several factors including the cross-shore sediment transport. For instance, in segment 3, during the period from 2017 to 2021, when a depression, a storm, and a typhoon occurred, which might cause the cross-shore sediment transport that potentially contributed to erosion at downdrift locations. However, the model exhibited accretion there, as the GENESIS model solely simulated longshore sediment transport without accounting for cross-shore processes. It was recommended to use GENESIS in scenarios where there was no presence of depressions, storms, or typhoons. However, to gain a more comprehensive understanding of the shoreline dynamics specific to Phan Thiet bay under the influence of these weather events, it was suggested to employ additional tools or models.

Moreover, the presence of big rivers like Ca Ty river, Phu Hai river, and some small rivers as the example shown in Figure 5-36 also might cause the discrepancies between simulated result and observed data. These rivers might supply additional sediment supply that was not fully considered in the model. In segment 2, where Ca Ty river and Phu Hai river exist, they were not accounted for in the model, which could be the main reason causing the underperformance of segment 2. To improve accuracy, it is recommended to include these rivers in the model by gathering observed data on sediment supply from river or calibrate that rate in the model. Thereby, the model can better capture the dynamics of sediment transport and improve the accuracy of the simulated shoreline.

Furthermore, human interventions and activities along the shoreline, such as sand dredging and exploitation, which were not captured in the simulations, can also contribute to differences between the model outputs and the observed changes. The factors of sea level rise, tidal, and beach slope are also important considerations in the analysis; however, they were not included in this study due to limitations in data availability. To gain a deeper understanding of the mechanisms driving shoreline change, it was essential to collect and integrate additional observed data on factors such as sand supply and removal, sea level rise, tides, and beach slope.

Figure 5-36 The satellite images (Google Earth Pro in Mar 2001)

There were noticeable differences in the down-drift areas of the beach reclamation project for each period, where the simulated erosion rates were higher than the actual rates. This could be due to human efforts to protect the shoreline, especially in densely populated residential areas. Additionally, the proximity of Hamubay location to the simulation boundary of the Segment 1 simulation may have influenced the results.

Additionally, the complex shape of the shoreline itself posed a challenge to GENESIS model. GENESIS tended to smoothen the shoreline shape as shown in Figure 5-37. This could explain why the simulated shoreline change differs from actual shoreline change. Therefore, GENESIS was recommended for simulating the more consistently smooth shorelines.

The differences also could be attributed to the structure data that could not be observed on satellite image and recorded by authorities due to illegal constructions. The difference observed in segment 2 from 2008 to 2011 could possibly be attributed to human intervention in the form of a soft embankment constructed in the area, as mentioned in news reports (Nam, 2008). However, despite efforts to locate actual data regarding this intervention, it was not found to be the available information, including on Google Earth images. The absence of accessible data posed a challenge in fully understanding and incorporating the impact of this intervention on the simulated shoreline changes. It was recommended to record the construction of structures in the Phan Thiet bay. Therefore, for other future research, the more accurate input data of structures could be incorporated into the model.

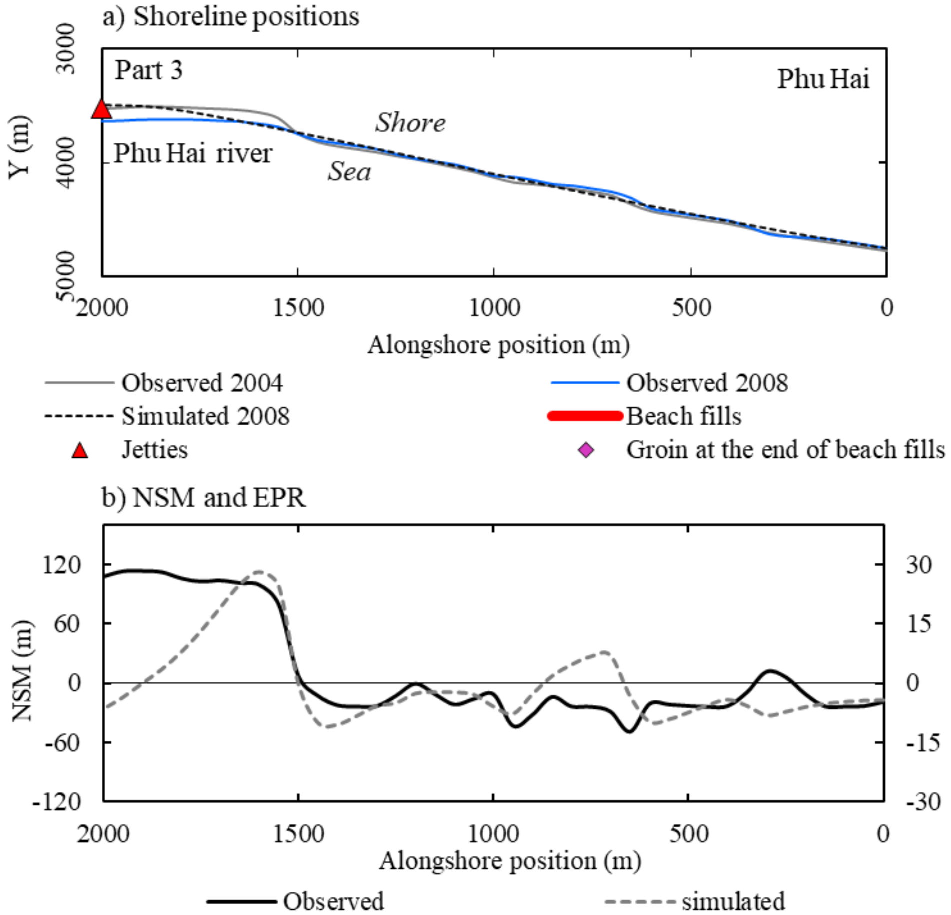

Figure 5-37 Calibration result of part 1 segment 2
(03 Jan 2004 to 15 Feb 2008)

Moreover, the discrepancies also can be attributed to the input data such as wave data, and shoreline data which was not the observed data, but the simulated wave data, and digitized shoreline. Improving the accuracy of those input data would lead to the improvement of accuracy of GENESIS model as well.

While GENESIS could capture the shoreline change trend in most of the locations in segment 1 and segment 3, it still needed to be improved by incorporating observational data. Therefore, it was recommended to collect the observational longshore sediment transport rate, and wave data.

5.4.2 Sediment transport direction

The result from GENESIS showed that the direction of longshore sediment transport most likely from the East to the West, as shown in Figure 5-38, aligning with expected direction of sediment transport based on the shoreline orientation, wave direction and the observation of Google Earth images. Since the oblique incident waves from the East and Southeast dominated the incident wave from other direction, the longshore sediment transport from the East was expected to be higher than the one from the West, which was as same as the result from GENESIS model. Moreover, observing Google Earth images also found that the land spit happened with the sediment trapped in the East. That could be the evidence of longshore sediments transport from the East as well.

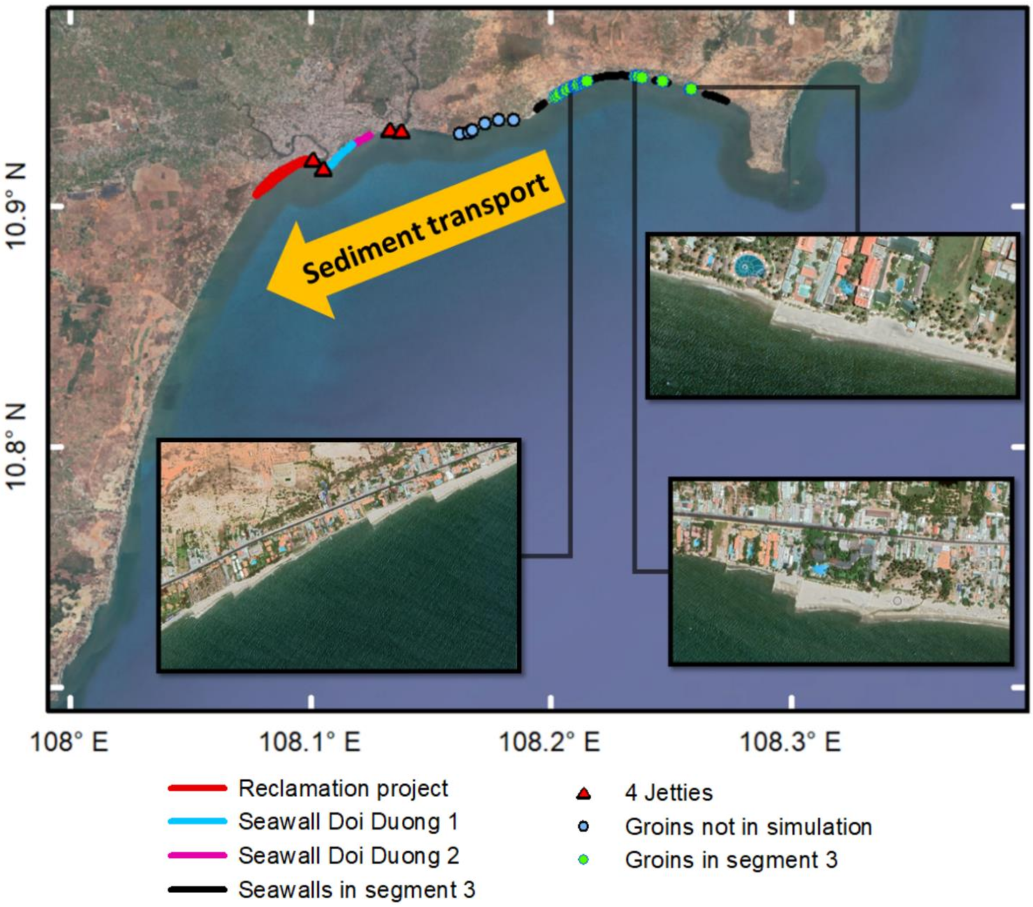

Figure 5-38 Evidence of longshore sediment transport direction by observing Google Earth images

This indicated that the movement of sediment along the shoreline was primarily influenced by the orientation of the shoreline, the incident wave patterns, and the existing structures. Taking into account wave pattern, sediment transport, and overall evolution of shoreline gave the better understand how coastal structures interact with natural sediment transport processes. This knowledge allowed for more accurate assessments of the effects of these structures on shoreline change and helped to make decisions for coastal management and engineering projects.

CHAPTER 6
CONCLUSION AND RECOMMENDATION

6.1 Conclusion

2 main objectives of this study were 1) to investigate the behaviors of shoreline changes in Phan Thiet bay, Vietnam, and 2) to investigate the effects of coastal structures to the shoreline in Phan Thiet bay, Vietnam from 1988 to 2021. ArcMap was used for extracting shoreline from Landsat images. SWAN model was used for GENESIS model was used for simulating shoreline change.

6.1.1 Shoreline change investigation

The first objective was achieved by assessing the relationship between the shoreline change and the existences of typhoon and coastal structures. The shoreline change including shoreline change rate, and area of land loss and land gain was determined by the movement of the shorelines digitized from Landsat satellite images.

The shoreline in Phan Thiet Bay underwent significant changes over four distinct periods. Initially, from 1988 to 1995, there was substantial erosion, accounting for 76% of shoreline changes without any structures yet, and with 2 typhoons. This trend shifted in the second period, spanning from 1995 to 2004, with the shoreline experiencing a more balanced pattern of erosion and accretion (50% erosion) with 2 jetties and 1 typhoon. However, in the third period, from 2004 to 2016, a shift towards accretion was observed, with 81% of shoreline changes attributed to accretion processes with 4 jetties, 1 beach reclamation project, 5 seawalls, and two typhoons. Most recently, in the fourth period from 2016 to 2021, a significant 83% of shoreline changes attributed to erosion, marking the most serious period of change with 41 structures in total and 3 storms. In this last period, 20% of the total erosion observed to be moderate erosion.

The study identified a clear correlation between shoreline change rates and the presence of coastal structures, as well as the frequency of typhoons. It's worth noting that while other factors, such as sediment from the Ca Ty and Phu Hai rivers, could influence shoreline dynamics in Phan Thiet Bay, these factors could not be thoroughly investigated due to limitations in observed sediment data from these rivers.

6.1.2 Effect of coastal structures on the shoreline change

The second objective was achieved by comparing the shoreline change of 2 cases of simulating shoreline with and without the presence of coastal structures including reclamation project, jetties, groins, and seawalls. The differences between 2 cases suggested the effect of those coastal structures on the shoreline change.

In order to simulate the shoreline, beside the shoreline achieved by the method of previous part, the study utilized wave data as an important input for the GENESIS model, which was used for simulating shoreline change. To achieve higher resolution compared to available global, and longer time coverage in more locations compared to observed data, the wave characteristics were simulated using the SWAN model.

The result of wave simulation SWAN model revealed that wave heights and directions varied across different points and were influenced by factors such as wind characteristics, bathymetry, and the presence of headlands. Comparing the simulated wave heights to the observed wave heights, the MAE ranged from 0.06 m to 0.08 m. Additionally, there was noticeable agreement between the simulated and observed wave directions, as the dominant wave directions aligned with each other. Furthermore, when comparing the EPR values resulted from the simulated wave data and the observed wave data, the mean absolute difference was found to be 0.15 m/year. This indicates a reasonably close agreement between the two datasets. Based on this result, it can be suggested that the SWAN model was suitable for simulating waves as input for the GENESIS shoreline change model.

GENESIS shoreline simulation model's performance varied across different segments and time periods, with overall reasonable agreement with observed shoreline changes in segment 1 and segment 3. Especially, the result suggested the ability of GENESIS model on determining the location of erosion and accretion.

In segment 1 from Ke Ga to Ca Ty, from 2004 to 2021, the beach reclamation project Hamubay was found to possibly intensify erosion down-drift to to 1600 m from its location.

The effects of 4 jetties at the river's mouth and seawalls in segment 2 were attempted to be investigated. However, despite efforts to calibrate the GENESIS model, there were noticeable discrepancies between the simulated and actual shorelines. These differences could be attributed to the lack of sediment input from Ca Ty and Phu Hai rivers in the model. This finding indicates that the sediment from rivers plays a crucial role in shoreline changes in Phan Thiet bay and should be considered in future studies.

The presence of groins in segment 3 from Ong Dia to Lang Chai resulted in shoreline accretion updrift of their positions and erosion down-drift, as expected. The extent of these effects varied depending on the location of the groin, ranging from approximately 300 m to 2250 m along the nearby shoreline.

This study investigated the effects of 4 seawalls in segment 3 from 2006 to 2017, and their impact on shoreline change varied. The seawall that had the most influence was less perpendicular to the direction of incoming waves. It affected a shoreline length of about 1700 m. This suggests that the location of seawalls should be chosen carefully to ensure they protect the land while minimizing unintended erosion in nearby areas.

The result from this study may be used as the additional fundamental data of shoreline change for other works in Phan Thiet bay.

6.2 Recommendations

Due to the time limitations of this master's thesis, certain aspects of the study could not be included. Therefore, there would be some recommendation for further activities as following:

In case of high-resolution images such as Google Earth images and Sentinel-2 images are available during the study time, it would be recommended to use them instead of Landsat satellite image for the higher resolution images and more accurate shoreline digitization. Additionally, it was suggested to gather observed shoreline positions in long term to validate and correct the shoreline extracted from those satellite images, moreover, for being the more accurate input in the shoreline change model. It was recommended to collect tide and beach slope data for improving the shoreline digitization result by correcting tidal effect on shoreline position.

To better understand how typhoons affect the shoreline in Phan Thiet bay, it was recommended to gather long-term wave measurements and conduct field observations of shoreline before and after typhoon to study shoreline erosion after typhoons.

Collecting observed wave data, which was considered as the most accurate wave data, in the bay over an extended period and during different seasons would be valuable for validating the wave simulation model and being the input in shoreline change simulation to improve the accuracy of those models.

It was recommended that if it is possible, the swell and the tidal effects should be analyzed in Phan Thiet bay to gain more accurate magnitudes of wave heights.

To validate the GENESIS model, it would be valuable to conduct the measurement of alongshore sediment transport. Besides that, more data of sediment should be collected such as cross-shore sediment transport by storm, sediment from 2 big rivers and other small rivers introducing additional sediment supply, and human interventions along the shoreline such as sand dredging or exploitation.

REFERENCES

Akpınar, A., van Vledder, G. P., Kömürcü, M. İ., & Özger, M. (2012). Evaluation of the numerical wave model (SWAN) for wave simulation in the Black Sea. *Continental Shelf Research*, *50*, 80-99.

ASTM, A. S. f. T. a. M. (1995). Standard Specification for Wire Cloth and Sieves for Testing Purposes. In.

ASTM, A. S. f. T. a. M. (2004). Standard Test Methods for Particle-Size Distribution (Gradation) of Soils Using Sieve Analysis. In.

Bagli, S., Soille, P., & Fermi, E. (2004). Automatic delineation of shoreline and lake boundaries from Landsat satellite images. *proceedings of initial ECO-IMAGINE GI and GIS for Integrated Coastal Management, Seville*, 13-15.

Battjes, J., & Stive, M. (1985). Calibration and verification of a dissipation model for random breaking waves. Journal of geophysical research: Oceans,

Battjes, J. A., & Janssen, J. (1978). Energy loss and set-up due to breaking of random waves. Proceedings of the 16th International Conference of Coastal Engineering, American Society of Civil Engineers, New York.

Bertotti, L., & Cavaleri, L. (1995). Accuracy of wind and wave evaluation in coastal regions. 24th International Conference on Coastal Engineering, New York.

Boak, E. H., & Turner, I. L. (2005). Shoreline definition and detection: a review. *Journal of Coastal Research*, 688-703.

Booij, N., Ris, R. C., & Holthuijsen, L. H. (1999). A third-generation wave model for coastal regions: 1. Model description and validation. *Journal of Geophysical Research*, *104*(C4), 7649-7666.

Brooks, & Cole. (2002). Factors Affecting Wind Wave Development. In.

Bruun, P. (1954). *Coast erosion and the development of beach profiles* (Vol. 44). US Beach Erosion Board.

Burningham, H., & Fernandez-Nunez, M. (2020). Shoreline change analysis. In *Sandy beach morphodynamics* (pp. 439-460). Elsevier.

Cat, N. N., Tien, P. H., Sam, D., & Binh, N. (2006). *Status of coastal erosion of Vietnam and proposed measures for protection*. Retrieved 2021, February 4 from

Cavaleri, L., & Rizzoli, P. M. (1981). Wind wave prediction in shallow water: Theory and applications. *Journal of geophysical research: Oceans*, *86*(C11), 10961-10973.

Center of Meteology and hydrography Vietnam. (2021). *historical data of typhoon in Vietnam*. Retrieved 2022, January 10 from https://www.nchmf.gov.vn/kttv/

Chisholm, A., & Dumsday, R. (1987). *Land degradation: problems and policies*. Cambridge University Press.

Church, J. A., Clark, P. U., Cazenave, A., Gregory, J. M., Jevrejeva, S., Levermann, A., Merrifield, M. A., Milne, G. A., Nerem, R. S., & Nunn, P. D. (2013). *Sea level change*.

Collins, J. I. (1972). Prediction of shallow-water spectra. *Journal of Geophysical Research*, *77*(15), 2693-2707.

Crowell, M., Leatherman, S. P., & Buckley, M. K. (1991). Historical shoreline change: error analysis and mapping accuracy. *Journal of Coastal Research*, 839-852.

Davidson, M., Splinter, K., & Turner, I. (2013). A simple equilibrium model for predicting shoreline change. *Coastal Engineering*, *73*, 191-202.

Dean, R. G. (1977). *Equilibrium beach profiles: US Atlantic and Gulf coasts*. Department of Civil Engineering and College of Marine Studies, University of Delaware, Newark.

Delft University of Technology. (2007). SWAN user manual. *Delft University of Technology. The Netherlands*.

Dewidar, K., & Bayoumi, S. (2021). Forecasting shoreline changes along the Egyptian Nile Delta coast using Landsat image series and Geographic Information System. *Environmental Monitoring and Assessment*, *193*(7), 429.

DHI. (2023). *Metocean data on demand through a centralised portal*. Retrieved 2023, January 17 from https://www.metocean-on-demand.com/

Do, A. T., Vries, S. d., & Stive, M. J. (2019). The estimation and evaluation of shoreline locations, shoreline-change rates, and coastal volume changes derived from Landsat images. *Journal of Coastal Research*, *35*(1), 56-71.

Duc, N. M., & Luan, N. T. (2014). *Impact of nearshore hydrodynamic regime to accretion and erosion processes of Phan Thiet coastline, Binh Thuan province* Proceedings of the 19th IAHR-APD Congress 2014, Hanoi, Vietnam.

ECMWF. (2020). *ERA5 hourly data on pressure levels from 1940 to present*. Retrieved 2020. March 8 from https://cds.climate.copernicus.eu/

ECMWF. (2021). *ERA-20C Ocean Wave, Daily*. Retrieved 2021, June 16 from https://apps.ecmwf.int/datasets/data/era20c-wave-daily/type=an/

GEBCO Compilation Group. (2020). GEBCO 2020 grid. In: British Oceanographic Data Centre, National Oceanography Centre, NERC ….

Hallermeier, R. J. (1983). Sand transport limits in coastal structure designs. Coastal Structures' 83,

Hanson, H. (1989). GENESIS: a generalized shoreline change numerical model. *Journal of Coastal Research*, *5*, 1-27.

Hasselmann, K. (1974). On the spectral dissipation of ocean waves due to white capping. *Boundary-Layer Meteorology*, *6*(1-2), 107-127.

Hasselmann, K., Barnett, T., Bouws, E., Carlson, H., Cartwright, D., Enke, K., Ewing, J., Gienapp, H., Hasselmann, D., & Kruseman, P. (1973). Measurements of wind-wave growth and swell decay during the Joint North Sea Wave Project (JONSWAP). *Ergänzungsheft zur Deutsehen Hydrographischen Zeitschrift*

Hoang, V. C., Thanh, T. M., Viet, N. T., & Tanaka, H. (2015). Shoreline change at the Da Nang River Mouth, Vietnam. Proceedings of the 5th International Conference on Estuaries and Coasts,

Holthuijsen, L. H. (2010). *Waves in oceanic and coastal waters*. Cambridge university press.

Horikawa, K. (1988). *Nearshore dynamics and coastal processes: Theory, measurement, and predictive models*. University of Tokyo press.

Hue, N. H., & Thanh, N. H. (2019). Assessing the Impact of Massive Development of Beach Resorts on Current Status of Coastal Erosion Along the Central Coast of Vietnam. International Conference on Asian and Pacific Coasts,

Hung, N. M., & Larson, M. (2014). "Coastline and river mouth evolution in the central part of the Red River Delta". In *Coastal Disasters and Climate Change in Vietnam* (pp. 43-79). Elsevier.

Janssen, P. A. (1991). Quasi-linear theory of wind-wave generation applied to wave

forecasting. *Journal of Physical Oceanography*, *21*(11), 1631-1642.
Janssen, P. A. (2008). Progress in ocean wave forecasting. *Journal of Computational Physics*, *227*(7), 3572-3594.
Kakisina, T. J., Anggoro, S., & Hartoko, A. (2016). NEMOS (Nearshore Modelling of Shoreline Change) Model for Abrasion Mitigation at the Northern Coast of Ambon Bay. *Aquatic Procedia*, *7*, 242-246.
Komen, G., Hasselmann, S., & Hasselmann, K. (1984). On the existence of a fully developed wind-sea spectrum. *Journal of Physical Oceanography*, *14*(8), 1271-1285.
Larson, M., & Kraus, N. C. (1989). *SBEACH: numerical model for simulating storm-induced beach change. Report 1. Empirical foundation and model development*.
Li, W., Du, Z., Ling, F., Zhou, D., Wang, H., Gui, Y., Sun, B., & Zhang, X. (2013). A comparison of land surface water mapping using the normalized difference water index from TM, ETM+ and ALI. *Remote Sensing*, *5*(11), 5530-5549.
Linh, M. T. Y. (2018). *Assessment of Coastal Vulnerability in Central Vietnam: Case study of Binh Thuan and Ba Ria – Vung Tau Province* Ho Chi Minh University of Technology].
Liu, J. P., DeMaster, D. J., Nguyen, T. T., Saito, Y., Nguyen, V. L., Ta, T. K. O., & Li, X. (2017). Stratigraphic formation of the Mekong River Delta and its recent shoreline changes. *Oceanography*, *30*(3), 72-83.
Maxar. (2023). *Optical imagery*. Retrieved 2023, March 28 from https://www.maxar.com/products/optical-imagery
McFeeters, S. K. (1996). The use of the Normalized Difference Water Index (NDWI) in the delineation of open water features. *International journal of remote sensing*, *17*(7), 1425-1432. https://doi.org/10.1080/01431169608948714
Mentaschi, L., Vousdoukas, M. I., Pekel, J.-F., Voukouvalas, E., & Feyen, L. (2018). Global long-term observations of coastal erosion and accretion. *Scientific reports*, *8*(1), 12876.
MONRE, M. o. N. R. a. E. (2010). *Vietnam-Netherlands Mekong Delta Masterplan project*.
MONRE, M. o. N. R. a. E. (2020). *Scenario of Climate Change and Sea Level Rise for Vietnam*.
Mullick, M. R. A., Islam, K. A., & Tanim, A. H. (2019). Shoreline change assessment using geospatial tools: a study on the Ganges deltaic coast of Bangladesh. *Earth Science Informatics*, 1-18.
Nam, V. (2008). *Building soft embankment against sea erosion*. Retrieved 2020, October 23 from https://thesaigontimes.vn/xay-ke-mem-chong-xam-thuc-bien/
Narayana, A. C. (2016). Shoreline Changes. In M. J. Kennish (Ed.), *Encyclopedia of Estuaries* (pp. 590-602). Springer Netherlands. https://doi.org/10.1007/978-94-017-8801-4_118
NCAR. (2023). *Climate Forecast System Reanalysis (CFSR)*. Retrieved 2023, April 14 from https://climatedataguide.ucar.edu/climate-data/climate-forecast-system-reanalysis-cfsr
NOAA. (2023a). *National Centers for Environmental Information*. Retrieved 2023, March 20 from https://www.ncei.noaa.gov/
NOAA. (2023b). *WaveWatch III (WW3) Global Wave Model*. Retrieved 2023, March 20 from

https://coastwatch.pfeg.noaa.gov/erddap/griddap/NWW3_Global_Best.html
Ozturk, D., & Sesli, F. A. (2015). Shoreline change analysis of the Kizilirmak Lagoon Series. *Ocean & Coastal Management*, *118*, 290-308.
Pham, B. T., & Prakash, I. (2018). Application of Simple Remote Sensing Techniques for the Detection and Extraction of Coastline-A Case Study of Diu Island, India. *Indian Journal of Ecology*, *45*(4), 778-784.
Phillips, M. R., & Jones, A. L. (2006). Erosion and tourism infrastructure in the coastal zone: Problems, consequences and management. *Tourism Management*, *27*(3), 517-524.
Phillips, O. M. (1957). On the generation of waves by turbulent wind. *Journal of fluid mechanics*, *2*(5), 417-445.
Pierson Jr, W. J., & Moskowitz, L. (1964). A proposed spectral form for fully developed wind seas based on the similarity theory of SA Kitaigorodskii. *Journal of Geophysical Research*, *69*(24), 5181-5190.
Pilkey, O. H. (1991). Coastal erosion. *Episodes*, *14*(1), 46-51.
Polsomboon, P., & Sriariyawat, A. (2019). *Application of SWAN Model for Simulate Wave Height in Gulf of Thailand during tropical storm Pabuk* The 24th National Convention on Civil Engineering, Udonthani, Thailand.
Prasad, D. H., & Kumar, N. D. (2014). Coastal Erosion Studies—A Review. *International Journal of Geosciences*, *5*.
Quang Tuan, N., Cong Tin, H., Quang Doc, L., & Anh Tuan, T. (2017). Historical monitoring of shoreline changes in the Cua Dai Estuary, Central Vietnam using multi-temporal remote sensing data. *Geosciences*, *7*(3), 72.
Quoc, L. N. (2019). *Erosion and coastal structure situations, the consequences and solutions of coastal erosion.*
Reeve, D. E., & Valsamidis, A. (2014). On the stability of a class of shoreline planform models. *Coastal Engineering*, *91*, 76-83.
Ris, R., Holthuijsen, L., & Booij, N. (1999). A third-generation wave model for coastal regions: 2. Verification. *Journal of geophysical research: Oceans*, *104*(C4), 7667-7681.
Sorensen, R. M. (2005). *Basic coastal engineering* (Vol. 10). Springer Science & Business Media.
Sorensen, R. M. (2006). *Basic coastal engineering* (Vol. 10). Springer Science & Business Media.
Sutikno, S., Murakami, K., Handoyo, D. P., & Fauzi, M. (2015). Calibration of numerical model for shoreline change prediction using satellite imagery data. *Makara Journal of Technology*, *19*(3), 113-119.
Swift, D. J., Stanley, D., & Swift, D. (1976). *Coastal sedimentation*.
Takagi, H., Esteban, M., & Tam, T. T. (2014). Coastal Vulnerabilities in a fast-growing Vietnamese city. In *Coastal Disasters and Climate Change in Vietnam* (pp. 157-171). Elsevier.
Thao, N. D., Takagi, H., & Esteban, M. (2014). *Coastal disasters and climate change in Vietnam: Engineering and planning perspectives*. Elsevier.
The European Space Agency. (2015). *Sentinel-2 delivers first images*. Retrieved 2023, March 24 from https://www.esa.int/
Thinh, N. A., & Hens, L. (2017). A Digital Shoreline Analysis System (DSAS) applied on mangrove shoreline changes along the Giao Thuy coastal area (Nam Dinh,

Vietnam) during 2005-2014. *Vietnam Journal of Earth Sciences*, *39*(1), 87-96.

Thomas, R. C., & Frey, A. E. (2013). *Shoreline change modeling using one-line models: General model comparison and literature review*.

Thomas, T. J., & Dwarakish, G. (2015). Numerical wave modelling–A review. *Aquatic Procedia*, *4*, 443-448.

Tien, P. H., Thanh, T. D., Long, B., & Cu, N. (2003). Coastal Erosion and Sedimentation in Vietnam.. Marine resources and environment. *Science and Technics Publishing House, Hanoi*, *10*, 20-33.

Tolman, H. L. (1992). Effects of numerics on the physics in a third-generation wind-wave model. *Journal of Physical Oceanography*, *22*(10), 1095-1111.

Trung, P. B. (2019). The effects of projects of dredging and recovering saline sand at estuaries in Binh Thuan-Ninh Thuan provinces. *Vietnam Journal of Marine Science and Technology*, *19*(4A), 55-66.

Trung, P. B., & Mau, L. D. (2011). Status of erosion-deposition processes along the coast of Binh Thuan province. *Vietnam Journal of Earth Sciences*, *33*(3), 322-328.

Uda, T. (2018). *Morphodynamic Model for Predicting Beach Changes Based on Bagnold's Concept and Its Applications*. BoD–Books on Demand.

United States Geological Survey. (2023a). Landsat 5. https://www.usgs.gov/landsat-missions/landsat-5

United States Geological Survey. (2023b). *Landsat 8*. Retrieved 2023, March 20 from https://www.usgs.gov/landsat-missions/landsat-8

US Army Corps of Engineers. (1984). *Shoreline Protection Manual* (Vol. 1).

US Army Corps of Engineers. (1995). Chapter 7 Sediment properties. In *Sedimentation Investigations of Rivers and Reservoirs*.

Vallarino Castillo, R., Negro Valdecantos, V., & Moreno Blasco, L. (2022). Shoreline Change Analysis Using Historical Multispectral Landsat Images of the Pacific Coast of Panama. *Journal of Marine Science and Engineering*, *10*(12), 1801.

Van To, D. (2006). Beach erosion in Doi Duong–Phan Thiet tourist resort and its proposed measure. Vietnam-Japan Estuaries workshop,

Van To, D. (2008). The equilibrium stages of headland-bay beaches in the coastal provinces of Vietnam. *Tạp chí Khoa học kỹ thuật Thủy lợi và Môi trường*(23), 95.

Vietnamnet. (2017). *Shifting sands: illegal VN sales to Singapore*. Retrieved 2023, June 23 from https://vietnamnet.vn/

Vo, P. L., Lin, T., & Nguyen, B. G. (2018). Threat of coastal hazards to socio-economic development in the Central coast of Vietnam.

Vuong, N. D. (2009). *Plan of shoreline protection structures in Binh Thuan from 2011 to 2020*.

Vuong, N. D. (2012). *Scientific and technology research for disaster prevention, environmental protection and reasonable use of natural resources*.

Vuong, N. D. (2014). *Scientific and technology research for disaster prevention, environmental protection and reasonable use of natural resources*.

Vuong, N. D., & Dat, P. V. (2015). *Hard countermeasure to protect shoreline and reduce accretion in Ca Ty estuary Phan Thiet, Binh Thuan province (in Vietnamese)*.

Vuong, N. D., Hung, L. M., & Phuong, N. T. (2015). *Propose countermeasure to* *stabilize La Gi estuary, Dinh river, Binh Thuan (in Vietnamese)*.

WAMDI Group. (1988). The WAM model—A third generation ocean wave prediction model. *Journal of Physical Oceanography*, *18*(12), 1775-1810.

Wentworth, C. K. (1922). A scale of grade and class terms for clastic sediments. *The journal of geology*, *30*(5), 377-392.

WMO, S. (1998). *Guide to wave analysis and forecasting*.

Xu, H. (2006). Modification of normalised difference water index (NDWI) to enhance open water features in remotely sensed imagery. *International journal of remote sensing*, *27*(14), 3025-3033.

Zuzek, P. J., Nairn, R. B., & Thieme, S. J. (2003). Spatial and temporal considerations for calculating shoreline change rates in the Great Lakes Basin. *Journal of Coastal Research*, 125-146.

APPENDIX A

THEORIES OF SWAN WAVE SIMULATION MODEL

SWAN is the third-generation numerical wave model which is used to compute random, short-crested wave in the coastal region with shallow water and inland water. SWAN can be applied in the area whose width is less than 20-30 km and water depth less than 20-30 m. The model is based on an Eulerian formulation of the discrete spectral balance of action density that accounts for refractive propagation over arbitrary bathymetry and current fields (Booij et al., 1999). SWAN can consider shallow water physics and provide the large scale of time simulation.

The below spectral action balance equation describes the evolution of the wave spectrum (Booij et al., 1999) as equation (A-1)

$$\frac{\partial}{\partial t}N+\frac{\partial}{\partial x}c_xN+\frac{\partial}{\partial y}c_yN+\frac{\partial}{\partial \sigma}c_\sigma N+\frac{\partial}{\partial \theta}c_\theta N=\frac{S}{\sigma} \qquad \text{(A-1)}$$

Where $\frac{\partial}{\partial t}N$ represents the local rate of change of action density in time

$\frac{\partial}{\partial x}c_xN+\frac{\partial}{\partial y}c_yN$ represents propagation of action in x and y of Cartesian coordinates with propagation velocities c_x and c_y.

$\frac{\partial}{\partial \sigma}c_\sigma N$ represents the changing of the relative frequency with progation velocity c_σ in σ space due to changing of depths and currents.

$\frac{\partial}{\partial \theta}c_\theta N$ represents depth-induced and current-induced refraction (with propagation velocity c_θ in θ space.

S represents the effects of wind, dissipation, and nonlinear wave-wave interactions. S is the source term in term of energy density.

In SWAN, diffraction and wave-induced currents are not be directly considered.

Phillips (1957) and Hasselmann et al. (1973) describe the transformation of wind energy to the waves as equation *(2-5).*

$$S_{in}(\sigma,\theta) = A + BE(\sigma,\theta) \tag{A-2}$$

$S_{in}(\sigma,\theta)$ is wind source energy density, representing the effect of wind.

$E(\sigma,\theta)$ is energy density spectrum.

A and B depend on wave frequency and direction, and wind speed and direction. The linear growth is described by A due to Cavaleri and Rizzoli (1981) and mentioned by Holthuijsen (2010) as equation (A-3).

$$A = \begin{cases} \dfrac{1.5\times10^{-3}}{g^2 2\pi}[u_* \cos(\theta-\theta_{\text{wind}})]^4 G & \text{for } |\theta-\theta_{wind}| \le 90^o \\ 0 & \text{for } |\theta-\theta_{wind}| > 90^o \end{cases} \tag{A-3}$$

u_* is friction wind velocity.

$u_*^2 = C_D U_{10}^2$

C_D is wind-drag coefficient as equation (A-4).

$$C_D = \begin{cases} 1.2875\times10^{-3} & \text{for } U_{10} < 7.5m/s \\ (0.8+0.065U_{10})\times10^{-3} & \text{for } U_{10} \ge 7.5m/s \end{cases} \tag{A-4}$$

θ_{wind} is wind direction.

G is the cut-off function as

$$G = \exp[-(\sigma/\sigma_{PM}^*)^{-4}] \tag{A-5}$$

The Pierson-Moskowitz frequency (σ_{PM}^*) (Tolman, 1992) is the peak constrain of the frequency growth.

$$\sigma^{*}_{PM} = 2\pi \frac{0.13g}{28u_*} \quad \text{(A-6)}$$

The exponential wave growth is described by two formulation of B which is taken from Komen et al. (1984) as equation (A-7).

$$B = \max\left\{0; \gamma \frac{\rho_{air}}{\rho_{water}} \left(\frac{u_*}{c}\right)^2 \cos^2(\theta - \theta_{wind})\right\}\sigma \quad \text{(A-7)}$$

Where $\gamma = \frac{1.2}{\kappa^2}\lambda \ln^4 \lambda$ (Janssen, 1991) (A-8)

$$\lambda = \frac{gz_e}{c^2}\exp\left[\kappa c / \left|u_* \cos\left(\theta - \theta_{wind}\right)\right|\right] \quad \text{(A-9)}$$

for $\lambda \le 1$

$$B = 0 \quad \text{for } \lambda > 1 \quad \text{(A-10)}$$

κ is the von Kármán constant, equal to 0.41.

z_e is the effective surface roughness.

SWAN considers effects of currents according to apparent local wind speed and direction.

Wave energy dissipation includes whitecapping $S_{ds,w}(\sigma,\theta)$ which depends on the steepness of the waves, bottom friction $S_{ds,b}(\sigma,\theta)$, and depth-induced wave breaking $S_{ds,br}(\sigma,\theta)$. In SWAN, whitecapping $S_{ds,w}(\sigma,\theta)$ is described according to Hasselmann (1974) and WAMDI Group (1988) as equation (A-11).

$$S_{ds,w}(\sigma,\theta) = -\Gamma \tilde{\sigma} \frac{k}{\tilde{k}} E(\sigma,\theta) \quad \text{(A-11)}$$

Γ is the steepness dependent coefficient.

$$\Gamma = C_{ds}((1-\delta) + \delta \frac{k}{\tilde{k}}) \left(\frac{\tilde{s}}{\tilde{s}_{PM}}\right)^p$$

C_{ds} and δ are tunable coefficients. C_{ds} =4.1$\times$10^{-5}, δ =0.5 and p =4.

$\tilde{s}$ is the overall wave steepness.

$$\tilde{s}_{PM} = \sqrt{3.02\times10^{-3}} \text{ (Pierson Jr \& Moskowitz, 1964)} \quad \text{(A-12)}$$

k is wave number.

$\tilde{\sigma}$ and $\tilde{k}$ represent mean frequency and mean wave number

The sea bottom disspipate wave energy because of bottom friction, bottom motion, percolation, or wave backscattering due to irregularities of the seabed. For continental shelf sea with sandy bottoms, the dominant mechanism appears to be bottom friction (Bertotti & Cavaleri, 1995).

$$S_{ds,b}(\sigma,\theta) = -C_{bottom}\frac{\sigma 2}{g^2\sinh^2(kd)}E(\sigma,\theta) \quad \text{(A-13)}$$

Equation (2-16) represent the effect of bottom to dissipate wave energy due to friction. C_{bottom} is bottom friction coefficient.

In SWAN, there are 3 types of friction model which are:

- The empirical Joint North Sea Wave Project (JONSWAP) with $C_{bottom} = 0.038\ m^2s^{-3}$ for swell conditions and $C_{bottom} = 0.067\ m^2s^{-3}$ for wind sea conditions (Hasselmann et al., 1973);
- The drag law model with $C_{bottom} = C_f gU_{rms}$ where C_f is bottom friction coefficient, g is gravitational acceleration and U_{rms} is root mean square velocity (Collins, 1972);
- The eddy-viscosity model with $C_{bottom} = f_w gU_{rms}/\sqrt{2}$ where f_w is wave friction factor. As the default of SWAN model, $C_{bottom} = 0.038\ m^2s^{-3}$ is used for swell dissipation, and $C_{bottom} = 0.067\ m^2s^{-3}$ is used for wind-sea conditions (WAMDI Group, 1988).

The process of depth-induced wave breaking $S_{ds,br}(\sigma,\theta)$ is represented in equation (A-14).

$$S_{ds,br}(\sigma,\theta) = -\frac{S_{ds,br,tot}}{E_{tot}} E(\sigma,\theta) \qquad \text{(A-14)}$$

$S_{ds,br,tot}$ is the rate of dissipation of wave energy and E_{tot} is the total wave energy (Battjes & Janssen, 1978). The value of $S_{ds,br,tot}$ depends on the breaking parameter $\gamma = \mathrm{H}_{\max}/\mathrm{d}$ where $\mathrm{H}_{\max}$ is the highest wave height in the local water depth (d). The value of breaking parameter γ may be constant $\gamma = 0.73$ which is the value from Battjes and Stive (1985) or it changes depending on the bottom slope.

APPENDIX B
THEORIES OF GENESIS ONE-LINE MODEL

This appendix mentions the theories of GENESIS One-line model based on its manual Hanson (1989).

1. Assumptions and limitations

The GENESIS model has been widely used to simulate shoreline behavior under different scenarios and applied for various purposes. It is important to recognize the assumptions and limitations of GENESIS model.

The first assumption of the GENESIS model is that the shape of the beach profile is constant over time and locations. That means the beach profile moves parallel to itself. Thereby, the beach change can be described by the shoreline change with the consistent beach profile. While this may be true for some beaches, it is not always the case, particularly in areas where there are significant changes in sediment supply due to the structures or wave energy such as storms. For example, the slope where the wave is stronger should be steeper compared to the location of lower waves. Moreover, the beach profile also changes in terms of the wave energy and sediment size. Beach made of coarser sand will have a steeper slope of the beach profile. Beaches exposed to higher wave energy will have a steeper slope (Sorensen, 2006).

The second limitation of the Genesis model is that it assumes constant shoreward and seaward limits of sediment transport. The shoreward boundary is at the active berm where the elevation is highest. The seaward boundary is at the depth of closure. Beyond the depth of closure, there are no significant depth changes. In reality, the berm elevation and depth of closure can vary over time as a result of changes in sea level, sediment supply, and other factors.

The third limitation is that the predictions of the total longshore sand transport rate are assumed to be influenced by the height and direction of breaking waves along the shore, without considering the details and effects of the nearshore current pattern. In some real cases, the nearshore current can play a significant role in sand transport processes, particularly in areas with complex nearshore bathymetry and hydrodynamic factors. Instead, the model parameterizes the transport rate based on breaking wave quantities.

The fourth limitation is that the shoreline changes following the long-term trend, which is controlled by the waves inducing longshore sediment transport, and by the boundary conditions of structures or other barriers. While this may be appropriate for some coastal settings, it may not work well in areas where rapid changes in shoreline position occur due to storms or other factors.

For example, in the case that there is the barrier interrupting the longshore sediment transport such as a groin, the slopes of the updrift groin and downdrift groin are different in reality. However, in GENESIS, the slope is consistent. On the other hand, the long-term shoreline behavior is simulated according to that groin while the beach slope is not reproduced.

2. Governing equation for shoreline change

Conservation of sand volume is the main principle of the governing equation for shoreline change. As shown in Figure B-1, the x axis is parallel to the shoreline. The y axis is cross-shore. Considering the segment Δx the interval time Δt, the change in shoreline position is Δy. D_B is the berm height, and D_c is the depth of closure from vertical datum. The berm is the part of the beach where sand accumulates and it's typically the highest point. The berm height is the distance between the highest point of the berm and the waterline. Water depth D_c is the seaward boundary of beach profile change. The volume change in segment Δx is $\Delta V = \Delta x \Delta y (D_B + D_c)$.

The shoreline changes when the volume of sediment entering and sediment existing that Δx segment is different. That could be considered in longshore and line source. For the longshore sediment transport, the volume of sediment entering Δx segment is $Q\Delta t$. The net volume change which is the difference between sediment entering and sediment existing is $\Delta Q \Delta t = \frac{\partial Q}{\partial x} \Delta x \Delta t$. Another contribution of sediment volume change is the line source or the sink of sand, for example the river mouth or inlets correspondingly. The volume of sediment from shoreward is $q_s \Delta x \Delta t$. The volume of sediment from offshore is $q_o \Delta x \Delta t$. The volume change considering both directions is $q\Delta x\Delta t$. Considering both longshore and line source, the volume change is $\Delta V = \frac{\partial Q}{\partial x}\Delta x\Delta t + q\Delta x\Delta t$.

Therefore, $\Delta V = \Delta x\Delta y(D_B + D_c) = \frac{\partial Q}{\partial x}\Delta x\Delta t + q\Delta x\Delta t$ (B-1)

Deriving equation (B-1), it becomes

$$\frac{\partial y}{\partial t} + \frac{1}{(D_B + D_c)}\left(\frac{\partial Q}{\partial x} - q\right) = 0 \qquad \text{(B-2)}$$

In order to determine the position of final shoreline, the required data are the initial shoreline position, and the distance of shoreline movement which is calculated by the change of sediment volume in the equation (B-2). To solve that equation, the boundary condition at the beginning and the end of the segment, and values of Q, q, D_B and D_c must be given.

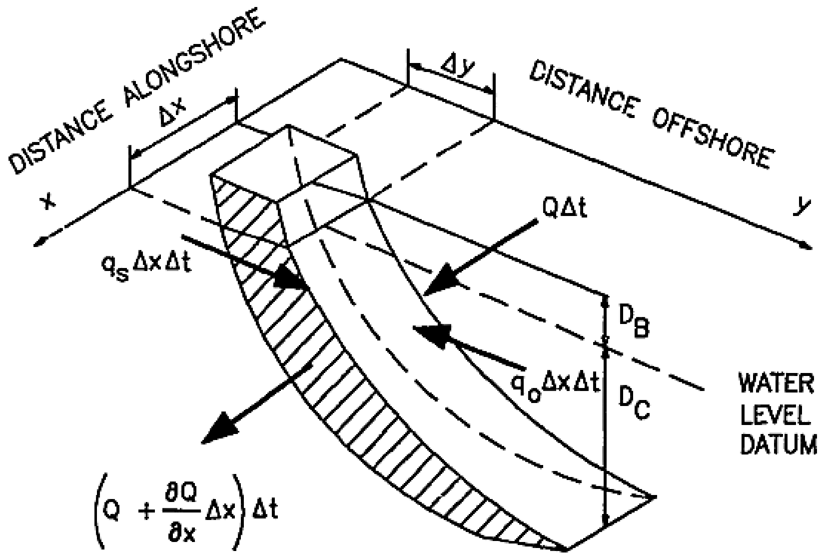

Figure B-1. Cross-section view of sand transportation (Hanson, 1989)

3. Sediment transport rate prediction

GENESIS predicts sediment transport rate based on the longshore sediment transport, sources and sinks, and direct change in shoreline position by human activities.

A longshore sediment transport is generated by the wave coming to the shoreline with an oblique wave angle and then breaking. In GENESIS, the empirical predictive formula for longshore sand transport rate is in equation (B-3).

$$Q = \left(H^2 C_g\right)_b \left(a_1 sin2\theta_{bs} - a_2 cos\theta_{bs}\frac{\partial H}{\partial x}\right)_b \qquad \text{(B-3)}$$

Where

H is breaking wave height

C_g is the wave group speed given by linear wave theory

b is subscript representing wave breaking condition

θ_{bs} is the angle of wave crests to the shoreline.

a_1 and a_2 are determined as equation (B-4) and (B-5) .

$$a_1 = \frac{K_1}{16(\rho_s/\rho - 1)(1-p)(1.416)^{5/2}} \qquad \text{(B-4)}$$

$$a_2 = \frac{K_2}{8(\rho_s/\rho - 1)(1-p)tan\beta(1.416)^{7/2}} \qquad \text{(B-5)}$$

K_1, K_2 are empirical transport coefficients for calibrating. K_1 is calibration parameter of sand transport due to oblique incident waves. K_2 is calibration parameter of longshore variation in the breaking wave height. In case the diffraction is not applied, the longshore variation in the wave height is random and very small, and K_2 can be neglected.

ρ_s is the density of the sediment (taken to be 2.65×10^3 kg/m^3)

ρ is the density of water (1.03×10^3 kg/m^3 for seawater)

p is the sediment porosity (taken to be 0.4)

$tan\beta$ is the average seabed slope from the shoreline to depth of active longshore sand transport. The cross-shore transport is assumed to be ignored.

GENESIS requires the input of significant wave height for converting to root mean square wave height with the factor of 1.416.

In equation (B-4), the first term including K_1 accounts for the longshore sediment transport that induced by the breaking of oblique incident wave. The second term including K_2 accounts for the longshore sediment transport induced by the longshore gradient in breaking wave height. In an open-coast, the contribution of the second term is much smaller than the first term. However, in the area near the structures, K_2 should be considered well since the diffraction affects the breaking wave height.

In GENESIS, K_1 and K_2, or called transport parameters, are calibrated to account for the actual sand transport since the shoreline response model has many assumptions and approximations that were made during its formulation. The value of transport coefficient K_1 cooperating with $1/(D_B + D_c)$ determines both the duration of the simulated shoreline shift and the amount of sand transported alongshore. The value of transport coefficient K_2 determine the shoreline change mainly in the vicinity of structures.

Sources and sinks factor is also considered for predicting sediment transport. In equation (B-2), the variable q indicates a source or sink of sand in the system. Rivers and cliffs are common sources, while inlets and entrance channels are typical sinks. On the landward boundary, wind-blown sand can act as a source or sink, depending on the direction of the wind. The rates q_s and q_o in the shoreward and seaward directions values are specific to each situation and may vary over time and distance along the shore. GENESIS simulates the sources and sinks by the Beach Fills volume.

Besides the longshore transport rate, and sources and sinks, the direct change should be considered for calculating the sediment transport such as beach fill or dredging. This can result in the profile being moved shoreward or seaward by a specified amount, which can vary over time and distance alongshore. GENESIS offers the option to directly change the shoreline position by a specified amount of Beach

Fills, either positive (seaward) due to beach fill or negative (landward) due to sand mining.

4. Empirical parameters

Depth of longshore transport

The depth of longshore transport is the offshore limitation of longshore sediment transport area which is close to the surf zone area. The depth of longshore transport is calculated in GENESIS for determining the sediment bypassing over the groins and jetties. Assuming certain standard conditions, the depth of longshore transport (D_{LT}) is calculated with the significant wave height $(H_{1/3})$, which is a parameter utilized in GENESIS.

$$D_{LT} = \frac{1.27}{\gamma}(H_{1/3})_b \quad \text{(B-6)}$$

Where

1.27 is the conversion factor between one-tenth highest wave height and significant wave height

γ is breaker index, ratio of wave height to water depth at breaking (normally is 0.78)

$(H_{1/3})_b$ is significant wave height at breaking

Compared to the depth of closure $(D_{C)}$, depth of longshore transport (D_{LT}) is much smaller except under extremely high waves.

Not only D_{LT}, but also maximum depth of longshore transport (D_{LTo}) is determined in GENESIS as in equation (B-7), in order to calculate the average beach slope $tan\beta$ in equation (B-5) by Hallermeier (1983).

$$D_{LTo} = (2.3 - 10.9H_o)\frac{H_o}{L_o} \quad \text{(B-7)}$$

Where

$\frac{H_o}{L_o}$ is wave steepness in deep water

H_o is significant wave height in deep water

L_o is wavelength in deep water

GENESIS calculates L_o based on linear wave theory

$L_o = gT^2/2\pi$

g is the acceleration due to gravity

T is the wave period. If the wave data includes spectral information, then the peak spectral wave period is used to determine the wave period (T). However, if spectral data is not provided, the period associated with the significant waves is used instead.

GENESIS calculates D_{LTo} at each time step based on the deep-water wave data. However, the value of D_{LTo} is constant throughout the entire stretch of the coastline being modeled.

Average profile shape and slope

The average profile shape is required to be determined for solving longshore sediment transport equation which requires the wave breaking location, and average nearshore bottom slope. The profile is illustrated by depth of water (D) at each y location, not changes by x axis as shown in equation (B-8) according to Bruun (1954) and Dean (1977).

$$D = Ay^{2/3} \qquad \text{(B-8)}$$

Where

A is the empirical scale parameter whose value depends on the median sediment size (D_{50}) as shown below. Therefore, each median sediment size gives a different beach profile. In a GENESIS simulation, only the beach profile does not change, thereby only 1 sediment size is assigned. The A-value that produces the most representative profile shape is determined by that effective grain size.

$$A = 0.41(D_{50})^{0.94} \qquad , D_{50} < 0.4$$

$$A = 0.23(D_{50})^{0.32} \qquad , 0.4 \leq D_{50} < 10.0$$

$$A = 0.23(D_{50})^{0.28} \qquad , 10.0 \leq D_{50} < 40.0 \qquad \text{(B-9)}$$

$$A = 0.46(D_{50})^{0.11} \qquad , 40.0 \leq D_{50}$$

If the beach profile is available from the survey (D vs. y), the median sediment size should be determined based on that profile. If the beach profile is not available, the median sediment size at the surf zone should be collected for being assigned in GENESIS.

After determining A value, the average nearshore slope $(tan\beta)$ is calculated as the average value of the integral of the slope $\partial D/\partial y$ from 0 to y_{LT}. After the derivation, the formula of calculating $tan\beta$ is equation (B-10) .

$$tan\beta = (\frac{A^3}{D_{LT}})^{1/2} \qquad \text{(B-10)}$$

Depth of closure

Depth of closure (D_C) should be determined based on the beach profiles by years or empirical equation similar to D_{LT}. By checking the profiles by years, the area that profiles do not change could be found. The depth of the starting of that area is the Depth of closure. Another way is applying the equation (B-11) below (Horikawa, 1988) when wave height and period are calculated by the highest significant waves that occurred during a 12-hour period over the course of a year.

$$D_C = (2.3 - 10.9\frac{H_o}{L_o})H_o \qquad \text{(B-11)}$$

GENESIS uses one value of D_C for the whole simulated area. In reality, that can be true in the open coast, when the depths of closure are relatively consistent along a stretch of coastline due to the consistent wave climate and sediment characteristics. However, in the lee of large structures where the wave climate is milder, the depth of closure is smaller than other open coast areas.

5. Structures and beach fill in GENESIS

In the GENESIS model, we can simulate how coastal structures and engineering activities affect the position of the shoreline. The model can represent common types of structures such as groins, breakwater, seawalls, and beach fill, which is a type of "soft structure."

In modeling shoreline change, structures can have two primary effects to the shoreline change. First, structures that extend into the surf zone block the movement of sand along the shore, reducing the amount of sand on the down-drift side. Second, detached breakwaters and structures that extend beyond the surf zone produce wave diffraction, which changes local wave height and direction, affecting the longshore sand transport rate.

Nondiffracting groins:

In shoreline protection, groins and short jetties are usually as long as the surf zone's average width. In shallow water, waves usually arrive almost perpendicular to the tip of the structure or have already broken. As a result, the wave diffraction produced by these structures can be regarded as insignificant. Therefore, groins and short jetties used for shore protection should be treated as non-diffracting structures.

Diffracting groin

Long jetties and harbor breakwaters that are several surf zone widths long can almost completely block longshore sand transport. These structures extend beyond the surf zone where waves may arrive at a large oblique angle, causing a wide diffraction zone. The diffraction option in modeling is used to describe these types of structures.

For both nondiffracting groin and diffracting groin, both bypassing and permeability are the important parameters. While GENESIS automatically calculates the process of sand bypassing around the seaward end of groins, permeability needs to be assigned into GENESIS model. Regardless of whether the structures cause wave diffraction or not, they should be listed in order of where they are located on the grid, from the beginning to the end. This order helps the model to correctly calculate the impact of each structure on the water flow.

The permeability value of groins can range from 1.0 to 0.0. A permeability value of 1.0 means that the groin is entirely transparent, allowing sand to pass through and over it. On the other hand, a permeability value of 0.0 indicates that the groin is highly impermeable and does not permit any sand to pass through or over it.

There is no established way to determine the permeability of a groin in the GENESIS model, so it is best to calibrate the model to find out. If there are many different types of groins in the area being modeled, it is recommended to estimate the relative permeability first and then refine it during calibration. To estimate permeability, fully functioning groins with a crest above MSL are given an initial value of 0.0 to 0.1, while groins with gaps or are overtopped during parts of the tidal cycle may have a permeability in the range of 0.1 to 0.5. Comparing the condition of groins on aerial photographs can also help estimate relative permeability.

When the depth at the groin tip (D_G) is smaller than depth of longshore transport D_{LT} ($D_G < D_{LT}$), the sediment bypasses around a groin. When the depth at the groin tip D_G is higher than depth of longshore transport D_{LT} ($D_G > D_{LT}$), $BYP =$ 0.

Bypassing factor (BYP) in equation (B-12) represents the bypassed sediment amount. $(0 \le BYP \le 1)$

$$BYP = 1 - \frac{D_G}{D_{LT}} \qquad \text{(B-12)}$$

Seawalls

A seawall is a structure built along the shoreline to protect land from erosion and flooding caused by waves. The seawall acts as a barrier that prevents the beach from eroding and moving landward beyond the wall's position. In other words, the presence of a seawall limits the possible position of the shoreline because the beach cannot erode beyond the wall.

Beach fills

When multiple beach fills occur, it is important to provide information in the order in which they happened. Although the fills may overlap in time and location, they still need to be entered in the same order each time. GENESIS considers beach fill to have the same grain size and berm height as the original beach. GENESIS does not operate directly using the volume of beach fill. Instead, it calculates the total distance of shoreline movement after the fill and beach profile have reached an equilibrium shape due to wave action. The fill is placed in all cells between and including the starting and ending cells. When a beach fill operation occurs, GENESIS places the fill and advances the shoreline in equal amounts at each time step, between the start and end dates of the fill operation, even if the wave conditions are not strong enough to cause sediment transport and shoreline changes.

APPENDIX C
COMPARE WIND ERA5 TO OBSERVATIONAL WIND DATA

This appendix provides the comparison of global wind data which is wind ERA 5 to observational wind data from Phan Thiet station as their locations shown in Figure C-1.

The only observational wind station was Phan Thiet station located at 10.9 N 108.1 E, close to the coastline (Less than 1 km from the coastline) as shown Figure C-1. The data was collected from Binh Thuan Provincial Hydrometeorological Center. The characteristics of wind at this station is shown as the wind rose in Figure C-2. The wind is from many directions with a frequency range from 3.12 % of SSW (South South West) wind to 16.00 % West wind. At this location, 3.59 % of winds have a speed of more than 10 m/s. The most frequent wind speed is from 2 m/s to 4 m/s which covered around 42.90 %.

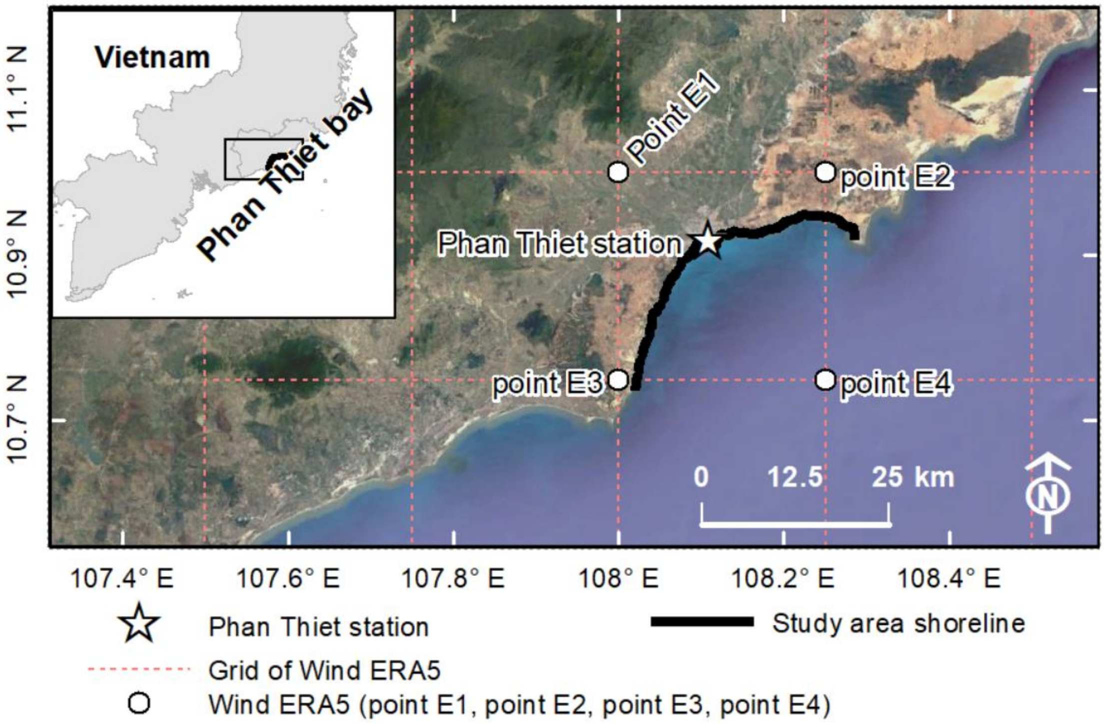

Figure C-1 Locations of observed wind data (Phan Thiet station) and 4 points of ERA5 wind data (E1, E2, E3, E4)

In Phan Thiet bay, observed wind data was collected at the Phan Thiet meteorological station from 2015 to 2018 only. While these observed wind data is the most accurate compared to global wind data, it has spatial limitations as it does not cover the entire computational grid, and the time limitation as it does not span from 1988 to 2021. To overcome these spatial and temporal limitations, global wind data from ERA5 was utilized to supplement the analysis and provide a broader understanding.

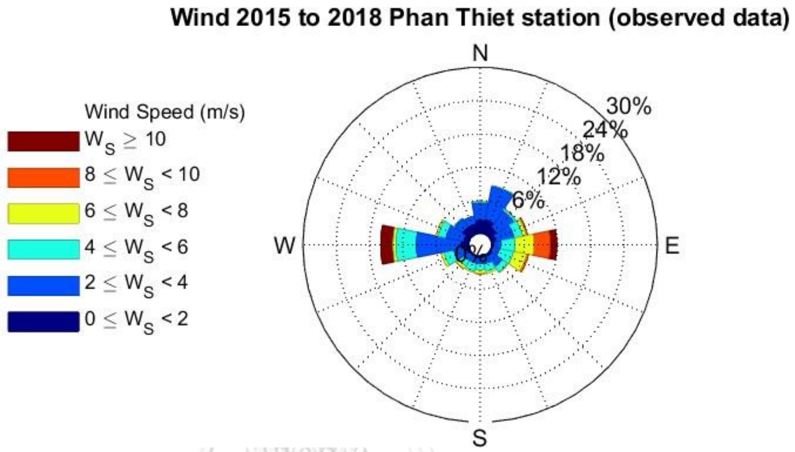

Figure C-2 Wind data at Phan Thiet station

Point E1, point E2, point E3, and point E4 are the nearest points of ERA5 to Phan Thiet observational station, as the resolution of ERA5 wind data is 0.25 arc-degree. The ERA wind data from 2015 to 2018 at 4 points are shown in Figure C-3. Point E1 is situated on land, while points E2 and E3 are close to the coast, and point E4 is located in the sea. The difference in the wind characteristics in land and on sea could be seen through the wind roses of these 4 points.

According to the analysis of those points which was summarized in Table C-1, the wind on land points that are point 1, point 2, point 3 had lower wind speeds compared to point 4 in the ocean. That shows how different the wind in land from the wind on sea in Phan Thiet area. The dominant wind directions are ENE, E and WSW in coastal area (point 2 and point 3) and on sea (point 4). At point 1 in land, the dominant directions are ENE and West, which are slightly different from coastal area. In Phan Thiet, the wind at the inland point 1 was distributed in all directions more evenly than other points at the coastal area and on sea point.

Moreover, in those 3 points, the wind barely blew from the North, East and adjacent directions.

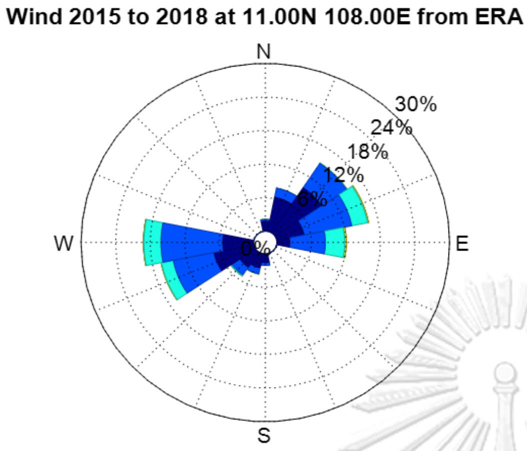

a) *ERA5 wind data point E1*

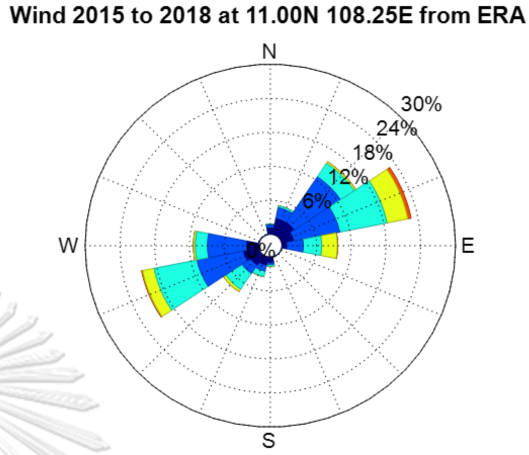

b) *ERA5 wind data point E2*

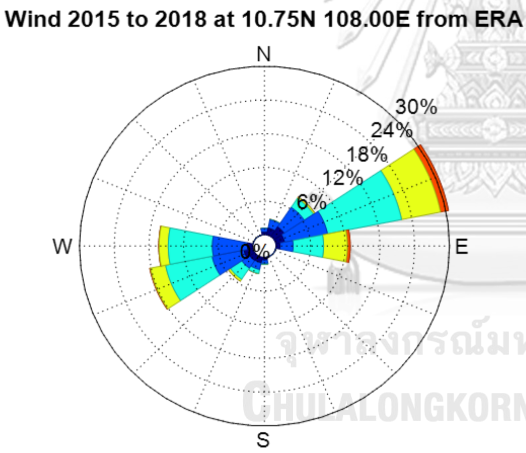

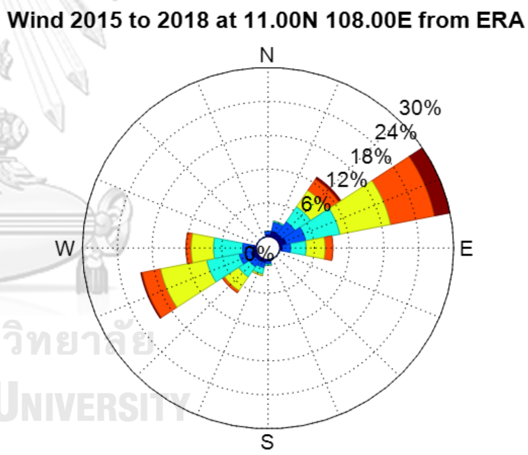

c) ERA5 wind data point E3

d) ERA5 wind data point E4

Figure C-3 Wind rose or ERA5 wind data
a) ERA5 wind data point E1,) b) ERA5 wind data point E2, c) ERA5 wind data point E3, and d) ERA5 wind data point E4

There are some differences and similarities between the characteristics of the observational wind data and ERA5 wind data. The ERA5 wind data has direction distribution similar to the wind at point 1, which is quite even among all the directions. In both of them, even the most predominant direction only plays 18.91 %. Because the observational data was the hourly-instantaneous data, while the ERA data is hourly-mean wind data. The distribution of the observational wind data was more even than ERA data in coastal area and onshore. The wind speed of Phan Thiet station is quite comparable with wind data point 4. At Phan Thiet station, wind with the wind speed higher than 10 m/s happened 3.59 %, which is close to 3.76% in wind data point 4. Moreover, the direction of those highest wind speed is from the West and East at Phan Thiet station, while they are WSW and ENE at point 4. Four stations of ERA5 have distance 14 km, 18 km, 22 km, and 25 km correspondingly from the Phan Thiet wind station. With those distances, the similarity of the distribution of wind speed, predominant wind frequency, and direction could suggest the similarity of ERA5 data and observed wind data.

Table C-1 Comparison of wind inland at E1, close to the coast E2 and E3, and nearshore E4

	Phan Thiet station	**E1**	**E2**	**E3**	**E4**
Distance to shore	*< 1km*	*On land* 14 km	*On land* 5 km	*On land* 2 km	*Nearshore* 25 km
Highest wind speed	> 10 m/s *0.85%*	8 to 10 m/s *0.02%*	> 10 m/s *0.02%* 8 to 10 m/s *0.97%*	> 10 m/s *0.09%* 8 to 10 m/s *1.94%*	> 10 m/s *3.76%*
Most frequent speed	2 to 4 m/s *46.06%*	0 to 2 m/s *42.96%* 2 to 4 m/s *44.63%*	2 to 4 m/s *41.40%*	4 to 6 m/s *40.03%*	6 to 8 m/s *30.86%*
Most frequent direction	West 13.77%	West *18.91%*	WSW *18.82%* ENE *21.97 %*	ENE *29.14%*	ENE *30.34%*

135

APPENDIX D
COMPARE WAVEWATCH III DATA TO OBSERVATIONAL WAVE DATA

The seaward boundary condition is based on wave data from Global wave data, since only 1 buoy of observing wave data were available in the simulating area. Observational wave data was collected at Bach Ho from Institute of Meteorology Hydrology and Climate Change Vietnam, as shown in Table D-1, and Figure D-1. The wave characteristics at this station were then compared with WaveWatch III data to confirm the reliability and applicability of WaveWatch III as a wave boundary condition for simulating nearshore wave dynamics in Phan Thiet bay.

Table D-1 Observed wave data in Phan Thiet bay

Locations	Coordinate (WGS84)	Time	Interval time
Bach Ho	10.442 ^{o}N 108.381 ^{o}E	10 Jun 2017 to 12 Jun 2017	Everyday, every 3 hours, start at 1:00 am

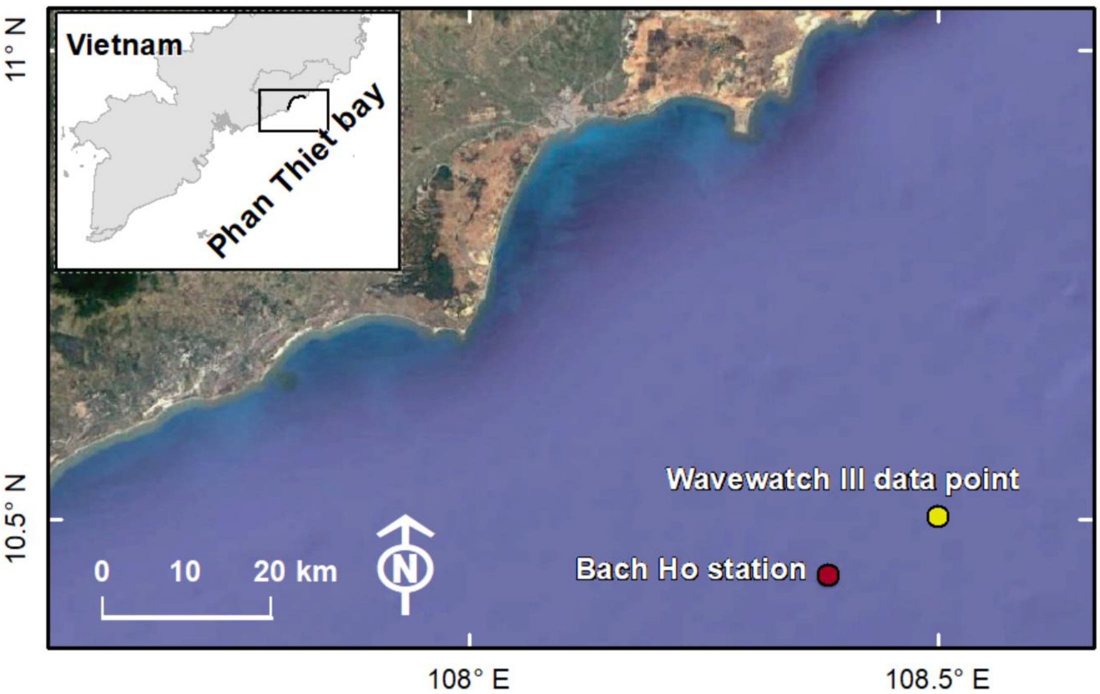

Figure D-1 Locations of WaveWatch III data and their closest observational data (Bach Ho station)

The observed wave directions and heights closely align with the corresponding values provided by the WaveWatch III model as shown in Figure D-2. Most of the directions were from South or SW. Even though there are some differences in the range of significant wave height, this comparison conclusively validates the application of the WaveWatch III model in representing the wave characteristics of the study site. Therefore, WaveWatch III can be used to be the boundary conditions for simulating the wave characteristics in Phan Thiet bay in the higher resolution.

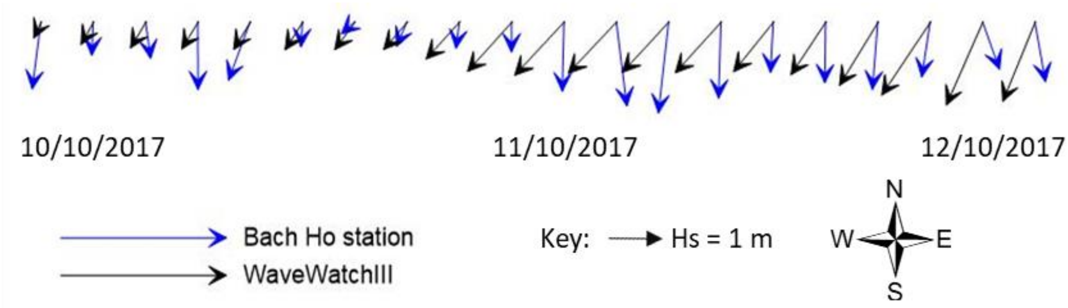

Figure D-2 The comparison of Wavewatch III data at 10.5 °N 108.5 °E and wave at Bach Ho station from 10 Jun 2017 to 12 Jun 2017

APPENDIX E
SWAN MODEL SETUP AND SENSITIVITY

1/ Model setup

The first step of using SWAN was setting up the model with spatial conditions, bathymetry data, wind data, and wave boundary data. The spatial and temporal details of those data were shown in Table E-1 and Table E-2.

Table E-1 Description of the grid of computation, bathymetry data, wave data, wind data size and their sources

Item	**Latitude (Degree)**	**Longitude (Degree)**	**Mesh size (Degree)**	**Sources**
Computation grid & Bathymetry	From 10.505 to 11.505	From 107.5 to 109.0	0.0125	GEBCO
Wind	From 10.5 to 11.5	From 107.5 to 109.0	0.25	ERA5
Wave	From 10.505 to 11.505	From 107.5 to 109.0	0.5	WAVEWATCH III

Table E-2 Description of the time of wind input and wave boundary

Item	**Start (dd/mm/yyyy)**	**End (dd/mm/yyyy)**	**Interval time**
Wind	01/01/1988	31/12/2021	1 hour
Wave	01/01/1988	31/12/2021	3 hours

The spatial domain of SWAN model was Phan Thiet bay and the adjacent areas as shown in Figure 3-12. The simulated grid of this area included 80 rows and 120 columns from latitude 10.505° N to 11.505° N longitude 107.5° E to 109.0° E. The size of each grid cell was 0.0125 arc-degree × 0.0125 arc-degree (approximate 1.3875 km × 1.3875 km).

Bathymetry data was the gridded bathymetry data of the General Bathymetric Chart of the Oceans (GEBCO), whose website for downloading data was https://download.gebco.net/ (GEBCO Compilation Group, 2020). When the SWAN model in this study was conducted in 2021, the GEBCO_2020 grid was the latest global bathymetric product released by GEBCO. For bathymetry input in this study, the GEBCO_2020 including the elevation data of the area from 10.505°N to 11.505°N of latitude, and 107.5°E to 109°E of longitude as shown in Figure E-1 was used. The grid resolution was 15 arc-second which was about 0.004167 arc-degree or 0.4624 km. The elevation value represented the elevation at the center of each grid cell. Most of the seabed elevation was referred to mean sea level, except for some shallow water areas. The data sources did not have mean sea level vertical datum. The GEBCO data was downloaded with 3 separate table variables of latitude, longitude, and elevation. In order to preprocess the GEBCO bathymetry data into the format that was used in SWAN, the software Matlab and Delft3D version 3.04 were used. The grid cell was still 0.004167 arc-degree. That file was imported into Delft3D and changed to the grid cell of 0.0125 arc-degree for matching the computation grid in SWAN.

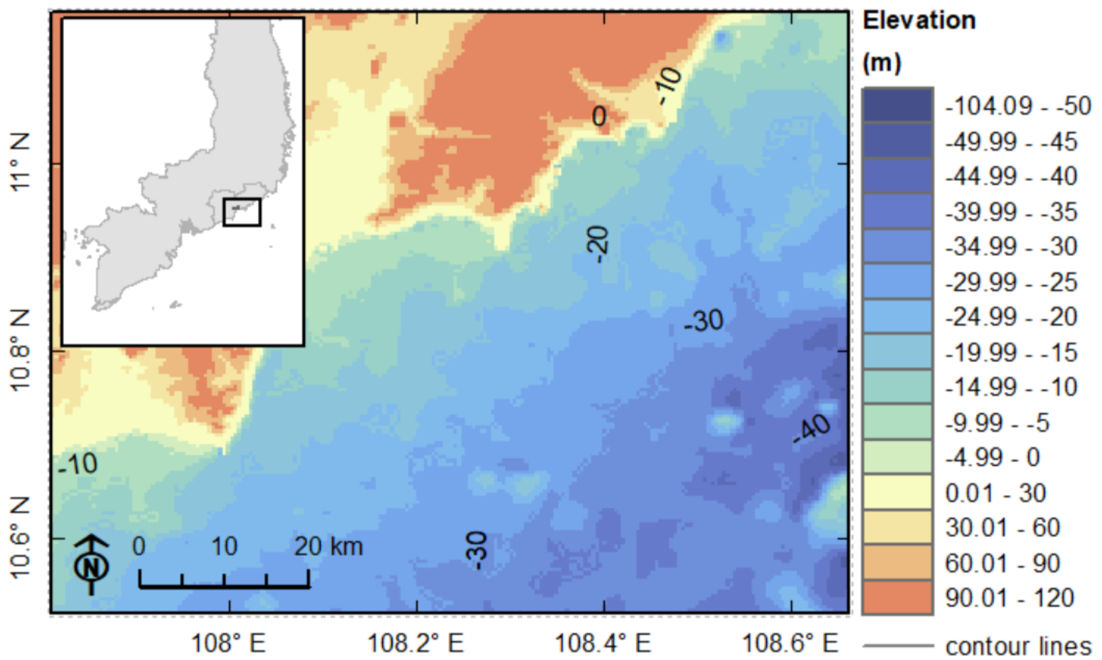

Figure E-1 Topography assigned in SWAN (GEBCO_2020 with 15 arc-second resolution)

ERA5 wind data from 1988 to 2021 with an interval time of every hour was used for simulating the wave in this study. The wind data was from latitude 10.5 °N to 11.5 °N, and from longitude 107.5 °E to 109.0°E with the 0.25 arc-degree grid is wide enough to cover beyond all the sea area of computation grid. The wind data includes the wind speed in the zonal direction (u direction) and meridional direction at a height of 10 m above the surface. The wind from the West to the East (u direction) and the wind from the South to the North (v direction) were set to be positive. Every set of u wind and v wind represents the wind speed in that grid of 0.25 arc-degree × 0.25 arc-degree.

After downloading the ERA wind data, Matlab was used for preprocessing wind data into the format that can be understood by SWAN. The ERA wind data originally include 2 different files of the u wind, and v wind by location and time. This format should be changed into 1 file only in which SWAN can read all u wind by location, and then read all v wind by location of a certain time; and then, the next time step would be read.

Wavewatch III wave data was considered to meet the requirements in quality and quantity as the wave boundary. The resolution is 0.5 arc-degree and the interval time is 3 hours, available more than from 1988 to 2021 (NOAA, 2023b) which is the simulation time that SWAN does. The wave boundary is from latitude 10.505 ^{o}N to 11.505 ^{o}E, and from longitude 107.5 ^{o}E to 109 ^{o}E. The grid resolution of Wavewatch III wave is 0.5 arc-degree × 0.5 arc-degree. That means there are 4 boundary points for simulating wave in SWAN as shown in Figure 3-12. The time interval is 3 hours.

The next step of preparing the input and boundary data was creating the code in SWN file (.swn) to be read and run in SWAN version 41.31. Some main parts of the code were the start-up of coordinate setting, the spatial condition, the input, the boundary, the parameters of physical processes, and the output setting.

Firstly, the Start-up of the model was set up. The wind and wave direction of SWAN input and output were in Nautical convention instead of default Cartesian convention. All coordinates of locations and geographical grid sizes were given in degrees. Greenwich meridian was longitude x=0. Equator was latitude y=0. The study area was in the East and in the Northern hemisphere with positive values of x and y. Secondly, the detail of SWAN model in this study was described. The computation grid was uniform and rectangular. The x and y Geographic location of the origin of the computational grid in the spherical coordinate were 107.5 ^{o}E and 10.505 ^{o}N. The direction of the positive x-axis of longitude value of the computation grid was the East direction. The direction of the positive y-axis of latitude value of the computation grid was the North direction. The length of the computation grid in x-direction was 1.5 degree. The length of the computation grid in y-direction was 1.0 degree. The grid includes 120 x 80 meshes. The spectral directions covered the full circle. The grid of bottom input was also uniform and rectangular with the origin coordinate 107.5 ^{o}E and 10.505 ^{o}N. The grid size was 120 x 80 meshes. The size of each mesh was 0.0125 x 0.0125 degree. The input bottom grid was in the same unit scale as required in SWAN. The input grid of the wind velocity field was defined with the origin at 107.5 ^{o}E and 10.5 ^{o}N. The number of meshes were 6 in x-axis and 4 in y-axis. The mesh size was 0.25 x 0.25 square degree. JONSWAP wave spectrum was default in SWAN. The wave boundary segment went around the sea boundary following the South edge and East edge boundary. The start point was at coordinate 107.5 ^{o}E 10.505 ^{o}N in the SW of the boundary, and end point was at coordinate 109.0 ^{o}E 11.505 ^{o}N. In this study, the physical processes included whitecapping, wave breaking, and bottom fiction. The parameters of these processes were calibrated in SWAN model by comparing to observed wave data. The coefficients for determining the rate of whitecapping dissipation, friction, and wave breaking were calibration parameter. The friction coefficient of JONSWAP formulation was 0.037. The constant breaker index was used. The proportionality coefficient of the dissipation rate was 1.0 as the default. The breaker which was the ratio of maximum individual wave height over depth is 0.7. Afterward, the model was set up to run with the time step of the nonstationary computation was 0.5 hour. The output was the file of the coordinate (XP,YP) in World Geodetic System WGS84, water depth (DEPTH) in meter, significant wave height (HS) in meter, swell wave height (HSWELL) in meter, mean absolute wave period in second, and wave direction (DIR) in degree of Nautical Convention. The time interval tween fields were 0.5 hour.

(Example code of 18 Aug 2014 to 26 Aug 2014)

$Set up******

```
PROJ 'Phan Thiet'

SET NAUTICAL
```

```
MODE NONSTATIONARY TWODIMENSIONAL
COORDINATES SPHERICAL
```

$South Vietnam sea Long 107.5E-119.0E Lat 10.505N-11.505N (grid of 0.0125x0.0125 degree)******

```
CGRID REG 107.5 10.505 0. 1.5 1.0 120 80 CIRCLE 36 0.1 2.5 41
INPGRID BOTTOM REG 107.5 10.505 0. 120 80 0.0125 0.0125
READINP BOTTOM 1.0 'BOTNOW' 4 0 FREE
INPGRID WIND REG 107.5 10.5 0. 6 4 0.25 0.25 NONSTAT 20140801.000000 1 HR 20140830.230000
READINP WIND 1. 'PT_Wind2014_Aug.dat' 2 FREE
$
```

$BOUNDARY AND INITIAL CONDITION******

```
BOUN SHAPE JONSWAP 3.30 PEAK DSPR DEGREE
$***SOUTHERN BOUNDARY***
BOUN SEGM XY 107.5 10.505 108.0 10.505 &
CON FILE 'waveboundary/TPAR_108.0_10.5_1.bnd' 1
BOUN SEGM XY 108.0 10.505 108.5 10.505 &
VAR FILE  0.00 'waveboundary/TPAR_108.0_10.5_2.bnd' 1 &
          0.50 'waveboundary/TPAR_108.5_10.5_1.bnd' 1
BOUN SEGM XY 108.5 10.505 109.0 10.505 &
VAR FILE  0.00 'waveboundary/TPAR_108.5_10.5_2.bnd' 1 &
          0.50 'waveboundary/TPAR_109.0_10.5_1.bnd' 1

$*****************EASTERN BOUNDARY******************
BOUN SEGM XY 109.0 10.505 109.0 11.005 &
```

```
VAR FILE  0.00 'waveboundary/TPAR_109.0_10.5_2.bnd' 1 &
          0.50 'waveboundary/TPAR_109.0_11.0_1.bnd' 1
BOUN SEGM XY 109.0 11.005 109.0 11.505 &
CON FILE 'waveboundary/TPAR_109.0_11.0_2.bnd' 1
INIT ZERO
GEN3 KOM 1.4e-5 3.02e-3
WCAP KOM 1.4e-5 3.02e-3 2 1 1
FRIC JONSWAP 0.037
BREA CONST 1.0 0.7
PROP BSBT
NUM ACCUR 0.010 0.020 0.020 99.50 NONSTAT mxitns=1
$***OUTPUT REQUEST***
POINTS 'PT' FILE 'PH01_TN.loc'
TABLE  'PT' HEAD 'PH01_TN.out' TIME XP YP DEPTH HS TMM10
DIR DSPR OUT 20140818.175600 0.5 HR
BLOCK 'COMPGRID' NOHEAD 'PT.mat' LAYOUT 4 XP YP DEPTH HS
HSWELL TMM10 DIR WIND DHSIGN DRTM01 OUT 20140818.175600
0.5 HR
TEST 1,0
COMPUTE NONSTAT 20140818.175600 0.5 HR 20140826.235600
STOP
```

3/ Model sensitivity

Sensitivity analysis revealed parameter impacts on the model output, guiding calibration and validation. It identifies key factors controlling the model's behavior and highlights areas needing more data to reduce uncertainties and improve accuracy. In the present study, sensitivity analysis focused on three parameters: whitecapping

(WCAP), bottom friction (FRIC), and depth-induced wave breaking (BREAK). The objective was to gain a comprehensive understanding of how these parameters affect the resulting wave heights.

The whitecapping parameter (WCAP) controls the representation of wave energy dissipation due to whitecapping or wave breaking. Sensitivity analysis of the WCAP in the SWAN model revealed the insights into its influence on wave characteristics. By systematically varying the values of WCAP, the study examined the resulting wave patterns and identified a notable sensitivity to changes in this parameter. Increasing the value of WCAP was found to intensify wave energy dissipation, leading to a significant reduction in wave heights. Conversely, decreasing the WCAP value allowed for relatively less energy dissipation and consequently yielded higher wave heights in the simulated wave patterns.

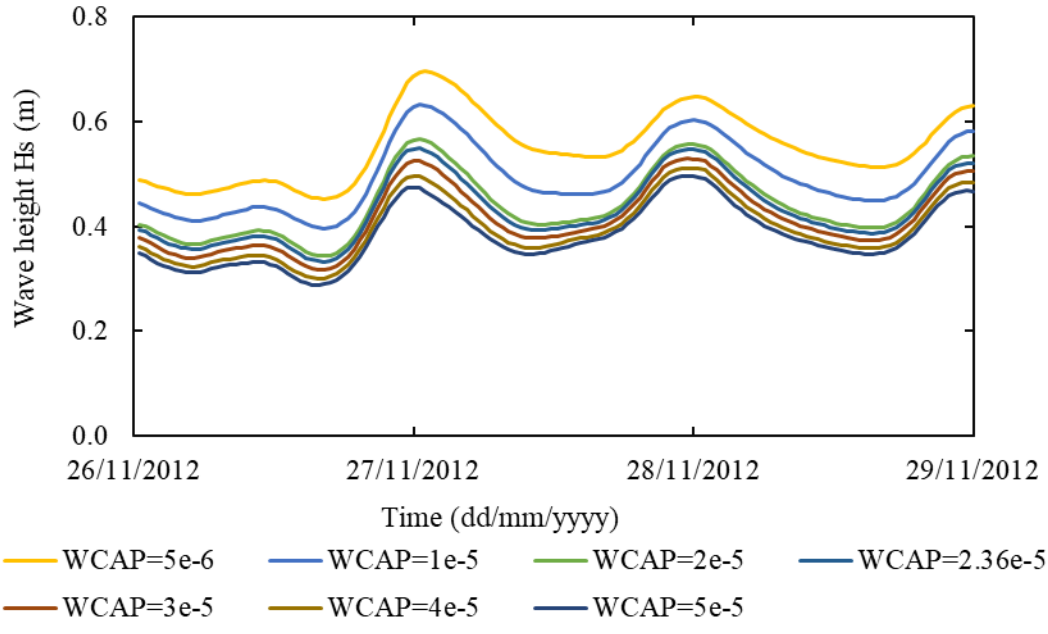

Figure E-2 Sensitivity of whitecapping parameter (WCAP)

The bottom friction parameter (FRIC) is a factor in the SWAN model that controls the dissipation of wave energy caused by interactions with the seabed. The influence of FRIC on wave characteristics was assessed by conducting a sensitivity analysis of the FRIC parameter. When the FRIC value was increased, the dissipation of wave energy through enhanced interactions with the seabed was intensified. As a result, a decrease in wave heights was observed. Conversely, reducing the FRIC value resulted in less energy dissipation, allowing for higher wave heights in the simulations.

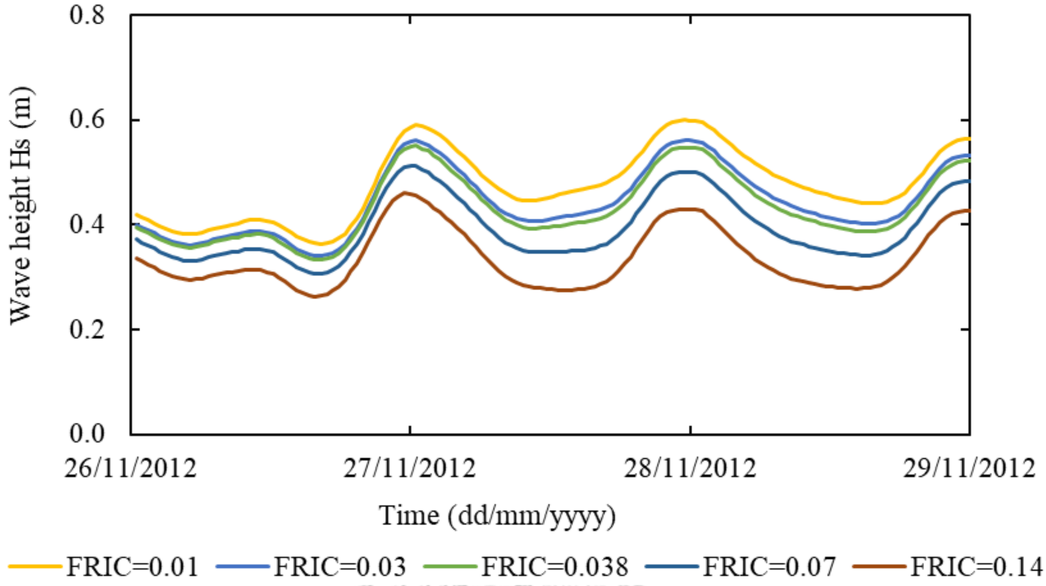

Figure E-3 Sensitivity of Bottom friction parameter (FRIC)

The Depth-induced wave breaking parameter (BREAK) controls the dissipation of wave energy caused by depth-induced wave breaking. The sensitivity analysis of the BREAK parameter in the SWAN model provided insights into its influence on wave characteristics. During the investigation, the BREAK was systematically varied, yet no observable changes in wave height over time were detected. The simulations indicated that increasing or decreasing the BREAK value did not yield any visible impact on wave heights at station PH01, which was used for doing sensitivity analysis. That could mean wave breaking did not happen in this area possibly due to low wave steepness, high wave period, or low wave energy. These findings suggest that wave breaking was not significant in the study area during the analyzed period.

The sensitivity analysis revealed significant differences in the impacts of the whitecapping parameter (WCAP) and bottom friction parameter (FRIC) compared to the wave breaking parameter (BREAK). WCAP and FRIC demonstrated a considerably larger influence on the model than BREAK. Consequently, in the subsequent calibration and validation process, greater attention will be given to WCAP and FRIC, considering their stronger impact. On the other hand, BREAK will be considered as a lower priority parameter in the calibration and validation process. These findings guide the prioritization of parameters to ensure an effective and efficient calibration and validation procedure.

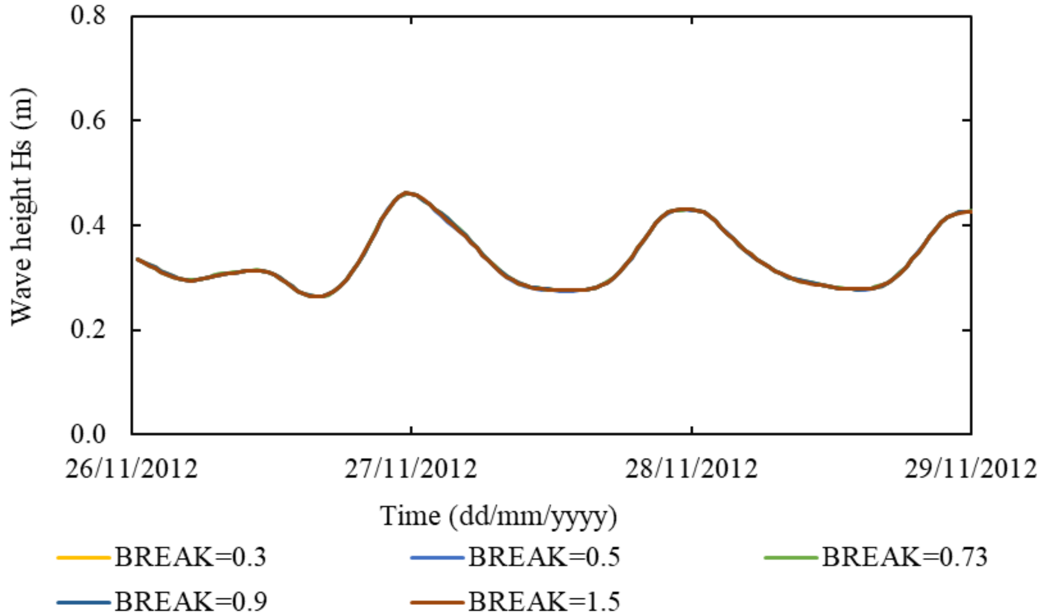

Figure E-4 Sensitivity of Depth-induced wave breaking (BREAK)

APPENDIX F
GENESIS MODEL SETTING UP

In this study, in order to get the input for GENESIS model, the Grid Generator and WWWL programs were used as shown in Figure F-1. The first program is Grid Generator, in which the bathymetry and the shoreline were imported before building the uniform grid for GENESIS model later. The second program is WWWL. In this WWWL program, the wave data from the previous model SWAN would be formatted as the requirement of GENESIS model. The last program is GENESIS model, where the shoreline is simulated from the initial shoreline and other input such as wave data, sediment size, and structure. The initial shoreline is from part 1 shoreline change assessment of this study. In GENESIS, after setting up the model is the sensitivity analysis, calibration, and validation for determining the parameters including K1, D_c, D_{50}, D_b, K2. The outputs of this process are the positions of shorelines with the difference between initial shoreline and final shoreline, and longshore sediment transport rate.

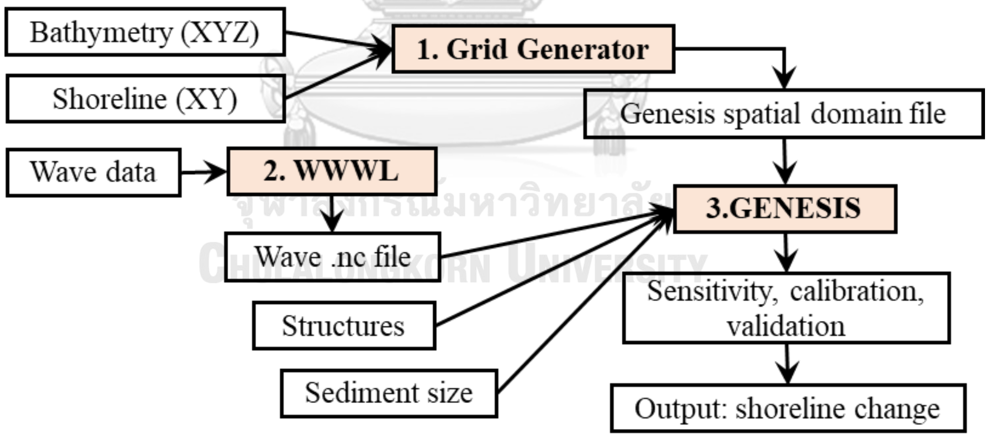

Figure F-1 CEDAS process including Grid Generator, WWWL, and GENESIS

The first step is supposed to be preparing the input including the bathymetry, shorelines, wave data, structures, and sediment size. The bathymetry and shoreline input are the same for all 3 segments, while wave data, sediment size and structures are different depending on each segment. The locations of wave data and structures of segment 1, segment 2, and segment 3 were illustrated in Figure F-2, Figure F-3, and Figure F-4.

Table F-1 shows the details of the shorelines used as the initial shorelines and reference shorelines in GENESIS. Most of the shorelines were obtained from Landsat images. Only 1 shoreline for segment 2 in 15 Mar 2011 was manually digitized in Google Earth since the Landsat images have low quality with the cloud in Segment 2 during the year 2011.

Table F-1 Landsat images to do shoreline digitization for GENESIS model

Date	Time (UTC+7:00)	Source	Segment
07/01/1988	9:36	Landsat 5	1, 3
09/03/1993	9:29	Landsat 5	1, 3
10/01/1995	9:20	Landsat 5	1
04/05/1996	9:17	Landsat 6	3
07/07/1996	9:21	Landsat 5	1
03/01/2004	9:46	Landsat 5	1, 2
14/04/2006	9:59	Landsat 5	3
15/02/2008	9:58	Landsat 5	1, 2
07/02/2011	9:57	Landsat 5	1
15/03/2011	Use Google Earth Pro image		2
03/03/2014	10:07	Landsat 8	1
15/06/2017	10:06	Landsat 8	3
10/02/2018	10:07	Landsat 8	1
06/09/2018	10:06	Landsat 8	2
06/03/2021	10:07	Landsat 8	1, 2, 3

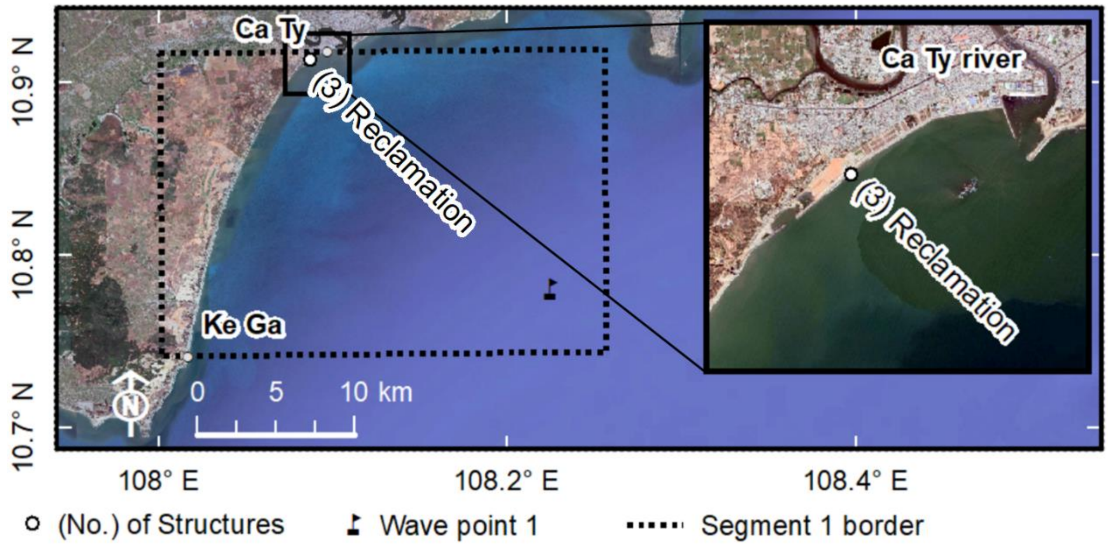

Figure F-2 Location of wave data and structures for segment 1 in GENESIS

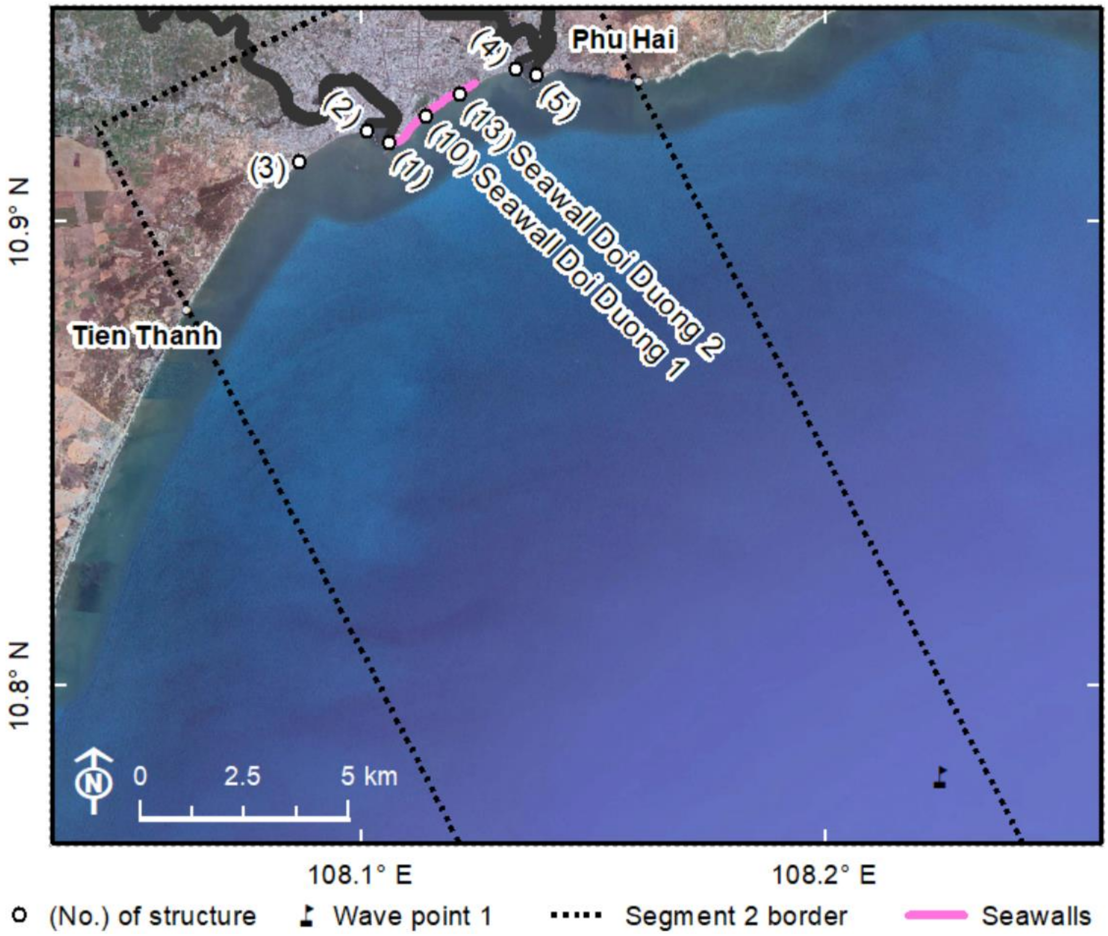

Figure F-3 Location of wave data and structures for segment 1 in GENESIS

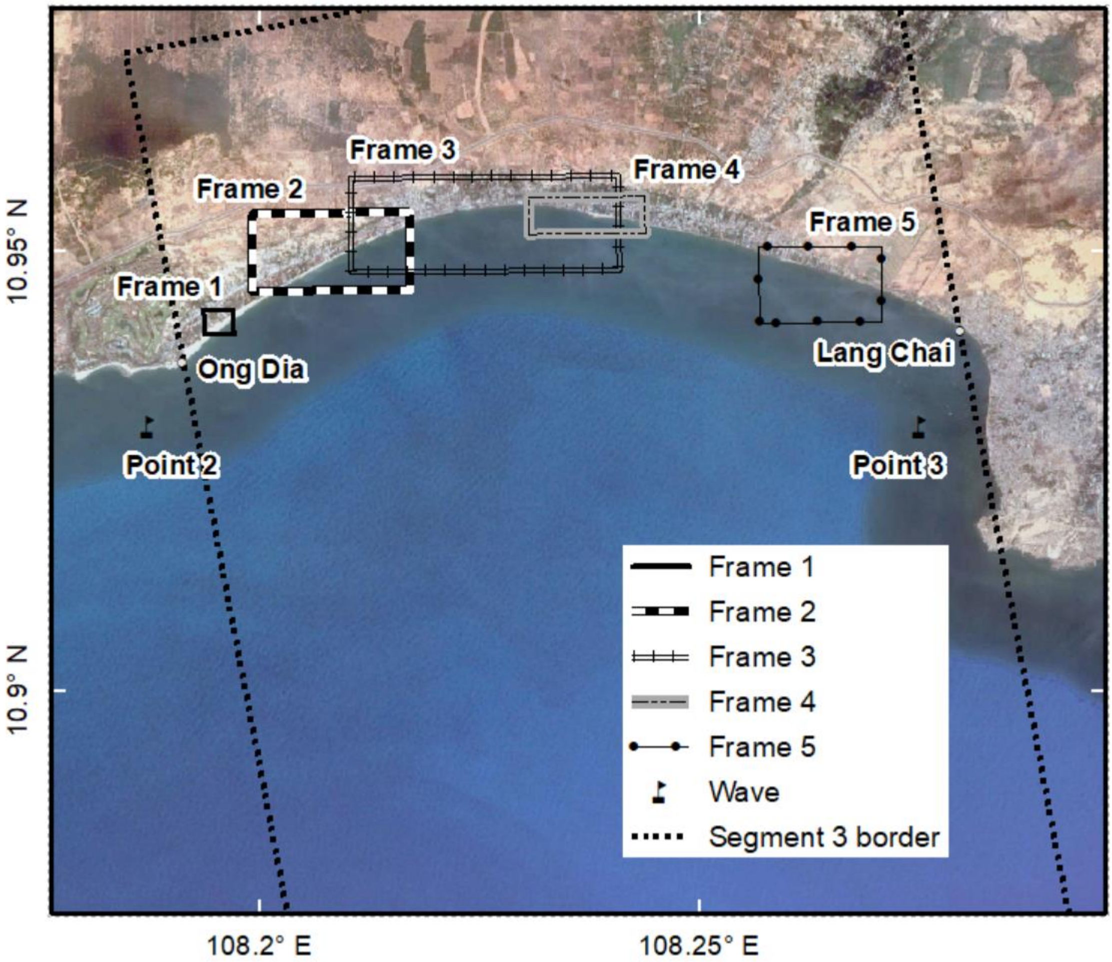

Figure F-4 Location of wave data and structures for segment 3 in GENESIS

In case of segment 3, due to the large number of structures in long shoreline, the map was zoomed into 5 frames as shown in Figure F-5 and Figure F-6.

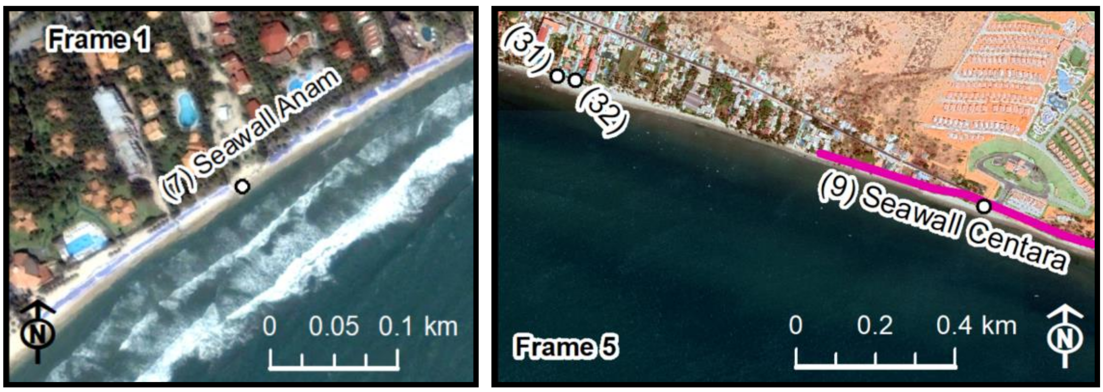

Figure F-5 Zoon in to Frame 1 and Frame 2 of segment 3 in Figure F-4

150

Figure F-6 Zoon in to frame 1, frame 3, and frame 4 of segment 3 in Figure F-4

Depending on the type of structure, different information is required in GENESIS as shown in Table F-2.

Table F-2 The data required for GENESIS to run the structures

Structure	Required data
Non-diffracting Groins and Jetties	Start X1 (m), Position Y1 (m), End X2 (m), Position Y2 (m), Model X-Index, Model length, Permeability
Diffracting Groins and Jetties	Start X1 (m), Position Y1 (m), End X2 (m), Position Y2 (m), Model X-Index, Model Length, Seaward Depth (m), Permeability
Detached Breakwaters	Start X1 (m), Start Index, Position Y1 (m), Depth 1 (m), End X2 (m), End Index, Position Y2 (m), Depth 2 (m), Transmission Coefficient (m)
Seawall	Start X1 (m), Start Index, Position Y1 (m), End X2 (m), End Index, Position Y2 (m)
Beachfills	Start yyyymmdd, End yyyymmdd, Start Coordinate (m), Start Index, End Coordinate (m), End Index, Added Berm Widths (m)

In Genesis, there is no available option to assign the beach reclamation project into the model. In order to determine the most appropriate way of assigning the beach reclamation project Hamubay into the GENESIS model and accurately simulate its effects on the shoreline, different approaches were tested in this study. The beach reclamation project involves the process of filling an area of the sea to create new land, and in this case, it is protected by a seawall along the edge of the beach. The tested methods included:

+ Beach fills only: it was not possible to determine the erosion result downstream of Hamubay accurately due to the spilling of sediments from the beach fills into the adjacent area.

+ Combining beach fills and seawall along the edge of the beach fills: it was also not possible to determine the erosion result downdrift of Hamubay accurately due to the spilling of sediments from the beach fills into the adjacent area. The seawall does not give the effect to the shoreline downdrift of Hamubay.

+ Combining beach fills with a groin at the end of the project: the erosion at the downdrift of Hamubay was simulated in a better way compared to the 2 upper methods.

+ Adjusting the initial shoreline while adding a seawall: The result shows the final shoreline as a gradual and smooth shoreline due to GENESIS simulation. This method is particularly suitable for the final phase of the Hamubay project, where the edge of the beach reclamation aligns seamlessly with the downdrift shoreline. Meanwhile, this approach may not be applicable during earlier stages of the project when the alignment between the beach reclamation and the downdrift shoreline is not as consistent.

The results recommended that the beach reclamation project Hamubay be assigned to the GENESIS model as beach fills with a groin at the end for the period between 2004 to 2018. However, for the simulation with the final year of 2021, where the end of the beach reclamation project was more aligned with the shoreline, it is suggested to adjust the initial shoreline to match the final edge of Hamubay and add a seawall along that edge.

After preparing all the required inputs, the model was implemented. Firstly, the Bathymetry with the data of sea bed elevation of mean sea level vertical datum was imported to Grid Generator (GridGen). After the bathymetry data is the location of the initial shoreline. Next steps is defining the GENESIS grid of segment 1, segment 2, and segment 3 as illustrated in Figure F-7, Figure F-8, and Figure F-9 correspondingly. The grid size DX'×DY' is 50 m × 50 m for all 3 segments.

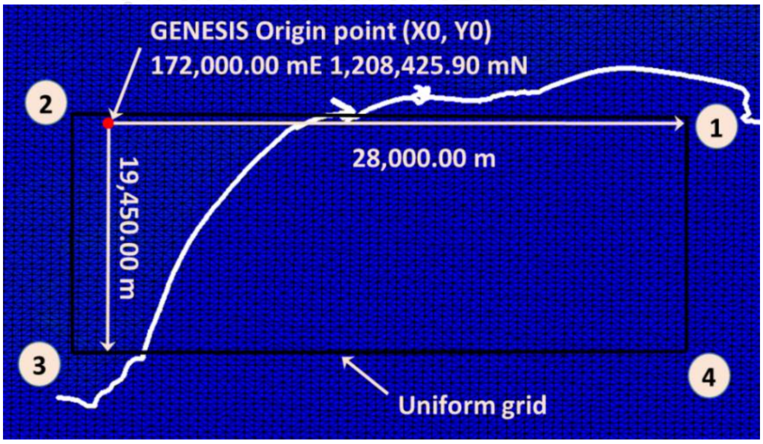

Figure F-7 The uniform grid of segment 1 in GENESIS

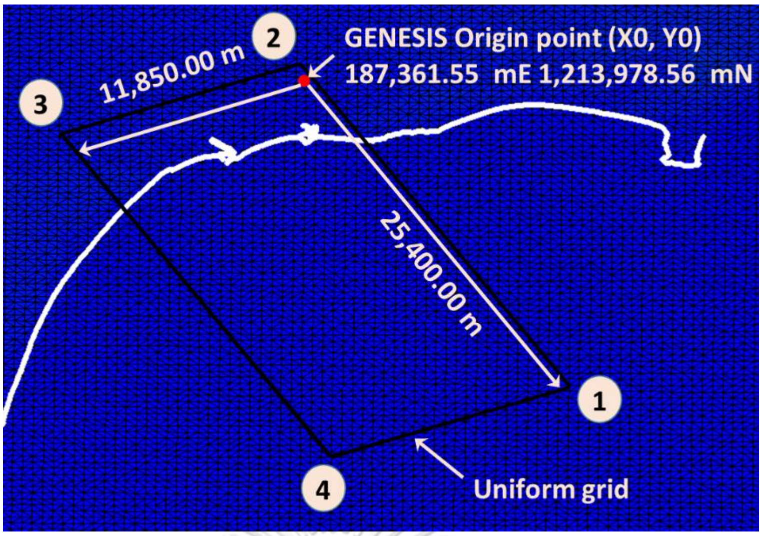

Figure F-8 The uniform grid of segment 2 in GENESIS

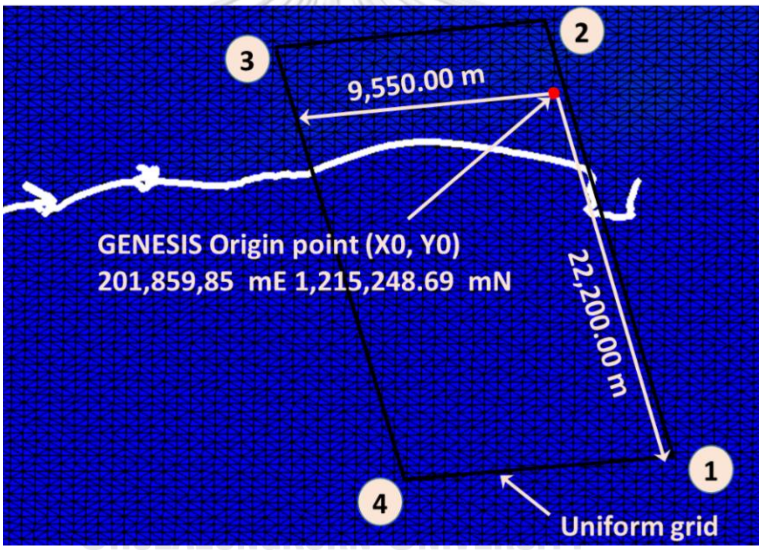

Figure F-9 The uniform grid of segment 3 in GENESIS

Beside the Grid Generator, the wave data was supposed to be prepared in WWWL program before being assigned to GENESIS model. WWWL program transforms the wave data into the required formatted file including time of wave data, wave height, wave period, wave direction, and mean depth and coordinates of that wave location. In WWWL program, the coordinate system was set up to be the UTM zone 49N; the vertical datum was set up to be Mean Sea Level as same as in Grid Generator. The time is Greenwich Mean Time; and the direction convention is Meteorologic which are the same as the wave data from SWAN. That means 0 degree is at the North direction; the wave rose shows the direction of where the wind is from. In other words, 0-degree waves are from the North.

After obtaining the wave file, the GENESIS spatial domain file, and the inputs of structures and sediment size, GENESIS model was ready to be used. The GENESIS spatial domain file was first imported into GENESIS model. Next was the GENESIS configuration which includes the wave file, the simulation temporal data such as the simulation period, and the time step. The configuration also should specify the location to save the output file and the visualization file which are necessary to export the result.

Other compulsory data for GENESIS to run are the sand and beach data, and the longshore sand transport calibration coefficients. The sand and beach data include effective grain size (D_{50}), average berm height (D_b) and Closure Depth (D_c). The longshore sand transport calibration coefficients include K1 and K2. In this study, these are also the calibration parameters. Beside these parameters, GENESIS also allows the users to set up the boundary conditions data such as setting up the Wave model applied to be internal in this study; setting up the number of wave components to apply; setting up the left and right boundary conditions to be pinned, gated, or moving.

In some simulation for the period that the coastal projects existed, the information of those structures needed to be assigned. GENESIS has some options of structures including Nondiffracting Groins and Jetties, Diffracting Groins and Jetties, Detached Breakwaters, Seawalls, and Beach Fills as shown in Table F-2.

Hereafter, GENESIS model could be run and export output data. The outputs of GENESIS are the shoreline comparisons and the average longshore transport rate. In the shoreline comparison, the initial shoreline, the final shoreline, and the difference at each X point were exported.

APPENDIX G
DETERMINING SEDIMENT SIZE FOR GENESIS SIMULATION

One of the main inputs in GENESIS is the sediment size D_{50}. The sediment size was determined based on the beach profile, and the sediment collected at the study area. Figure G-1and Figure G-4 show the locations where the beach profiles were drawn based on the survey data and GEBCO data.

1/ Sediment size based on beach profile

In order to determine the value of sediment size from the beach profile, that beach profile need to be compared to the graph between distance Offshore and Elevation by the equation (G-1) of Bruun (1954) and Dean (1977) as the details described in CHAPTER 2. Each sediment size value gives 1 line of beach profile in that graph.

$$D = Ay^{2/3} \quad \text{(G-1)}$$

The beach profile survey was conducted by Vuong (2012) and Vuong (2014) in 12 locations near the Ca Ty river mouth and Phu Hai river mouth as shown in Figure G-1.

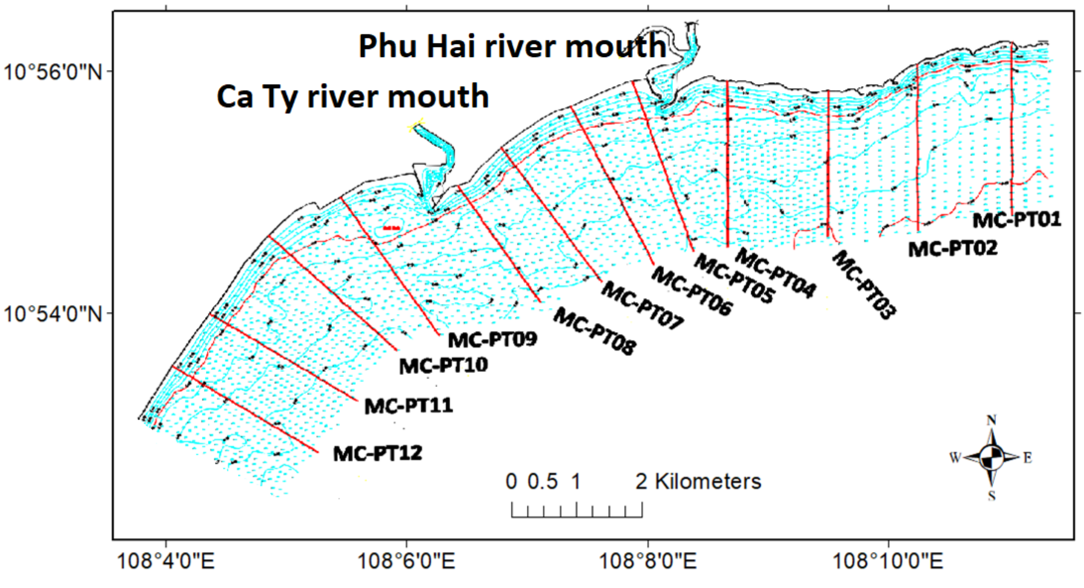

Figure G-1 locations of the beach profile survey

For example, in segment 1, the profiles of 4 segments were determined in 2 years, 2012 and 2014. That means there are in total 8 profiles for considering. Those 8 profiles give the result of sediment size in the range of 0.15 mm to 0.3 mm as shown in Figure G-2. The average profile of those 8 profiles gave the result of sediment size of 0.25 mm as shown in Figure G-3.

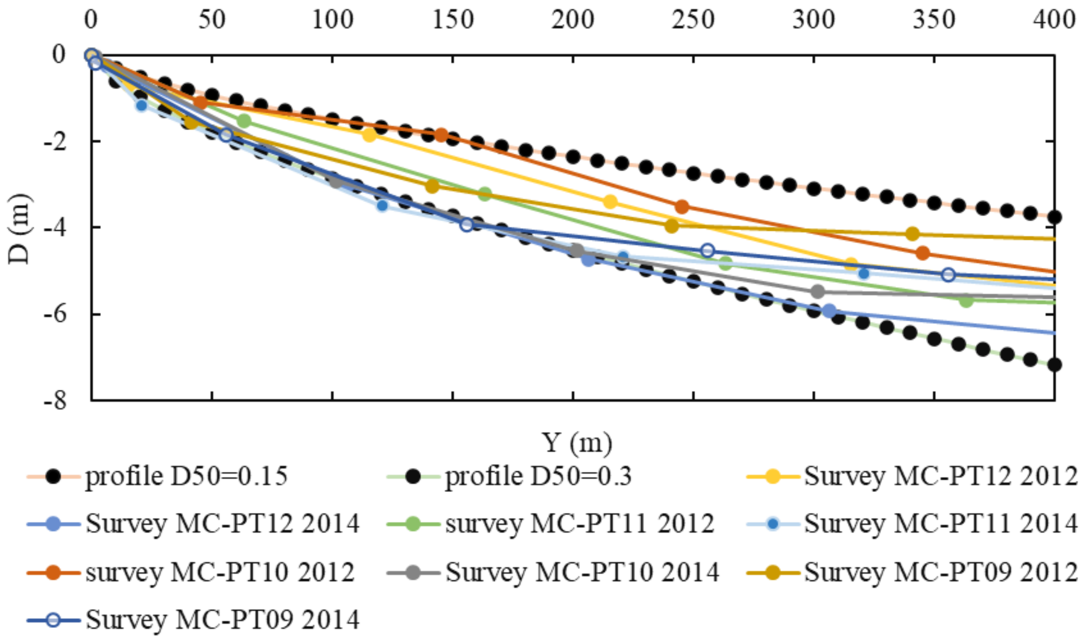

Figure G-2 The profiles of 4 survey locations in 2 times (2012 and 2014) in segment 1 (8 profiles)

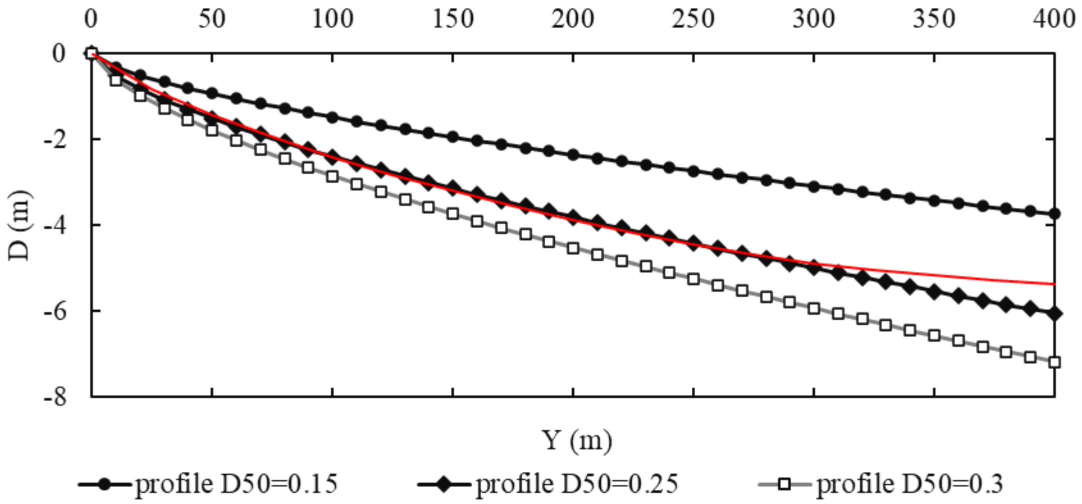

Figure G-3 The average profiles of 4 survey locations in 2 times (2012 and 2014) in segment 1 (8 profiles)

Beside the profile survey with the limited locations, the beach profile graphs were drawn based on GEBCO data by using the 3D analysis toolbar in ArcMap. For determining the sediment size, 20 beach profiles in all 3 segments of this study were plotted as shown in Figure G-4.

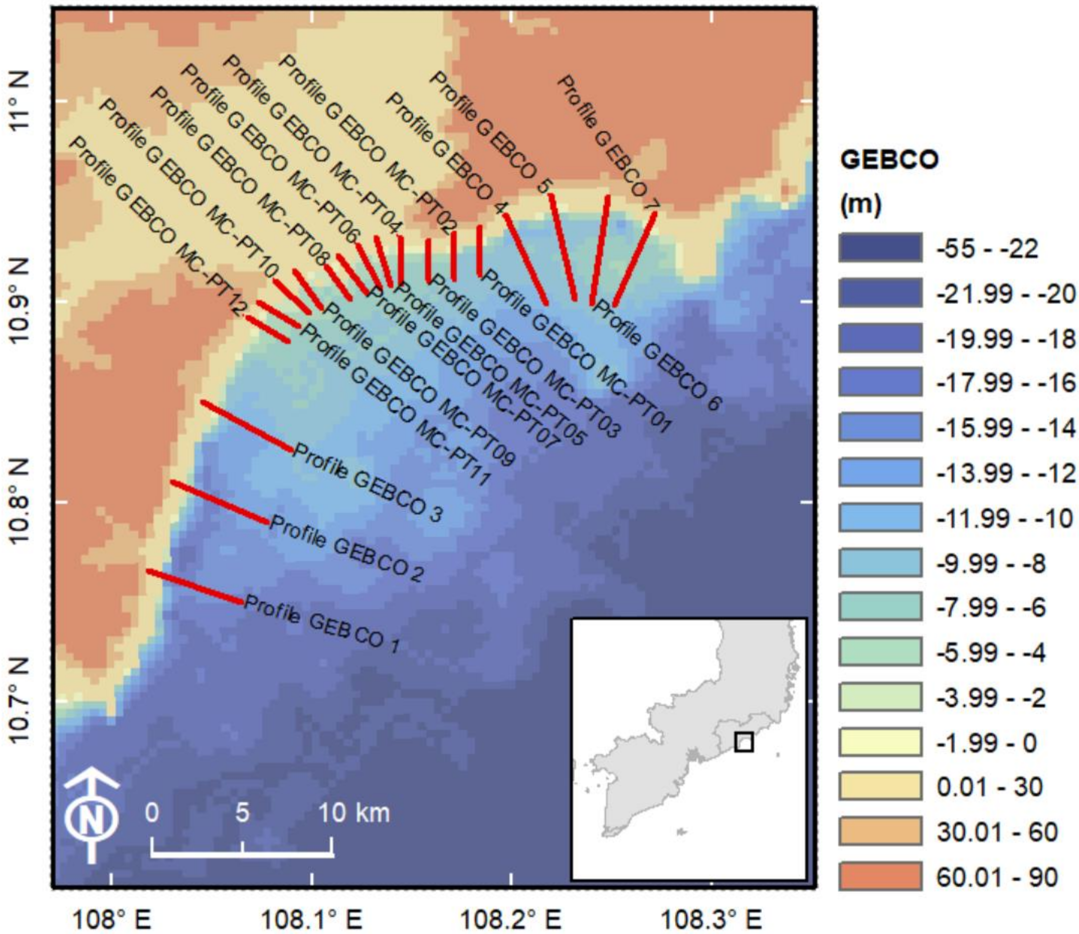

Figure G-4 Locations of beach profiles from GEBCO extracted in ArcMap

For example, in segment 1, 7 beach profile graphs were plotted at 7 locations including GEBCO 1, GEBCO 2, GEBCO 3 which are the locations for considering the south of segment 1, and GEBCO MC-PT12, GEBCO MC-PT11, GEBCO MC-PT10, GEBCO MC-PT09 which are at the same coordinates as in the profile survey. As shown in Figure G-5, those 7 profiles gave the result of sediment size in the range of 0.1 mm to 0.45 mm. The average profile of all 7 profiles gave the result of sediment size of 0.25, which is as same as the result by using the profiles in the survey.

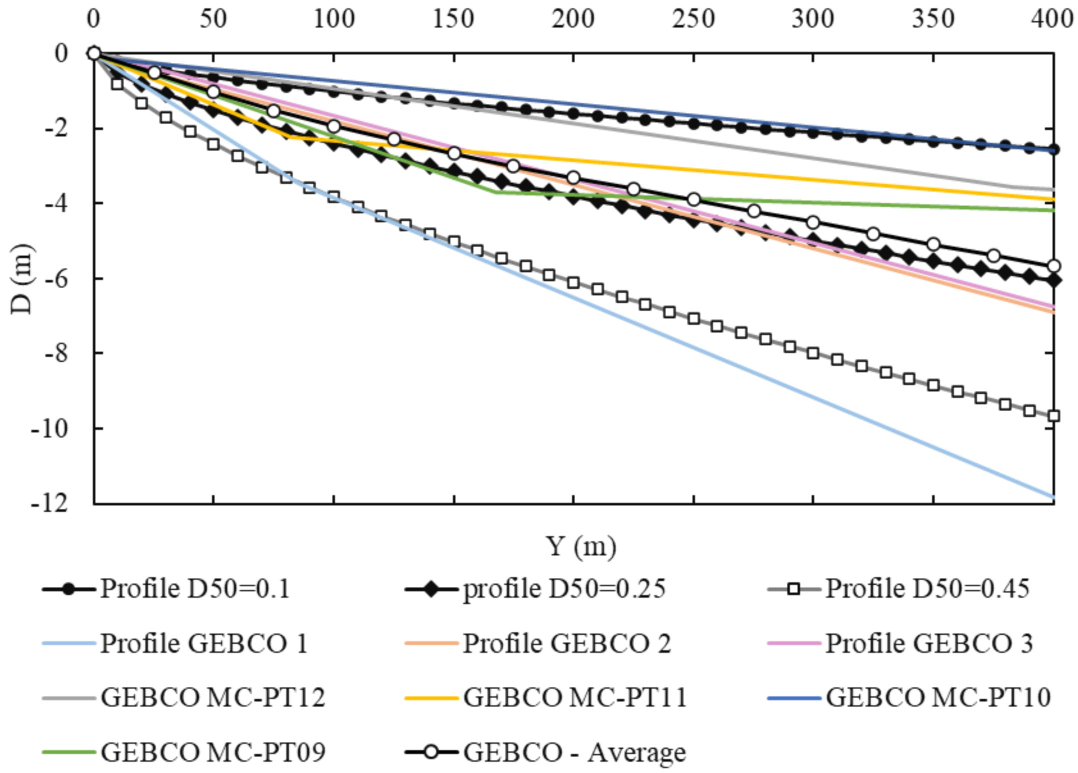

Figure G-5 The profiles of 7 locations in segment 1

As discussed above, the result of sediment size determined with the survey profiles and GEBCO profiles are the same. Therefore, in segment 3, even though the survey result is not available, the sediment size still can be estimated with the GEBCO profile with the same method as in segment 1. In segment 2, both survey data and GEBCO data are available, hence the same method as in segment 1 is used for segment 2.

2/ Sediment size based on sieve analysis experiences

Another way of estimating the sediment size in this study is doing the lab work for the sediment samples collected at 5 locations as shown in Figure G-6. Since the sediment size was estimated to be about 0.15 mm to 0.45 mm, the sieve analysis should be the suitable method to determine the size of sediment samples. Because sieve analysis is the typical method for the sediment between 0.0625 mm to 32 mm (US Army Corps of Engineers, 1995).

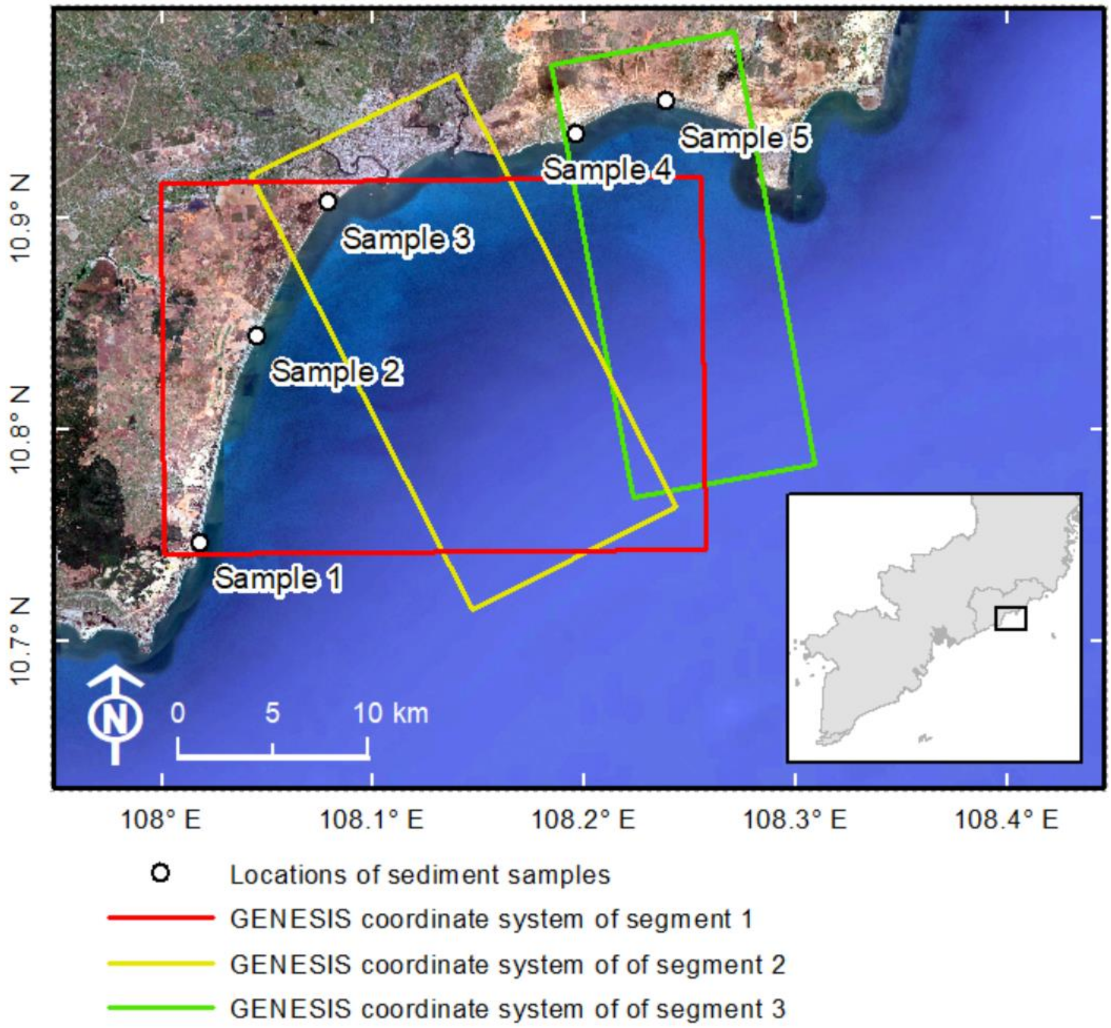

Figure G-6 Locations of sediment samples

The sieve analysis was done by using the USA Standard test sieve as shown in Figure G-7. The sieve follows ASTM E11 standard by ASTM (1995), while the experiment follows ASTM D6913 standard by ASTM (2004). The sieve test can determine the percentage of each particle size that retained in the sieve with the certain grid size. Subsequently the grain size distribution graphs could be plotted for estimating particle size.

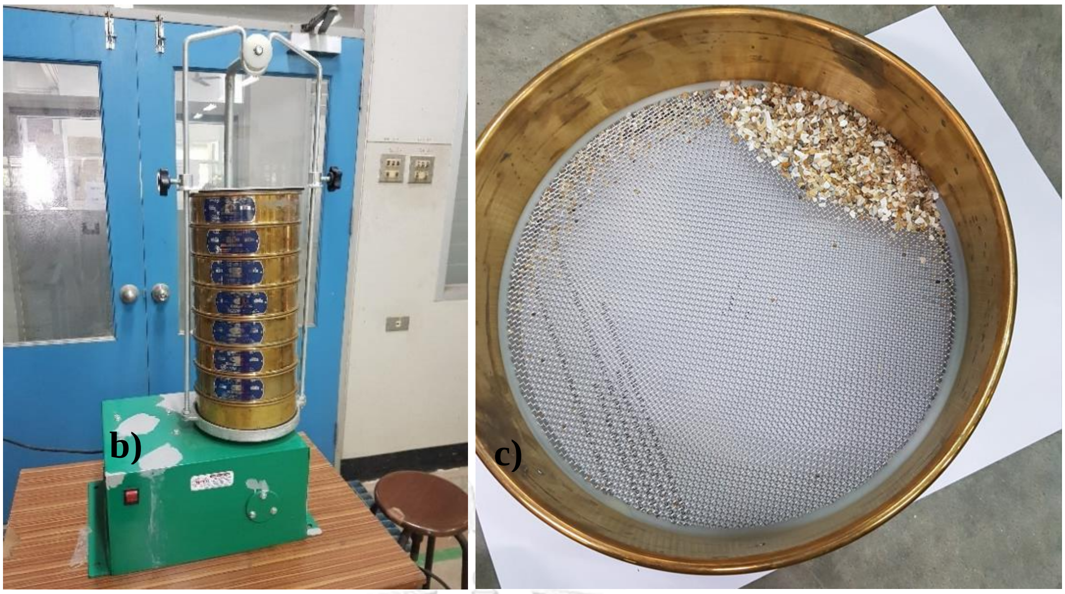

Figure G-7 Tools of sieve analysis: a) sieve (following standard ASTM E11), and the shaker, and b) sediment retained in sieve

The sieve analysis results of 5 sediment samples are respectively shown from Table G-1 to Table G-5. The cumulative mass distribution graphs of sediment 1 to sediment 5 are respectively shown in Figure G-8.

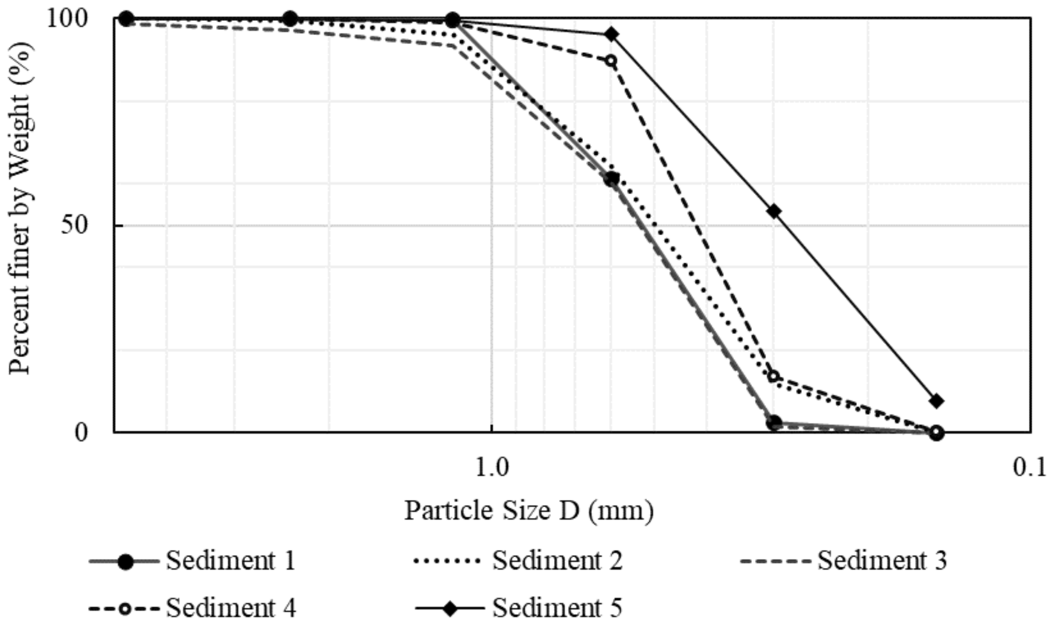

Figure G-8 Cumulative mass distribution of sediment sample 1

Table G-1 Sieve analysis results of sediment sample 1

	Sieve number	size (mm)	Soil retained (g)	Accumulative Retain (g)	% Mass retain	% Passing
1	No. 4	4.750	0.22	0.22	0.04	99.96
2	No. 8	2.360	0.54	0.76	0.15	99.85
3	No. 16	1.180	1.59	2.35	0.47	99.53
4	No. 30	0.600	191.29	193.64	38.81	61.19
5	No. 50	0.300	293.12	486.76	97.55	2.45
6	No. 100	0.150	12.01	498.77	99.95	0.05
7	No. 200	0.075	0.23	499.00	100.00	0.00
8	Pan	0.000	0.00	499.00	100.00	0.00

Table G-2 Sieve analysis results of sediment sample 2

	Sieve number	size (mm)	Soil retained (g)	Accumulative Retain (g)	% Mass retain	% Passing
1	No. 4	4.750	0.17	0.17	0.03	99.97
2	No. 8	2.360	3.11	3.28	0.66	99.34
3	No. 16	1.180	16.56	19.84	3.97	96.03
4	No. 30	0.600	158.10	177.94	35.62	64.38
5	No. 50	0.300	261.99	439.93	88.07	11.93
6	No. 100	0.150	59.29	499.22	99.93	0.07
7	No. 200	0.075	0.33	499.55	100.00	0.00
8	Pan	0.000	0.00	499.55	100.00	0.00

Table G-3 Sieve analysis results of sediment sample 3

	Sieve number	size (mm)	Soil retained (g)	Accumulative Retain (g)	% Mass retain	% Passing
1	No. 4	4.750	6.20	6.20	1.24	98.76
2	No. 8	2.360	8.69	14.89	2.98	97.02
3	No. 16	1.180	18.00	32.89	6.59	93.41
4	No. 30	0.600	165.85	198.74	39.81	60.19
5	No. 50	0.300	292.90	491.64	98.49	1.51
6	No. 100	0.150	7.42	499.06	99.97	0.03
7	No. 200	0.075	0.14	499.20	100.00	0.00
8	Pan	0.000	0.00	499.20	100.00	0.00

Table G-4 Sieve analysis results of sediment sample 4

	Sieve number	size (mm)	Soil retained (g)	Accumulative Retain (g)	% Mass retain	% Passing
1	No. 4	4.750	0.00	0.00	0.00	100.00
2	No. 8	2.360	0.29	0.29	0.06	99.94
3	No. 16	1.180	4.82	5.11	1.02	98.98
4	No. 30	0.600	45.99	51.10	10.23	89.77
5	No. 50	0.300	380.17	431.27	86.30	13.70
6	No. 100	0.150	67.17	498.44	99.74	0.26
7	No. 200	0.075	1.31	499.75	100.00	0.00
8	Pan	0.000	0.00	499.75	100.00	0.00

Table G-5 Sieve analysis results of sediment sample 5

	Sieve number	size (mm)	Soil retained (g)	Accumulative Retain (g)	% Mass retain	% Passing
1	No. 4	4.750	0.14	0.14	0.03	99.97
2	No. 8	2.360	1.20	1.34	0.27	99.73
3	No. 16	1.180	1.55	2.89	0.58	99.42
4	No. 30	0.600	16.91	19.80	3.96	96.04
5	No. 50	0.300	212.82	232.62	46.55	53.45
6	No. 100	0.150	228.45	461.07	92.26	7.74
7	No. 200	0.075	38.58	499.65	99.98	0.02
8	Pan	0.000	0.09	499.74	100.00	0.00

Finally the median sediment grain sizes (D_{50}) of 5 samples were estimated and shown in the Table G-6.

Table G-6 median sediment grain sizes (D_{50}) of 5 samples based on sieve analysis

	Sample 1	Sample 2	Sample 3	Sample 4	Sample 5
D_{50} (mm)	0.54	0.52	0.55	0.44	0.29

Based on all the sediment size above, the sediment can be classified into sand according to Wentworth (1922). In each simulation of GENESIS, only 1 sediment size could be assigned. Therefore, it is necessary to find the value for being the sediment size input of each segment. However, there are some different between the beach profiles from sieve result, survey results, and GEBCO as shown in Table G-7.

The difference can be because there are more factors other than sediment size affecting the beach profile. The values of sediment size for each segment were while doing the sensitivity analysis and calibration of GENESIS model.

Table G-7 Summary of the sediment size result of 3 segments with different methods and data sources

Unit: mm

	Segment 1	**Segment 2**	**Segment 3**
Beach profile - Survey	0.25	0.2	N/A
Beach profile - GEBCO	0.25	0.2	0.25
Experiment – Sieve analyssis	0.54	0.55	0.37

APPENDIX H
SENSITIVITY OF GENESIS

Sensitivity analysis evaluates how parameter changes affect the model output. By varying parameters systematically, it identifies key factors controlling model behavior and their impact on the output. These guides focus on important input parameters for calibration and validation. Sensitivity analysis also highlights areas requiring more data or research to reduce uncertainties and improve model accuracy. In this study, the sensitivity was done for the parameters including interval time of wave data input, Sediment size (D_{50}), Berm height (D_B), Depth of Closure (D_C), K1, Moving boundary, K2, Permeability of the groin, Model length, and Grid azimuth.

Simulation intend time

The length of wave data incorporated into every simulation of GENESIS model was limited. Therefore, the longer interval time of wave data was preferable, even though a longer interval time with less frequent and less precise wave data can result in less accurate shoreline predictions. The sensitivity was done on segment 1 for 3 different interval times which are 0.5 hours, 3 hours, and 6 hours. The impact of the interval time of wave data on the shoreline model result was minimal, as shown in Figure H-1. The simulated shoreline results for three different interval times are relatively consistent, as are the corresponding End Point Rate (EPR) results. This suggests that the wave climate does not undergo rapid changes over time. Therefore, it may be unnecessary to use high-frequency wave data if the objective of the study was to examine the long-term shoreline evolution.

Sediment size (D_{50})

The next sensitivity analysis was carried out to investigate the effect of sediment size (D_{50}) on the shoreline response by varying it at 0.05 mm, 0.2 mm, 0.54 mm, and 5 mm. The findings indicate that the shoreline result was only sensitive to sediment sizes below 0.2 mm, whereas larger sizes showed minimal sensitivity. In particular, the sediment size of 0.05 mm had more pronounced impact on the shoreline change, while changing the sediment size at 0.2 mm, 0.54 mm, and 5 mm had no significant effect on simulated shoreline change. These findings suggest that sediment size may not be a critical factor in simulating shoreline change in this segment 1, except in cases where very small sediment sizes are present. Sensitivity analysis was performed in segment 2 and 3 as well to test the impact of sediment size on shoreline change, which was not entirely in line with the theoretical expectation in segment 1. However, the results were consistent with segment 1.

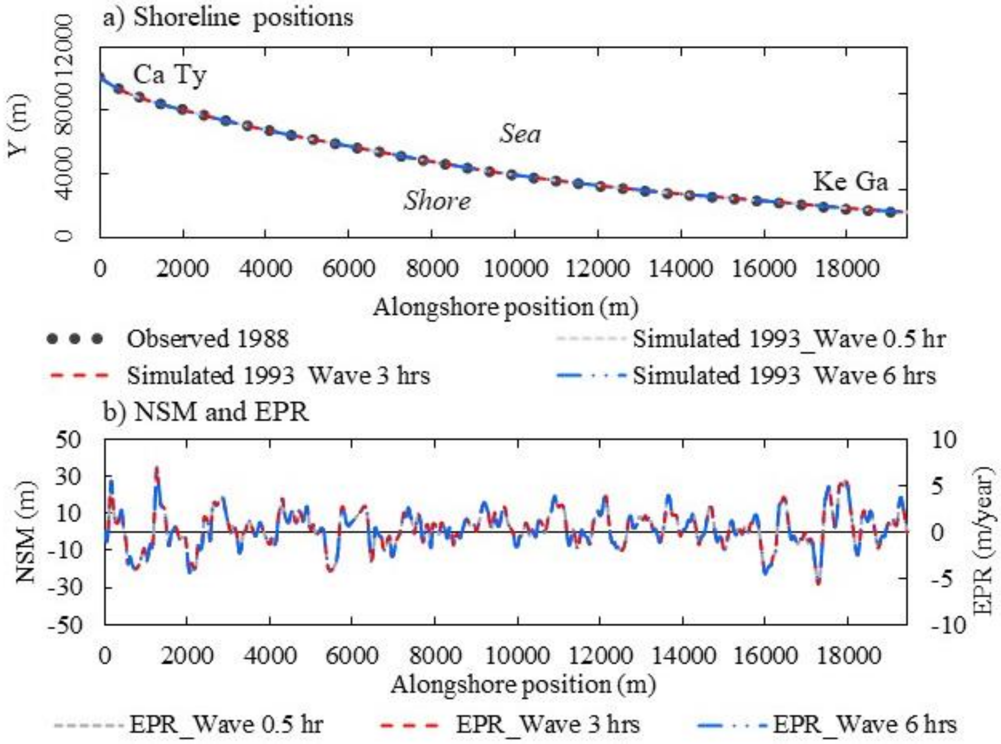

Figure H-1 Sensitivity of interval time of wave data

The low sensitivity of shoreline change to sediment size can be attributed to the consistent dominant wave direction and approach angle in the area. The uniformity in wave energy direction and angle as shown in Figure H-3 generates a relatively consistent flow of water and sediment, which results in a less varied sediment transport pattern. This means that the sediment particles move more predictably, reducing the sensitivity of shoreline change to variations in sediment size. In other words, when sediment transport is less variable, the impact of sediment size on the shoreline change becomes less significant.

Figure H-2 illustrates that it can be challenging to observe the shoreline movement unless the graph was significantly zoomed in about 39 times, as shown in Figure H-4. To improve the visualization, it is recommended to include the EPR on the graph. By adding the EPR to the graph, the changes in shoreline position can be better interpreted and understood, even at a larger scale. The EPR, or Erosion and Accretion Rate, is a key parameter in understanding shoreline change. By using this graph, we can easily observe the changes in the shoreline along the study area and determine whether it was eroding or accreting.

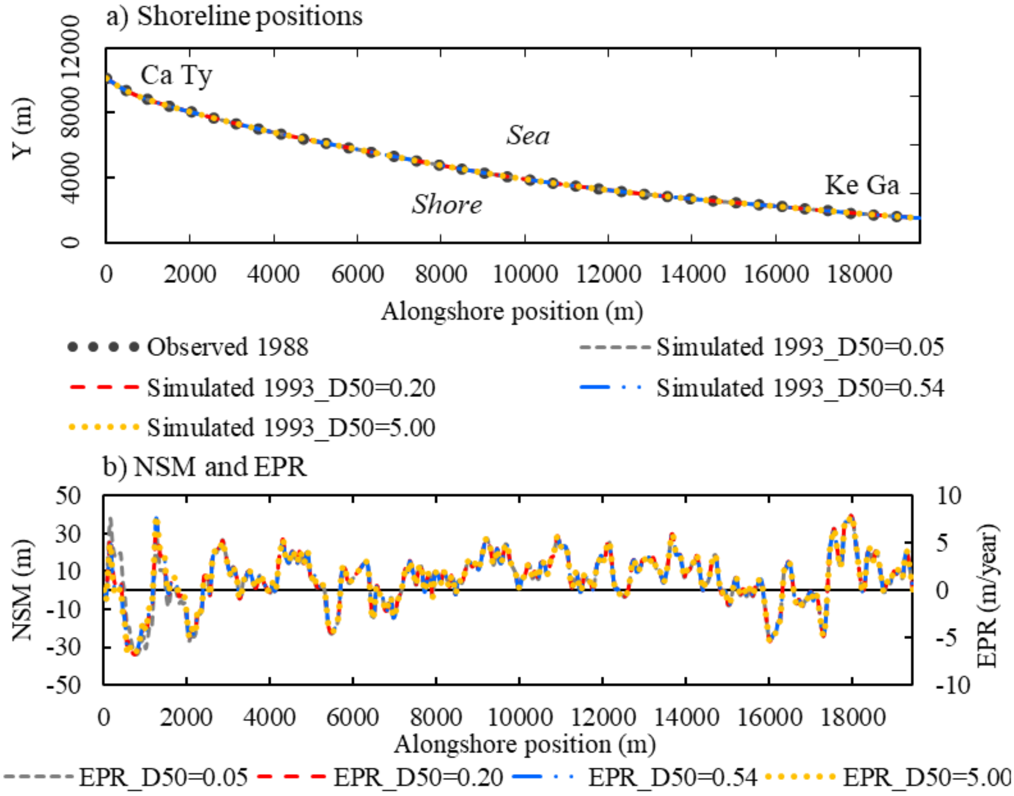

Figure H-2 Sensitivity of sediment size (D_{50})

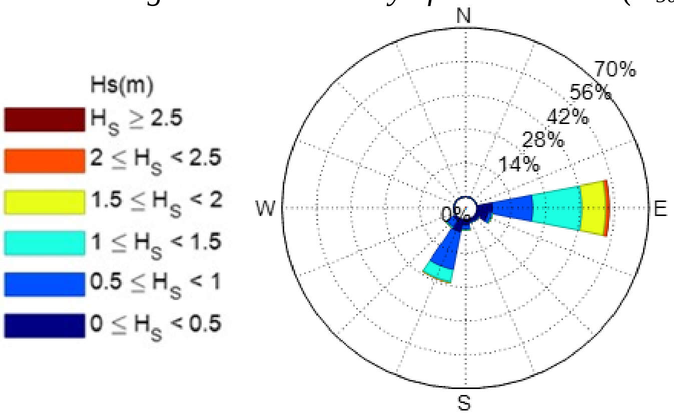

Figure H-3 Wave data at point 1 for use in GENESIS from 1988 to 1993

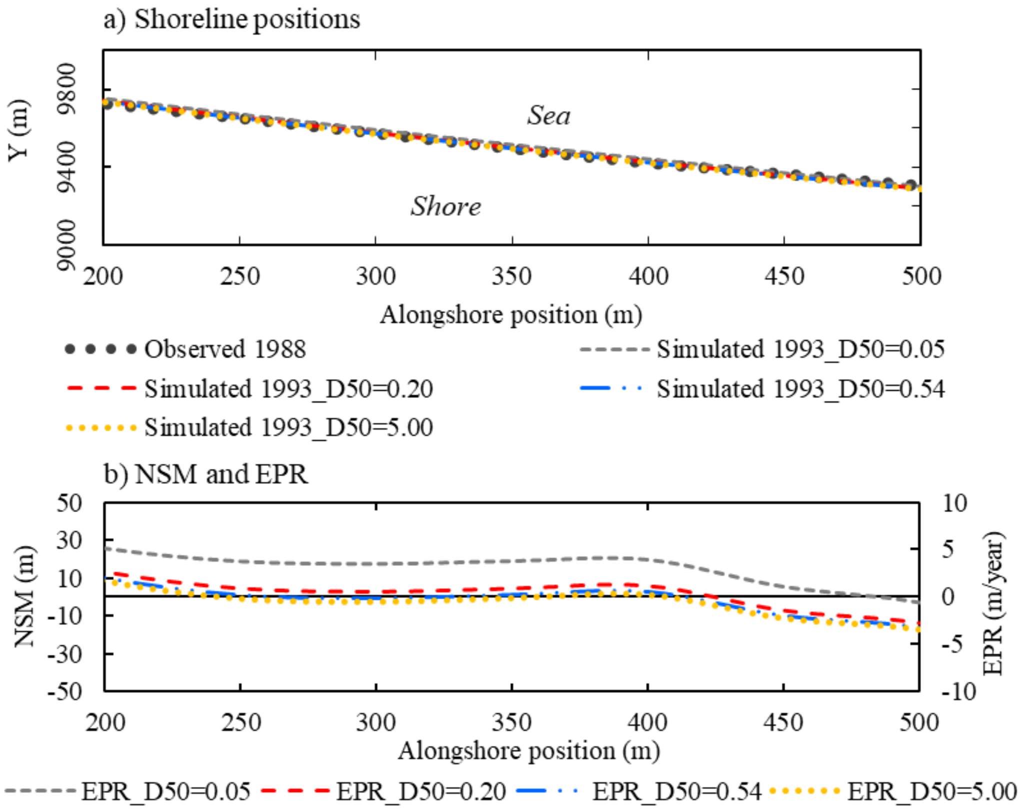

Figure H-4 The zoomed-in graph of the graph in Figure H-2

Berm height (D_B)

The berm height refers to the distance from the waterline to the highest point of the berm. Increasing the berm height (D_B) resulted in a more stable shoreline with less erosion and accretion as shown in Figure H-5. Because in GENESIS model, the berm height is considered as a boundary condition, affecting the nearshore hydrodynamics and sediment transport. According to the governing equation of GENESIS, with the same volume of sediment, when D_B is higher, the ∂y decreases. The effect of berm height (D_B) on shoreline change was more significant when the height changes from 0 m to 2 m, compared to when it changes from 2 m to 4 m. However, once the berm height reaches around 2 m to 4 m, further increases in height do not have a significant effect on shoreline change.

Depth of closure (D_c)

The seaward boundary of the GENESIS simulation is defined by the Depth of closure (D_c), and its increase leads to a more stable shoreline, similar to the (D_B) parameter discussed earlier, as seen in Figure H-6. However, the impact of D_c on shoreline change was more gradual compared to (D_B). In Phan Thiet bay, the impact of (D_c) on shoreline change was low, which can be attributed to the consistent wave direction and approach angle. When wave energy comes from a consistent direction and similar approach angle, the sediment transport pattern along the shoreline becomes more consistent and predictable. As a result, changes in depth have a relatively lower impact on the sediment transport pattern and shoreline change.

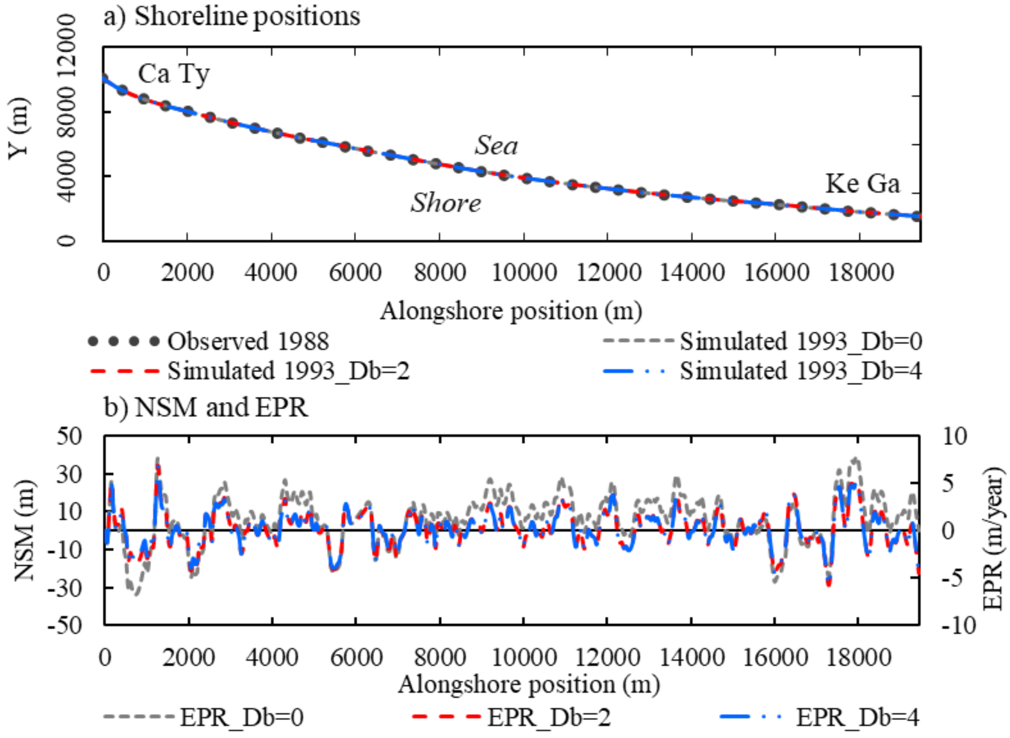

Figure H-5 Sensitivity of berm height (D_B)

Moving boundary

In GENESIS, the moving boundary defines how much the boundary moves in that simulation. To test the sensitivity of the moving boundary, simulations were run at different values ranging from -70 m/simulation to 70 m/simulation. The results showed that the moving boundary only had a significant impact on the shoreline from X=0 m to X=1200 m, as shown in Figure H-7. This means that the moving boundary likely has no impact on the shoreline in the larger area. To better visualize the impact of the moving boundary, the graph was zoomed in and shown in Figure H-8. When the moving boundary was negative, it was observed that the shoreline in that area experiences erosion, and conversely, it accretes when the moving boundary was positive.

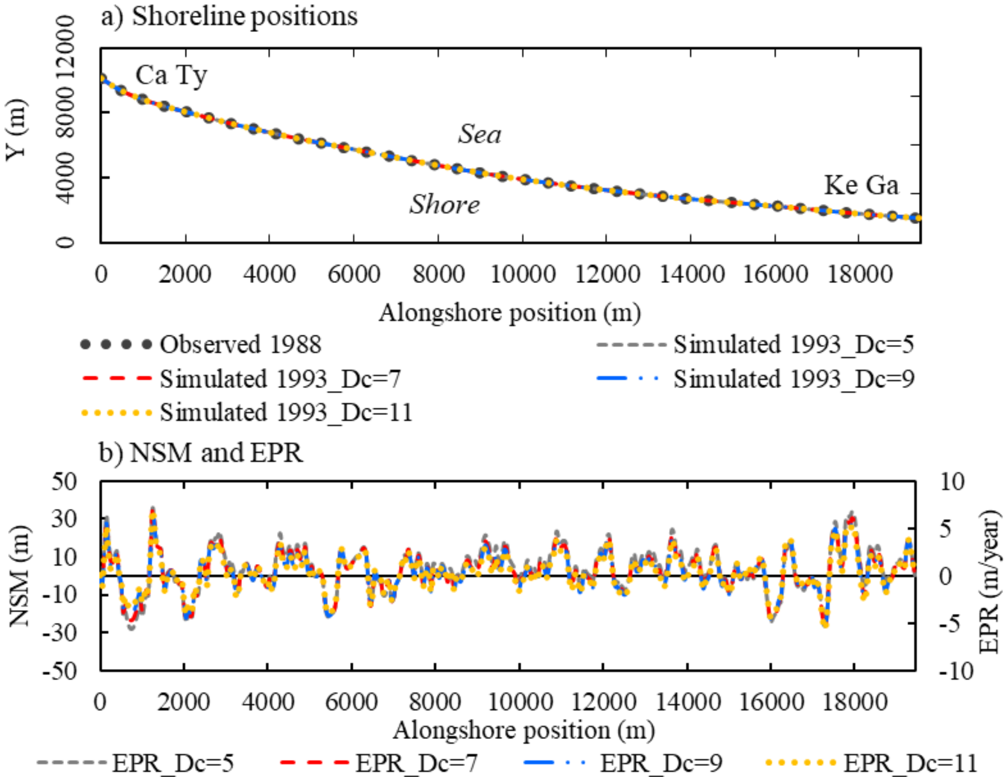

Figure H-6 Sensitivity of Depth of closure (D_C)

K1 parameter

The K1 parameter is an important factor in the GENESIS simulation, as it determines the coefficient of sand transport due to oblique incident waves. A higher value of K1 generally results in more shoreline change, since it increases the transport of sediment by waves at an angle to the shoreline. When K1 increases from 0.05 to 0.1, the shoreline change was relatively small. But when K1 increases from 0.1 to 0.5, there was a significant increase in shoreline change. This leads to more accretion along the shoreline, particularly near the left boundary of this segment 1. Overall, the value of K1 should be carefully selected to accurately represent the sediment transport processes in the study area.

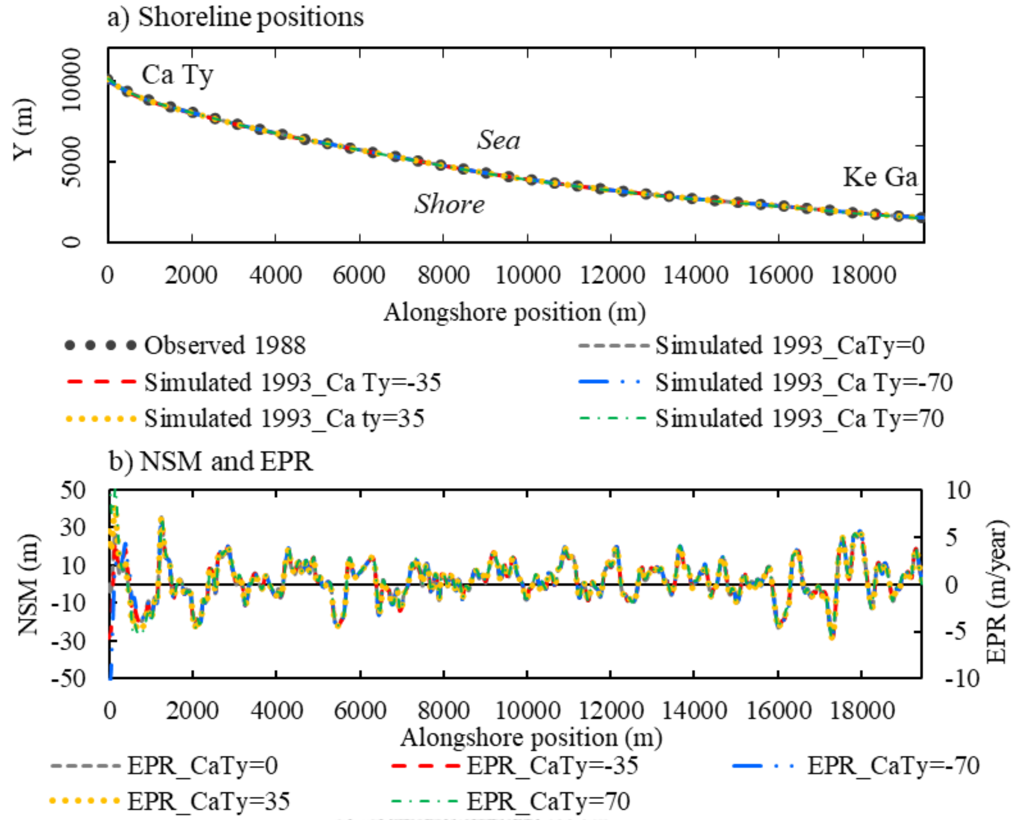

Figure H-7 Sensitivity of moving boundary (m/simulation) of Ca Ty boundary

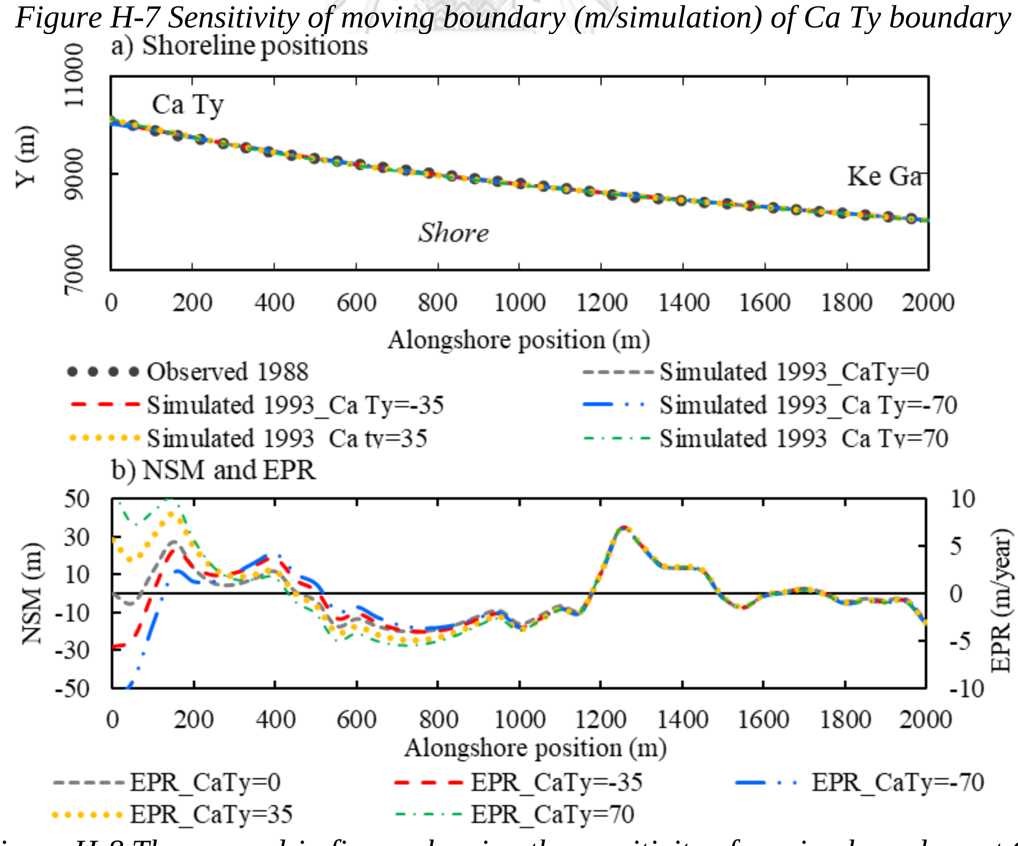

Figure H-8 The zoomed-in figure showing the sensitivity of moving boundary at Ca Ty boundary

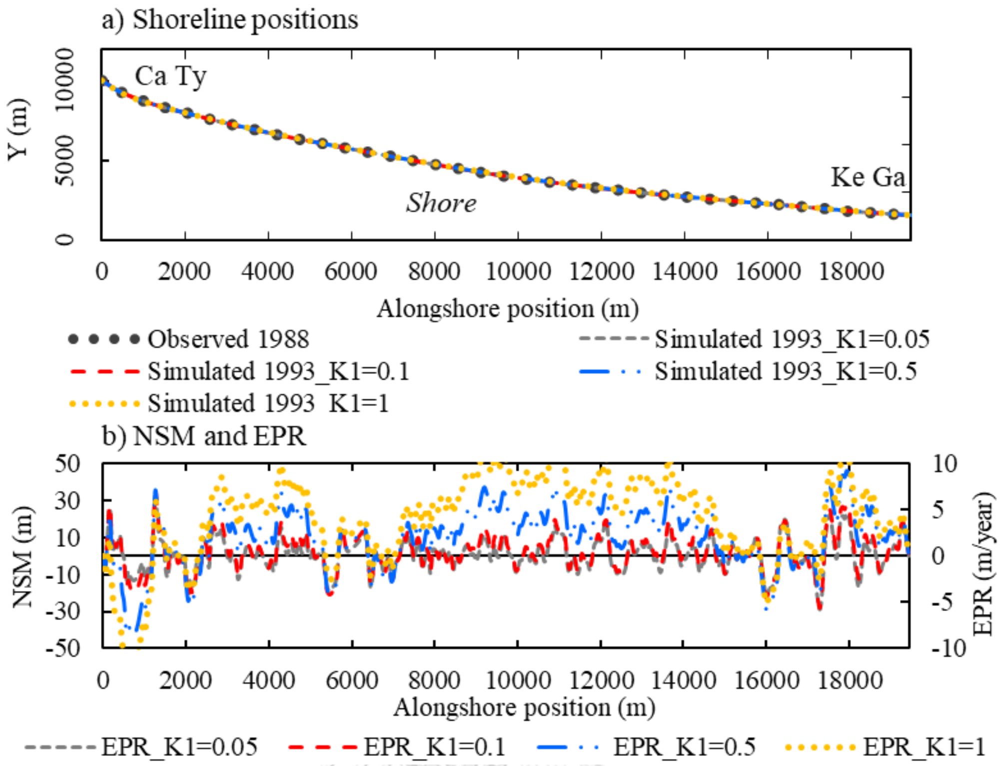

Figure H-9 Sensitivity of sediment transport coefficient K1

To make better sensitivity analysis, the focus of parameters related to structures, such as K2, permeability, and model length of the groins, should be on segment 2, which includes groins. Because segment 1, containing the Beach Fill structure near the boundary, may be influenced by boundary conditions.

Parameter K2

The sensitivity of K2, representing the sediment transport coefficient influenced by wave-breaking height, was examined in segment 2 with multiple jetties. Altering K2 affected the variation in wave-breaking height, resulting in changes to shoreline location and magnitude as shown in Figure H-10. Increasing K2 from 0.05 to 0.1 results in a minimal difference in shoreline change. However, further increasing K2 from 0.1 to 0.6 leads to significant shoreline changes, particularly near the Ca Ty river mouth between X=2550 m to X=5800 m and X=6250 m to X=7300 m. In simulations with structures, careful calibration of K2 is necessary to study their impact on shoreline change.

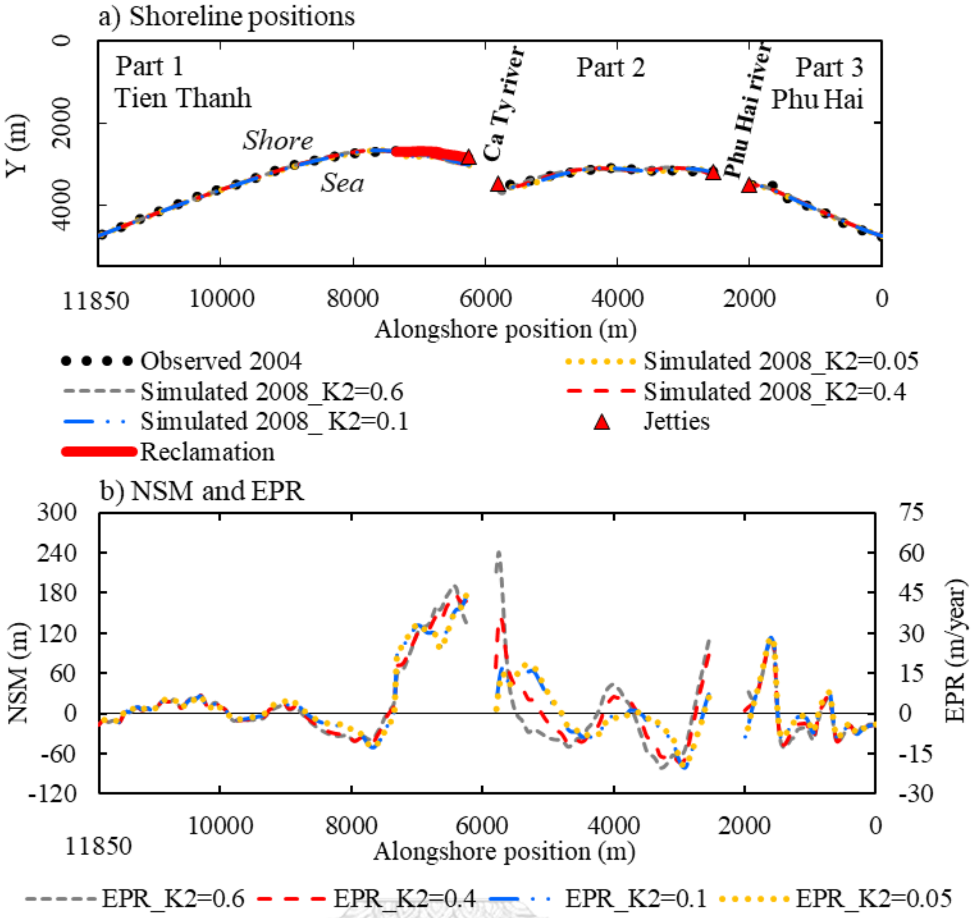

Figure H-10 Sensitivity of sediment transport coefficient K2

Permeability of groin near river mouth

The permeability of the groins determines the amount of sediment that can pass through the structure. A groin with a permeability equal to 0 would stop all sediment transport updrift, while a permeability value of 1 would allow all sediment to pass through the structure. For examining the impact of varying the permeability value, a sensitivity analysis was conducted on the jetty Phu Hai 1 represented by groin structure in GENESIS. The results indicated that as permeability increased from 0 to 1, the shoreline right down drift of the groin became more landward. This was because some of the sediment was able to move further down drift, resulting in less erosion in the down-drift area.

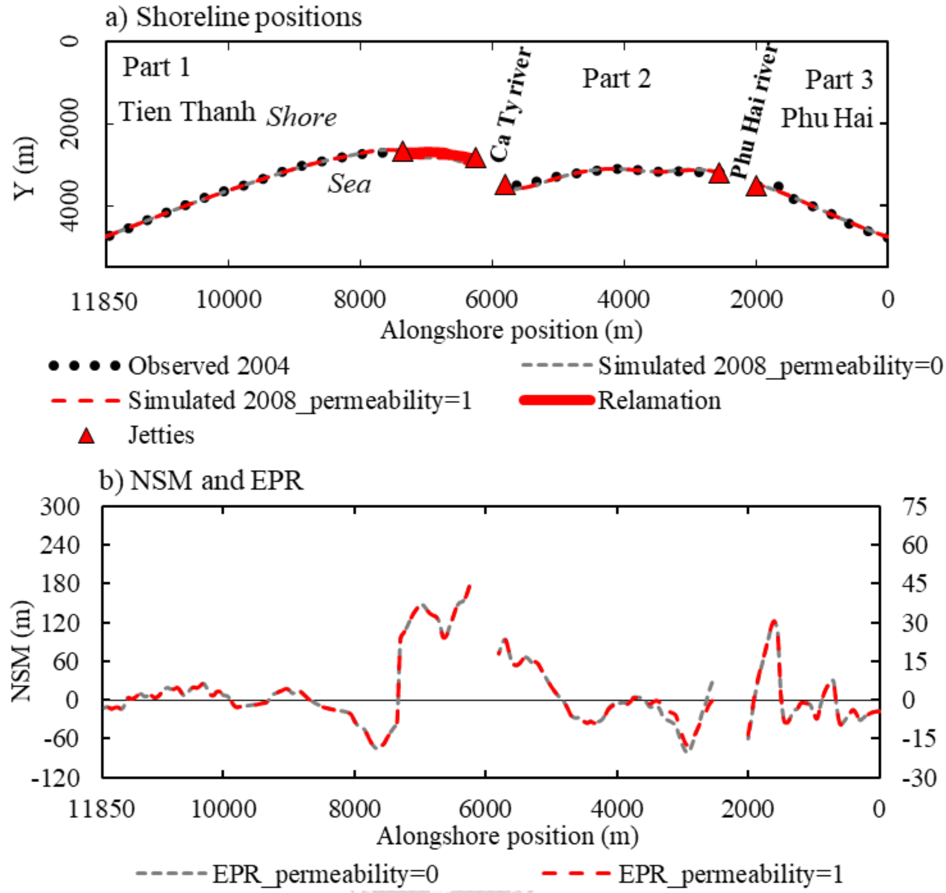

Figure H-11 Sensitivity of permeability of Jetty Phu Hai 1

Permeability of imaginary groin at the end of beach fills

In this study, Jetty Phu Hai 1 is located near the river mouth with a complex shoreline. To understand the impact of permeability value on the updrift and downdrift of the groin, the sensitivity analysis of permeability was also conducted on the groin at the end of Beach Fills, known as the beach reclamation project Hamubay. As shown in Figure H-12, At a permeability value of 0, sediment accumulates at the updrift side of the groin, preventing its movement downdrift and causing erosion downstream. Conversely, with a permeability of 1, sediment can freely pass through the groin, resulting in a more stable shoreline. These effects are observed in the vicinity of 2300 meters, specifically from X = 6650 m to X = 8950 m.

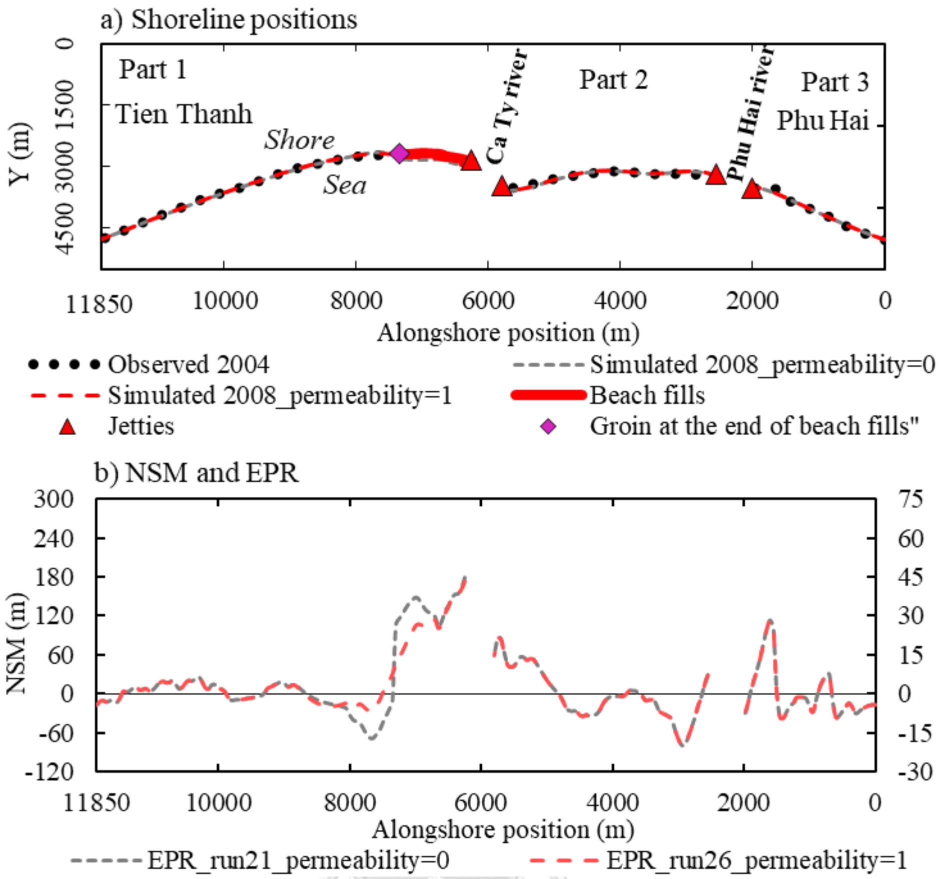

Figure H-12 sensitivity of permeability of groin at the end of Beach Fills

Model length

The model length of the groin at the end of Beach Fills is a parameter that requires calibration in the GENESIS model, as it represents the imaginary groin for simulating the beach reclamation project Hamubay, not the actual groin measured using Google Earth Pro. Therefore, a sensitivity analysis of it is necessary. The analysis revealed that the model length had a minimal influence on shoreline change, suggesting that the precise length of the groin is not critical for the model's accuracy in predicting shoreline dynamics in this particular location.

In this study, the sensitivity analysis for groin model length was not conducted for all groins since their lengths could be determined using Google Earth Pro. However, it is crucial to note that when the depth at the groin tip is smaller than the depth of longshore transport (DLT), the model length can influence shoreline change by regulating the sediment flow through the groin, like groin permeability.

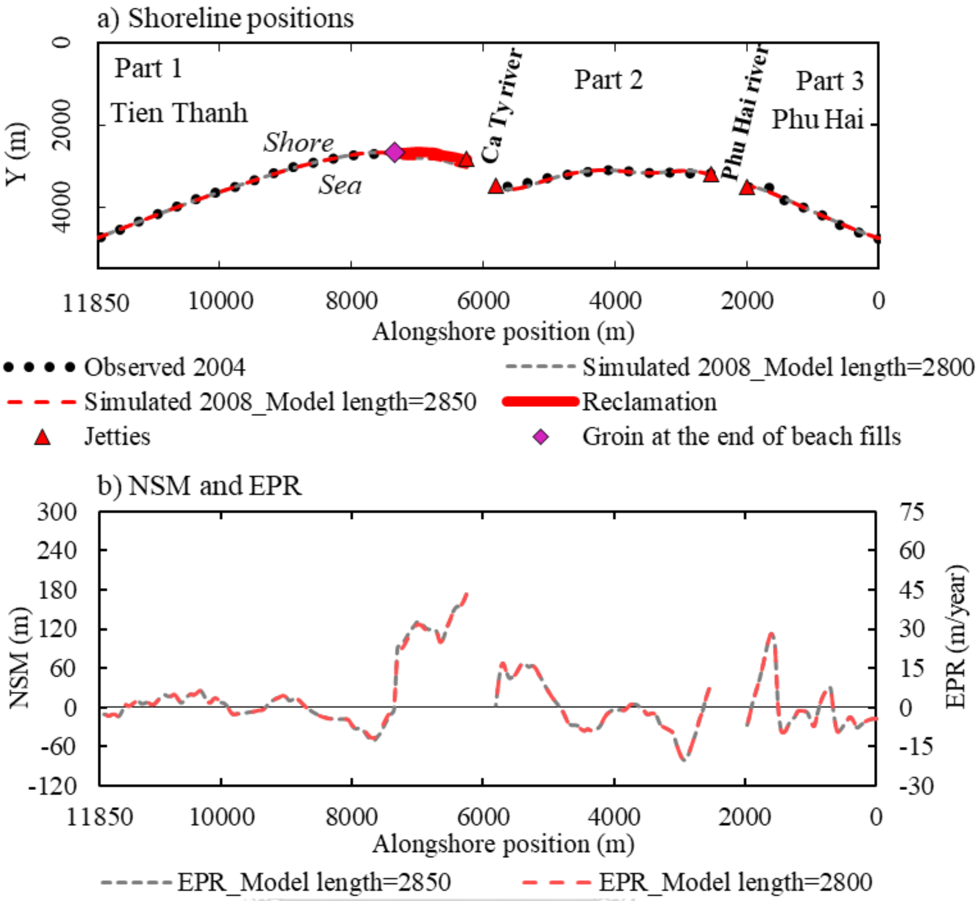

Figure H-13 Sensitivity of the Model length at the end of beach reclamation project

Azimuth angle of the grid

The azimuth angle of the grid determines the clockwise orientation of the X-axis relative to the West direction. In this study, we conducted a sensitivity analysis with three different azimuth angle values as shown in Figure H-14 and analyzed shoreline changes according to each angle as shown in Figure H-15. Generally, the azimuth angle influences shoreline change in most of the locations, especially near the boundaries. Notably, when the azimuth angle was set to zero, an unusual behavior was observed in shoreline change near the right boundary (Ong Dia boundary). Further analysis will be conducted during the calibration process to better understand this behavior.

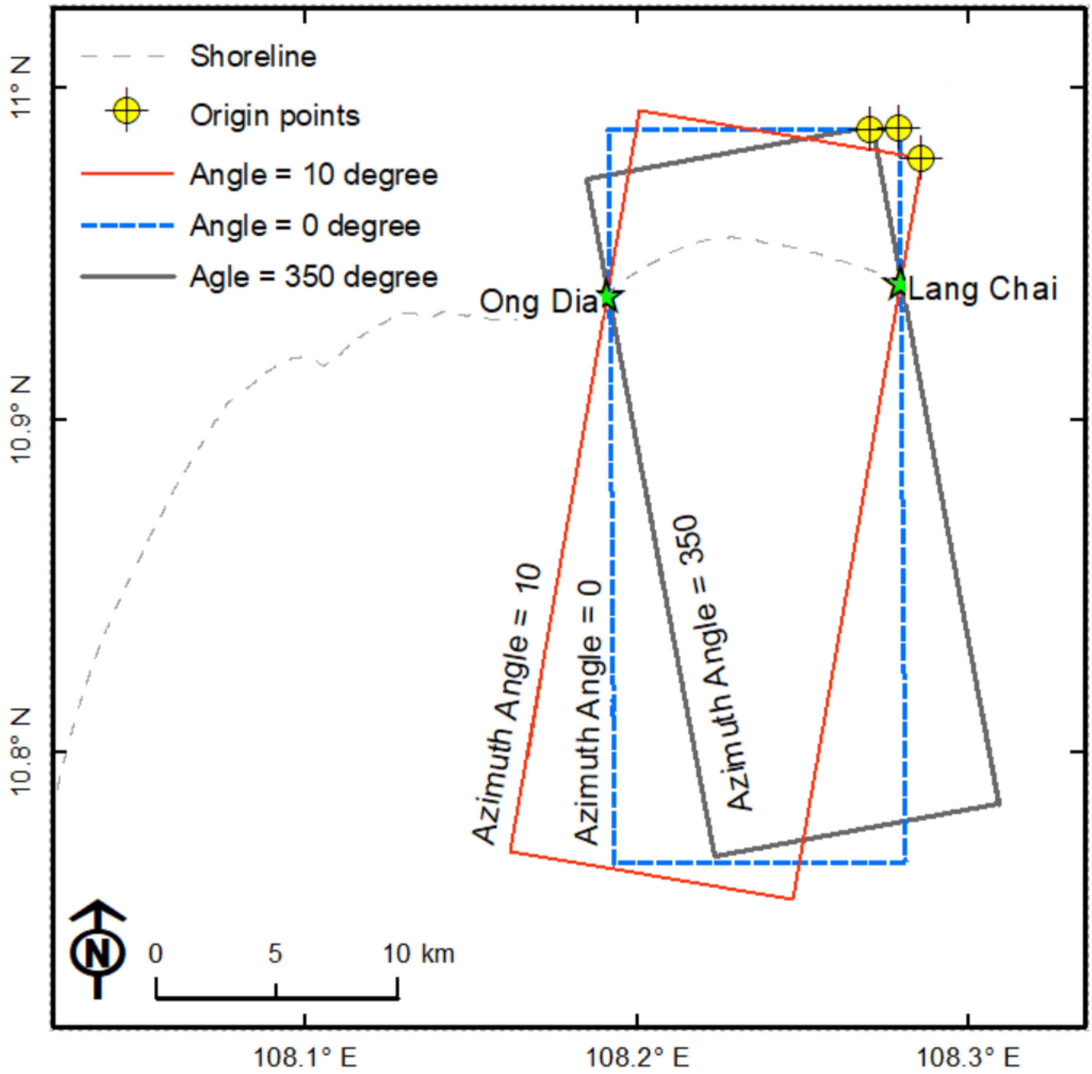

Figure H-14 The grid with different azimuth angles

The summary of sensitivity analysis of all above parameters were shown inTable H-1. The results of the sensitivity analysis highlight several critical parameters that need to be calibrated in the GENESIS model. First and foremost, the grid azimuth must be accurately set to surely avoid the potential bug creating the abnormal shoreline change in GENESIS model. Next, K1 and K2 (if applicable) must be calibrated to reflect the actual sediment transport rate in the study area. Depth of closure (D_c), sediment size (D_{50}), and berm height (D_b) are also crucial parameters that should be calibrated to accurately model the beach profile. The moving boundary is another important parameter that requires calibration to accurately represent the actual boundary movement. Finally, the permeability of the groin structure must be calibrated to simulate the sediment transport through the groin. It is suggested to calibrate these parameters in the above order to achieve the most precise and reliable results from the GENESIS model.

Table H-1 Summary of sensitivity analysis

Parameter	Sensitivity analysis
Interval time of wave data input	No effect, no calibration needed
Sediment size (D_{50})	Low effect
Berm height (D_B)	Low effect D_B increases, shoreline is more stable, and vice versa.
Depth of Closure (D_C)	Low effect D_C increases, shoreline is more stable, and vice versa.
K1	High effect Lower K1, shoreline is more stable, and vice versa.
Moving boundary	Low effect Negative moving boundary, shoreline is eroded, and vice versa.
K2	High effect with structure
Permeability of groin	Medium effect Permeability higher, shoreline is more stable, and vice versa.
Model length	Very low (for the groin at the end of the beach reclamation project Hamubay)
Grid azimuth	High effect azimuth angle = 0: abnormal shoreline change near right boundary

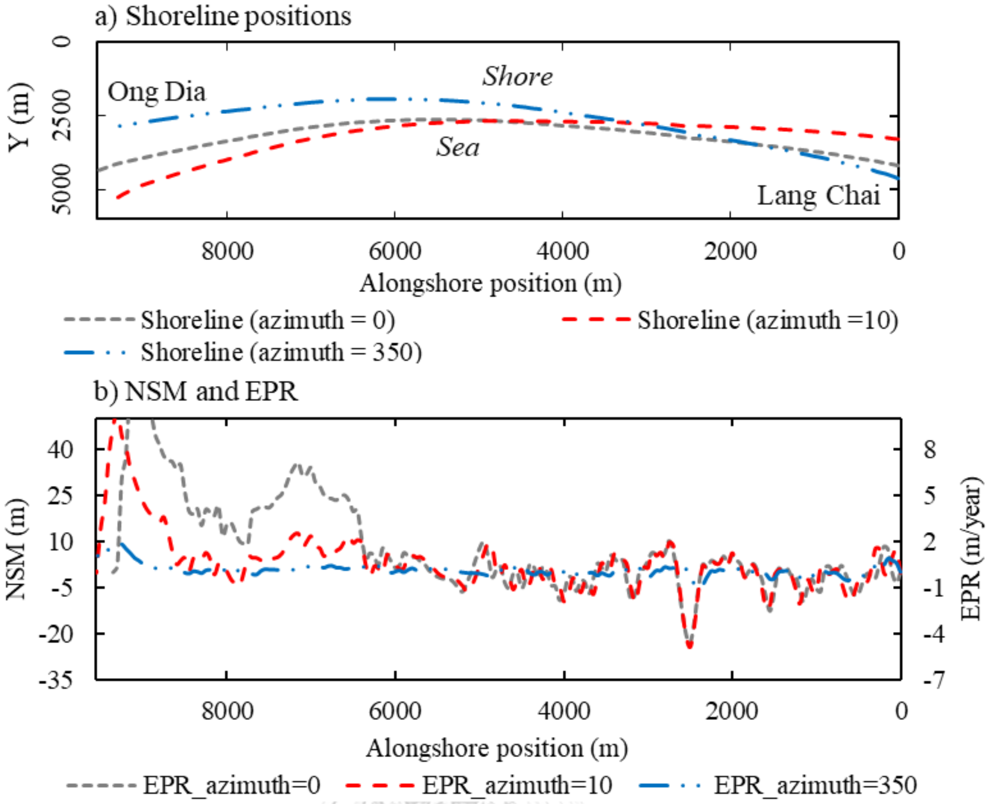

Figure H-15 Sensitivity of the azimuth angles of the grid

APPENDIX I

CALIBRATION OF GENESIS MODEL

In this study, the calibration process was conducted to optimize several key parameters of the GENESIS model, including the azimuth angle, K1, depth of closure (D_c), sediment size (D_{50}), and berm height (D_b) after finishing the sensitivity analysis of the impact of each parameter on the shoreline change result. The calibration involved comparing the model's output with observed data and adjusting the parameters to minimize the disparities between the model predictions and actual measurements.

In the CHAPTER 3, Figure F-7, Figure F-8, and Figure F-9 provide an overview of the calculation grid used for segment 1, segment 2, and segment 3 in GENESIS, with a more detailed illustration presented in Figure 5-9, Figure 5-10, and Figure 5-11 respectively.

1/ Segment 1

Calibration

The calibration of the model in segment 1 was performed by simulating from 07 Jan 1988 to 09 Mar 1993 (about 5 years) with the wave data at point 1 from 1988 to 1993. The interval time of the wave is 6 hours.

The parameters were calibrated with the orders of the grid azimuth, K1, depth of closure D_c, sediment size D_{50}, berm height D_b, left boundary conditions at Ca Ty, and right boundary conditions at Ke Ga as shown in Table I-1.

Table I-1 Values of calibration parameter of segment 1

Azimuth angle	**K1**	**D_c (m)**	**D_{50} (mm)**	**D_b (m)**	**Ca Ty 1 (m) left**	**Ke Ga (m) right**
0	0.05	5	0.05	0	0	0
290	0.1	7	0.25	0.6	-18	-24.19
	0.3	9	0.54	2	-36.38	-40
	0.5	11	1	4	-45	-45
				6		

The calibration process for the azimuth angle and K1 parameter yielded important results. The azimuth angle was calibrated between 0 degrees, which indicates that the X axis is parallel to the longitudinal direction, and 290 degrees, which indicates that the X axis is parallel to the shoreline. After comparing the results, the angle of 0 degrees was found to be the most accurate.

For the K1 parameter, four values were tested: 0.05, 0.1, 0.3, and 0.5. While the result for 0.05 was better than others, previous research suggests that the value of K1 should be between 0.1 to 1 only (Gravens et al., 1991). Therefore, K1 was chosen to be 0.1.

The depth of closure (D_C) was calibrated at values of 5 m, 7 m, 9 m, and 11 m. Although a value of 11 m gave a better result compared to the others, D_C should be controlled by the wave characteristics. By finding the highest significant waves that occurred during a 12-hour period over the course of a year, the H_o was determined to be 3.54 m and the L_o was 105.13 m. This yielded a D_C value of 6.76 m. However, according to observed data at Phu Quy station, H_o could be up to 5 m. Therefore, the D_C was chosen to be 9 m, which is compatible with the wave characteristics and provided a more accurate calibration result.

Determine the sediment size

The sediment size was determined based on the sediment collected in the study area, and the beach profile as the details of the calculation shown APPENDIX G. The beach profile was determined based on the beach profile survey and GEBCO bathymetry data.

The sediment size in this study is determined by doing lab work for the sediment samples collected from the study area as shown in APPENDIX G. After doing the sieve analysis, the result of the sediment size of segment 1 is 0.54 mm. Following estimating the sediment size by the processes is the calibration of the sediment size (D_{50}) in GENESIS model with various values of 0.05 mm, 0.25 mm, 0.54 mm, and 1 mm, it was found that the shoreline results from these different sediment sizes were not significantly different. The sediment size of 0.25 mm was chosen as it will be used to determine the profile shape in GENESIS. This profile shape determines the distance from the shoreline to the point of wave breaking at each grid cell and the zone of longshore sand transport. The location of wave breaking determines if diffraction occurs, which requires sources of diffraction to be seaward of the breaker zone.

Similar to D_c, D_B is also controlled by the wave characteristic according to (Larson & Kraus, 1989) with equation (*I-1*). While the average $tan\alpha$ is 0.0124. The result shows that D_B should be about 0.60 m. Although higher D_B values provided slightly better results, the difference was minimal. Thus, a value of 0.6 m was chosen for D_B.

$$\frac{D_B}{H_o} = 1.47\left[\frac{tan\alpha}{\sqrt{H_o/L_o}}\right]^{0.79} \tag{I-1}$$

Although the moving boundary parameters have a relatively small effect on the shoreline near the boundary, it is important to calibrate them to achieve more accurate results. Based on the calibration results, the final moving boundary may not match exactly with the actual moving boundary. However, it is important to note that the calibrated moving boundary parameters provided better results than other configurations. Therefore, for this period from 1988 to 1993, as well as other periods of segments 1 and other segments, it is recommended to assign the known actual moving boundary to be the moving boundary in the model, as this will improve the accuracy of the model performance. For segment 1, the moving boundary of Ca Ty 1 boundary was -36.38 m/simulation, while it was -24.19 m/simulation for Ke ga boundary.

The calibration was supposed to be done by comparing the simulated shoreline positions in 1993 to the actual shoreline in 1993 that was extracted from the Landsat image. However, due to the big scale of the whole shoreline segment compared to the net shoreline movement, it is difficult to discuss the shoreline position. Therefore, the graph presented in Figure I-1 provides a comparison between the simulated shoreline change rate and the actual shoreline change rate, as measured by the End Point Rate (EPR) in m/year (m/year). The simulated shoreline change rate was obtained from the

GENESIS simulation result. On the other hand, the actual shoreline change rate was derived from the actual shoreline positions in 1988 and 1993 in GENESIS coordinate system.

The comparison of the actual EPR and the simulated EPR in Figure I-1 shows that the simulated EPR closely follows the pattern of the actual EPR, with only minor deviations that the magnitudes of EPR are slightly different at some locations. However, it can be observed that the shoreline evolution of erosion and accretion is correctly simulated in most of the positions. Specifically, there is good agreement between the actual and simulated EPR from X=0 m to X=1200 m, and from X=11000 m to X=12500 m, where the shoreline has experienced both erosion and accretion, the simulated EPR closely matches the actual EPR.

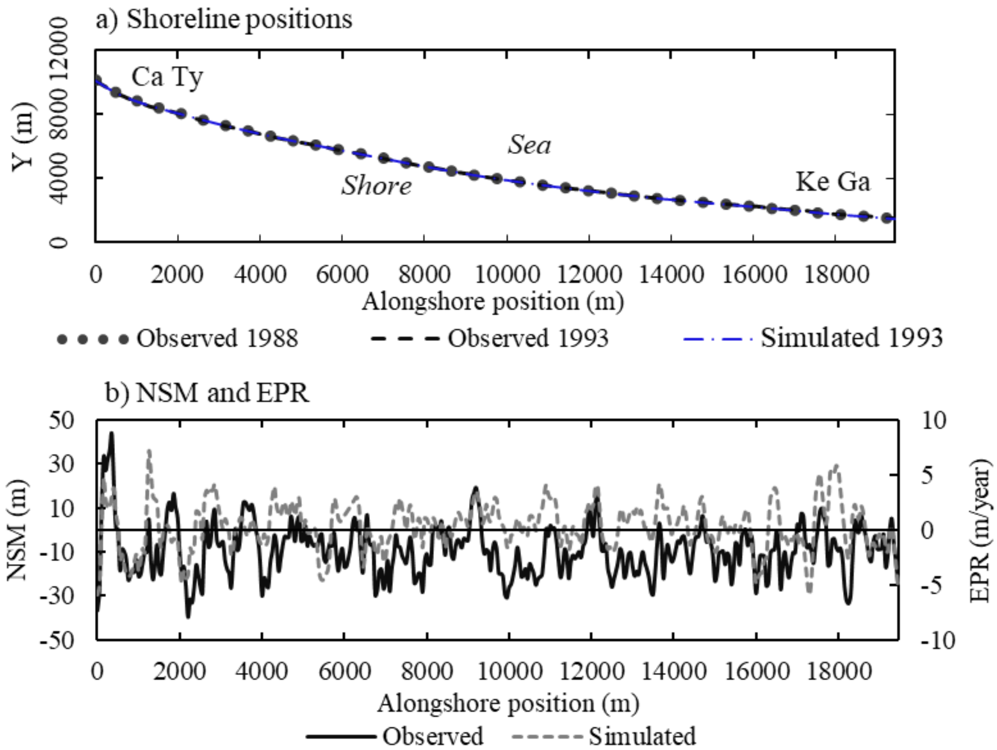

Figure I-1 Calibration result of segment 1 (07 Jan 1988 to 09 Mar 1993)

However, at X=10000 m, there was a noticeable difference between the actual EPR and the simulated EPR, indicating the need to investigate the adjacent area during the period of 1988 to 1993. Unfortunately, due to the limitations of available Google Earth imagery, the image from Mar 2001 was used instead, as shown in

Figure I-2. The presence of a small river in that area may be a contributing factor to the difference between the actual EPR and the simulated EPR. Therefore, it is suggested for future research to observe the sediment transport rate at the small river mouth and include it in the model. Thereby the model can better capture the dynamics of sediment transport and improve the accuracy of the simulated shoreline.

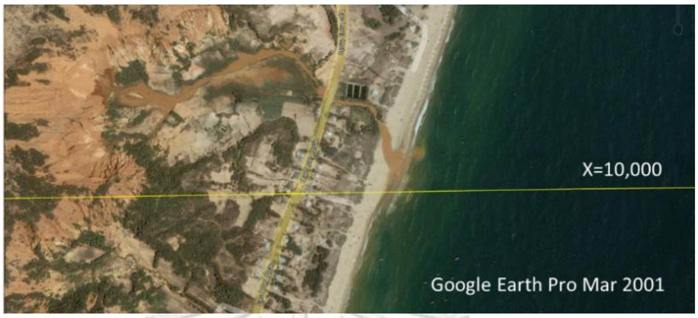

Figure I-2 The satellite images (Google Earth Pro in Mar 2001)

Mean Absolute Error (MAE) is a useful metric for evaluating the accuracy of numerical models, including shoreline change simulations. It provides a measure of how well the model predictions match the observed data, in terms of the absolute difference between the simulated and observed values as in the equation (I-2).

$$MAE = \frac{\sum_{i=1}^{n} |Y_{simulated} - Y_{actual}|}{total\ number\ of\ Y} \tag{I-2}$$

The Mean Absolute Error (MAE) was found to be 13.27 m, which is a measure of the average magnitude of the errors of the shoreline position (Y) in 1993 between the actual data and simulated data. While for the EPR of 1988 to 1993 (about 5 years), the MAE is 2.57 m/year. This suggests that there is some degree of error in the model, but the error is relatively small. Overall, the calibration results show that GENESIS can accurately simulate the shoreline evolution in the study area.

The sediment longshore transport rate was estimated from the calibrated simulation and presented in Figure I-3. The graph shows the net longshore transport rate, which is the balance between the sediment transported towards the right and the left direction. It also shows the sediment transport rates towards the right and left directions separately. The maximum net longshore transport rate was observed at approximately X = 1200 m, with a value of 150000 m3/year. It can be observed that the net longshore transport rate was positive for most of the shoreline when the right longshore transport rate was higher than the left longshore transport rate, indicating a dominant sediment transport towards the right direction from Ca Ty to Ke Ga as shown in Figure I-4, which aligns with the expected sediment transport patterns in the study area. This direction is likely influenced by the main wave direction from East to West and the shoreline orientation from NNE to SSW. These findings suggest that the calibrated model accurately simulates the sediment transport patterns in the study area, providing valuable information for coastal management.

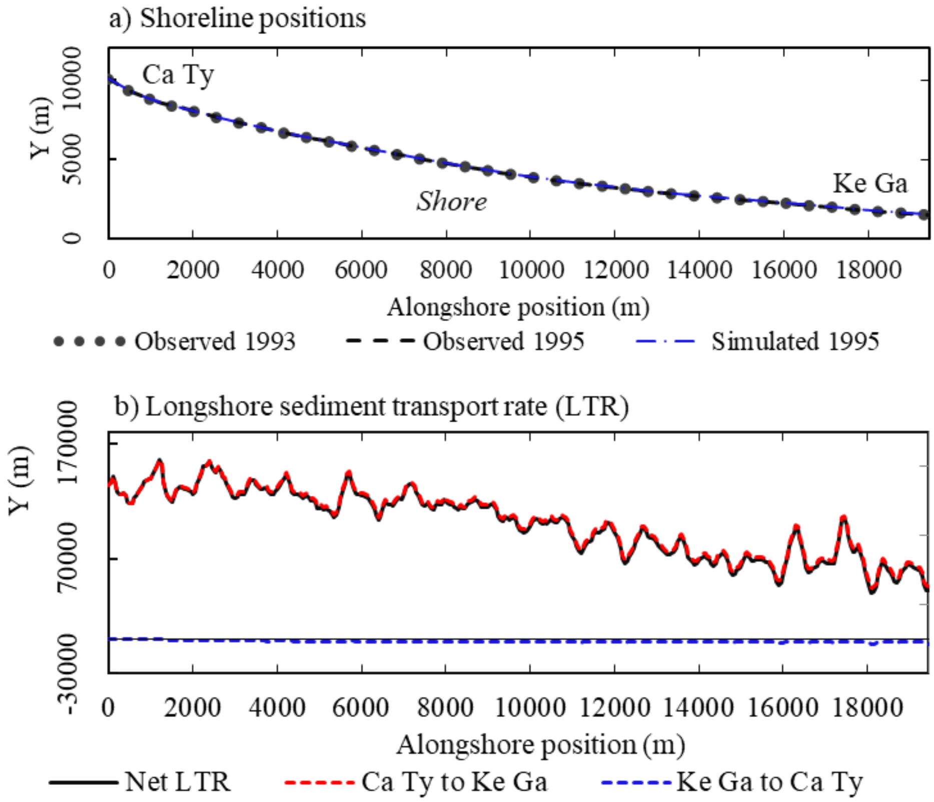

Figure I-3 Sediment longshore transport rate of segment 1 from 1988 to 1993

Validation

In order to validate the set of parameters as shown in Table I-2 for simulating other periods of segment 1 in GENESIS, those parameters were validated by simulating the period from 09 Mar 1993 to 10 Jan 1995.

The results of the validation, shown in Figure I-5, provide strong evidence that the simulated EPR was in good agreement with the actual EPR for most shoreline positions. Although some minor differences exist in the magnitudes of EPR at certain locations, the model correctly captures the shoreline erosion and accretion evolution. Specifically, the simulated EPR closely matches the actual EPR from X=12500 m to X=17000 m, where the shoreline experienced both erosion and accretion. Although there was a slight shift in the estimated location of accretion at around X=1500 m, the model still produced satisfactory results.

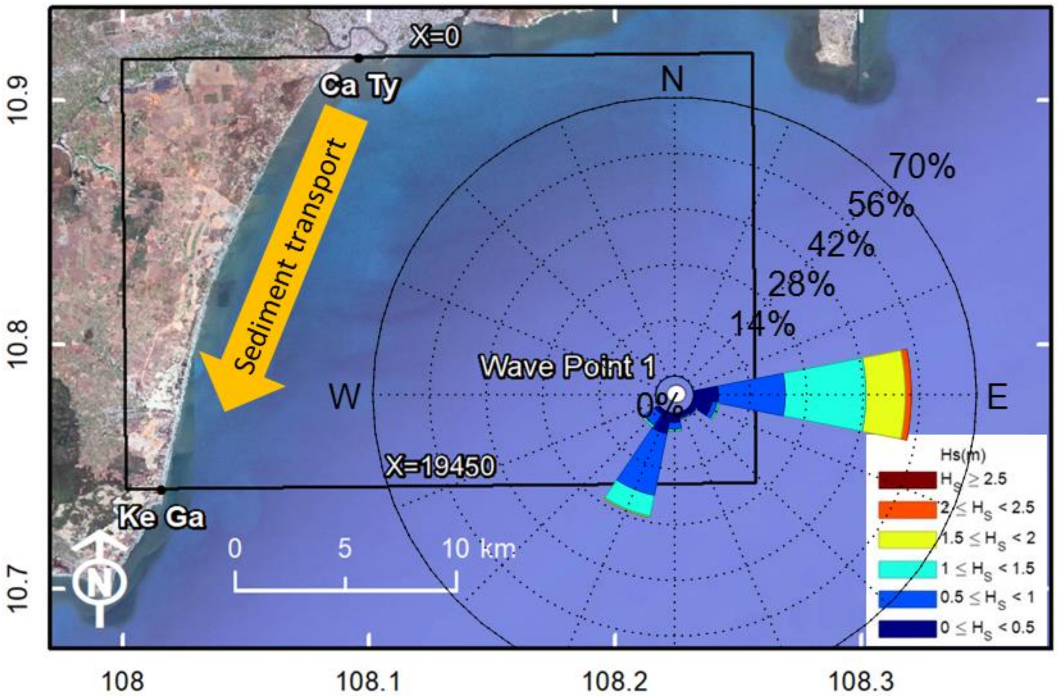

Figure I-4 Sediment transport direction, shoreline orientation, and wave characteristics at point 1 from 1988 to 1993

Table I-2 Set of parameters of segment 1 (calibration result)

Azimuth angle	**K1**	**D_c (m)**	**D_{50} (mm)**	**Berm height D_b (m)**	**Actual Ca Ty 1 (m) left**	**Actual Ke Ga (m) right**
0	0.1	9	0.25	0.6	37.64	5.18

However, the actual magnitude of erosion at X=9000 m and X=10500 m as shown in Figure I-6 was much higher than the simulated magnitude, and this could be attributed to the presence of two small rivers, as confirmed by the Google Earth Pro images, similar to the X=10000 m case in the calibration phase.

In the calibration phase, the model simulated the shoreline near Ca Ty boundary well. However, in this validation phase, the model could not simulate the erosion near the Ca Ty boundary, which could be due to the complex shoreline geometry with varying beach profile slope or sediment properties, or human intervention for ship navigation into the river.

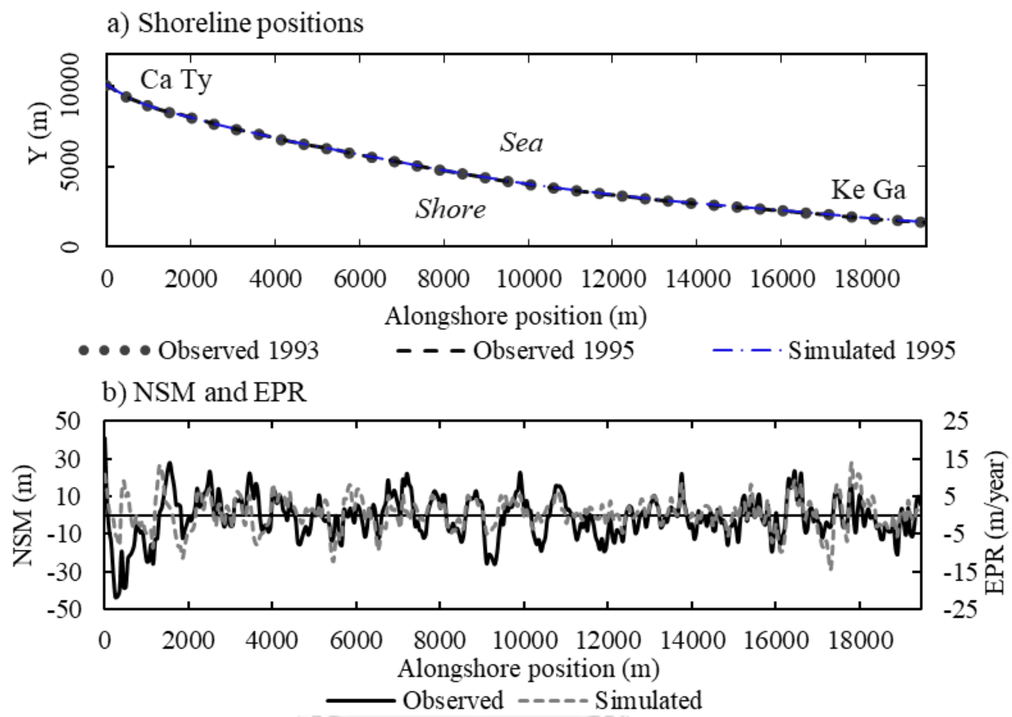

Figure I-5 Validation result of segment 1 from 09 Mar 1993 to 10 Jan 1995

Figure I-6 The existence of small rivers at X=9000 m, and X=10500 m

The Mean Absolute Error (MAE) between the actual data and simulated data was found to be only 6.82 m for shoreline position (which was lower than in the calibration phase) and 3.71 m/year for EPR (which was more or less the same as in the calibration phase). These results suggest that the model can be relied upon to provide valuable insights for coastal management in the study area. However, it was important to note that the model's accuracy may be impacted by other factors that were not considered in this study, such as the existence of small rivers, variations in sediment properties, beach profile slope, and human interventions. Further research may be necessary to better understand the impact of these factors and improve the model's performance for other applications. Nonetheless, the current results demonstrate the model's reliability and highlight its potential as a useful tool for coastal management in the study area.

2/ Segment 2

Calibration

The calibration of the model in segment 2 was performed by running the simulation from 03 Jan 2004 to 15 Feb 2008 (about 4 years) with the wave data at point 1 from 2004 to 2008. The interval time of the wave is 6 hours.

Similar to the calibration in segment 1 except for the K2 parameter since this simulation includes structures, the parameters are calibrated with the orders of the grid azimuth, K1, depth of closure D_c, sediment size D_{50}, K2, berm height D_b as shown in Table I-3.

Table I-3 Values of calibration parameter of segment 2

Azimuth angle	**K1**	**D_c (m)**	**D_{50} (mm)**	**K2**	**Db (m)**
0	0.05	5	0.05	0.07	0
270	**0.1**	7	**0.2**	0.1	**0.6**
334	0.3	**9**	0.5	**0.2**	2
	0.5	11		0.4	
				0.6	

In segment 2, the azimuth value of 334 degrees was selected as it resulted in a closer match between the simulated shoreline change and the observed shoreline change. Consistent with segment 1, the smallest K1 value of 0.1 was chosen, along with the highest values for D_c and D_b, to minimize the extent of shoreline change.

Additionally, the value of D_{50} calculated from the profile was adopted for this segment.

The K2 parameter was subjected to testing with three different values: 0.05, 0.2, and 0.55. Previous studies recommend that the value of K2 should fall within the range of (K1/1.5) to (K1/0.5) (Gravens et al., 1991). After calibration, it was observed that a value of 0.2 for K2 yielded the better results than others. Hence, a value of 0.2 was chosen as the K2 in GENESIS simulation of segment 2.

Finally, after the comparison of the simulated shoreline change and the actual shoreline change, the most compatible result is shown in Figure I-7.

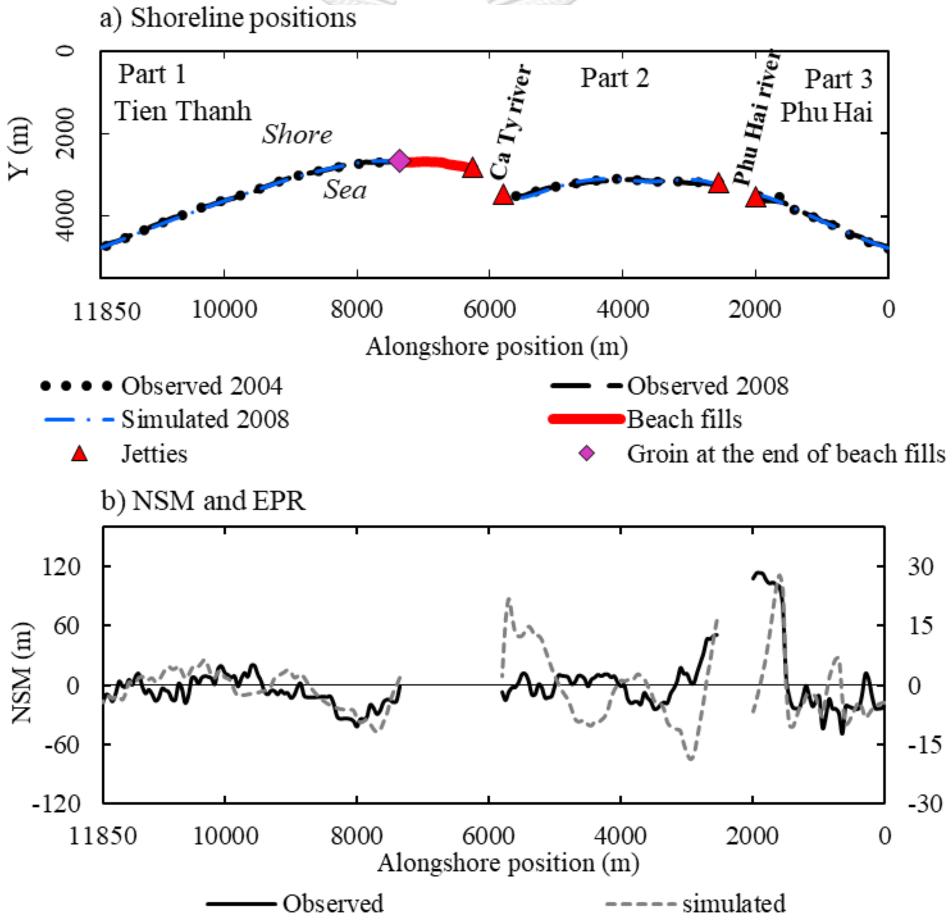

Figure I-7 Calibration result of segment 2 (03 Jan 2004 to 15 Feb 2008)

The sediment longshore transport rate was estimated in the calibrated simulation and is shown in Figure I-8. The graph indicates that although the longshore transport is disrupted at the two river mouths, the net longshore transport rate is mostly positive along the shoreline, with higher transport towards the right direction from Phu Hai to Tien Thanh. This aligns with the expected sediment transport patterns in the study area, influenced by the main wave direction from East to West and the shoreline orientation from NNE to SSW (Figure I-4 and Figure I-9). These findings demonstrate the reliable simulation result of sediment transport patterns by the calibrated model, providing valuable insights into longshore sediment transport for coastal management.

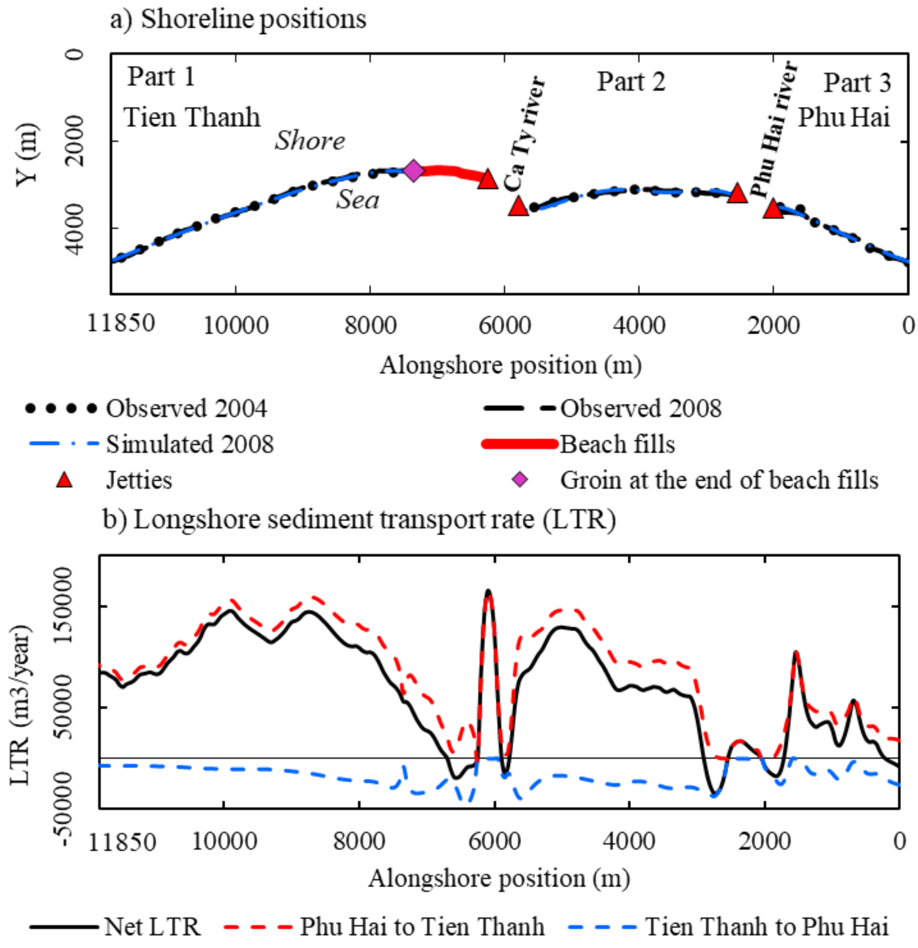

Figure I-8 Sediment longshore transport rate of segment 2 from 2004 to 2008

The calibration results for part 1, as zoomed in Figure I-10, demonstrate a generally good alignment between the calibrated End Point Rate (EPR) values and the actual EPR, effectively capturing the shoreline's erosion and accretion patterns at most shoreline positions with MAE 29.65 m for the shoreline, and 11.21 m/year for the EPR. However, some deviations exist where the EPR magnitudes differ at specific locations. For instance, between X=650 m to X=950 m, the actual shoreline experienced erosion, whereas the simulation indicated accretion. Conversely, from X=1650 m to X=2000 m, the actual shoreline exhibited accretion, while the simulation predicted erosion. These deviations could be attributed to the complex shape of the shoreline in this particular area. The actual shoreline profiles in 2004 and 2008, as illustrated in Figure I-10 and Figure I-11, display complicated shape that differs from the smoother shoreline simulated by GENESIS. This smoothing effect of GENESIS could explain why the simulated shoreline change differs from actual shoreline change. Another factor influencing the discrepancies could be the absence of consideration for nearby structures as shown in Figure 6.38, which have the potential to impact the shoreline in part 1 of segment 2. To achieve more accurate simulations of this complex shoreline area, it is recommended to employ a different shoreline model that incorporates the input of adjacent structures. GENESIS, on the other hand, is better suited for simulating the more consistently smooth shorelines.

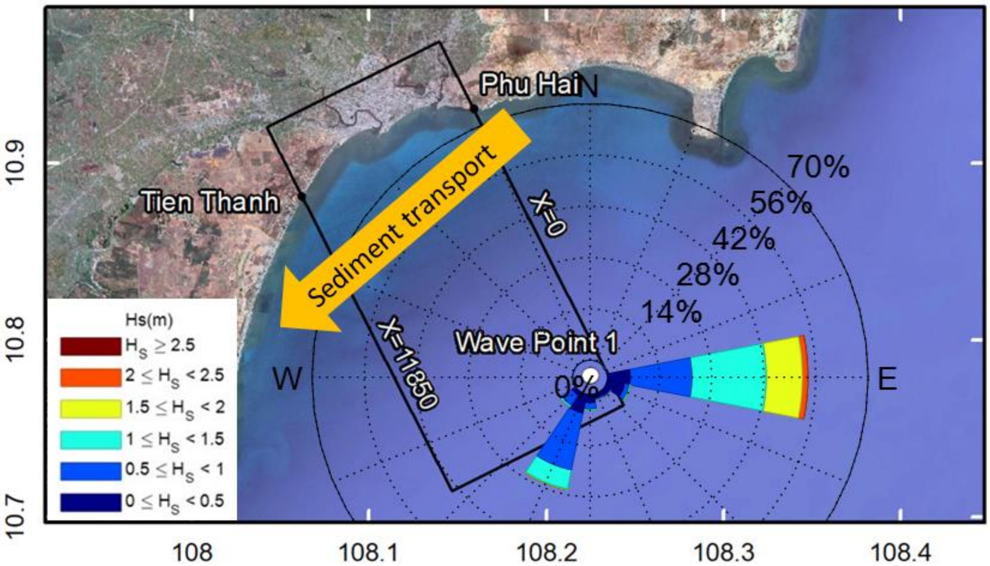

Figure I-9 Sediment transport direction, shoreline orientation, and wave characteristics at point 1 from 1988 to 1993

In part 2 of segment 2, situated between two rivers, despite extensive calibration efforts to achieve the highest level of accuracy, the model fails to capture the shoreline evolution in this specific area with MAE 37.40 m of the shoreline and 10.47 m/year of EPR. The actual shoreline exhibits a relatively stable pattern with a low End Point Rate (EPR). However, the GENESIS model produces a result indicating significant erosion downstream of Jetty Phu Hai 1, specifically from X=2550 m to X=3550 m, into where the sediment coming was very small as shown in Figure I-8. This discrepancy can likely be attributed to the lack of sediment supply from the Phu Hai river in the model's inputs. To improve the accuracy of other research, it is recommended to conduct the observation or calibration of sediment supply from the Phu Hai river.

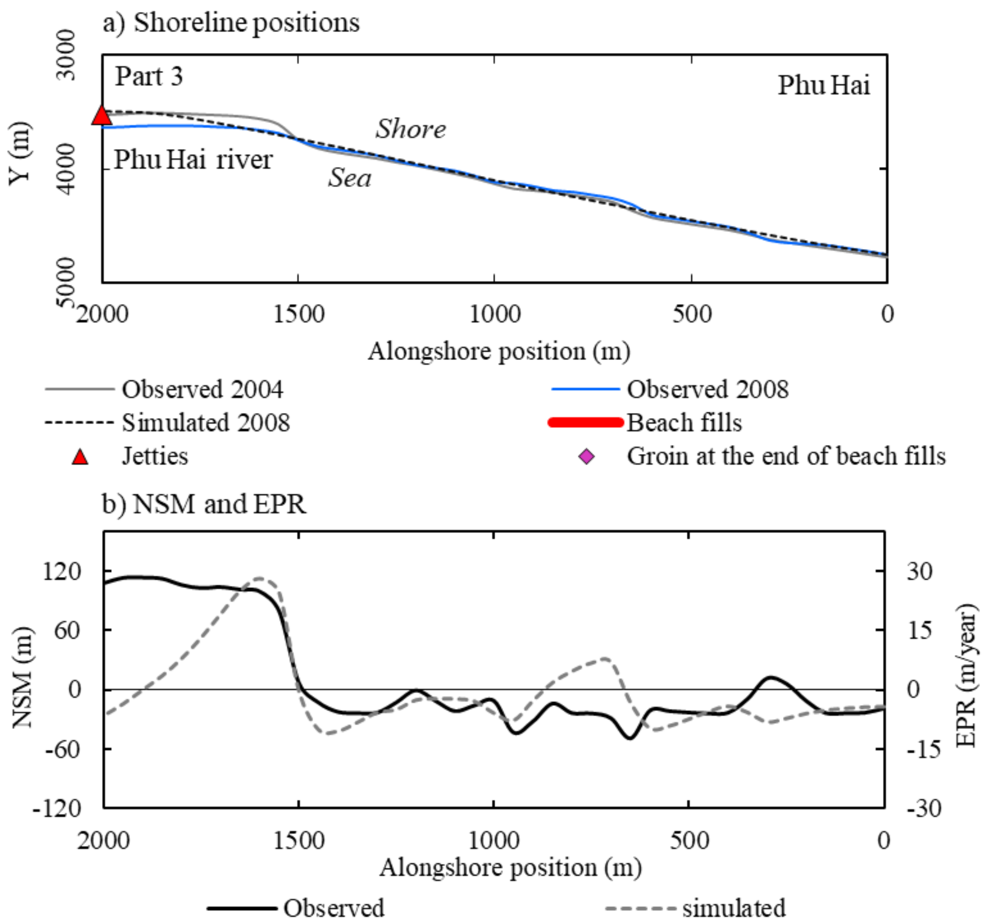

Figure I-10 Calibration result of part 1 segment 2
(03 Jan 2004 to 15 Feb 2008)

Part 3 of segment 2, located downs-drift of Jetty Ca Ty 1, includes beach reclamation project Hamubay that was simulated in segment 1 as well. The calibration generally gave a good result in this part with MAE of 14.12 m for the shoreline, and 9.08 m/year for EPR. Especially for the erosion down-drift of Hamubay, this simulation of part 2 in segment 2 gave the compatible result of simulated shoreline change and actual shoreline change, which was similar to a simulation of segment 1 from 2004 to 2008.

Figure I-11 Google Earth image of part 1 segment 2 (X=0 m to X=2000 m)

Part 3 of segment 2 is positioned downs-drift of Jetty Ca Ty 1 and includes the beach reclamation project Hamubay, which was also simulated in segment 1. The calibration process yielded satisfactory results overall, with a Mean Absolute Error (MAE) of 14.12 m for shoreline position and 9.08 m/year for End Point Rate (EPR). Notably, the simulation accurately captured the erosion occurring downstream of Hamubay, aligning closely with the actual shoreline changes. This outcome mirrors the simulation results from segment 1 between 2004 and 2008, showcasing consistency in the model's ability to replicate the shoreline dynamics in this region.

In conclusion, for the remaining simulations in Segment 2, the parameter set as shown in Table I-4 was selected for conducting the validation aiming to capture the most accurate shoreline change in segment 2.

Table I-4 Set of parameters of segment 2 (calibration result)

Azimuth angle	**K1**	**D_c (m)**	**D_{50} (mm)**	**K2**	**Db**
334	0.1	9	0.2	0.2	0.6

Validation

In order to validate the set of parameters for simulating other periods of segment 2 in GENESIS, those parameters as shown in Table I-4 were validated by running the simulation of the period from 15 February 2008 to 15 March 2011.

During period from 2008.02.15 to 2011.03.15 in segment 2, several existing structures were present, including Jetty Phu Hai 2, Jetty Phu Hai 1, Jetty Ca Ty 2, and

Jetty Ca Ty 1, as shown in the calibration phase. Additionally, there was an extension of the beach reclamation project, compared to its previous state during the calibration period.

The validation results, shown in Figure I-12, exhibit similarities to the calibration outcomes with slightly diminished performance. In part 1, characterized by a complex shoreline shape compounded by the presence of nearby structures, the model struggles to accurately simulate the shoreline dynamics. Conversely, in part 2, the model effectively captures the erosion downstream of the Jetty, spanning from X=2750 m to X=3950 m, as well as the erosion observed between X=8000 m and X=8650 m in part 1. Despite the disparities in the magnitudes of the End Point Rates (EPRs) between the simulated and actual shoreline changes in part 1, their patterns align closely, exhibiting comparable locations of peaks and troughs. This suggests that the model captures the overall behavior and trend of shoreline evolution, albeit with some discrepancies in magnitudes. The MAE of this period according to each part is shown in Table I-5.

Table I-5 The MAE of GENESIS from 2008 to 2011 in segment 2

Simulation	**MAE of Y (m)**	**MAE of EPR (m/year)**
Part 1	27.78	6.30
Part 2	25.37	11.58
Part 3	20.99	10.60

The difference observed in part 2 of segment 2 could possibly be attributed to human intervention in the form of a soft embankment constructed in the area, as mentioned in news reports (Nam, 2008). However, despite efforts to locate actual data regarding this intervention, it was not found available, including on Google Earth images. The absence of accessible data poses a challenge in fully understanding and incorporating the impact of this intervention on the simulated shoreline changes. Further investigation and access to reliable data sources are necessary to better simulate the shoreline change in this particular area.

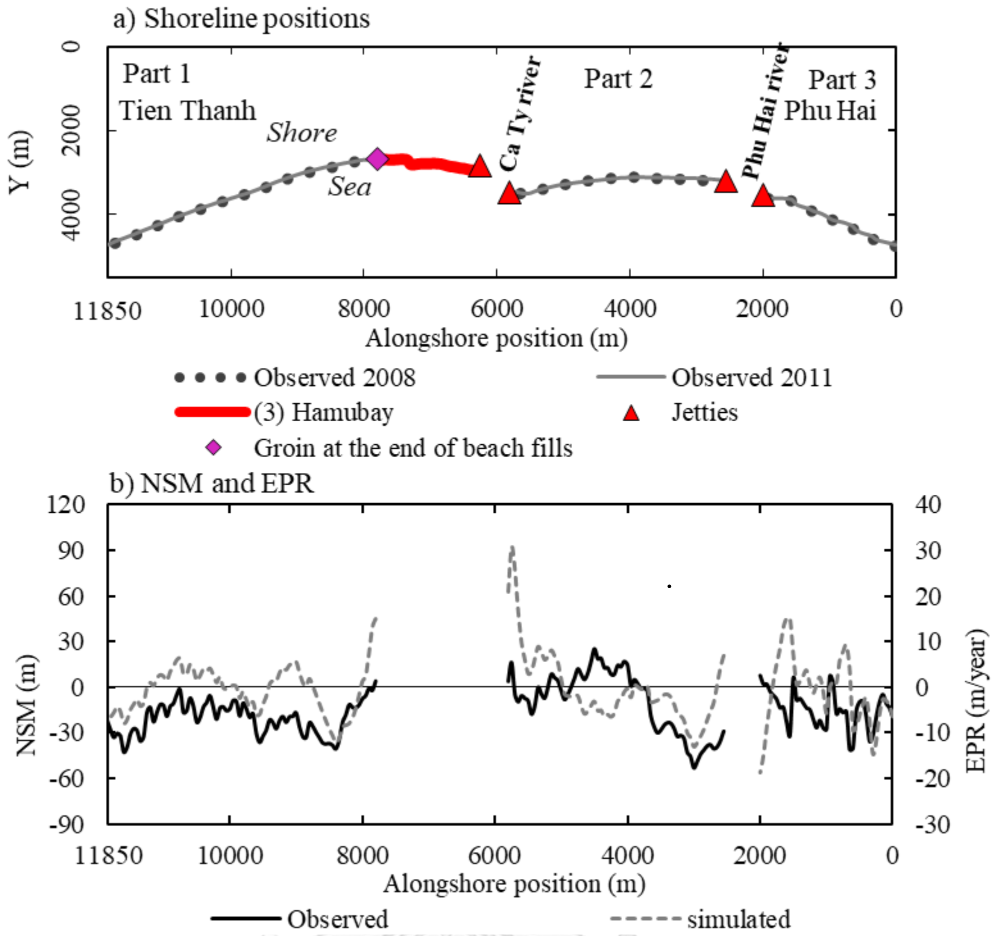

Figure I-12 Validation result of segment 2 (15 Feb 2008 to 15 Mar 2011)

3/ Segment 3

Calibration

The calibration of the model in segment 3 was performed by running the simulation from 07 Jan 1988 to 09 Mar 1993 (about 5 years) when there was no structure in this area yet.

The wave data from 2004 to 2008 with an interval time of 6 hours. In this segment 3, wave data at point 2 and point 2 were chosen to be used since that gave a better result compared to using wave data at point 1.

Similar to segment 1, the parameters are calibrated with the orders of the grid azimuth, K1, depth of closure D_c, sediment size D_{50}, K2, and berm height D_b as shown in Table I-6.

Table I-6 Values of calibration parameter of segment 3

Azimuth Angle	K1	**D_c (m)**	**D_{50} (mm)**	**D_b**
0; 10; **350**	0.01; **0.1;** 0.2; 0.5	5; 7; **9;** 11	0.05; **0.25;** 0.37; 0.5	0; **0.6;** 2

For segment 3, the azimuth value of 350 degrees was deliberately selected as it yielded a better alignment between the simulated shoreline change and the observed shoreline change. Following the approach applied in segment 1 and segment 2, a K1 value of 0.1, the smallest available, was chosen to minimize the extent of shoreline change. To further limit the magnitude of changes, the highest values of D_c and D_b were employed, with D_c set at 9 m and D_b at 0.6 m. Additionally, the calculated value of D_{50} from the profile, D_{50}=0.25, was used.

For segment 3, the azimuth value of 350 degrees was deliberately selected as it yielded a better alignment between the simulated shoreline change and the observed shoreline change. Following the approach applied in segment 1 and segment 2, a K1 value of 0.1, the smallest available, was chosen to minimize the extent of shoreline change. To further limit the magnitude of changes, the highest values of D_c and Db were employed, with D_c set at 9 m and Db at 0.6 m. Additionally, the calculated value of D_{50} from the profile, D_{50}=0.25, was used. Finally, the most compatible results of comparing the simulated shoreline change and the actual shoreline change is shown in Figure I-13.

The sediment longshore transport rate was estimated from the calibrated simulation and presented in Figure I-14. The graph shows that the net longshore transport rate is positive for most of the shoreline when the right longshore transport rate is higher than the left longshore transport rate, indicating a dominant sediment transport towards the right direction from Lang Chai to Ong Dia as shown in Figure I-14, which aligns with the expected sediment transport patterns in the study area. This direction is likely influenced by the main wave direction and the shoreline orientation as shown in Figure I-15. In this case, the main wave direction tends to be from the South to the North with high probability of wave from Southeast. These findings suggest that the calibrated model accurately simulates the sediment transport patterns in the study area, providing valuable information for coastal management.

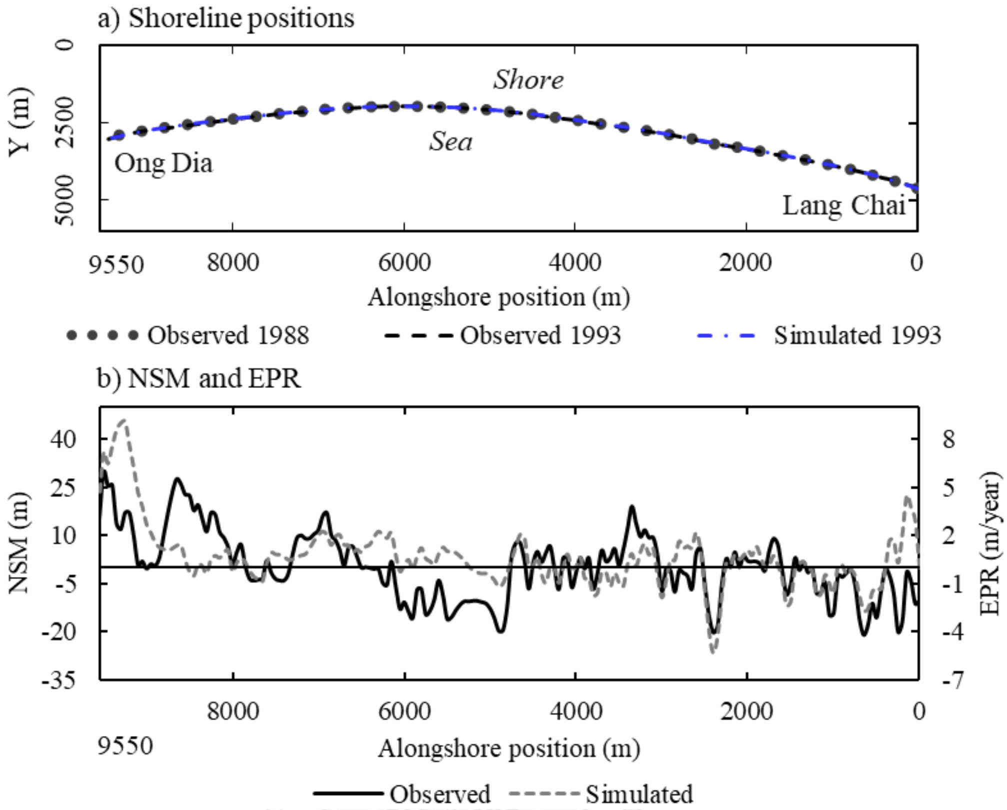

Figure I-13 Calibration result of segment 3 (07 Jan 1988 to 09 Mar 1993)

The calibration results for segment 3, as shown in Figure 6.49, reveal a generally agreement between the calibrated End Point Rate (EPR) values and the actual EPR, effectively capturing the erosion and accretion patterns along the shoreline. The calibration process yielded a mean absolute error (MAE) of 8.31 m for the shoreline and 4.24 m/year for the EPR, indicating a reasonably accurate simulation. However, some discrepancies were observed, particularly in the magnitudes of the EPR at specific locations. For example, from X=4800 m to X=6500 m, the actual shoreline change exhibited erosion, whereas the simulation showed a combination of erosion and accretion with a relatively small magnitude. Nevertheless, it is noteworthy that the overall patterns of the actual shoreline change and the simulated shoreline change align, with consistent peak and trough locations. This consistency is also observed for the shoreline near the boundaries, locating from X=0 m to X=400 m and X=8000 m to X=9550 m. Despite the slight deviations in magnitude, the calibrated GENESIS model successfully captures the general behavior and trends of shoreline dynamics in segment 3.

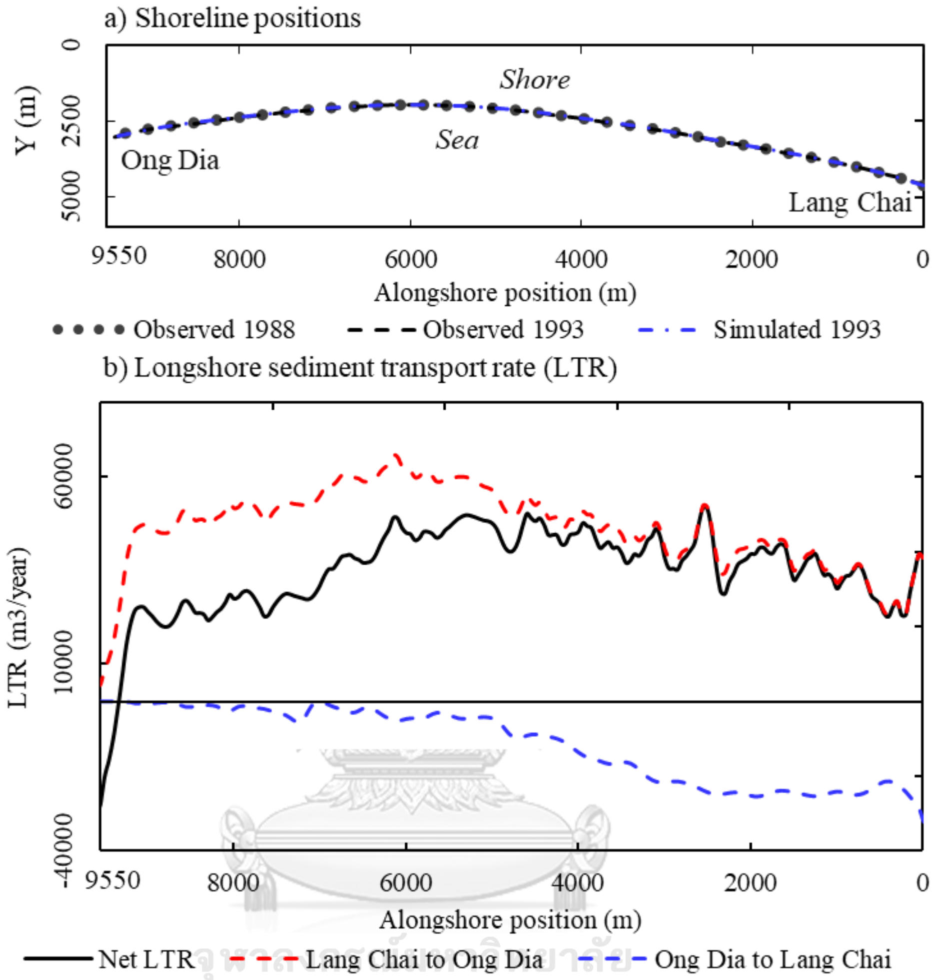

Figure I-14 Sediment longshore transport rate of segment 3 from 1988 to 1993

Validation

In order to validate the set of parameters for simulating other periods of segment 3 in GENESIS, those parameters as shown in Table I-7 were validated by running the simulation of the period from 09 Mar 1993 to 04 May 1996. During this period, there still no structure to be in the simulation yet.

The validation results, presented in Figure 6.52, strongly support the agreement between the simulated End Point Rate (EPR) and the actual EPR for most shoreline positions. The Mean Absolute Error (MAE) between the actual data and simulated data was found to be only 6.71 m for shoreline position (which is lower than in the calibration phase) and 4.59 m/year for EPR (which is more or less the same as in the calibration phase). Notably, the simulated EPR closely aligns with the actual EPR from X=0 m to X=5300 m, where both erosion and accretion occur. This region includes the Lang Chai boundary, which was not well-matched during the calibration phase.

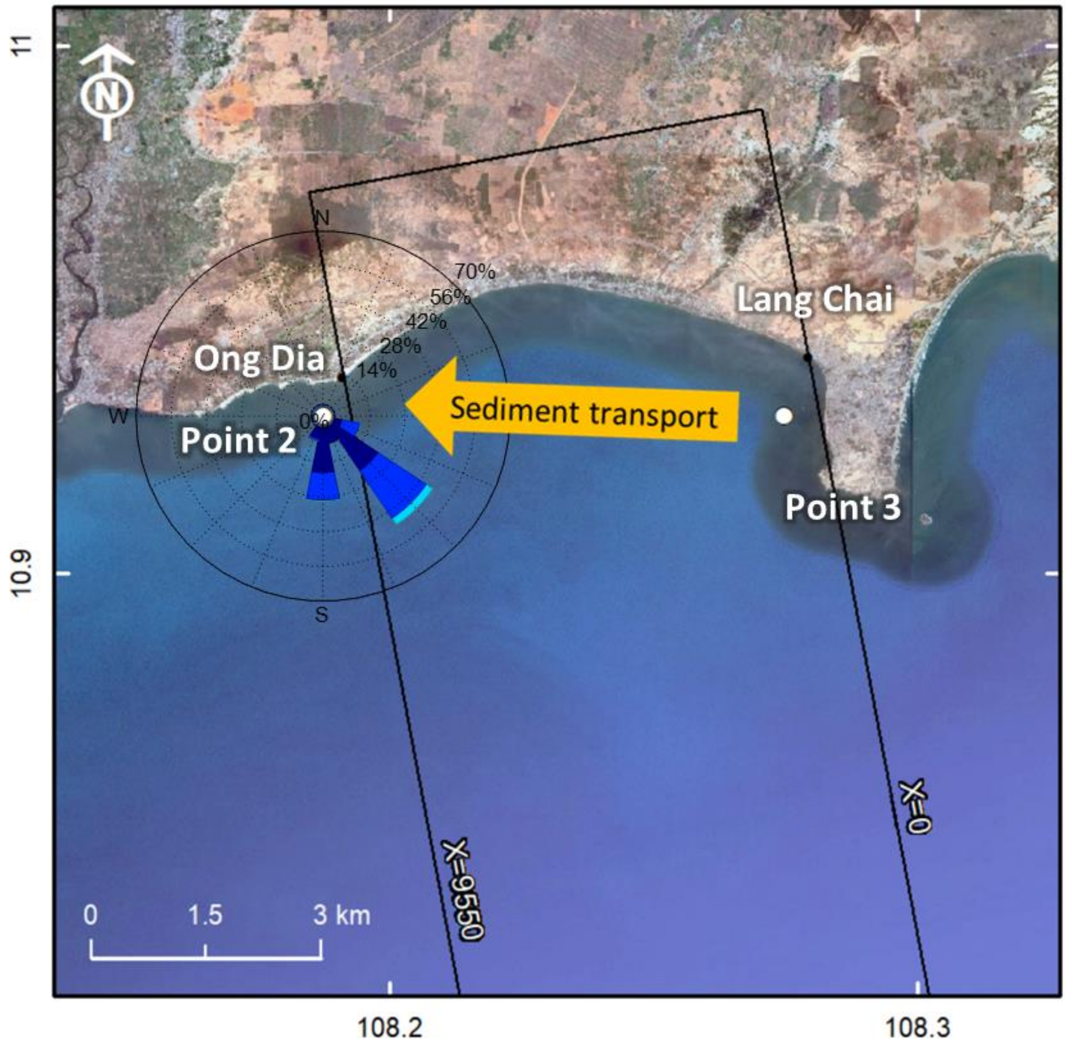

Figure I-15 Sediment transport direction, shoreline orientation, and wave characteristics at point 2 and point 3 from 1988 to 1993

Table I-7 Set of parameters of segment 3 (calibration result)

Azimuth angle	K1	D_c (m)	D_{50} (mm)	K2	Db
350	0.1	9	0.25	0.2	0.6

However, minor differences in EPR magnitudes are evident at certain locations, the model effectively captures the overall shoreline erosion and accretion dynamics. A discrepancy arises in the simulation of shoreline change from X=5300 m to X=7500 m, where the actual shoreline experiences erosion while the simulation showed greater stability. Consequently, this disparity affects the down-drift area near the Ong Dia boundary. In the simulation, less sediment is observed moving down-drift, resulting in reduced accretion compared to reality. Despite these minor differences, the overall performance of the GENESIS model in simulating the shoreline changes in segment 3 during the validation phase is promising and provides valuable insights into the shoreline change evolution.

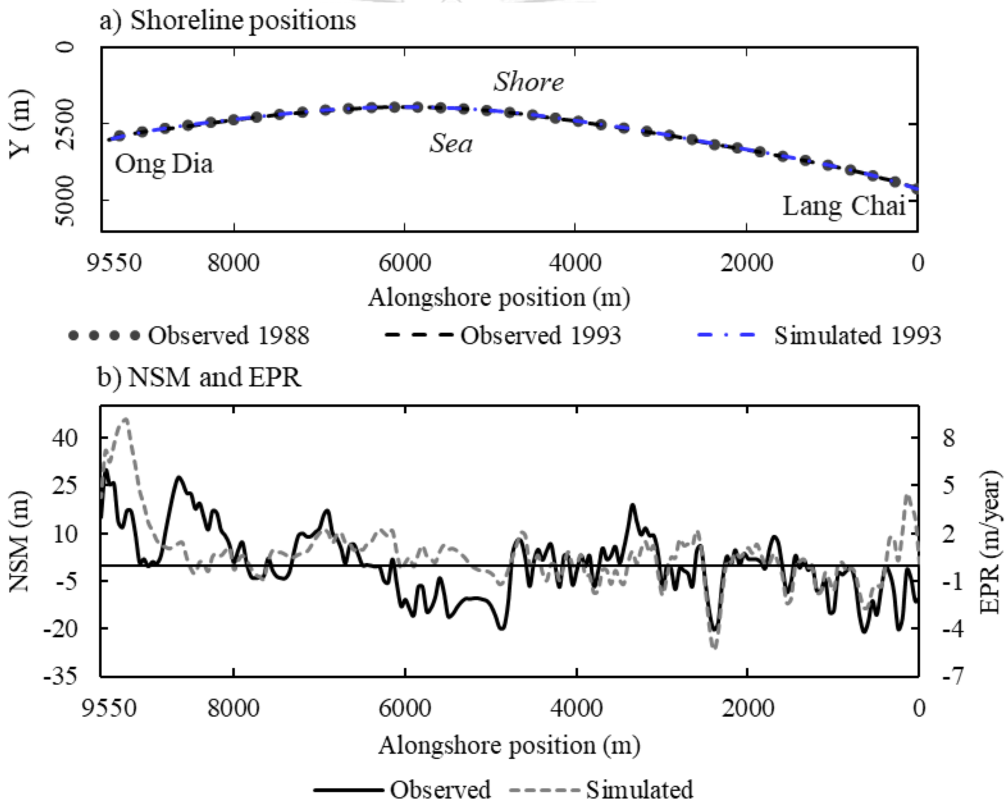

Figure I-16 Validation result of segment 3 from 09 Mar 1993 to 04 May 1996

VITA

NAME	PHAM THI PHUOC HOAI
DATE OF BIRTH	10 Sep 1995
PLACE OF BIRTH	Khanh Hoa province, Vietnam
INSTITUTIONS ATTENDED	Ho Chi Minh University of Technology
HOME ADDRESS	Ninh Hoa town, Khanh Hoa province, Vietnam